THE PETROGRAPHY, GEOCHEMISTRY AND PETROGENESIS OF ALKALINE DYKE ROCKS FROM THE COLDWELL ALKALINE COMPLEX, NORTHWESTERN ONTARIO

by

David G. Laderoute©

A thesis submitted in partial fulfillment of the requirements
of the degree
Master of Science

Faculty of Science
Lakehead University
Thunder Bay, Ontario

To my wife, Jackie, and my sons, Andrew and Mark, for the patience, forbearance and support they have shown while this work has become a reality.

ACKNOWLEDGEMENTS

First and foremost, I would like to thank Dr. Roger Mitchell, whose patience, guidance and criticism proved invaluable in the production of this thesis. I would also like to offer special thanks to Dr. Garth Platt, who filled in for Dr. Mitchell while the latter was away on sabbatical in Great Britain.

For their assistance in preparing this work, I would also like to offer thanks to the following people: Dr. Edward Mercy, Dr. Steve Kissin, Dr. Graham Borradaile and Dr. Phil Fralick for comments and suggestions for dealing with specific subjects and problems; Dr. Tom Griffith, Al MacKenzie and Keith Prignitz for assistance with various analytical procedures; Maureen Artist for assistance with neutron activation analysis and associated computer procedures; Ron Bennett and Diane Crothers for help in preparation of samples and thin and polished sections; Bruce Jago and Tom Dixon for helping me to understand the arcana of computers in general and FORTRAN in particular; Wendy Bons for help with paperwork, photocopying and other administrative details; Dr. Mel Gascoyne and Richard Everitt for use of computer time with Atomic Energy of Canada, Ltd.; and Mark Smyk and Jurate Lukosius-Sanders for assistance with field work.

TABLE OF CONTENTS

LIST OF TABLES

Table Page

LIST OF PLATES

Plate Page

LIST OF FIGURES

Figure Page

ABSTRACT

Dyke rocks occurring in the Coldwell alkaline intrusive complex, N.W. Ontario, were studied by various petrographic and geochemical means. The resulting observations indicate that 5 types of mafic alkaline lamprophyres, distinguished on the basis of chemistry and mineralogy according to the scheme of Rock (1977), and 1 type of felsic tinguaite occur in the complex (in approximate order of abundance):

a) ocellar camptonites
b) analcite tinguaites
c) sannaites
d) quartz-bearing camptonites
e) amphibole camptonites
f) monchiquites

Lamprophyres are characterized mineralogically by phenocrysts of clinopyroxene and brown amphibole, and remnant phenocrysts of olivine (all commonly zoned from Mg-rich cores to Fe-rich rims) in a groundmass of Fe-Na-clinopyroxene, brown amphibole, biotite, plagioclase and alkali feldspar (except in the case of the monchiquites, which contain an isotropic glassy material in place of feldspar), nepheline, calcite and minor opaque and accessory phases. All phases are commonly altered to a variety of secondary products. Quartz camptonites are distinct in containing incompletely resorbed quartz phenocrysts. All lamprophyres contain varying abundances of ocelli, which are globular segregations of carbonate minerals and silicate phases such as scapolite, chlorite, epidote, zeolites and fluorite. Tinguaites contain phenocrysts of alkali feldspar, nepheline, analcite and minor riebeckite in a groundmass of the former three phases plus

aegerine and minor accessory phases.

Application of multivariate statistical routines to major and minor element data from these rocks suggests that the quartz camptonites are distinct from the other lamprophyres on the basis of various chemical parameters other than silica. These routines are incapable of distinguishing the other lamprophyres on the basis of chemistry. Variation diagrams constructed from the major element data suggest that all of the dyke rocks except the quartz camptonites form a magmatic series. Studies of trace element abundances in these rocks suggest that they are related as a magmatic series by a fractional crystallization scheme involving those phases occurring as phenocrysts, crystallizing under varying physico-chemical conditions, with the parental liquid being a LREE- and volatile component-enriched alkali olivine basait related to the terminal stages of the Centre 2 magmatism in the complex. The quartz camptonites are derived separately from a similar liquid which was contaminated with silica-rich material, or from a thoeliitic parent related to the Centre 1 acitivity in the complex. Ocelli result from immiscibility of a carbonate or silicate liquid coexisting with the magma from which the dykes formed. Studies of material from dyke margins and corresponding centres suggest that minor flow differentiation has occurred. Following their emplacement, all dykes were subjected to varying degrees of alteration resulting from late-stage magmatic and post-magmatic processes.

CHAPTER 1- INTRODUCTION

It is the purpose of this thesis to describe in detail the petrography, mineralogy and geochemistry of selected minor intrusive units of the Coldwell Alkaline Intrusive Complex. This information will be used to assess the relationships between these rocks and to establish a petrogenetic model for their origin.

REGIONAL GEOLOGY

The Coldwell Complex is a sub-circular intrusive body of Neohelikian age (Platt and Mitchell,1982) located on the north shore of Lake Superior approximately 200 km east of Thunder Bay, Ontario (Figure 1.1). It is the largest alkaline intrusion in North America, having an areal extent of approximately 580 km^2. The complex is emplaced in Archean metavolcanic and metasedimentary rocks of the Superior Province of the Canadian Shield, which in this area form the essentially east-west trending Schrieber-White River greenstone belt. These Archean rocks have been subjected to greenschist and amphibolite facies metamorphism and at least two episodes of folding and have been intruded in turn by Archean granites and syenites (Ayres et al,1970; Einarsson,1972). The grade of metamorphism in the immediate

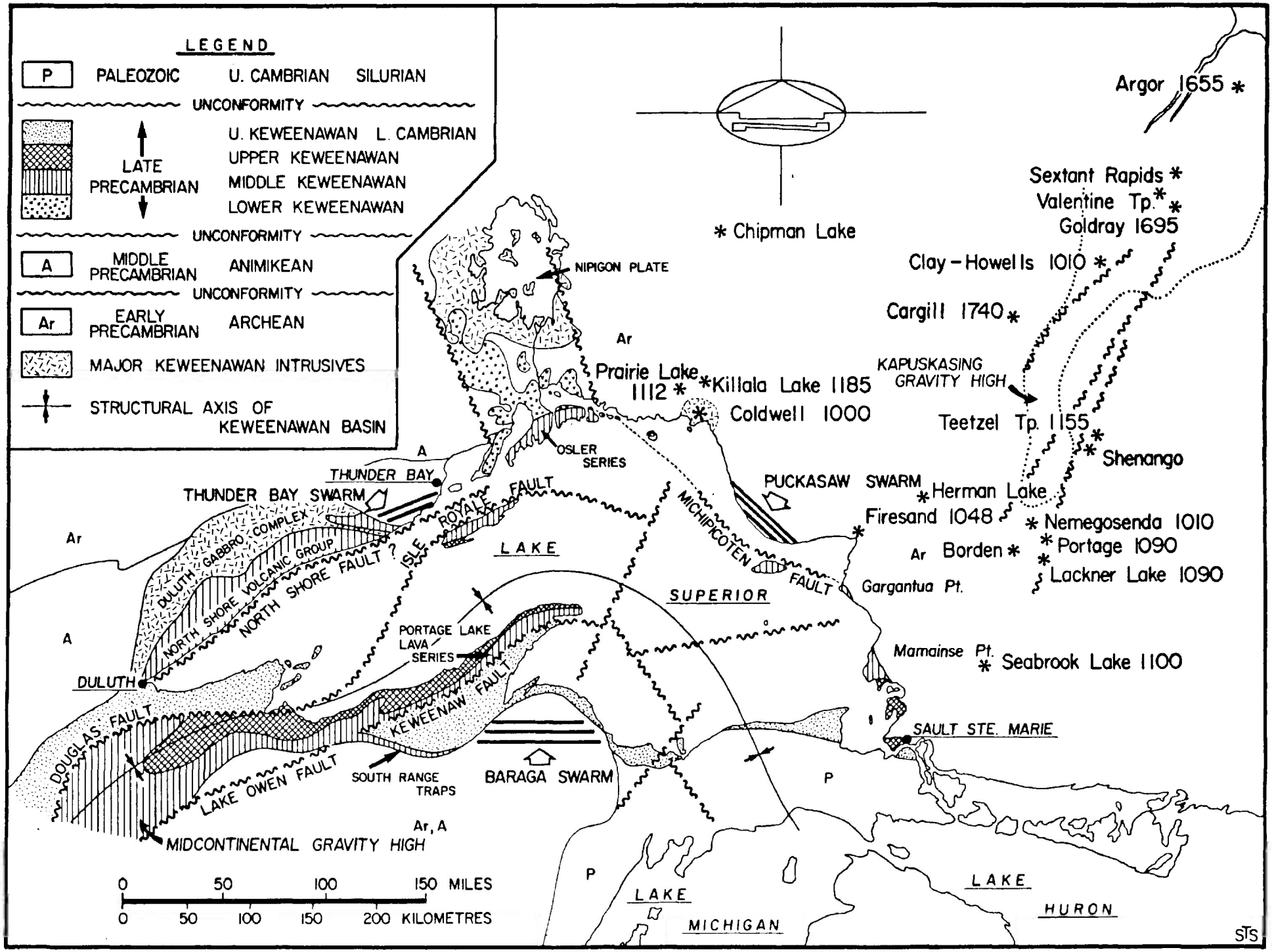

Figure 1.1 Regional Geological Setting of the Coldwell Complex

vicinity of the Coldwell Complex is raised to pyroxene hornfels facies in a thermal aureole approximately 2 km wide that surrounds the complex. Further information concerning the Archean geology of the area is given by Puskas (1967), Milne (1967), Walker (1967) and Thompson (1931).

The Coldwell Complex itself is emplaced at a northeasterly-trending bifurcation of the greenstone belt, which is coincident with the junction of two belts of thoeliitic volcanic rocks- the North Shore-Osler volcanics to the west, and the Mamainse-Michipicoten volcanics to the southeast (Figure 1.1). These latter rocks represent some of the extensive intrusive and extrusive basic magmatism associated with Keweenawan rifting in the Lake Superior region (Mitchell and Platt,1977). This rifting and related igneous activity is similar to that seen in the Gregory-Kavirondo rifts of East Africa and the Kangerdlugssuag region of Greenland (Mitchell and Platt,1978), where Brooks (1973) has suggested that mantle plume generated triple-junctions have occurred. Alkaline intrusions are, in some cases, associated with the failed arms of these triple-junction intracratronic rift systems, being brought about by crustal upwarping (Bailey,1964). The linear trend of the Coldwell, Prairie Lake, Killala Lake and Chipman Lake intrusions (Figure 1.1) may represent a similar

failed arm situation (Mitchell and Platt, 1982). However, Hinze and Wold (1982), found no evidence to support the existence of such a triple-junction in the Lake Superior region. An alternative explanation proposed by Klasner et al (1982), is that the complex was emplaced where a late transverse fracture intersected the Keewanawan rift system (i.e. the Trans-Superior Tectonic Zone).

GENERAL GEOLOGY OF THE COLDWELL COMPLEX

Introduction

Figure 1.2 shows the general geology of the Coldwell Alkaline Complex as determined by Puskas (1967) and as subsequently re-evaluated by Mitchell and Platt (1977,1982). This map is an oversimplification of the geology of the area; in fact, the detailed relationships are considerably more complex, and are obscured by the extensive cover of mature forest that characterizes the region. The geology of the complex is best exposed along the shore of Lake Superior, and along road and rail cuts and power lines that traverse the area. The geology of the interior portions of the complex is thus based largely on extrapolation of observations from these relatively limited exposures.

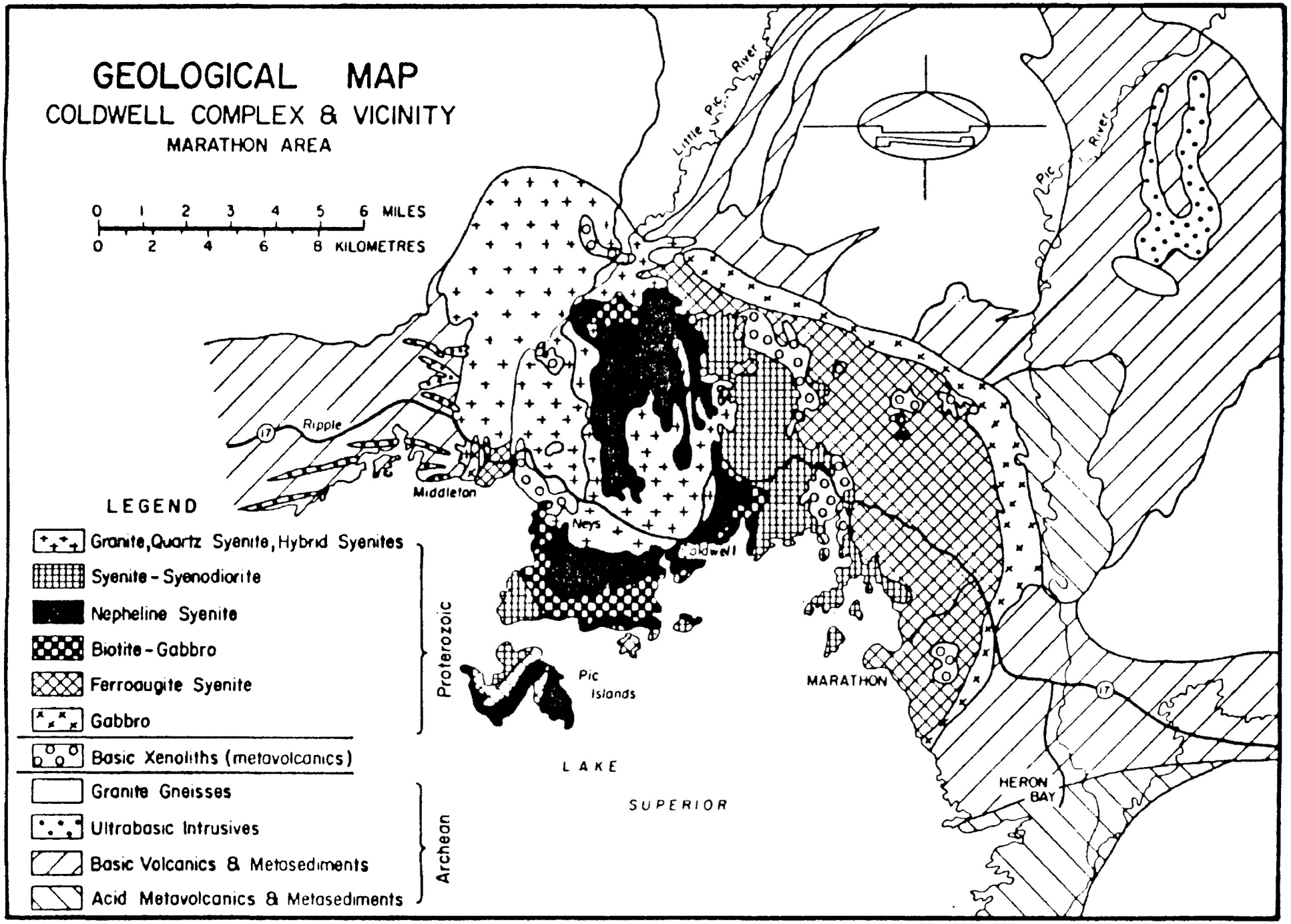

Figure 1.2 General geology of the Coldwell Complex from Platt and Mitchell (1982).

Structure

Lilley (1964) suggested that the intrusion was a funnel-shaped body of gabbro and ferroaugite syenite which was in turn intruded by nepheline syenites. Puskas (1967) believed that the complex was a lopolith. Mitchell and Platt (1977) rejected the idea of a single differentiated intrusion. Rather, they proposed that the complex comprises several centres of intusion (see below). Mitchell and Platt (1982) and Currie (1980) believe that the magmas of each centre were emplaced by cauldron subsidence and that the activity migrated in a westward direction. The evidence for such a style of intrusion is found in ring dykes represented by the eastern border gabbro of Centre 1 and the biotite gabbro of Centre 2, and in downfaulted and partially assimilated cap lavas that formed the roof of the complex in the area approximately defined by the Little Pic River and Redsucker Cove fault zones. The latter is a complex series of north to north-west trending faults that truncate the eastern Centre 1 ring structure (Mitchell and Platt, 1982). The result is that different structural levels are present in various parts of the complex.

Although the detailed three dimensional geology and structure of the complex is poorly understood, a gravity

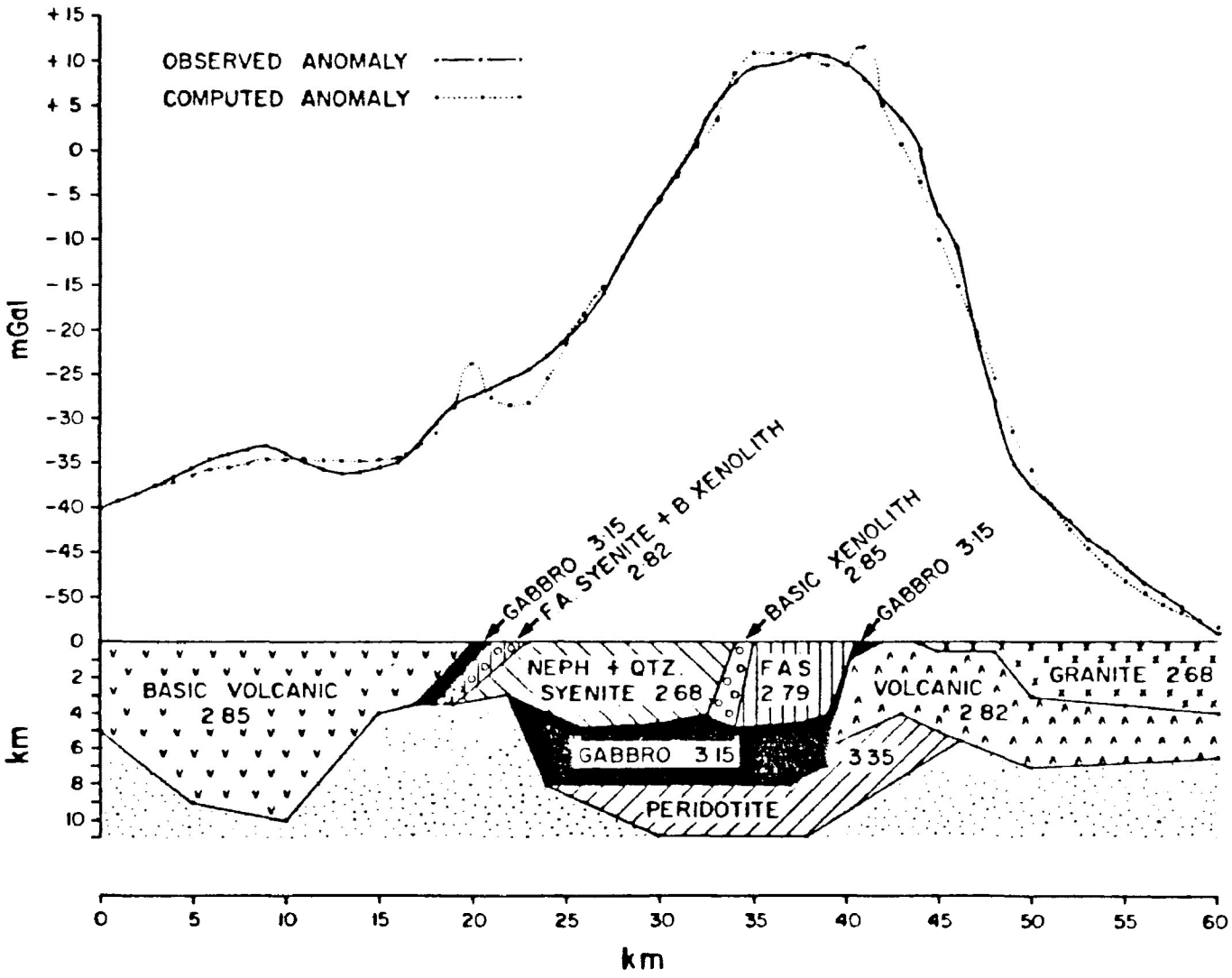

Figure 1.3 Geological Model of the Coldwell Complex based on the gravity study of Mitchell et al (1983)

study conducted by Mitchell et al (1983) provides a reasonable model that is also consistent with the petrology of layered intrusions. A prominent positive gravity anomaly (Figure 1.3) is interpreted to indicate the presence of a large body of peridotite and/or pyroxenite which forms the bulk of the complex. This layered intrusion, located at a depth of 8 to 11km, is overlain by gabbro (5 to 8km) and a thin (5km) layer of differentiated felsic rocks.

Centres of Magmatism

The complex comprises 3 distinct intrusive centres, each representing distinct magmatic episodes and each characterized by a distinct differentiation trend. In order of intrusion these are:

CENTRE 1- Saturated alkaline rocks with oversaturated peralkaline residua.

CENTRE 2- Miascitic alkaline rocks with undersaturated residua.

CENTRE 3- Alkaline rocks with oversaturated residua.

The following sections describe the petrology of each Centre:

CENTRE 1- The oldest rocks of the complex are the eastern border gabbros (Figure 1.2), which are intruded in turn by several "sub-centres" of ferroaugite syenite (Mitchell and Platt, 1977). These latter rocks typically display extreme iron enrichment, differentiate to quartz-bearing residua and are characterized by fayalite, ferroaugite, ferrorichterite, ferroedenite and aenigmatite (Mitchell and Platt, 1977). Both rock types display igneous layering in which cross bedding, slump-structures and diffuse turbulent or "wispy" layering are locally well developed.

CENTRE 2- An arcuate body of biotite-bearing gabbro that outcrops on the Coldwell Penninsula (Fig.1.2) represents the earliest expression of Centre 2 magmatism (Mitchell and Platt, 1982). This unit contains locally abundant suites of partially assimilated xenoliths of basic volcanic rocks, and consists of biotite, plagioclase, alkali feldspar, nepheline, olivine, pyroxene and amphibole, and in some cases significant amounts of magnetite and apatite. (Mitchell and Platt, 1982). The biotite gabbro is intruded and metasomatized by nepheline syenite that occurs in three principal "sub-centres" at Pic and Allouez Islands, the Mink Creek-Redsucker Cove area and east of the Killala Lake Road (Figure 2). These are coarse-grained leucocratic to melanocratic rocks composed of amphibole, nepheline and minor

and accessory olivine, pyroxene, biotite, natrolite, titanomagnetite, apatite, fluorite, zircon, sphene and sodalite. A wide range of textures have developed in response to high-temperature shearing and recrystallization (Mitchell and Platt, 1982). Layering is observed in the syenites on Pic Island where wispy modal layering is well developed, at Neys Park and on the West Coldwell Penninsula.

CENTRE 3- These rocks consist of magnesiohornblende syenites, ferroedenite syenites and quartz syenites. Ferroedenite syenites contain xenoliths of metavolcanic rocks presumably derived from the roof of the intrusion. Assimilation of these xenoliths has led to the development of a wide variety of contaminated ferroedenite syenites. The syenites are characterized by a paucity of pyroxene and an abundance of amphibole. The compositional evolution of the amphibole is towards sodic amphiboles and is unlike that observed in the nepheline syenites but similar to that of the Centre 1 ferroaugite syenites. Centre 3 quartz syenites are characterized by the presence of perthitic feldspars, and the presence of abundant zircon, fluorite, chevkinite, parrisite, synchysite and bastnasite (Mitchell and Lukosius-Sanders, unpublished data; Jago, 1980).

Minor Intrusions

Two forms of minor intrusion, dykes and diatremes, are recognized in the Coldwell Complex. The dyke rocks that are the subject of this thesis are apparently coeval with the Centre 2 magmatism as determined by cross-cutting relationships. A detailed description of the dykes is presented in subsequent sections. Three diatremes are also observed in the area. One of these, located on the west side of the Coldwell Penninsula (Fig.1.2) is definitely associated with the intrusion of the complex as it contains xenoliths of Centre 2 material (Balint, 1977). The origin of the other two diatremes is problematical, however, as they are located near the complex in the Archean country rock but have not yet been found to contain any Coldwell material as xenoliths.

FIELD GEOLOGY OF THE DYKE ROCKS

Introduction and General Observations

Those types of dyke rocks that are associated with Centre 2 may be broadly catagorized into several groups on the basis of field observation, in approximate order of abundance:

a) ocellar lamprophyres

b) analcite-bearing tinguaites (termed "heronites" by Coleman (1900))

c) lamprophyres with abundant clinopyroxene phenocrysts

d) lamprophyres with quartz phenocrysts

Examples of the above types of dykes have been examined in detail in terms of their field geology. All of these rocks display features characteristic of true dykes, such as cross-cutting relationships (Plate 1.1), brecciation (Plate 1.2), development of chilled margins (Plate 1.3) and alteration of host rocks (Kent, 1981). Where possible, attitudes of the dykes have been determined (Table 1.1), however, limited exposure and local pinch-outs and dislocations commonly obscure gross physical features.

Plate 1.1 Two tinguaite dykes exhibiting a cross-cutting relationship

Plate 1.2 A lamprophyre dyke incorporating fragments of syenitic wall-rock near the centre of the photograph

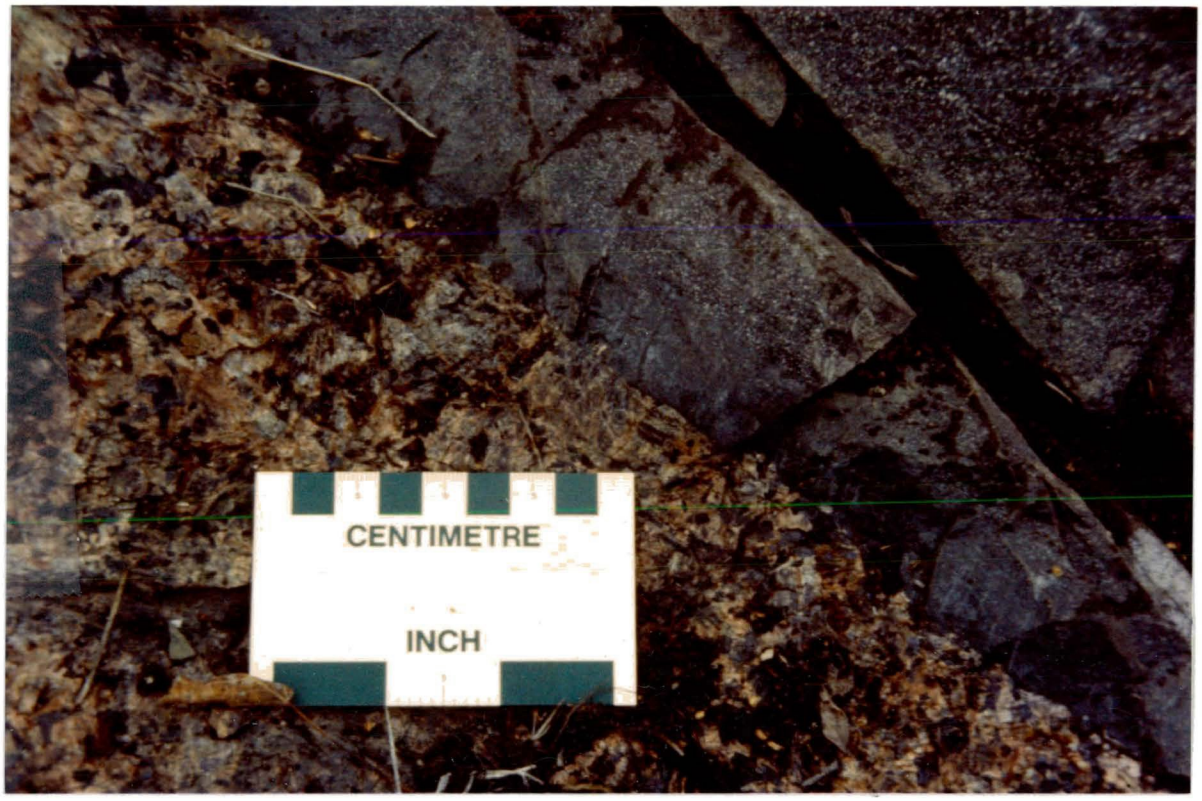

Plate 1.3 Chilled margin developed in a lamprophyre against the syenitic wall-rock; note the sharp contact between the dyke and the wall-rock

Plate 1.4 Lamprophyre dyke exhibiting internal banding parallel to the dyke contact as a result of multiple intrusion within the same conduit to form a composite dyke, or as a result of flow differentiation

Table 1.1 Physical Characteristics of Dykes

Dyke Type	Attitude	Width (m)
Lamprophyres	284-81	1.2
	340-48	0.3
	302-40	2.5
	17-34	0.9
	330-90	0.3
	328-60	1.0
	328-60	0.6
	328-60	0.3
	260-78	3.0
	297-80	2.0
	276-70	0.5
	260-70	3.0
	275-75	4.0
	306-80	1.5
	272-80	4.0
	100-70	0.7
	281-80	1.0
	310-90	2.0
	276-70	0.5
	317-74	2.0
Tinguaites	313-85	0.1
	20-90	0.1
	355-82	0.3
	45-18	0.5
	285-78	2.0
	324-87	1.5
	276-23	0.7
	311-67	1.1

Generally, the dyke rocks strike in a northwesterly direction and dip steeply to the north-east, although the felsic tinguaites display more variance from this general trend than the mafic dykes. Dyke widths are quite variable, ranging from 20cm (Plate 1.9) to several metres (Plate 1.5); considerable variation may be observed within a single dyke. Cross-cutting relationships between dykes and host rocks and other dykes are also difficult to determine for the reasons outlined above. Aubut (1977) developed a scheme to describe the cross-cutting relationships that exist among the dykes of the southwestern margin of the Coldwell Complex by categorizing the dykes into four "periods" based on apparent order of intrusion. However, the relationships throughout the Complex in general are not so clearly defined.

Contacts with the host rock are frequently undulatory and usually sharp (plate 1.3), although shearing and accumulation of leucocratic material along contacts is sometimes observed (Plate 1.6). Veinlets or dykelets of melanocratic material from the mafic dykes commonly penetrate the contact and extend some distance into the host rock (Plate 1.7). Alteration, including carbonatization and haematization of the host rock adjacent to the contact is also observed, but the degree and extent of this alteration is not apparently systematically related to the type of dyke

Plate 1.5 A tinguaite dyke approximately 2m wide

Plate 1.6 Accumulation of carbonate-rich leucocratic material along the margins of a tinguaite dyke

Plate 1.7 Lamprophyric dykelet derived from larger lamprophyre dyke intruding syenitic wall-rock

Plate 1.8 Lamprophyre dyke exhibiting considerable physical decomposition as a result of weathering

in question, but rather is quite variable. Alteration of the dykes themselves, particularily the lamprophyres, is usually quite extensive, resulting in significant decomposition during weathering (Plate 1.8).

The dykes themselves are commonly offset or dislocated (Plate 1.9) and intruded in en echelon fashion. Banding arranged parallel to the contacts with the host rock is sometimes evident (Plate 1.6) and has been interpreted to represent multiple episodes of intrusion forming a composite or multiple dyke (Platt, personal communication) or an effect of flow differentiation (Kent, 1980). The latter mechanism has also been associated with the development of elongation and preferred orientation as well as concentration in dyke centres of some features such as ocelli (Plate 1.10, 1.11) and phenocrysts (Plate 1.12). The mechanisms of dyke emplacement will be dealt with in Chapter 7.

Field Descriptions

Each of the dyke types has been examined in detail in terms of field petrology:

a) Ocellar lamprophyres: These are dark grey-green to

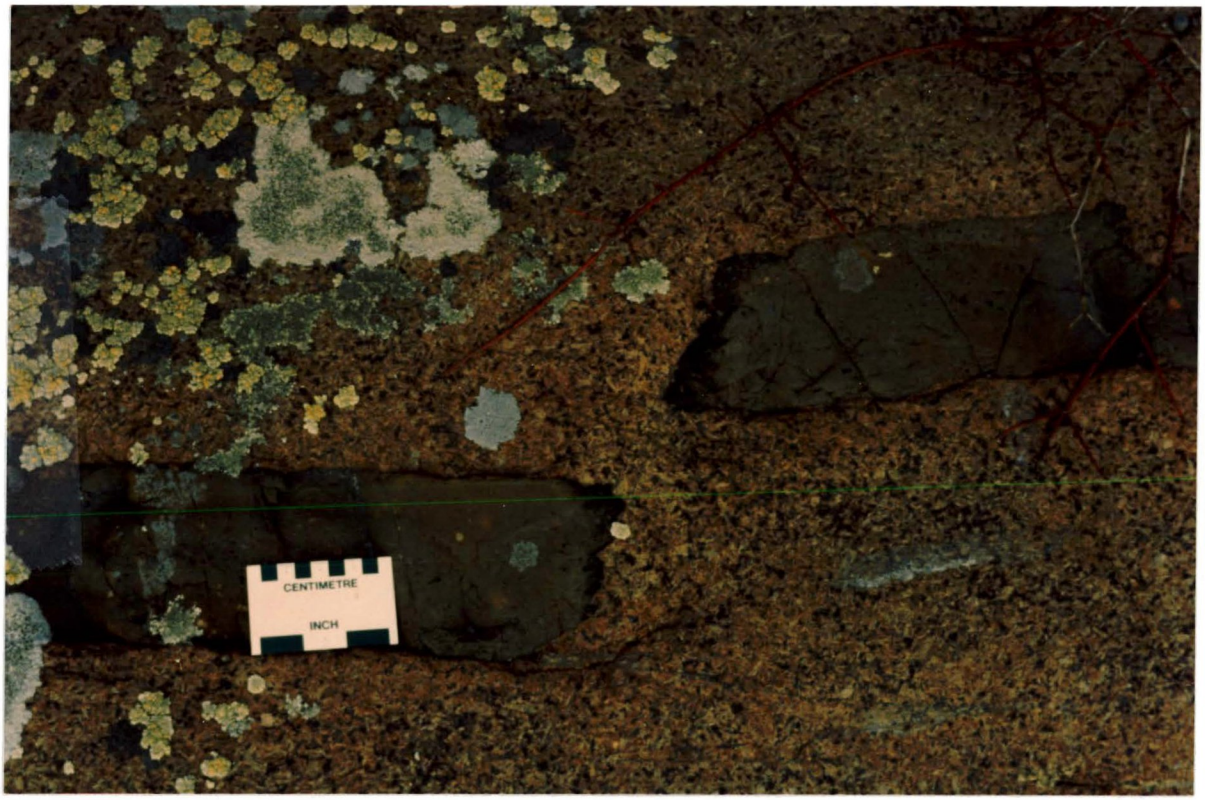

Plate 1.9 Lamprophyre dyke exhibiting offset probably as a result of injection of material along a pre-existing fracture not exposed in this outcrop

Plate 1.10 Lamprophyre dyke containing leucocratic ocelli which have been elongated in the direction of flow of the dyke

Plate 1.11 Lamprophyre dyke exhibiting concentration of leucocratic ocelli in the centre of the dyke as a result of flow differentiation

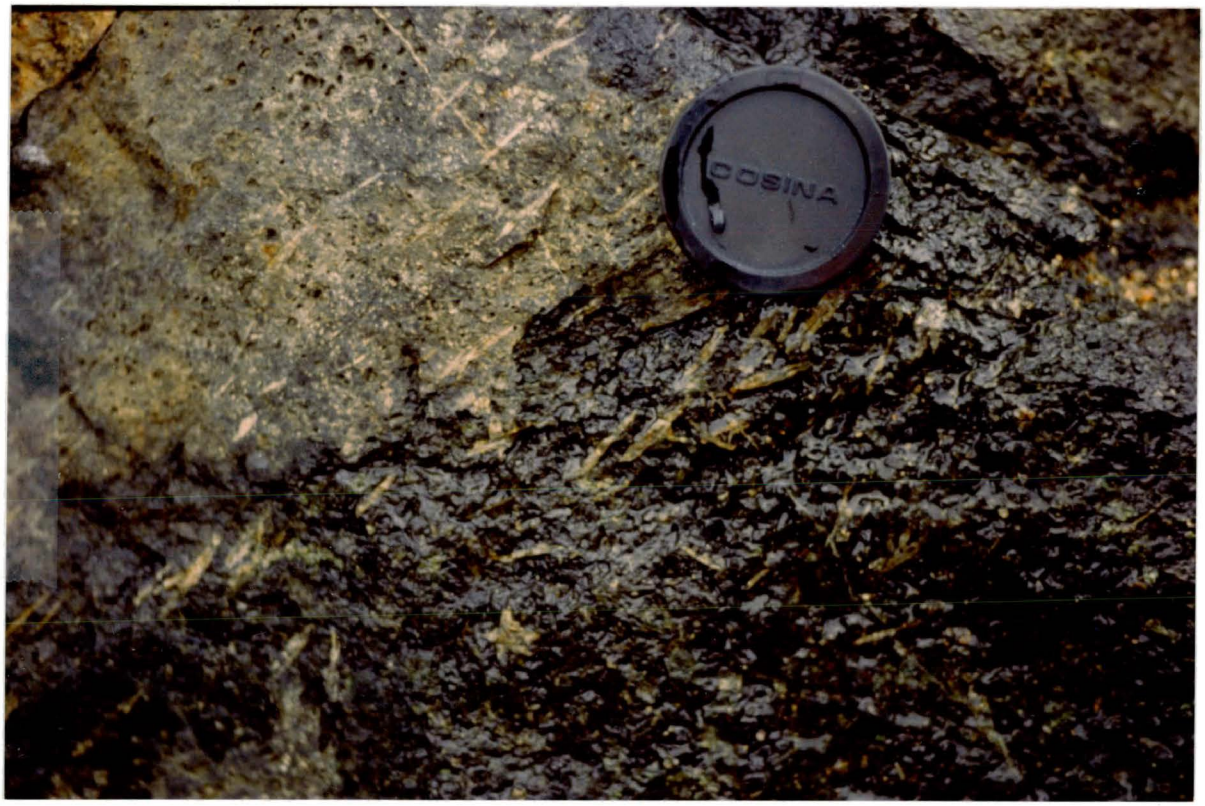

Plate 1.12 Lamprophyre dyke exhibiting concentration of clinopyroxene phenocrysts in the centre of the dyke as a result of flow differentiation; note the lack of phenocrysts in the marginal portion of the dyke in the upper left portion of the photograph

black porphyritic rocks with an aphanitic to fine grained groundmass (Plate 1.11). Typically, phenocrysts are dark green or black clinopyroxene and/or black amphibole. These rocks are characterized by the presence of globular segregations of white or pink felsic material and carbonate minerals termed ocelli. Preferential weathering of ocellar material results in many examples of this rock type developing a distinctive porous appearance on weathered surfaces. Occasionally, these rocks are massive but more frequently they display preferred alignment of elongate objects and non-uniform distribution of some features. For example, the ocelli and phenocrysts are commonly concentrated in the centre of the dykes (Plate 1.7), and ocelli are in some cases elongated parallel to the margins of the dykes in which they occur. Veinlets of carbonate are scarce to moderately abundant.

b) Analcite-bearing tinguaites: These are felsic dyke rocks, typically aphanitic to fine grained and pale to deep pink or orange-pink in colour (Plate 1.5). In some instances, pink or pale orange grains of analcite and alkali feldspar are observed. Generally, they are massive, although several display a slight increase in grain size towards the dyke centre. Veinlets and massive to colloform marginal accumulations of carbonate are common.

c) Lamprophyres with abundant clinopyroxene phenocrysts- These are grey, grey-green or dark grey porphyritic rocks with abundant large (up to 10mm) pheocrysts of dark green to black clinopyroxene (Plate 1.12). The phenocrysts range from fresh to highly altered, the latter resulting in a the formation of pits within the rocks. Concentration of phenocrysts in dyke centres is especially pronounced in some cases. Carbonate occurs as veinlets and rarely as ocelli.

d) Lamprophyres with quartz phenocrysts- These rocks are similar in appearance to the ocellar lamprophyres described above, but contain abundant rounded quartz grains from 0.5 to 5.0 mm in size, which invariably display thin (0.2mm or less) rims of dark material. Mafic phenocrysts and ocelli are considerably less abundant than in the ocellar lamprophyres, but the groundmass of both types is very similar in macroscopic appearance.

CHAPTER 2- PETROGRAPHY

PETROGRAPHY OF THE LAMPROPHYRES

Examination of a representative suite of lamprophyre dyke rocks from the Coldwell Complex in thin section indicates that the various types identified on the basis of field observations are petrographically distinct assemblages. In addition, a lamprophyre with abundant amphibole phenocrysts that was not distinguished from ocellar lamprophyre by macroscopic observation is identified. Table 2.1 summarizes the relative abundances and modes of each type. The following sections, arranged in order of dyke abundance, detail the petrography of the various types.

Ocellar Lamprophyre

Ocellar lamprophyre (see Plate 2.1) is massive, porphyritic, melanocratic rock containing abundant phenocrysts of clinopyroxene (1.0mm to 5.0mm) and to a lesser extent brown amphibole (1.0mm to 3.0mm). Clinopyroxene phenocrysts are generally euhedral and typically exhibit partial or complete concentric zoning from cores of grey to pale brown diopsidic clinopyroxene to mantles of colourless to pale green acmitic clinopyroxene. Reversed and

Table 2.1 Average Modes of Lamprophyres (Based on Averaged Point Counts of 3 Specimens of Each Type)

	1	2	3	4	5
Phenocrysts	4	21	2	7	5
Clinopyroxene	56	100	30	18	64
Hornblende	34	–	10	61	32
Kaersutite	8	–	–	21	2
Olivine	2	–	–	–	2
Quartz	–	–	60	–	–
Groundmass	46	41	61	46	68
Plagioclase	74	19	74	79	–
Alkali Feldspar	–	63	–	1	–
Clinopyroxene	7	10	6	4	2
Amphibole	6	–	5	8	7
Biotite	6	2	9	2	7
Nepheline	1	–	–	1	–
Apatite	1	1	<1	1	–
Calcite	3	4	1	1	5
Magnetite	2	1	3	3	–
Titanomagnetite	<1	<1	1	<1	2
Ilmenite	<1	–	1	<1	–
Sulphide Phases	<1	<1	<1	<1	–
Microlitic Phases	<1	<1	<1	<1	<1
Isotropic Material	–	–	–	–	77
Ocellar Phases	7	2	4	3	1
Calcite	72	67	71	68	60
Zeolites	4	6	13	14	14
Chlorite	6	2	9	2	7
Epidote	8	12	–	9	10
Scapolite	8	9	7	5	9
Cancrinite	1	2	–	–	–
Microlitic Phases	<1	<1	<1	<1	<1
Fluorite	1	2	–	–	–
Secondary Phases	43	35	35	44	23
Chlorite	44	57	55	51	13
Uralite	7	13	2	5	1
Iddingsite	3	–	–	–	1
Serpentine	11	19	2	2	<1
Cryptocrystalline Phases	35	11	41	42	84
Epidote*					
Clay Minerals*					
Sericite*					
Xenocrystic Phases	–	1	1	–	–

* Due to alteration of groundmass feldspars; no accurate determination of modal abundance possible (see text)

1- Ocellar Lamprophyre
2- Lamprophyre With Abundant Cpx Phenocrysts
3- Lamprophyre With Quartz Phenocrysts
4- Lamprophyre With Abundant Amphibole Phenocrysts

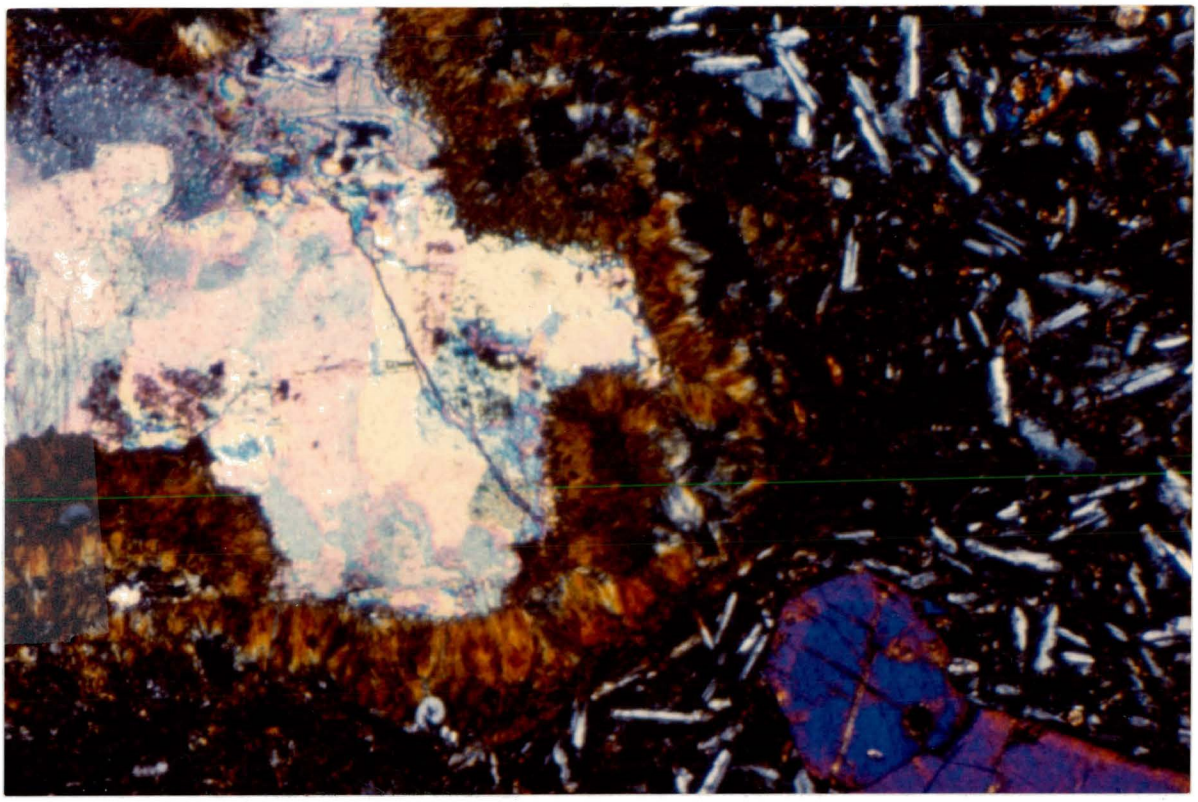

Plate 2.1 Ocellar lamprophyre; note the carbonate-filled ocellus in the left portion of the photograph, the clinopyroxeene phenocryst in the bottom right and the abundant subhedral plagioclase in the groundmass. (field-of-view (fov) 9.5mm; cross polarized light (xpl)).

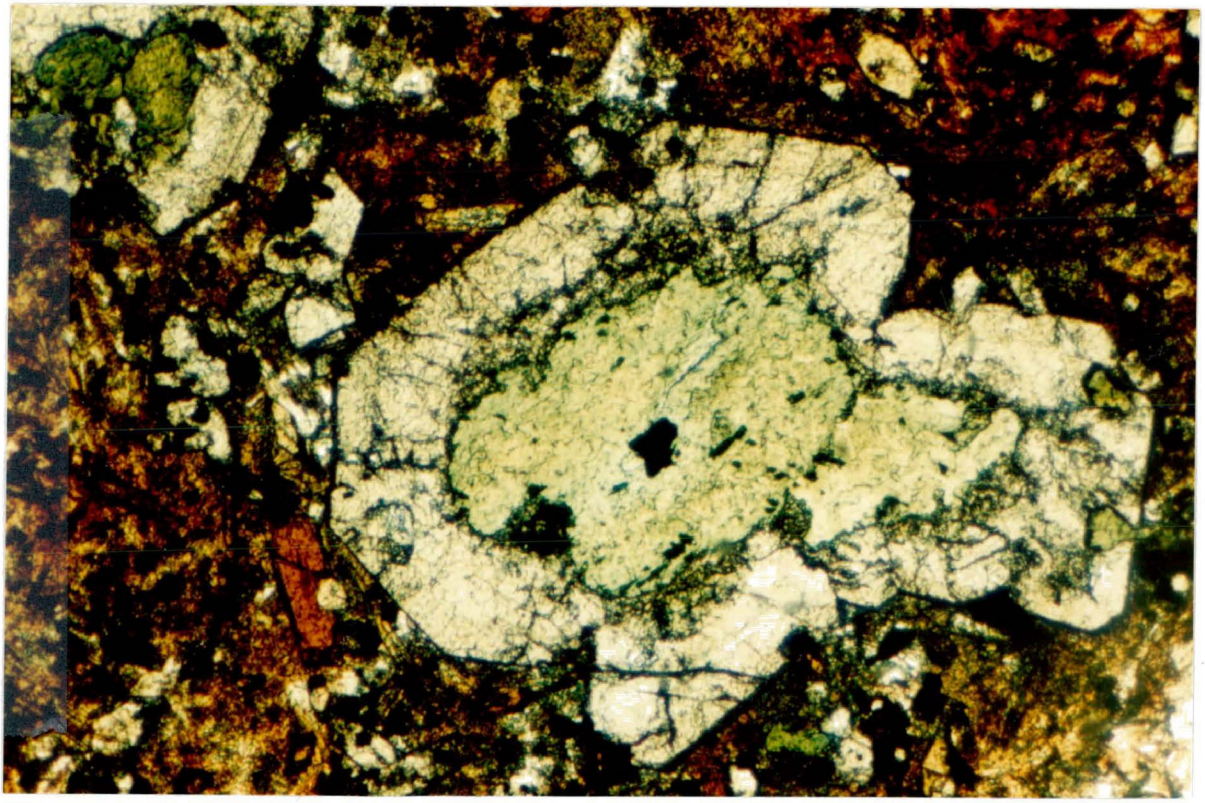

Plate 2.2 Reverse-zoned clinopyroxene phenocryst in an ocellar lamprophyre; note the embayed acmitic core in sharp contact with the diopsidic rim. Note also the biotite, brown amphibole and acmitic clinopyroxene in the groundmass (fov 9.5mm; plane polarized light (ppl)).

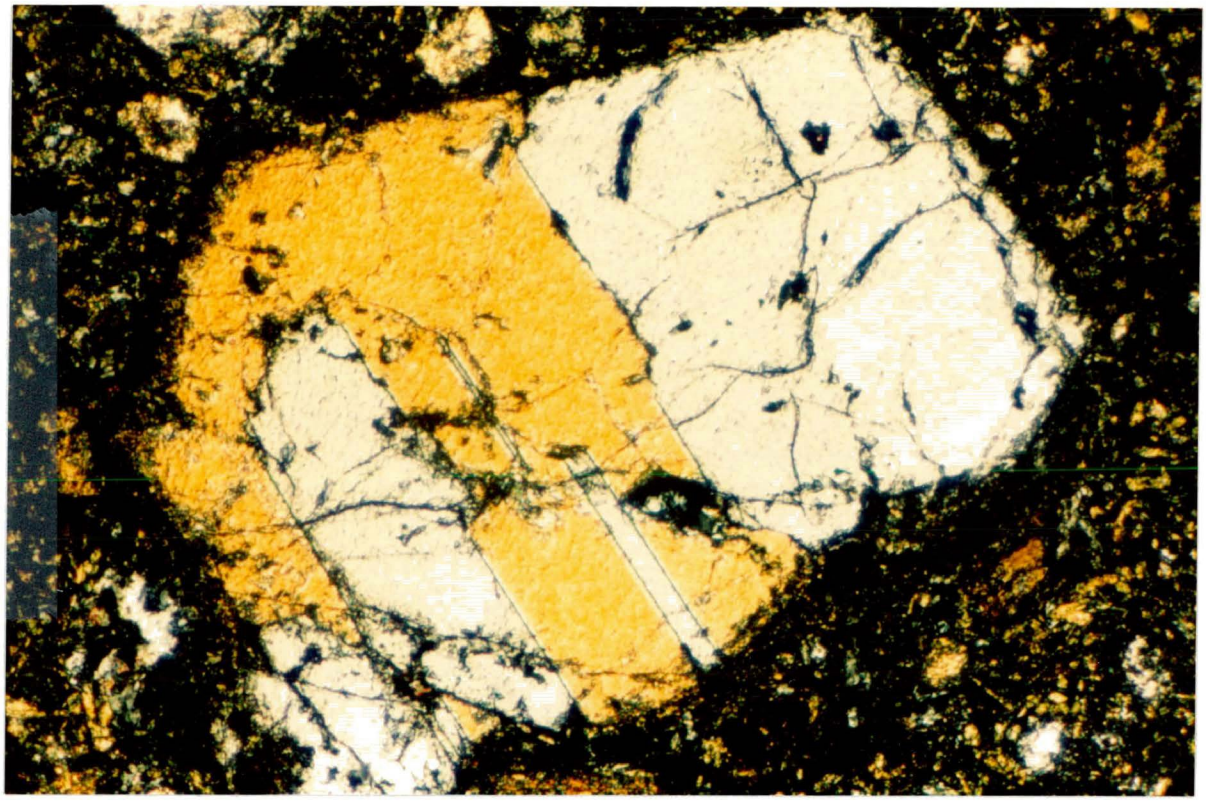

Plate 2.3 Clinopyroxene phenocryst exhibiting twinning along (100). Note development of secondary blue-green uralite along crystal margin and cleavage traces and fractures within crystal. Note also abundant brown biotite and dark green chlorite in groundmass (fov 9.5mm; xpl).

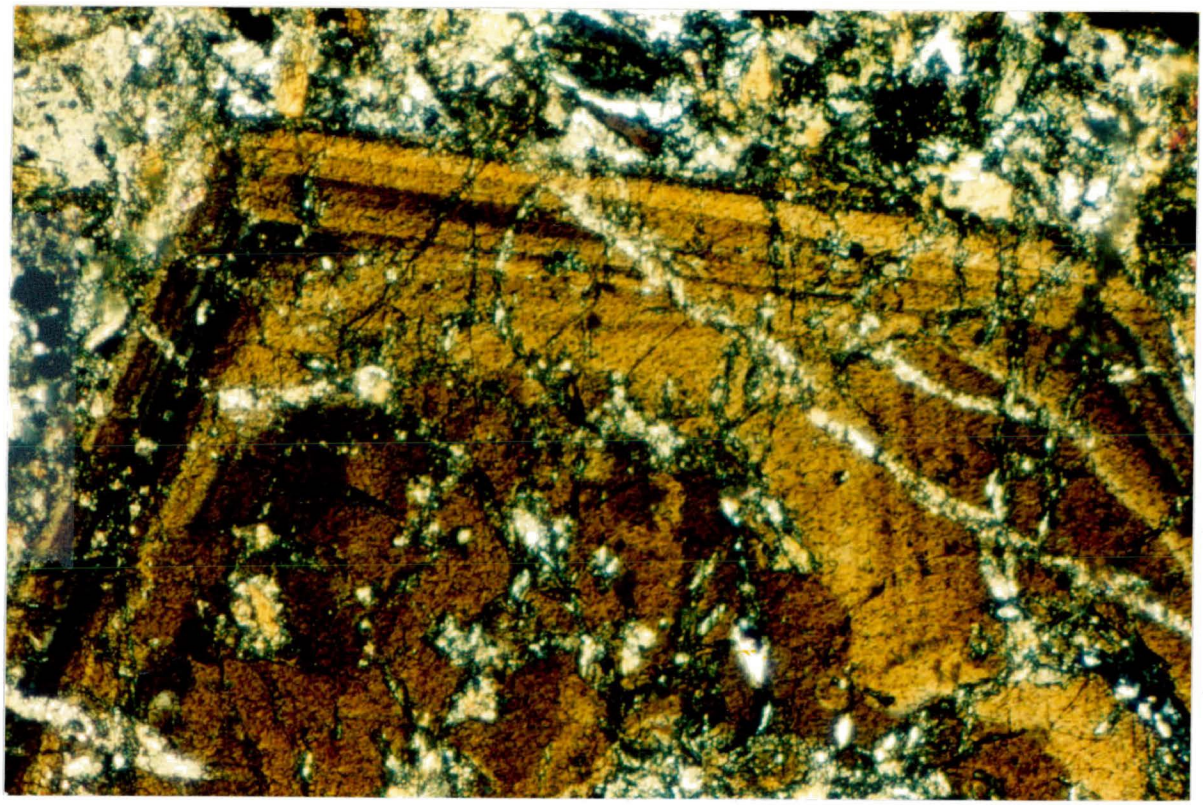

Plate 2.4 Zoned brown amphibole phenocryst in ocellar lamprophyre; note embayed core and rhythmic repetition of zoning in rim. Note also extensive alteration of amphibole to chlorite and uralite. (fov 9.5mm; ppl).

oscillatory forms of this zoning are observed in some instances, and contacts between adjacent zones are sharp (Plate 2.2). An hourglass sector zoning is sometimes superimposed upon the concentric zoning; adjacent sectors exhibit different birefringence and absorption colours of contrasting hue. In some cases, a narrow (0.05mm) rim of darker brown clinopyroxene surrounds the mantle zone; this rim zone commonly incorporates inclusions of very fine grained (less than 0.01mm) opaque grains. Twinning along (100) is common (Plate 2.3). Brown amphibole phenocrysts include strongly pleochroic yellow-brown hornblende and, to a lesser extent weakly pleochroic deep red-brown kaersutite. The hornblende is typically subhedral to euhedral and is commonly concentrically zoned from dark brown cores to pale yellow-brown rims, with rhythmic repetition of this pattern being common (Plate 2.4). Slight minor concentric variations in colour are sometimes noted within these zones. Kaersutite displays similar zoning in various shades of red-brown. In both cases, reversed zoning is occasionally observed. Twinning parallel to (100) is common. Many amphibole phenocrysts exhibit inclusions of finely disseminated opaque grains and clinopyroxene crystals. One dyke, C577, contains remnants of several extensively altered phenocrysts of olivine, 1.0mm to 5.0mm in size. These are surrounded by an unresolvable corona, which may include dark brown

clinopyroxene, and which may represent an effect of resorption or sub-solidus re-equilibriation. This will be discussed further in Chapter 4. The relict olivine contains numerous small (less than 0.05mm) inclusions of spinel.

The groundmass (Plates 2.1 to 2.4) is a fine grained assemblage of which up to 50% is comprised of cryptocrystalline aggregates of dark-coloured finely granular material. Of the remainder, the following phases have been identified as major primary constituents: plagioclase, nepheline, biotite, clinopyroxene of similar appearance to the phenocryst rims, brown amphibole and calcite, apatite and transluscent red-brown haematite. Various opaque phases including magnetite and titanomagnetite, ilmenite and rarely pyrite and chalcopyrite have also been observed as minor primary groundmass phases. Grain size averages 0.2 mm or less for groundmass minerals; apatite, which occurs as microlitic needles, rarely exceeds 0.05 mm. A more detailed description of the groundmass mineralogy is not possible due to the small grain size.

Pervasive alteration of the mafic phases results in the formation of a variety of secondary phases. In the case of clinopyroxene these include chlorite, uralite (used in the

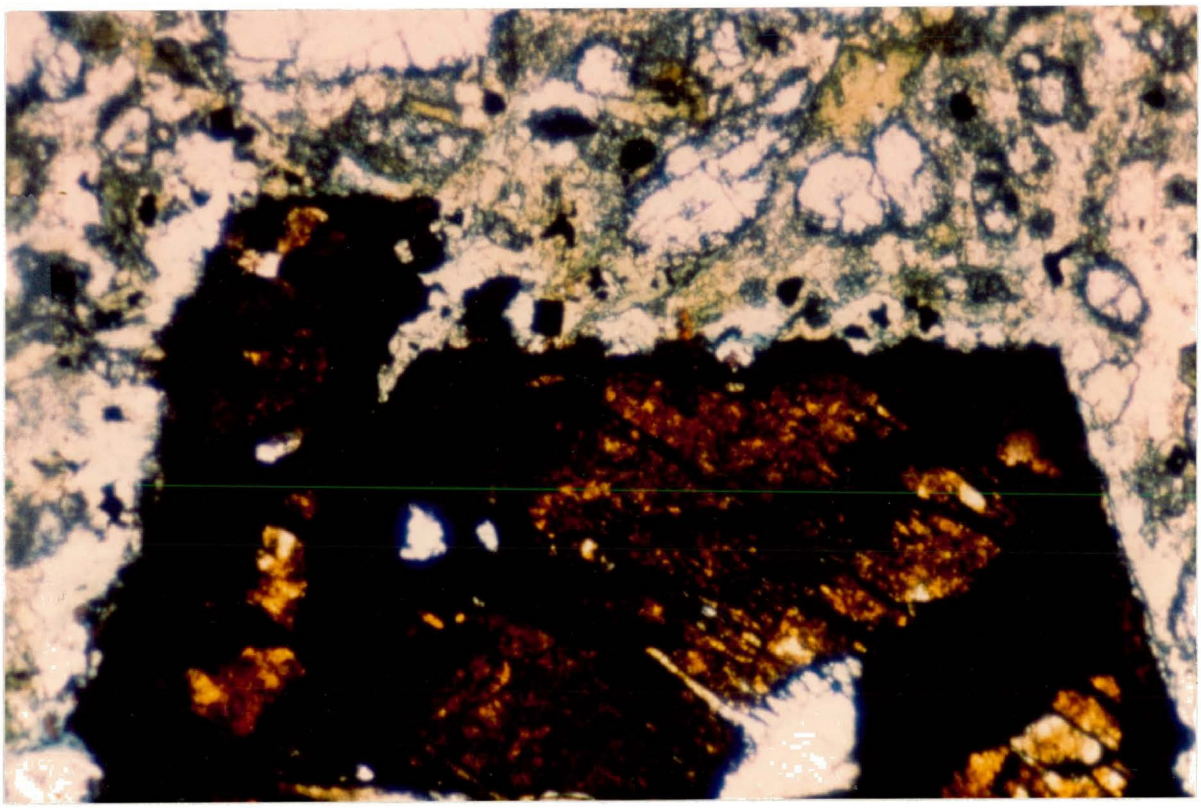

Plate 2.5 Clinopyroxene phenocryst in ocellar lamprophyre virtually completely altered to red-brown iddingsite and opaque phases (fov 9.5mm; ppl).

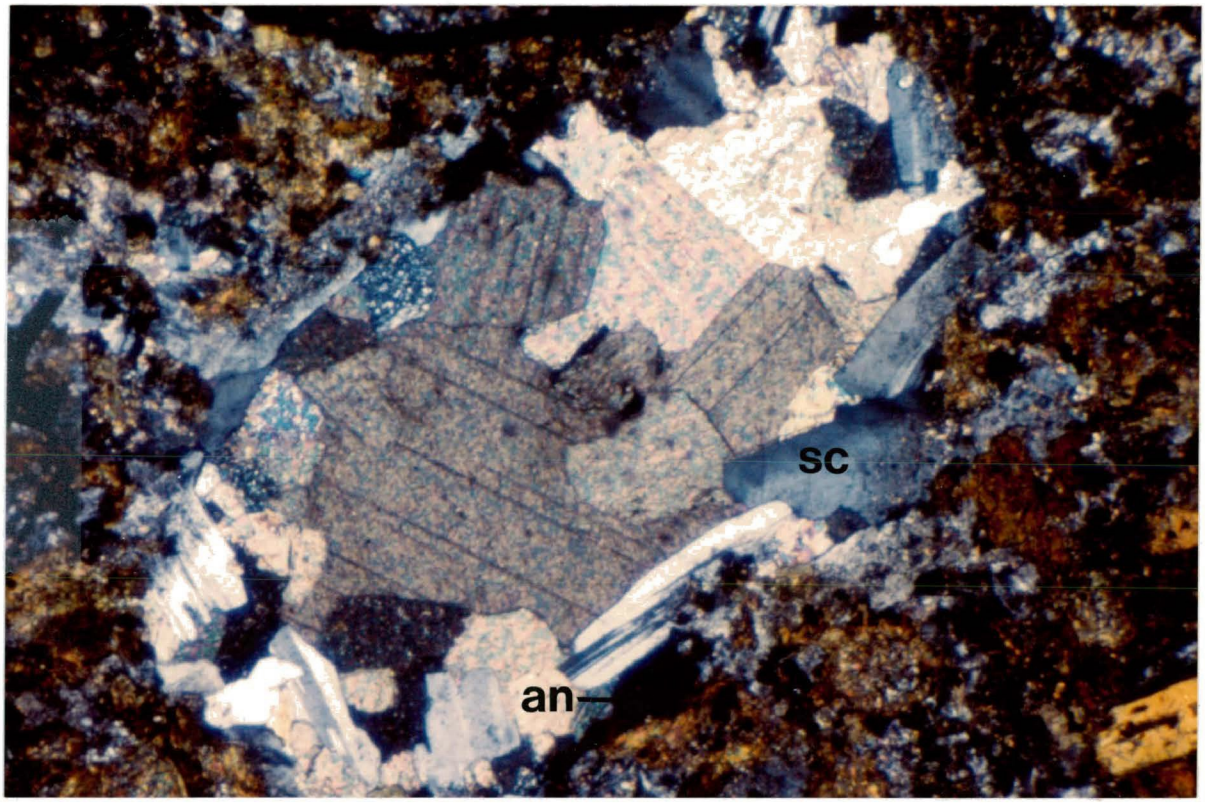

Plate 2.6 Ocellus in ocellar lamprophyre filled by carbonate minerals and scapolite (sc) and minor analcite (an). Note rounded shape and generally sharp contacts with groundmass

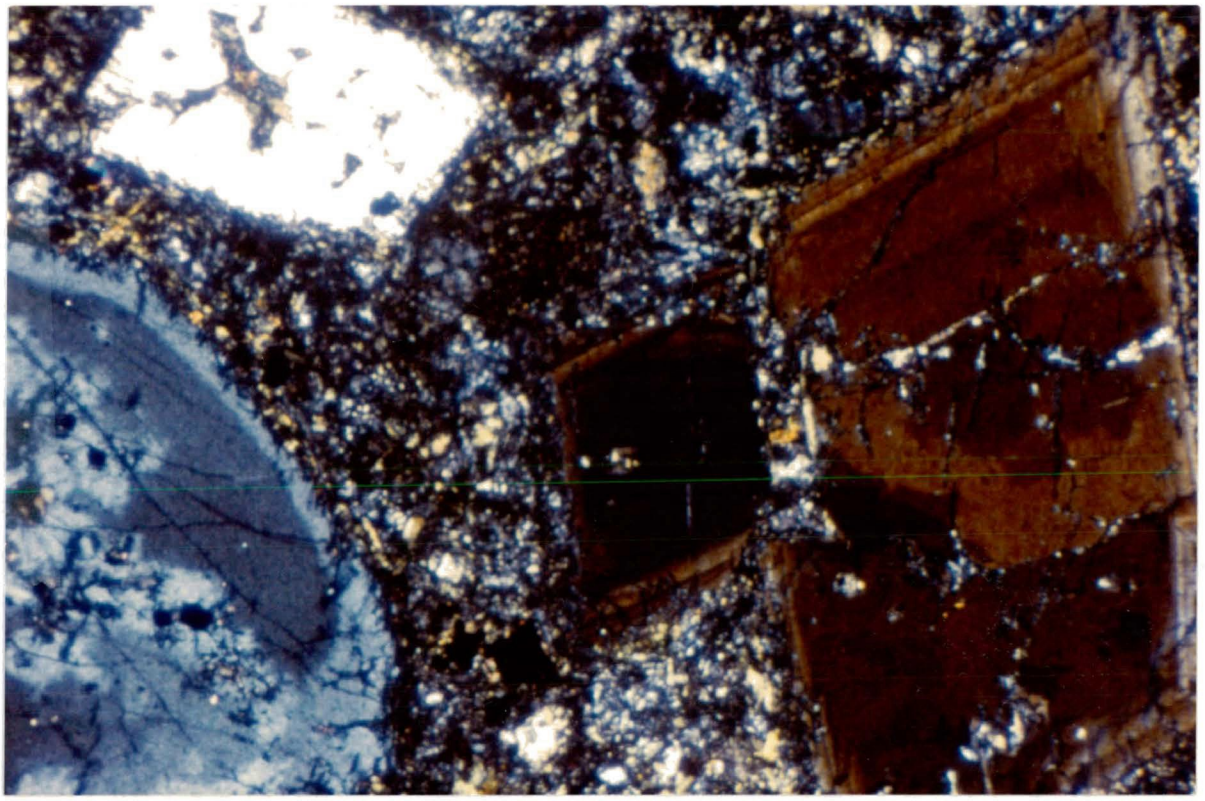

Plate 2.7 Lamprophyre with abundant clinopyroxene phenocrysts; note zoned euhedral clinopyroxene crystals and abundant feldspar (plagioclase and alkali feldspar) in groundmass (fov 9.5mm; xpl).

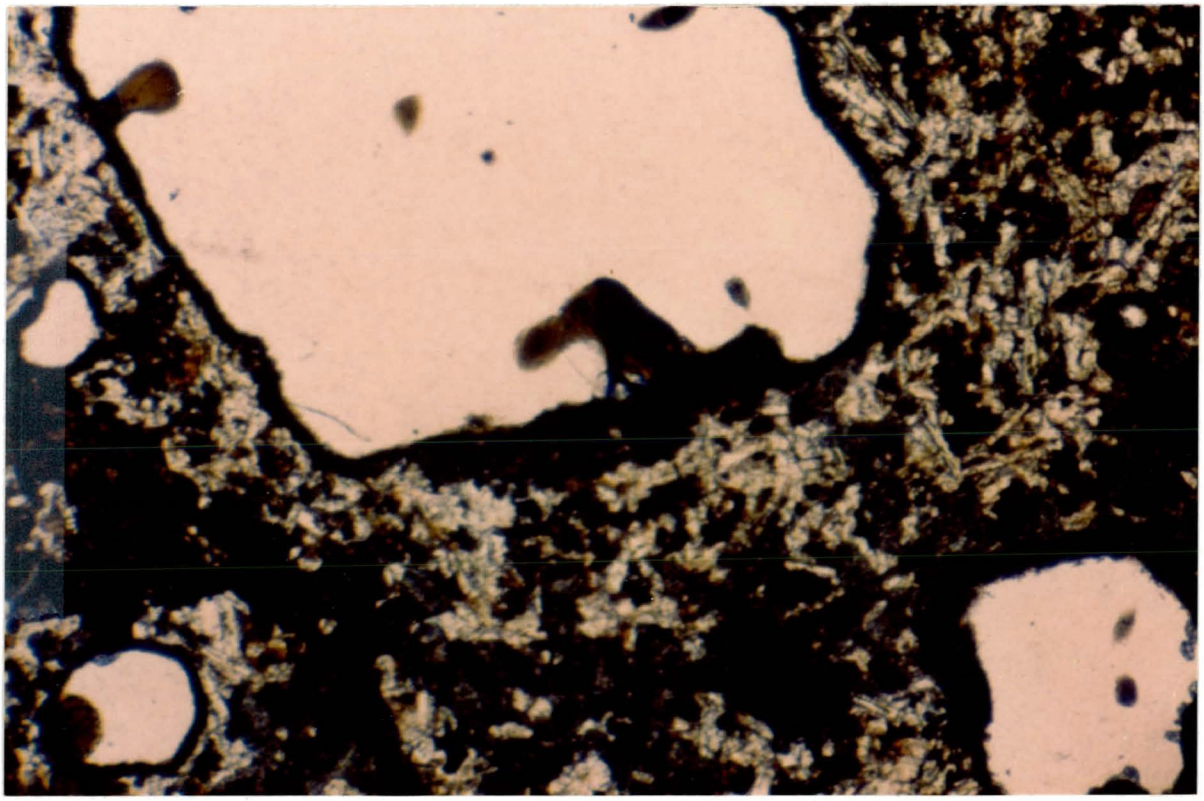

Plate 2.8 Lamprophyre with quartz phenocrysts; note rimming and embayment of quartz phenocrysts by melanocratic material (fov 9.5mm; ppl).

manner of Deer et al, 1966, to describe a secondary grey-green amphibole of indeterminate composition), rare iddingsite (Plate 2.5) and cryptocrystalline aggregates (probably serpentine, magnetite and carbonate). Amphibole alters to uralite and chlorite, while olivine is replaced by serpentine, magnetite and carbonate. The extent of this alteration ranges from incipient alteration along rims, fractures and cleavage traces of large grains to formation of complete pseudomorphs, and replacement of groundmass minerals. Plagioclase displays varying degrees of decomposition producing epidote, zeolites, sericite and clay minerals. Nepheline is commonly altered to cancrinite.

Ocelli (Plate 2.6) are globular to irregular segregations of calcite, zeolites including analcite and stilbite, chlorite, epidote, scapolite, cancrinite and, in rare instances, fluorite. These are common in this type of lamprophyre and range in size from 0.5mm to 30.0mm, with an average size of 5.0mm. The interface between the ocelli and the groundmass is generally sharp, with a tangential arrangement of elongate matrix crystals adjacent to the ocellus being common. In some cases, phenocrysts impinge upon the ocelli, compressing or even penetrating the ocellus-matrix interface. Ocelli occur singly or in clusters, with the latter arrangement commonly showing

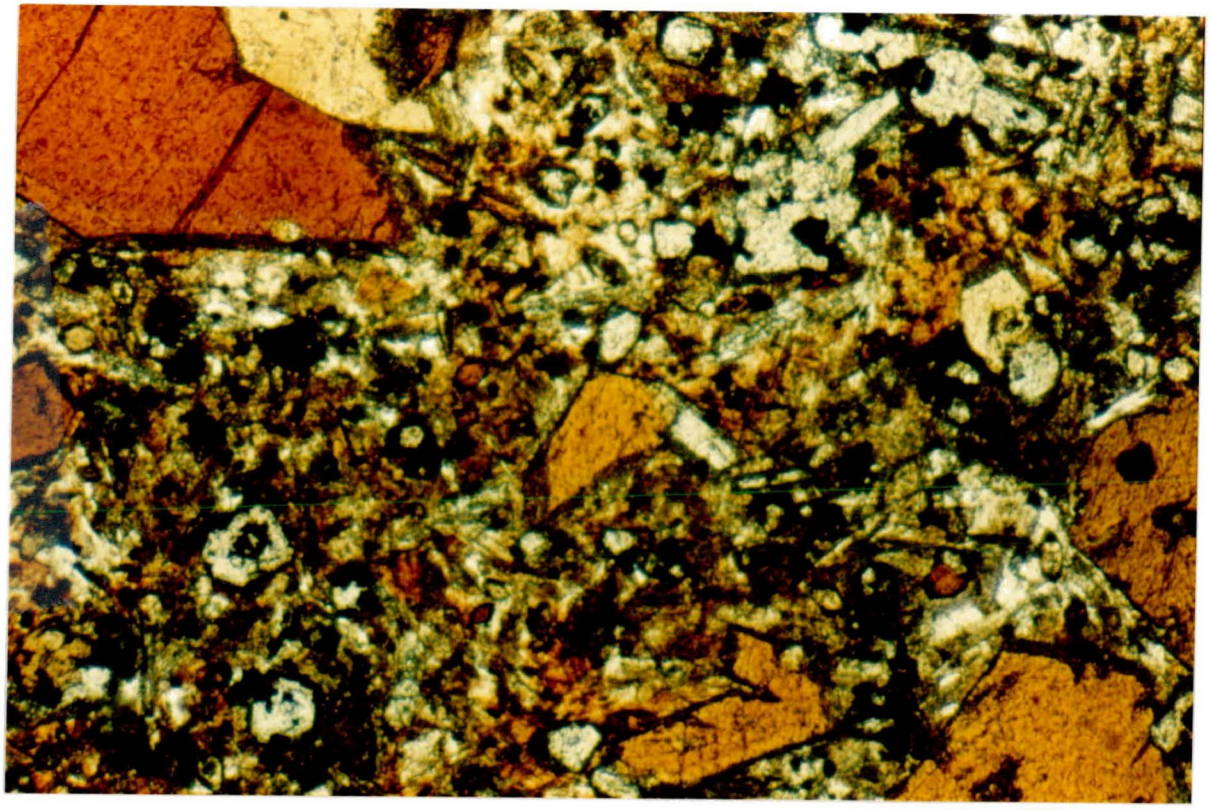

Plate 2.9 Lamprophyre with abundant amphibole phenocrysts (fov 9.5mm; ppl).

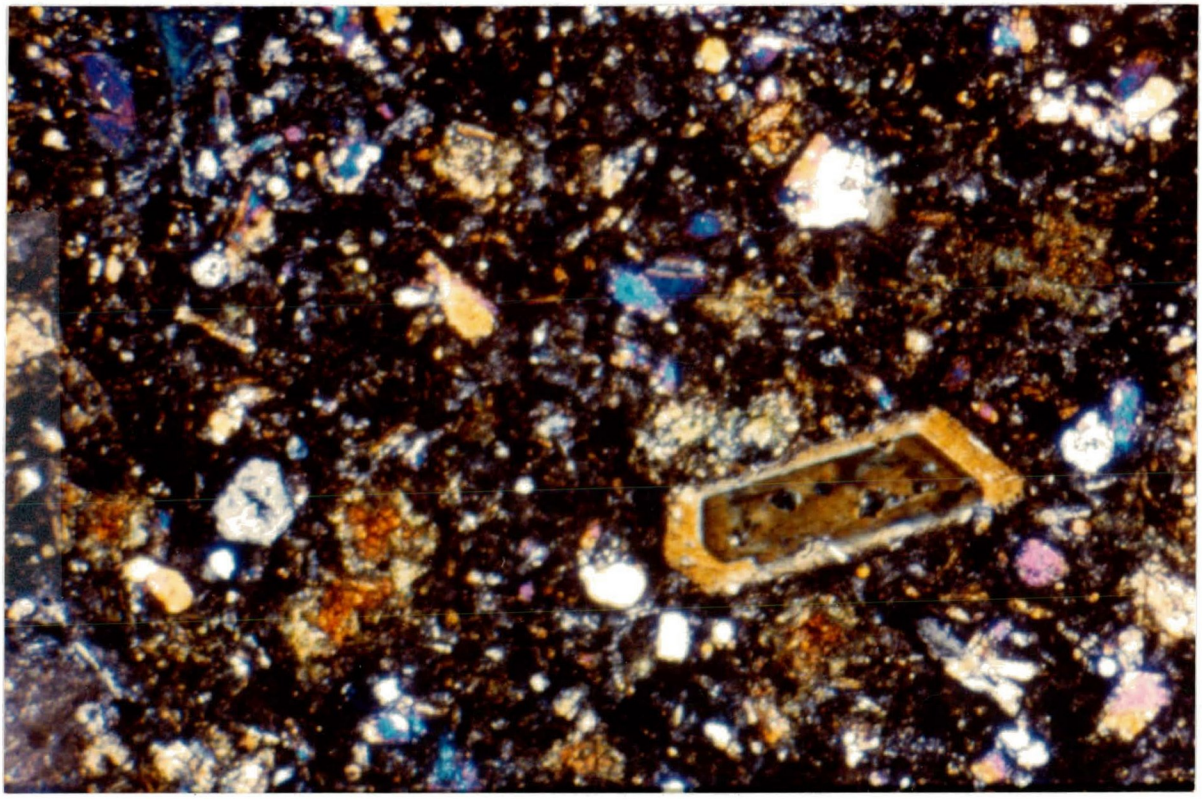

Plate 2.10 Lamprophyre with an isotropic base; abundant extinct material throughout the groundmass is the isotropic material. Note zoned clinopyroxene phenocryst in the lower right portion of the photomicrograph (fov 9.5mm; ppl).

overlapping or coalescence of individual ocelli to form complex lobate patterns. The ocelli will be discussed in more detail in Chapter 6.

Commonly, veinlets of calcite, haematite, zeolites including analcite and prehnite, and chlorite are observed to traverse the rock.

Lamprophyres with Abundant Clinopyroxene Phenocrysts

This type of lamprophyre is a porphyritic, melanocratic rock containing abundant large (5.0-15.0mm) euhedral clinopyroxene crystals as the only phenocryst phase (see Plate 2.7). These invariably exhibit a distinct concentric zonation from colourless to pale brown cores to pale green-brown rims. Narrow green rims similar to those observed surrounding clinopyroxene phenocrysts in the ocellar lamprophyres appear to be of the same composition as the groundmass clinopyroxene. This rim, where it occurs, displays a gradational contact with the adjacent mantle zone and contains abundant inclusions of very fine (0.05mm) dark coloured grains. Contacts between adjacent core and mantle zones are sharp, and the width of individual zones is variable, but mantle zones tend to be thinner than the corresponding cores. The pattern of zonation will only very

rarely repeat more than once, although rim zones sometimes display a complex series of concentric sub-zones distinguished by changes in birefringence. Hourglass sector zoning sometimes occurs within cores but does not overlap the concentric zonation; it is characterized by differing shades of brown absorption colour between adjacent zones. Twinning along (100) is common. Cores are commonly rounded and embayed by mantle material; this embayment cuts off the pattern of concentric zoning, suggesting the occurrence of resorption. Several large (1.0mm to 2.0mm), corroded laths of plagioclase are observed near and sub-parallel to the dyke margins; these appear to represent partially resorbed xenocrysts of wall rock material incorporated into the dykes.

The groundmass (Plate 2.7) is a medium to fine grained assemblage whose major primary phases include plagioclase, alkali feldspar and clinopyroxene of similar appearance to the phenocryst rims. Minor primary groundmass phases include biotite, apatite, calcite, magnetite, titanomagnetite and rarely sulphides such as pyrite and chalcopyrite. It is noteworthy that the abundance of primary hydrous phases is low compared to the other varieties of lamprophyre examined, in that only relatively small (less than 3%) amounts of biotite are observed. The various phases have undergone alteration similar to that observed in the ocellar

lamprophyre; chlorite and green-brown felted or fibrous material of indeterminate composition are dominant secondary products. Phenocrysts range from the virtually pristine to those completely pseudomorphed by the replacing phases. Ocelli are similar in composition and structure to those that occur in the ocellar lamprophyres but are smaller and considerably less abundant (see Table 2.1). In one dyke, C1, these ocelli are observed to be elongated along a common axis that is sub-parallel to the dyke margins.

Lamprophyres with Quartz "Phenocrysts"

This type of lamprophyre (Plate 2.8) is most similar to the ocellar lamprophyres, in that zoned phenocrysts of clinopyroxene and amphibole are set in a groundmass of plagioclase, biotite, brown amphibole, clinopyroxene, apatite, calcite, magnetite and titanomagnetite and rare pyrite. However, the abundance of phenocrysts is much lower than in the case of the ocellular lamprophyres (see Table 2.1), while quartz grains, ranging from euhedral (i.e. hexagonal) to rounded, and of variable size (0.1-10 mm) are abundant (see Plate 2.8). Without exception, the quartz grains are mantled by narrow (approximately 0.05mm) rims of very small (0.5mm or less), radially oriented, dark coloured material (see Plate 2.8) which cannot be identified by

optical methods. These rims, which are interpreted to be clinopyroxene resulting from the resorption of the quartz by melt that is not in equilibrium with it, and the origin of the quartz are discussed in detail in the Chapter 4. A few ocelli, composed of calcite, zeolites, chlorite and scapolite are observed. Alteration and veining by secondary minerals is similar to that observed in the ocellular lamprophyres.

Lamprophyres with Abundant Amphibole Phenocrysts

These are similar to the ocellar lamprophyres, however, considerable differences exist in the relative abundances of the various phenocryst phases and in the types of groundmass minerals. They are characterized by abundant large (0.5mm to 3.0mm) phenocrysts of brown amphibole (see Plate 2.9). As in the case of the ocellar lamprophyre, two distinct types are identified. Hornblende, strongly pleochroic from pale yellow to deep yellow-brown or brown is more common than weakly pleochroic, intensly red-brown kaersutite. Clinopyroxene occurs as phenocrysts similar to those observed in the ocellar lamprophyres (0.5mm to 2.0mm), but in considerably lesser abundance than the amphiboles. All phenocryst phases are similar in composition and character to those that occur in the ocellar lamprophyres.

In addition to the ubiquitous cryptocrystalline finely granular or felted material, the major primary groundmass phases include plagioclase, sodic clinopyroxene (both 0.1mm), kaersutite (0.05mm to 0.5mm) and biotite, (0.1mm to 0.3mm). Minor primary groundmass phases include apatite, calcite, and opaque phases such as titanmagnetite, minor ilmenite, chalcopyrite and minor pyrite (all 0.05mm to 0.1mm). Calcite also occurs in ocelli (0.5mm to 1.0mm) with epidote, scapolite and zeolites similar to the ocelli observed in the other lamprophyres. Alteration patterns and secondary mineral veining is similar to that observed in the ocellar lamprophyres.

Lamprophyres with an Isotropic Base

Dyke rocks of this type are distinguished by the presence of a primary, grey or brown, near to fully isotropic material comprising most of the groundmass (see Plate 2.10). The composition of this material is the subject of debate but is usually postulated to be glass (e.g. Rock, 1977; Troger, 1939) or analcime (e.g. Pirsson, 1900). This will be discussed further in Chapter 4. Alteration of this isotropic material results in the formation of apparently randomly distributed patches and streaks of colourless felted, fibrous or granular material of indeterminate composition. The

remainder of the primary groundmass mineralogy consists of kaersutite, brown amphibole, biotite, calcite and minor phases including apatite, microlitic phases, titanomagnetite and minor pyrite (all 0.5mm or less). Calcite also occurs with zeolites and chlorite in veinlets, and sometimes with epidote, chlorite, analcite and scapolite in ocelli similar in structure to those observed in the ocellar lamprophyres, although these are smaller (0.5mm) and less common than in the other lampophyre types (Table 2.1).

Phenocryst phases are similar to those that occur in the ocellar lamprophyres, although they tend to be smaller (0.5mm to 1.0mm) and less abundant (Table 2.1). Concentric zoning patterns are not repeated in any given phenocryst. Alteration types are also similar to those of the ocellular lamprophyre, however, the extent of alteration is generally less advanced in lamprophyres with an isotropic base.

PETROGRAPHY OF THE TINGUAITES

Average modal abundances of the various phases occurring in the tinguaites are given in Table 2.2.

Analcite Tinguaites

Tinguaites are leucocratic rocks containing abundant phenocrysts of alkali feldspar and nepheline (see Plate 2.11). Riebeckite is a minor phenocrystal phase (Plate 2.12), and analcite is observed to be common in some tinguaites (Plate 2.11). Alkali feldspar occurs as large (0.5-1.5mm), anhedral, Carlsbad-twinned crystals. The range of 2V values for 15 alkali feldspar phenocrysts is 45° to 65°, with an average value of 53°, which strongly suggests that these are anorthoclase or possibly orthoclase (Kerr, 1977). No perthitic exsolution is observed. Nepheline forms subhedral to anhedral crystals of similar size to alkali feldspar, but the latter is more common (Table 2.2). Riebeckite, pleochroic from indigo blue to deep yellow, is a relatively rare phase (Table 2.2) that is present as large (1.0-3.0mm) elongated subhedral laths arranged sub-parallel to dyke margins. These do not display twinning or zoning.

The fine-grained groundmass consists of alkali feldspar,

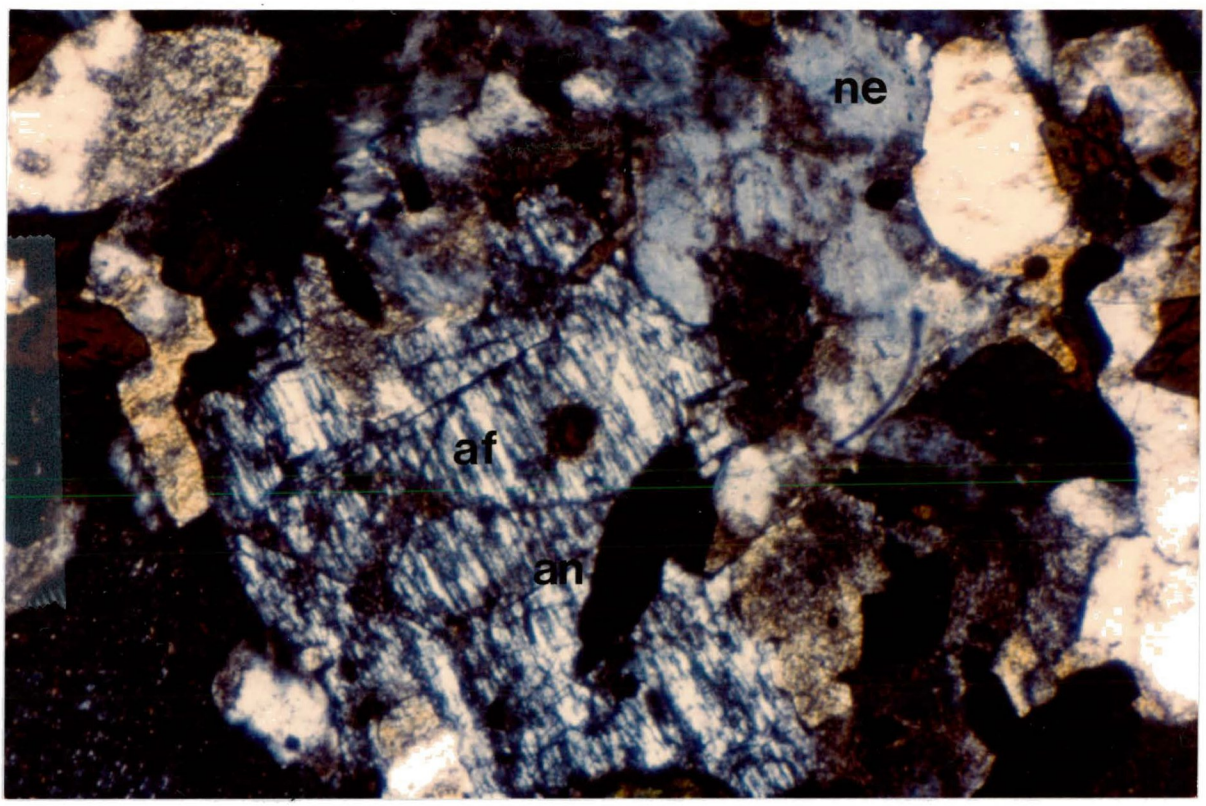

Plate 2.11 Tinguaite containing alkali feldspar (af), nepheline (ne) and analcite (an). Note pink haematite staining on phases on right side of photomicrograph (fov 9.5mm; xpl).

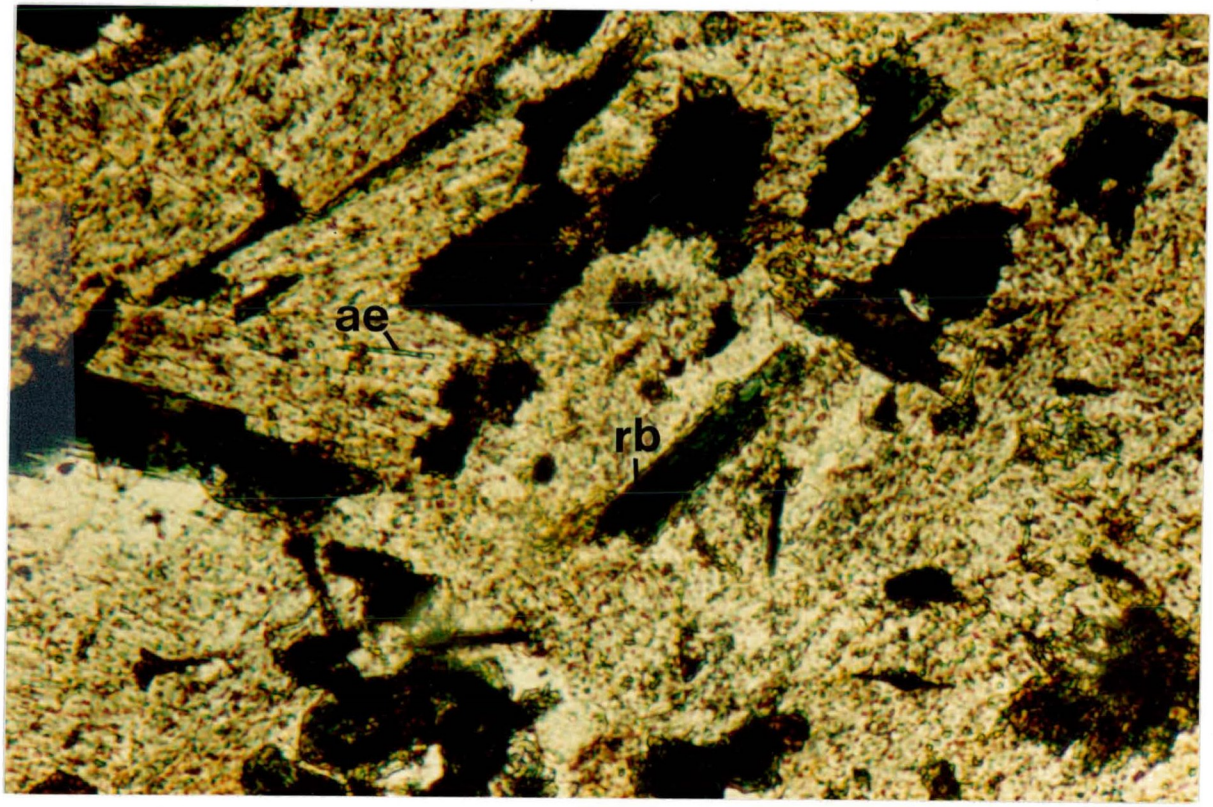

Plate 2.12 Tinguaite showing riebeckite phenocrysts (rb) and aegerine as a groundmass phase (ae). Note pale pervasive pale pink-brown colouration of felsic phases as a result of haematite staining (fov 9.5mm; ppl).

Table 2.2 Average Modes of Tinguaites (Determined by Averaged Point Counts of 3 Specimens)

Phenocrysts	62
Alkali Feldspar	63
Nepheline	22
Riebeckite	4
Analcite	11
Groundmass	29
Alkali Feldspar	30
Aegerine	47
Nepheline	14
Calcite*	11
Apatite	1
Zircon*	3
Aenigmatite	2
Magnetite	1
Microlitic Phases	1
Secondary Phases*	8
Zeolites	54
Sericite	19
Clay Minerals	11
Cancrinite	7
Cryptocrystalline Phases	5
Haematite	4
Xenocrystic Phases	1

* Considerable variation exists in the modal abundance of these phases

acicular aegerine, nepheline and calcite (all 0.1mm to 0.2mm) as major phases. Calcite associated with stilbite forms veinlets traversing the rock. More commonly, it occurs as coarsely crystalline accumulations along dyke margins. Zircon, apatite, aenigmatite (all less than 0.05mm) and minor magnetite (0.1mm) are minor phases, however, the zircon content is considerably higher in several dykes (e.g. C210 and C478; see Table 2.2). Phenocrysts typically form an intimately interlocking matrix with the groundmass phases filling the interstices. All phases commonly display pervasive staining by iron oxide, and the occurence of translucent reddish-brown haematite, interstitial to the other phases, is common.

Alteration of all phases is of varying intensity but is generally less advanced than that observed in the lamprophyres. Alkali feldspar decomposes along grain margins to form zeolites, sericite and clay minerals, while nepheline alters in a similar manner to zeolites and cancrinite. Analcite is replaced by other zeolites, which include natrolite and stilbite, and calcite. Riebeckite alters to an ill-defined, gray-brown fibrous material along grain margins and cleavage traces.

CHAPTER 3- CHEMICAL CLASSIFICATION OF THE COLDWELL DYKE ROCKS

WHOLE ROCK MAJOR ELEMENT CHEMISTRY

A representative suite of the various types of Coldwell dyke rocks were analysed to determine the abundance of SiO_2, Al_2O_3, FeO, Fe_2O_3, MgO, CaO, K_2O, Na_2O, MnO, P_2O_5 and TiO_2. Analytical methods are detailed in Appendix A. Table 3.1 presents representative compositions of each type; a full listing of these data is given in Appendix B. Table 3.2 lists descriptive statistics for the compositions of each type of dyke. Table 3.3 outlines their general petrological character.

General Discussion

All of the lamprophyres with the exception of the quartz-bearing variety are basic (SiO_2 = 45-52 wt%) or ultrabasic (SiO_2 < 45 wt%). The quartz lamprophyres and the tinguaites are intermediate (SiO_2 in the range 52 to 66 wt%). The lamprophyres are primarily metaluminous [$(CaO + Na_2O + K_2O) > Al_2O_3 > (Na_2O + K_2O)$]; a few are peraluminous [$Al_2O_3 > (CaO + Na_2O + K_2O)$]. These latter tend to display a modal abundance of biotite and clinopyroxene in excess of that determined for the corresponding average dyke of that type

	1	2	3	4	5	6	7	8	9	10	11	12	13
mple No.	C266	C135	C128	C454	C430	C461	C553	C555	C560	C566	C161	C478	Alk Bas
ide Wt%													
i02	44.90	41.05	44.50	45.81	52.20	56.05	44.61	47.26	44.80	41.60	61.28	60.83	46.53
l203	14.63	13.86	12.96	10.73	14.86	13.62	14.55	15.53	14.22	12.84	16.76	18.05	14.31
e203	3.76	3.06	3.05	4.48	4.05	2.59	3.44	4.73	3.68	4.62	2.14	4.99	3.16
e0	6.74	8.57	7.82	4.64	4.08	4.35	6.74	4.98	6.59	4.56	0.52	0.96	9.81
g0	6.45	6.40	9.30	10.30	5.66	6.25	6.50	5.14	7.25	6.34	0.14	0.17	9.54
a0	9.23	13.85	12.69	15.10	8.45	4.95	11.28	9.15	10.98	13.93	4.15	2.00	10.32
a20	3.77	2.77	3.21	2.05	2.86	3.76	3.78	5.49	3.72	3.28	6.17	5.16	2.85
20	1.92	2.68	1.64	0.16	2.04	2.46	2.34	2.27	2.41	2.73	6.27	5.45	0.84
n0	0.23	0.27	0.30	0.23	0.14	0.18	0.22	0.22	0.20	0.18	0.06	0.12	0.18
i02	1.51	1.13	1.08	0.95	1.24	1.01	1.59	1.17	1.42	1.31	0.37	0.05	2.28
205	1.60	1.82	1.04	0.73	0.65	0.62	1.04	0.97	1.18	0.89	0.10	0.07	0.28
12	1.81	2.25	0.24	1.81	0.77	0.96	0.71	0.51	0.62	2.90	1.76	1.03	0.09
30	3.08	2.01	1.91	2.34	2.61	3.27	3.21	3.08	2.78	3.69	0.54	0.99	0.05
tal	99.63	99.72	99.74	99.33	99.61	100.07	100.00	100.50	99.85	98.87	100.26	99.87	100.24
orm													
	-	-	-	-	6.40	7.39			-	-	-	8.43	-
r	11.34	15.83	4.69	0.95	12.05	14.53			14.24	16.13	37.04	32.20	5.28
h	30.21	4.20	6.56	17.34	24.19	31.81			12.26	7.39	50.23	43.65	20.04
s	17.48	17.49	16.13	19.61	21.70	13.04			15.00	12.26	-	3.00	23.63
e	0.91	10.42	11.16	-	-	-			10.41	11.03	0.60	-	2.20
i	6.02	21.54	31.65	31.28	9.12	1.44			23.01	26.33	0.75	-	20.89
l	-	-	-	11.96	12.14	19.39			-	-	-	0.42	-
l	14.72	12.51	13.36	1.86	-	-			10.14	4.32	-	-	18.48
i	5.45	4.44	4.42	6.50	5.87	3.76			5.34	6.70	0.80	3.34	4.53
l	2.67	2.15	2.05	1.80	2.36	1.92			2.70	2.49	0.70	0.09	4.41
p	3.50	3.98	2.27	1.60	1.42	1.35			2.58	1.94	0.22	0.15	0.67
c	4.12	5.12	0.55	4.09	1.75	2.18			1.41	6.60	4.00	2.34	-
c	-	-	-	-	-	-			-	-	0.76	-	-
n	-	-	-	-	-	-			-	-	3.30	-	-
e	-	-	-	-	-	-			-	-	1.33	2.69	-
	-	-	-	-	-	-			-	-	-	2.57	

1 & 2 Ocellar Lamprophyre
3 & 4 Lamprophyre With Abundant Cpx Phenocrysts
5 & 6 Lamprophyre With Quartz Phenocrysts
7 & 8 Lamprophyre With Abundant Amphibole Phenocrysts
9 & 10 Lamprophyre With Isotropic Base
11 & 12 Tinguaite
13 Typical Alkali Basalt (Carmichael et al, 1974)

Table 3.2 Descriptive Statistics for Major Element Data

Dyke Type (No. Samples)	SiO2	Al2O3	Fe2O3	FeO	MgO	CaO	Na2O	K2O	MnO	TiO2	P2O5
Cpx Lamprophyres (6)											
Mean	45.11	13.32	4.63	7.13	8.97	13.47	2.57	1.74	0.37	1.40	1.15
Standard Deviation	2.25	1.85	1.39	1.47	1.61	3.07	1.15	1.11	0.18	0.53	0.34
Quartz Lamprophyres (6)											
Mean	55.75	14.51	3.70	3.93	6.07	7.79	3.01	2.90	0.27	1.26	1.14
Standard Deviation	1.50	0.55	0.70	0.77	0.39	1.36	1.12	0.53	0.13	0.19	1.14
Ocellar Lamprophyres (19)											
Mean	46.84	14.85	3.61	8.41	6.71	10.11	4.05	2.36	0.27	1.51	1.11
Standard Deviation	1.96	1.10	0.60	1.72	1.76	2.18	0.98	0.74	0.07	0.60	0.48
Isotropic-Base Lamprophyres (5)											
Mean	45.79	15.32	4.44	6.40	7.17	11.87	3.85	2.76	0.21	1.26	0.95
Standard Deviation	0.56	2.15	0.49	1.02	0.61	3.36	0.60	0.42	0.01	0.22	0.21
Amphibole Lamprophyre (5)											
Mean	45.82	15.67	4.47	7.14	5.53	10.41	4.71	2.80	0.25	1.92	1.31
Standard Deviation	4.32	1.86	1.07	1.69	1.25	2.89	0.74	0.99	0.07	0.61	0.92
Tinguaites (9)											
Mean	61.81	18.17	2.67	2.01	0.34	2.49	6.59	5.24	0.14	0.40	0.12
Standard Deviation	1.81	1.77	1.51	1.36	0.21	1.12	0.93	1.36	0.06	0.19	0.08

Table 3.3 General Observations Concerning the Major Element Chemistry

Parameter	Cpx Lamprophyre	Quartz Lamprophyre	Ocellar Lamprophyre	Isotropic-base Lamprophyre	Amphibole Lamprophyre	Tinguaite
SiO2 Content	ultrabasic-basic	intermediate	ultrabasic-basic	ultrabasic-basic	ultrabasic-basic	intermediate
SiO2 Saturation	saturated-undersaturated	oversaturated	undersaturated	undersaturated	undersaturated	undersaturated-oversaturated
Al2O3 Saturation	peraluminous-metaluminous	peraluminous-metaluminous	peraluminous-metaluminous	peraluminous-metaluminous	peraluminous-metaluminous	peraluminous

Figure 3.1 Degree of Silica Saturation As Shown By A Plot of Alkalis Versus Silica (after Cox et al, 1979)

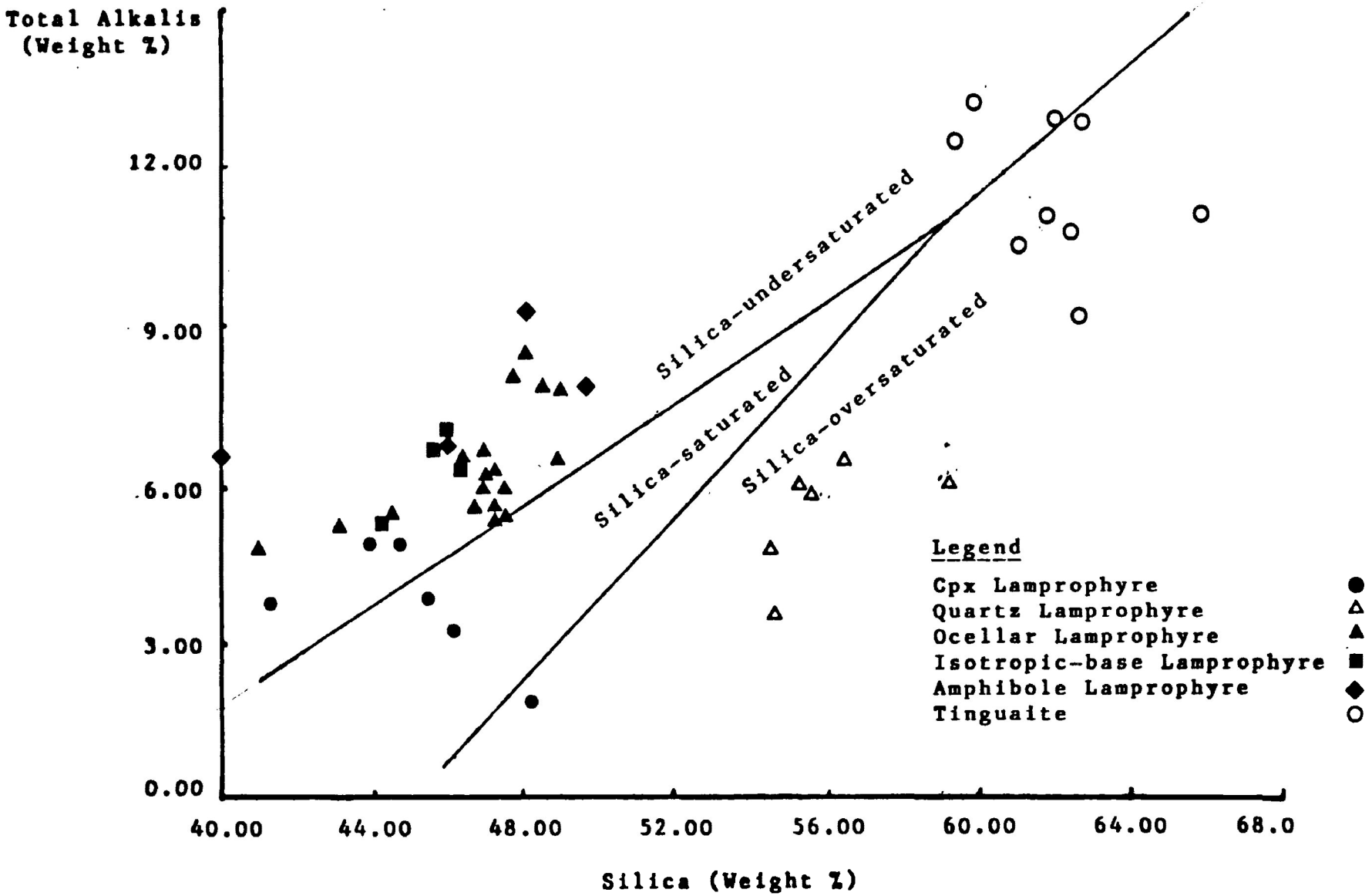

(see Table 2.1); the excess Al_2O_3 with respect to (CaO + Na_2O + K_2O) is therefore likely present in those phases (Hyndman, 1972). The tinguaites are without exception peraluminous, and may even exhibit normative corundum (e.g. sample C478 in Table 3.1).

Inspection of Figure 3.1, a plot of total alkalis versus silica after Cox et al (1979), shows that of the lamprophyres, the ocellular, amphibole and isotropic base varieties are without exception silica under-saturated, the cpx lamprophyres are both silica saturated and under-saturated, and the quartz lamprophyres are silica over-saturated. The tinguaites are both silica under- and over-saturated. The normative mineralogy (Table 2.3) is in good agreement with these observations.

Distribution of the Data

Figure 3.2 depicts absolute frequency histograms showing the distribution of the data of each of the oxides for the various types of dyke rocks. Inspection of these diagrams shows that the distribution of each oxide is polymodal. Since the major element chemistry of the tinguaites is distinct from that of the relatively mafic lamprophyres in the case of each oxide (see Table 3.1), an empirical

Figure 3.2

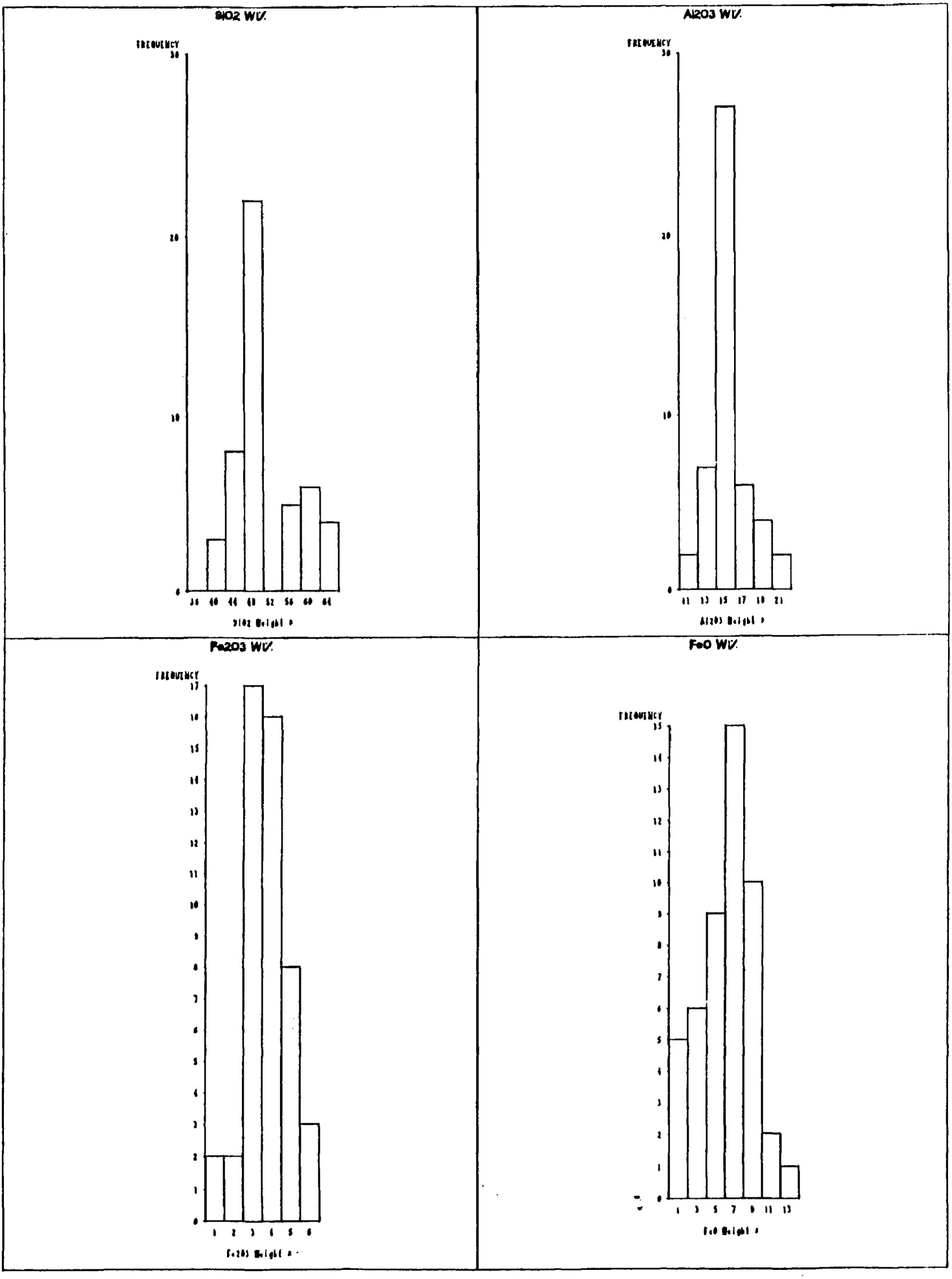
SiO2 Wt%
FREQUENCY
30
20
10
0
36 40 44 48 52 56 60 64
SiO2 Weight %
Al2O3 Wt%
FREQUENCY
30
20
10
0
11 13 15 17 19 21
Al2O3 Weight %
Fe2O3 Wt%
FREQUENCY
17
16
15
14
13
12
11
10
9
8
7
6
5
4
3
2
1
0
1 2 3 4 5 6
Fe2O3 Weight %
FeO Wt%
FREQUENCY
15
14
13
12
11
10
9
8
7
6
5
4
3
2
1
0
1 3 5 7 9 11 13
FeO Weight %

Figure 3.2 (Cont.)

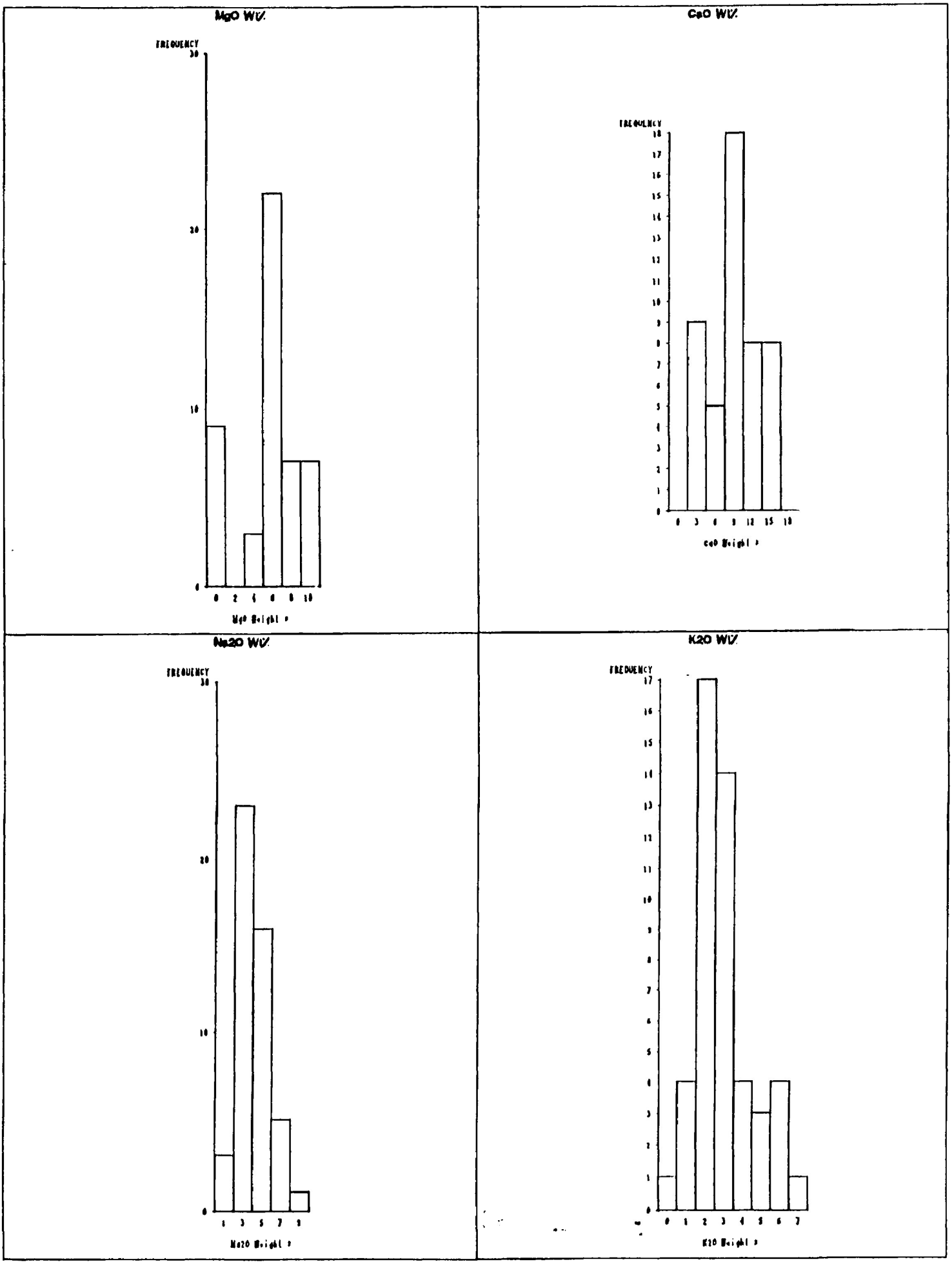

Figure 3.2 (Cont.)

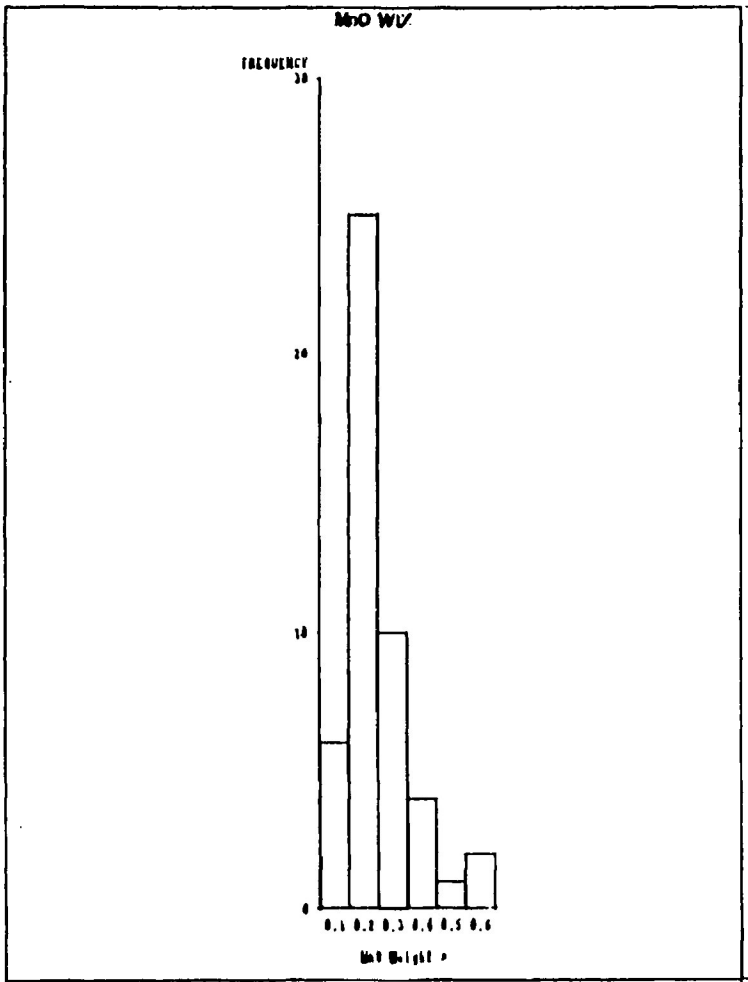

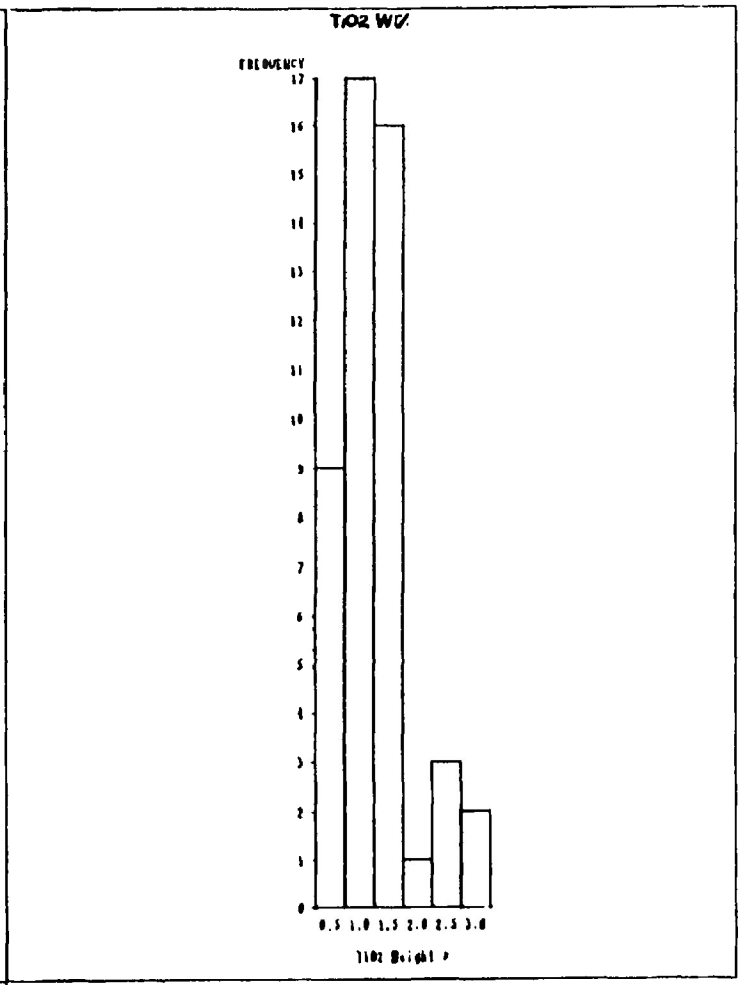

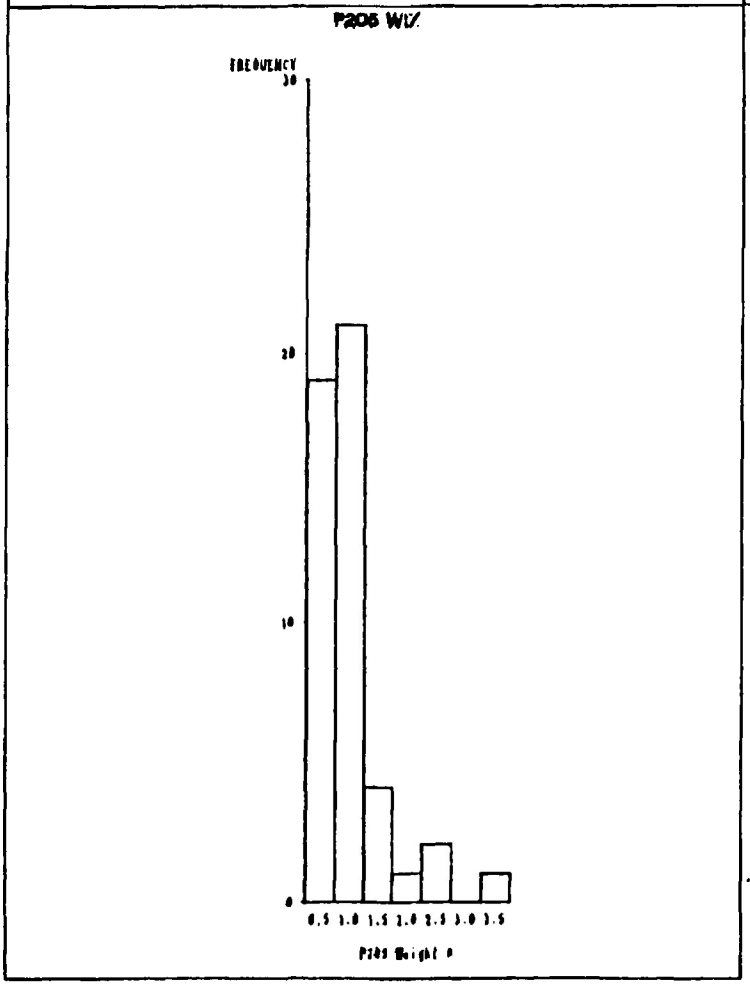

Table 3.4 Descriptive Statistics for Lamprophyre Major Element Data Distributions

Oxide	Minimum	Maximum	Range	Skewness	Kurtosis
SiO2	39.59	58.48	18.89	0.84	1.01
Al2O3	11.27	18.50	7.23	-0.02	1.04
Fe2O3	2.70	6.50	3.80	0.94	0.71
FeO	2.68	12.38	9.70	0.11	0.18
MgO	3.74	10.82	7.08	0.55	-0.12
CaO	5.16	16.33	11.17	0.55	-0.56
Na2O	0.83	5.97	5.14	-0.42	0.24
K2O	0.17	4.27	4.10	-0.51	0.59
MnO	0.12	0.60	0.48	1.70	3.09
TiO2	0.98	3.21	2.23	1.76	2.86
P2O5	0.37	3.46	3.09	2.32	6.18

Table 3.5 Results of Kolmogorov-Smirnov Goodness of Fit Test on Lamprophyre Major Element Data Distributions

Ho: The data is normally distributed.

Oxide	Result	Significance Level
SiO2	Ho rejected	0.05
Al2O3	Ho accepted	0.05
Fe2O3	Ho accepted	0.05
FeO	Ho accepted	0.05
MgO	Ho accepted	0.05
CaO	Ho accepted	0.05
Na2O	Ho accepted	0.05
K2O	Ho accepted	0.05
MnO	Ho rejected	0.05
TiO2	Ho rejected	0.05
P2O5	Ho rejected	0.05

conclusion is that one maximum in each histogram represents the tinguaite data (note that the quartz lamprophyres will also contribute to such a maximum in the SiO_2 histogram). The significance of other maxima in the these diagrams is evaluated by means of a statistical test, described below. Descriptive statistics are given in Table 3.4

Statistical analysis of the lamprophyre data (see the subsequent section "Statistical Discrimination of the Lamprophyres") involves parametric methods that are sensitive to the distribution of the data; specifically, a normal distribution (symmetrical variance σ of the data about a mean value λ) is ideal. Ahrens (1953,1954) describes a lognormal distribution of elements in nature as being a fundamental geochemical principle. In such a case, the logarithms of the data values are normally distributed. However, Chayes (1954) and Miller and Goldberg (1955) argued that a normal distribution is possible in a natural system; Gubac (1986) states that all natural systems tend towards a normal distribtion of their chemical components as a result of thermodynamic considerations. The normality of the distributions of the Coldwell lampropyre data were evaluated by means of the Kolmogorov-Smirnov one-sample goodness-of-fit test, which is used to determine how well a an observed distribution fits a hypothetical normal distribution

(Cheeney, 1983; see Appendix C). Table 3.5 summarizes the results of the Kolmogorov-Smirnov test. The null hypothesis (H_o), that the data are normally distributed, is rejected at the 5% significance level (5% being the level at which such rejection is considered statistically significant (Cheeney, 1983)) for SiO_2, MnO, TiO_2 and P_2O_5. However, there is insufficient evidence to reject H_o at the 5% significance level for the other oxides, in spite of the apparently polymodal distributions for several of them (i.e. MgO and CaO). The additional maxima are interpreted to be the an artifact of the intervals chosen to classify these data, so they are not real and do not affect the nature of the distribution (Cheeney, 1983); this effect diminishes with increasing sample size. In the case of SiO_2, however, this polymodal behaviour is real, as a result of the elevated silica contents of the quartz lamprophyres relative to the other types (see Table 3.1), so the distribution is not normal as confirmed by the Kolmogorov-Smirnov test. In the case of MnO, TiO_2 and P_2O_5, polymodal behaviour may be a factor in the rejection of H_o by the test, but examination of Table 2.6 shows also that the distribution of the data for each of these oxides is strongly positively skewed, which results in deviation from a normal distribution.

Since the probability of commiting a Type II error (i.e.

accepting H_o when it is actually false) at the 5% significance level is approximately 5% (Cheeney, 1983; Le Maitre, 1982), it is reasonable to assume that the data for Al_2O_3, Fe_2O_3, FeO, MgO, CaO, Na_2O and K_2O are normally distributed.

Variation Diagrams

Variation diagrams are given for the Coldwell dyke rock major element compositional data in order to examine the relationships between the various oxides. Diagrams were constructed by plotting each oxide against the Solidification Index of Kuno, and by plotting eigenvectors representative of the variance within the data as determined by a principal components analysis against one another.

Oxide-Solidification Index Diagrams

Figures 3.3 to 3.13 are variation diagrams constructed by plotting the weight percentage of each of the major and minor oxides against the Solidification Index (S.I.) of Kuno, which is defined as:

$$S.I. = \frac{100\ MgO}{MgO+FeO+Fe_2O_3+Na_2O+K_2O}$$

This particular index was chosen as the abscissa for these variation diagrams for the following reasons:

a) It responds well to changes in the absolute and relative abundances of the ferro-magnesian components.

b) It attempts to account for changes in the FeO concentration brought about by deuteric and secondary processes (i.e. oxidation during post-magmatic alteration) (Cox et al, 1979).

c) It incorporates changes in the alkaline components, since these tend to be enriched in residual phases. This helps to offset the potentially poor performance of the S.I. in the case of intermediate and acid suites showing little or no Fe enrichment relative to Mg (Cox et al, 1979).

d) It forms relatively strong linear relationships with the data for the various oxides when compared to other indices, such as the Harker Index or SiO_2 (see Table 3.6). However, taken in the absolute sense, these correlations must be viewed with some caution, as emphasized by Chayes (1960,1962) and Skala (1979). Since the data are all closed, in that the sum of the various oxides is 100%, none of the

Table 3.6 Correlation Statistics for Major Oxide-Solidification Index Variation Diagrams

Oxide	Correlation Coefficient r	Standard Error of Estimate	Intercept a	Slope b
SiO2	-0.702	4.83	59.47	-0.384
Al2O3	-0.769	1.39	18.44	-0.135
Fe2O3	0.352	1.07	2.94	0.033
FeO	0.440	2.59	3.78	0.103
MgO	0.977	0.65	-0.04	0.240
CaO	0.833	2.32	2.21	0.283
Na2O	-0.850	0.84	6.85	-0.110
K2O	-0.704	1.07	4.94	-0.085
MnO	-0.091	0.27	0.33	-0.001
TiO2	0.402	0.59	0.77	0.021
P2O5	0.500	0.59	0.29	0.027

KEY TO FIGURES 3.3 TO 3.13

Coldwell Dyke Rocks

filled circles- cpx lamprophyres

open stars- quartz lamprophyres

filled triangles- ocellar lamprophyres

filled stars- isotropic-base lamprophyres

filled squares- amphibole lamprophyres

open circles- tinguaites

Dyke Rocks From Other Occurrences

a- monchiquite, Monteregian Hills, Quebec (Eby, 1980)

b- camptonite, Monteregian Hills, Quebec (Eby, 1980)

c- camptonite, Serra de Monchique, Portugal (Rock, 1982)

d- monchiquite, Serra de Monchique, Portugal (Rock, 1982)

e- camptonite, Sines Complex, Portugal (Rock, 1982)

f- monchiquite, Sines Complex, Portugal (Rock, 1982)

g- tinguaite, Beemerville Complex, New Jersey (Maxey, 1976)

h- sannaite, Aillik Bay, Labrador (Malpas, 1986)

i,j- lamprophyre dykes, Ubekendt Ejland, West Greenland (Clarke et al, 1983)

Fig. 3.3

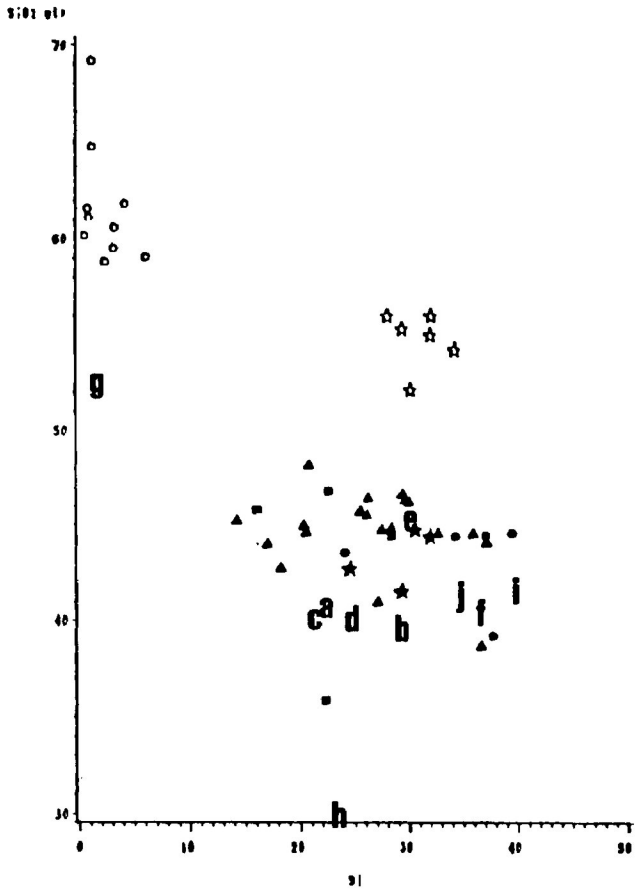

Fig. 3.4

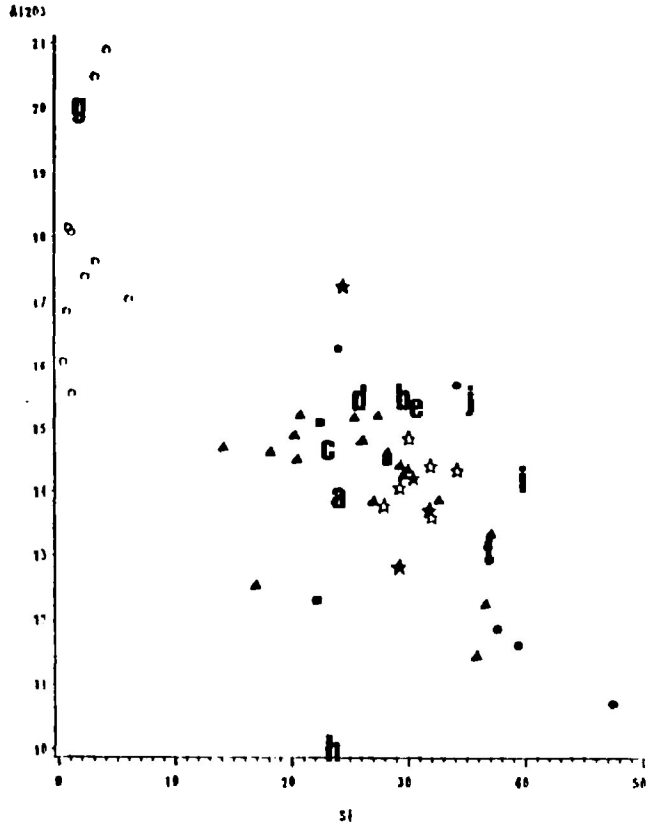

Fig. 3.5

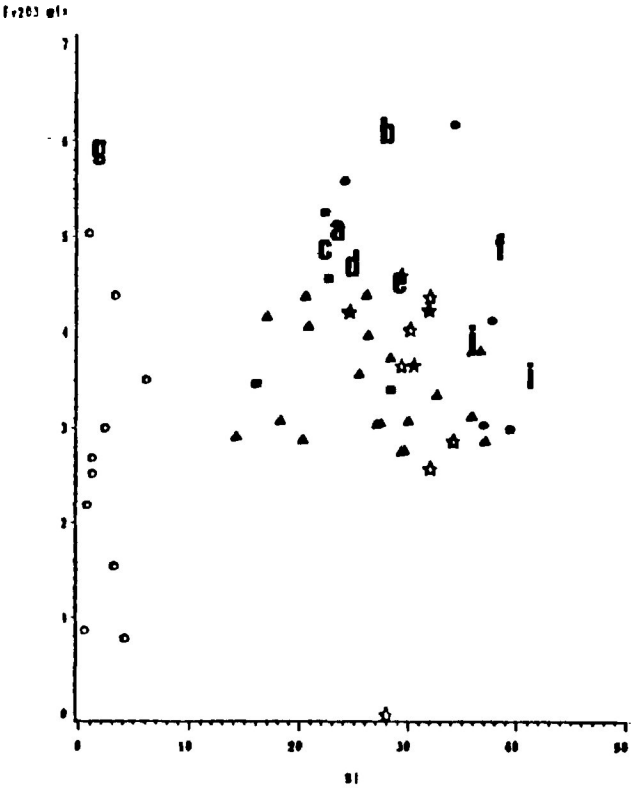

Fig. 3.6

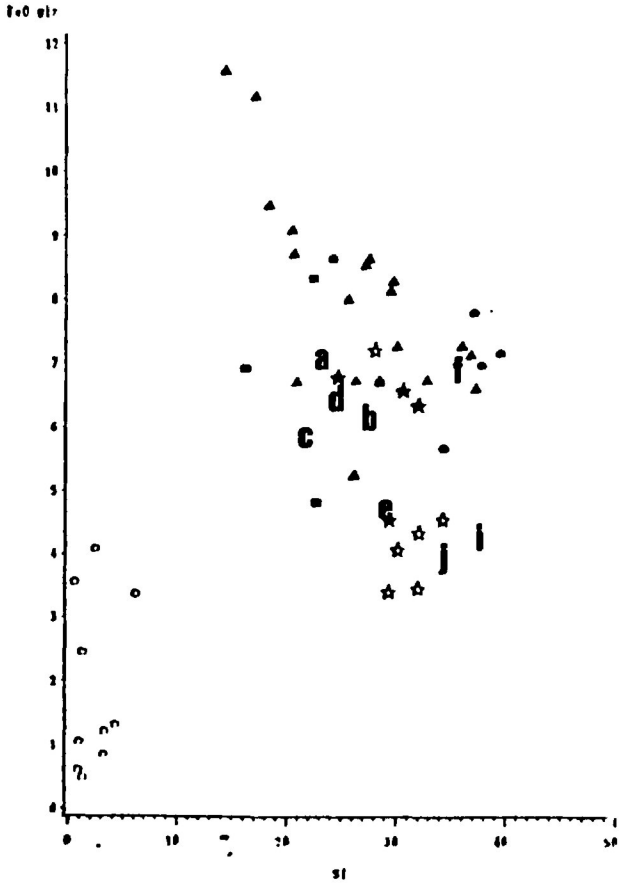

Fig. 3.7

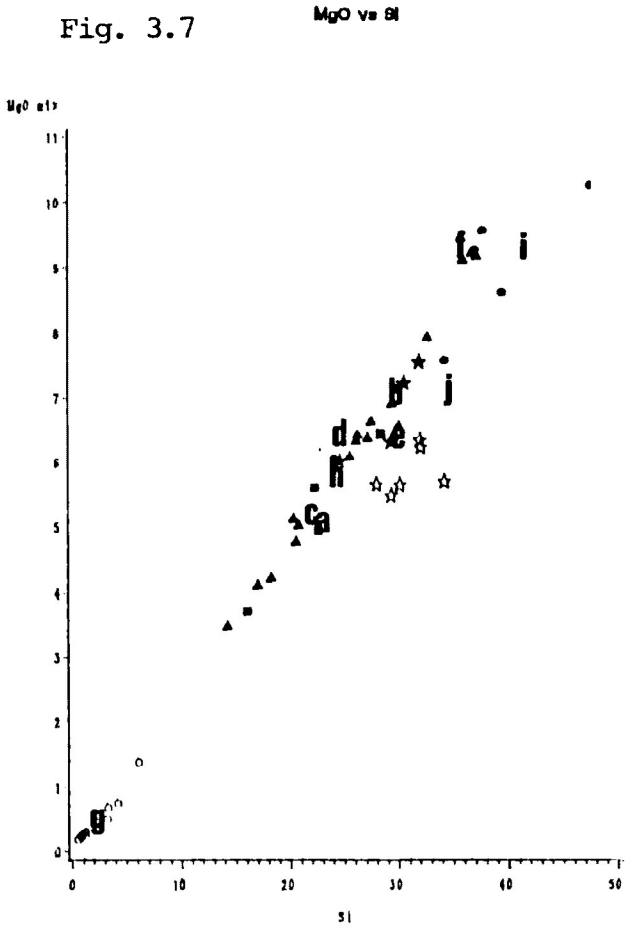

Fig. 3.8

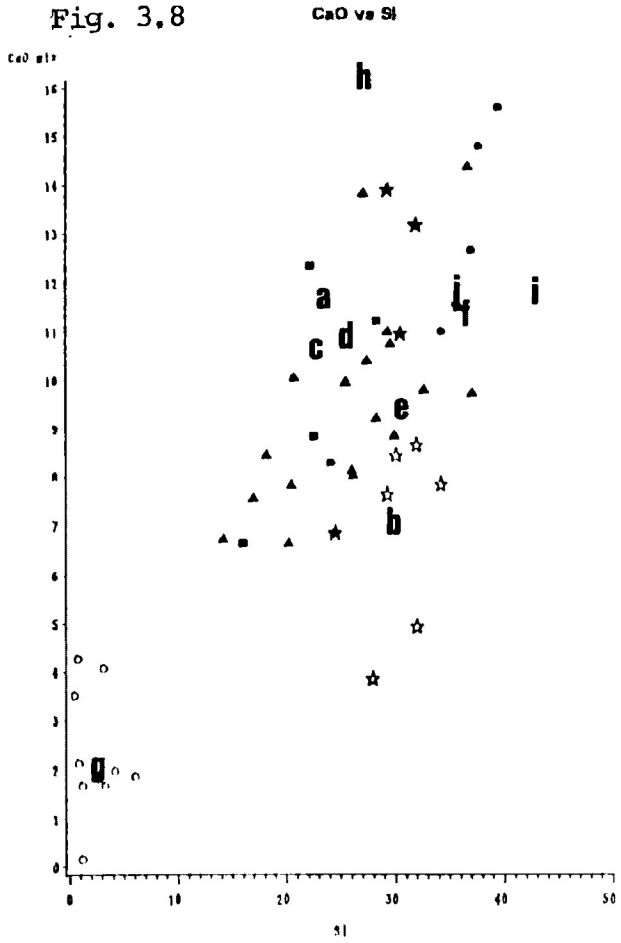

Fig. 3.9

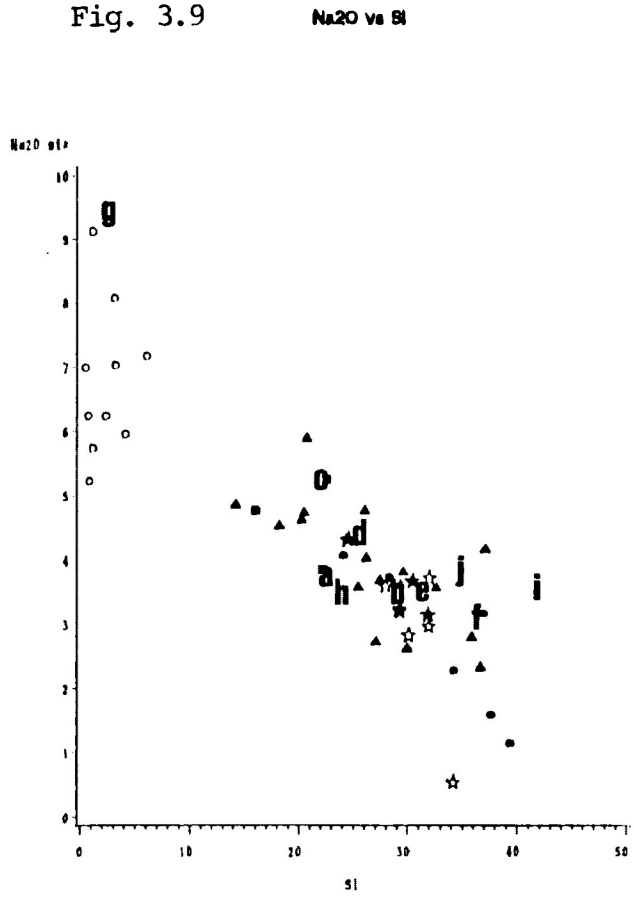

Fig. 3.10

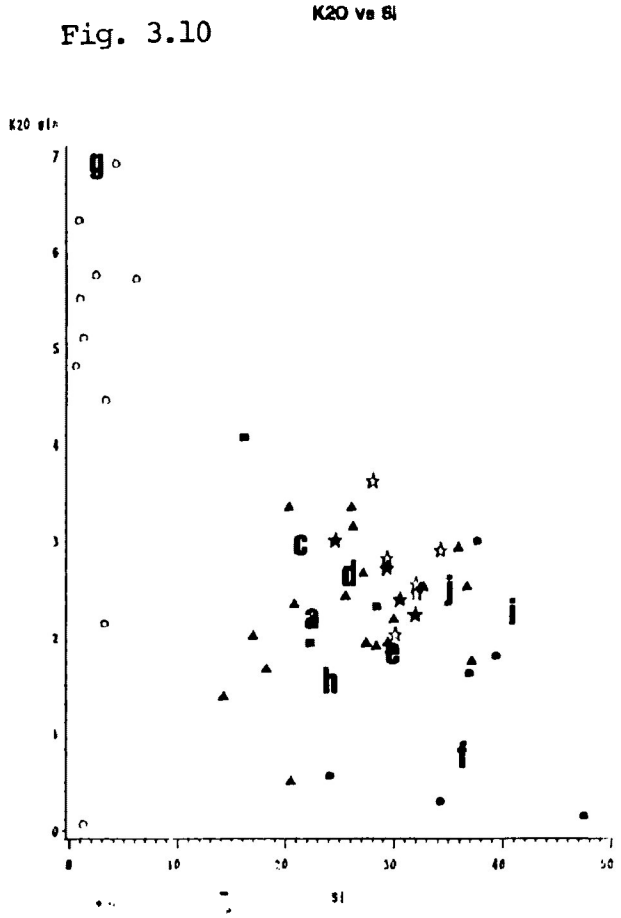

Fig. 3.11

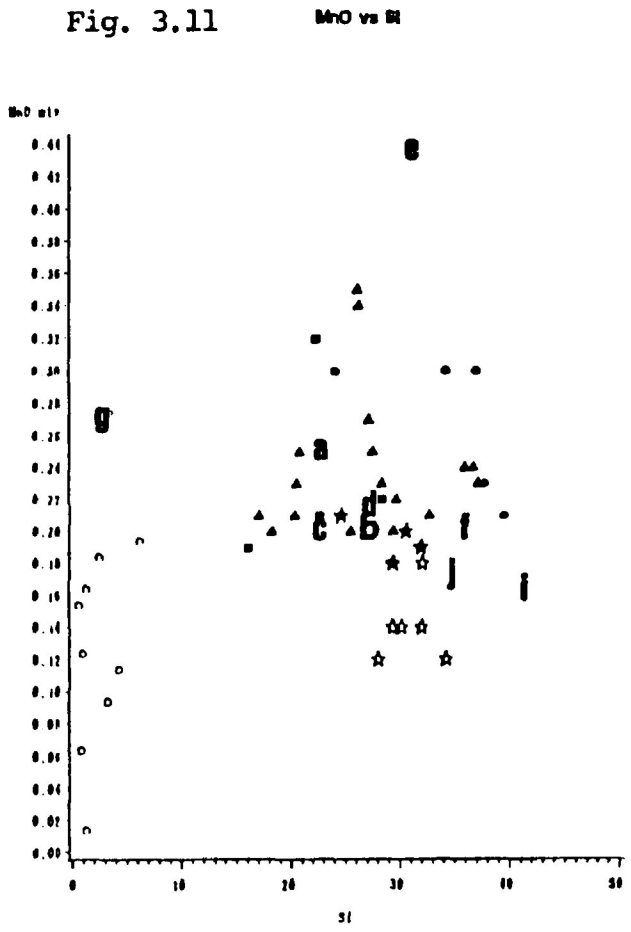

Fig. 3.12

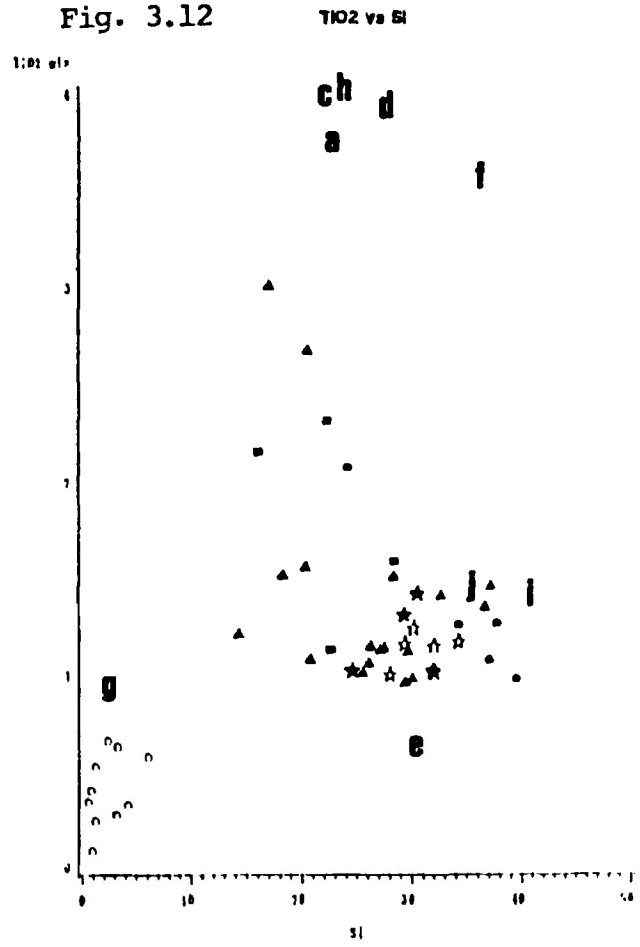

Fig. 3.13

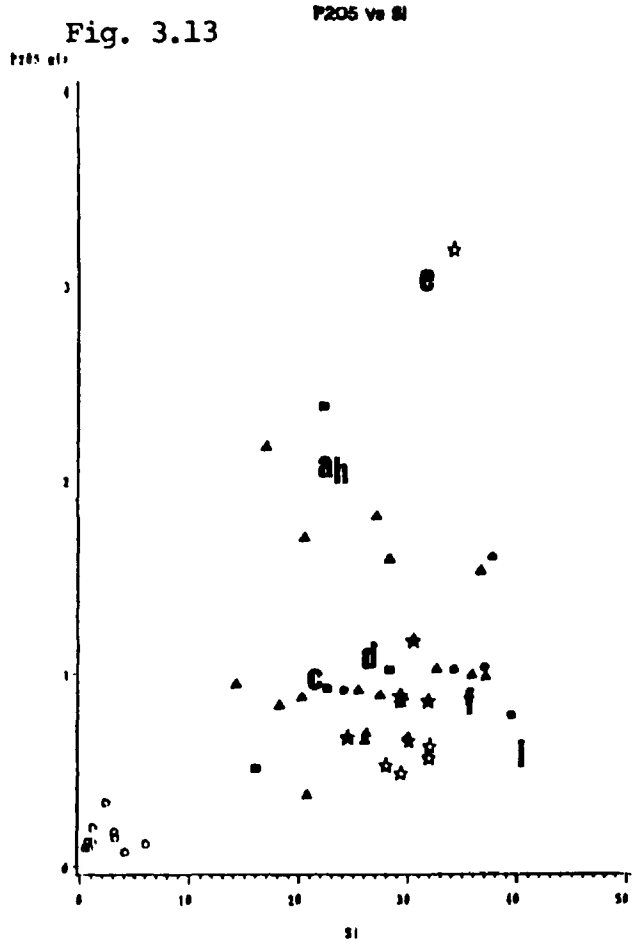

variables are independant. Closure tends to induce artificial correlations (Chayes, 1960). Various solutions to the problem of closure have been proposed by several authors (e.g. Chayes and Kruskal, 1966; Skala, 1977; Aitchison, 1981), but application of these methods is beyond the scope of this study. It is sufficient to emphasize that the correlation coefficient (r) is used in this work as a sample descriptor only, rather than as a means of predicting statistical parameters of the population (Le Maitre, 1982).

General relationships between the various oxides and the S.I. are as follows:

a) In Figures 3.3 to 3.13 the tinguaite data forms a distinct cluster separate from the lamprophyre data. This is largely a function of the separation of the values of the S.I. between the tinguaites and the lamprophyres.

b) On every diagram except those of MnO and P_2O_5 the data for the quartz lamprophyres form a relatively tight cluster, which may be distinctly separate from the data of the other lamprophyres, as in the case of SiO_2, or it may overlap the other data to some degree. The inference is that the quartz lamprophyres, as a group, are chemically coherent, and distinct from the other lamprophyres. This chemical

distinction extends beyond a simple separation on the basis of SiO_2 content, which would be expected empirically, to include all of the other oxides except MnO and P_2O_5.

c) MgO and CaO are positively correlated with the S.I., while SiO_2, Al_2O_3, Na_2O and K_2O define negative correlations (Table 3.6). The other oxides do not display any significant linear relationship with the S.I., although the FeO values for the lamprophyres, exclusive of those for the tinguaites, appear to display a moderate negative correlation.

d) A trend, either in a postive or negative sense relative to the S.I. as described in (c) above, is defined by the progession with decreasing S.I. from the cpx lamprophyres, to the other lamprophyres excluding the quartz bearing variety, to the tinguaites. The quartz lamprophyres do not lie on this trend.

Comparitive data for lamprophyres from other occurrences are also presented in Figures 3.3 to 3.13. Generally, there is considerable similarity between the Coldwell dyke rocks and these rocks in terms of whole rock major element composition.

Principal Components Analysis Eigenvector Diagrams

Principal components analysis (PCA) is a multivariate statistical method which transforms a given set of data composed of p variables, by means of rigid rotation of axes (Le Maitre, 1982), into a new set of p variables termed principal components. Each principal component is a linear combination of the original variables, with coefficients equal to the eigenvectors of the covariance matrix (as opposed to the correlation matrix- Davis, 1973; Le Maitre, 1982). The eigenvectors are usually taken with unit norm. The principal components are sorted by descending value of the eigenvalues, which are equal to the variances of the components (SAS Institute, 1985). The principal components are characterized by a number of properties:

a) The eigenvectors are orthogonal, so the principal components represent mutually perpendicular directions through the space defined by the original variables.

b) The principal component scores, constructed by projecting the original data onto the eigenvectors, are mutually uncorrelated (Le Maitre, 1982).

c) The magnitude and orientation of each principal

component is a function of the proportion of the variance that each variable in the original data set contributes towards the total variance (Davis, 1973).

d) The first principal component has the largest variance of any unit-length linear combination of the original variables, the jth prinicpal component has the largest variance of any unit length linear combination orthogonal to the first j-1 principal components, and the last principal component has the smallest variance of any linear combination of the original variables (SAS Institute, 1985).

e) The scores on the first j principal components have the highest possible generalized variance of any set of unit-norm linear combinations of the original variables (SAS Institute, 1985).

f) In geometric terms, the j-dimensional space spanned by the first j principal components gives the best possible fit to the data points as measured by the sum of squared perpendicular distances from each point to the j-dimensional space (SAS Institute, 1985).

It is likely that only the first few principal

Table 3.7 Results of Principal Components Analysis

Oxide	1st Eigenvector	2nd Eigenvector	3rd Eigenvector
SiO2	0.8008	-0.3373	-0.2493
Al2O3	0.1166	0.3724	0.4990
Fe2O3	-0.0474	-0.0009	0.2593
FeO	-0.2245	0.4993	-0.6711
MgO	-0.1759	-0.4045	-0.0791
CaO	-0.5050	-0.5088	0.0828
Na2O	0.0454	0.2609	0.2939
K2O	0.0523	0.0224	0.2320
MnO	-0.0017	0.0014	-0.0029
TiO2	-0.0223	0.0832	-0.0554
P2O5	-0.0352	0.0144	-0.1221
Eigenvalue	24.0062	9.1305	2.0760
% of Variance	60.6851	23.0809	5.2479

Figure 3.14 1st Eigenvector vs 2nd Eigenvector

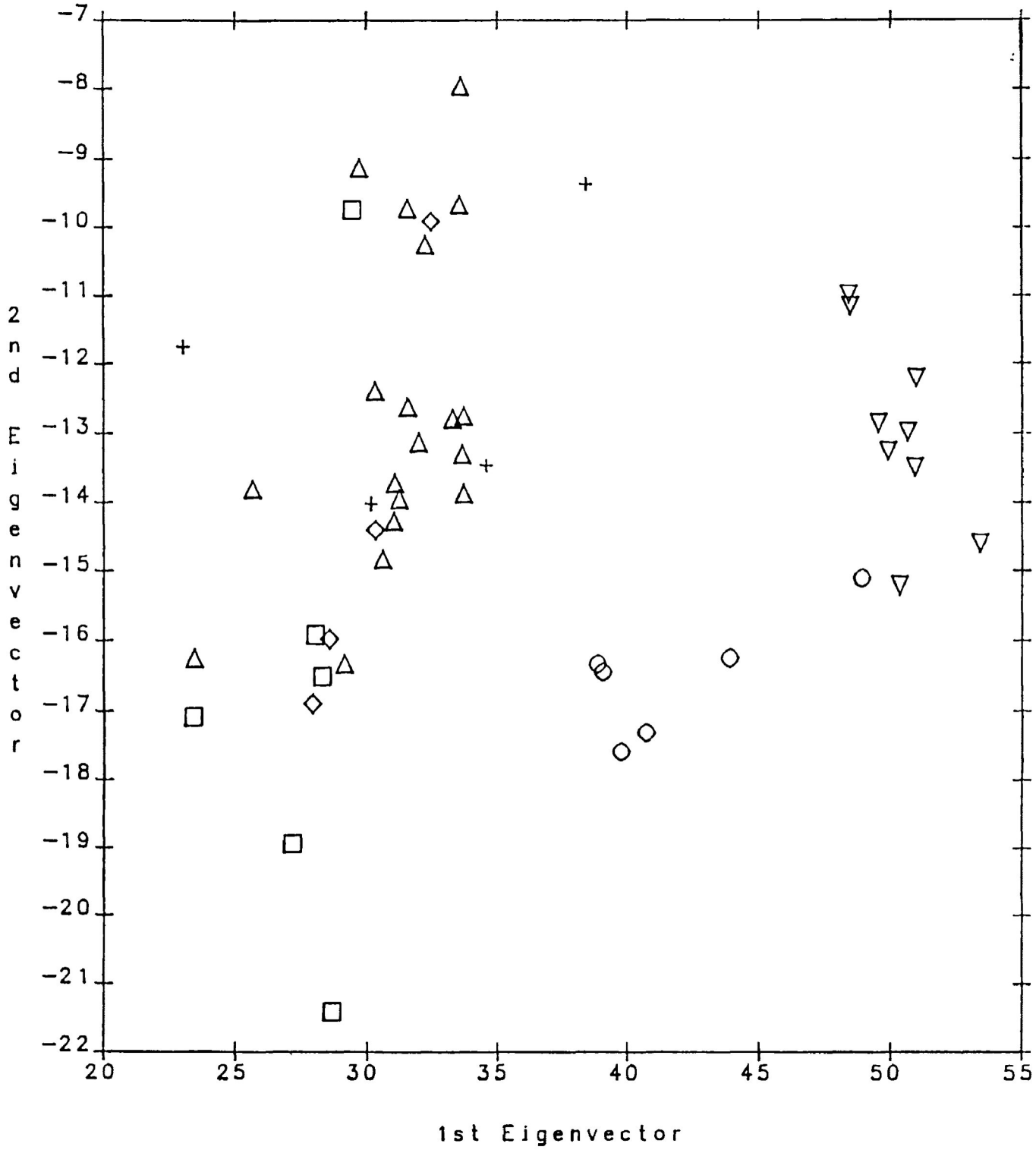

components will be required to portray effectively the overall variance in the data (Le Maitre, 1982; Cooley and Lohnes, 1962). Le Maitre (1968) states that the first three principal components will usually account for at least 95% of the total variance. By plotting these principal components against one another, the number of divariant variation diagrams required to express the compositional variation in the data is also reduced. PCA has the advantage of requiring no assumptions about the original variables, such as the nature of their distribution, since the results are purely representative of the variation that is inherent in the data (Le Maitre, 1982).

The data for the Coldwell dyke rocks were transformed into PCC by the FORTRAN progam PCA (Davis, 1973). The eigenvectors were extracted from the covariance matrix. Inspection of Table 3.7 shows that the first three eigenvectors account for approximately 89% of the variance in the data. The 1st eigenvector (Table 3.7) accounts for 61% of this variance, therefore, it defines the dominant trend exhibited by the data; this may represent some petrologically significant process (Le Maitre, 1982). Inspection of this eigenvector indicates that SiO_2 and Al_2O_3 vary inversely with FeO, MgO and CaO; SiO_2 and CaO appear to dominate as their terms are relatively large. This is in agreement with the

observed behaviour of these oxides in the oxide-S.I. variation diagrams. The 2nd eigenvector comprises 23% of the total variance; this is still quite significant, therefore, this may reflect some subsidiary petrological process, such as alteration (Le Maitre, 1982). Inspection of this eigenvector suggests that SiO_2, MgO and CaO vary inversely with Al_2O_3, FeO and Na_2O. The 3rd eigenvector accounts for only 5% of the total variance, while the remaining eigenvectors contribute even less information, so no significant interpretation can be based on these eigenvectors (Le Maitre, 1982). It would appear, therefore, that most of the variation in the data is related to changes in SiO_2, Al_2O_3, FeO, CaO and MgO, with the changes in SiO_2 and CaO contributing most to the variation.

Figure 3.14 is a plot of the 1st eigenvector versus the 2nd eigenvector. Inspection of this diagram shows that the tinguaites and quartz lamprophyres form distinct groups along the 1st eigenvector, while the other lamprophyres are not effectively separated. There is no significant separation of any rock type along the 2nd eigenvector.

Conclusions

A dominant trend in the major element data defined by

inverse variation of SiO_2, Al_2O_3 and Na_2O with MgO and CaO is indicated by inspection of variation diagrams constructed by plotting the various oxides versus the Solidification Index of Kuno, and by principal components analysis. SiO_2, Al_2O_3 and Na_2O content increase, and MgO and CaO decrease with increasing S.I. The inference is that the various dyke rocks are related by some evolutionary process which resulted in the observed changes in the various oxides; this process may be reflected by the 1st eigenvector, since it accounts for most of the variation in the data (Le Maitre, 1982), while the 2nd eigenvector, which also accounts for a considerable amount of the variation in the data may reflect some subordinate process such as alteration.

In terms of distinguishing the various types of dykes on the basis of their major element chemistry, the tinguaites are distinct from the lamprophyres, as would be empirically expected. The quartz lamprophyres appear to form a separate type on the basis of major element chemistry, however, there is apparently no similar distinction among the other lamprophyres. This is examined in the following section in more detail.

STATISTICAL DISCRIMATION BETWEEN THE LAMPROPHYRES

Separation of the tinguaites from the lamprophyres on the basis of whole rock major and minor element chemistry is trivial, since the former are very definitely distinct from the latter in this respect (see Table 2.3). Discrimination between the Coldwell basic lamprophyres was attempted here using the methods of divisive cluster analysis and multivariate discriminant analysis. Discrimination between various lamprophyre types has been attempted by Metais and Chayes (1964a; 1964b) and Rock (1977).

Cluster Analysis

Cluster analysis is a statistical procedure whereby the cases in a matrix of n cases (specimens), described by m variables (oxides), are grouped by a measure of similarity, in the case of agglomerative cluster analysis, or dissimilarity, in the case of divisive cluster analysis (Le Maitre, 1982). The objective is to classify the cases according to inherent groupings in the data, while making no initial assumptions concerning the data (Le Maitre, 1982). The method used in the case of the Coldwell lamprophyres was that of divisive cluster analysis, using the FORTRAN program TWINSPAN (Two Way Indicator Species Analysis), (Hill, 1979). Essentially,

TWINSPAN divides the cases into groups by means of repeated dichotomization using the variables as a basis, and similarily divides the variables into groups using the groups of samples as a basis, then combines the results into an ordered two-way table which identifies the natural groups in the data (Hill, 1979). The process of dicotomization is central to the method; it is described in detail by Hill (1979), and summarized below:

a) A direction of variation in the data is identified by ordinating the cases into a primary ordination according to the method of reciprocal averaging (Hill, 1973).

b) This primary ordination is then divided at its middle to establish a crude dichotomy. A refined ordination is constructed on the basis of differential variables that are preferential to one side or the other of this crude dichotomy.

c) The refined ordination is then divided at an appropriate point to derive a a new dichotomy.

d) Finally, an indicator ordination is established, based on the most highly preferential variables. The dichotomy suggested by the refined ordination is tested for reproduceability by a division of the indicator ordination.

A similar process of dichotomization is used to group the variables on the basis of the grouped cases.

TWINSPAN offers a number of options concerning the construction and use of "pseudo-variables" to deal with special scales of abundance used in the data. However, none of these options were selected for use with the Coldwell lamprophyre data, since their use is arbitrary and requires pre-suppositions concerning the data. Tables 3.8 and 3.9 summarize the groupings extracted from the ordered two-way table constructed by TWINSPAN for the cases (specimens) and variables (oxides), respectively, for the Coldwell lamprophyre data.

Inspection of Table 3.8 shows that TWINSPAN has identified 11 natural groupings or clusters in the specimens. Examination of the clusters shows that the quartz lamprophyres are largely separated into clusters 1 and 2. Similarily, the cpx lamrophyres are separated into clusters 7,8 and 9, although some overlap with other types occurs. The ocellar, isotropic-base and amphibole lamprophyres occupy the remaining clusters (3,4,5,6,10 and 11) with essentially no separation occuring among each type. Inspection of Table 3.9 shows that 7 clusters are identified by TWINSPAN in the oxides. Although the significance of this grouping scheme is unclear, it is noteworthy that FeO_t and to a lesser extent Na_2O, TiO_2 and P_2O_5 tend to be more abundant in the higher numbered specimen clusters than in the lower numbered ones,

Table 3.8 Results of TWINSPAN Cluster Analysis on Coldwell Lamprophyr Data

Group No.	No. of Cases in Group	Breakdown of Cases in Each Group by Rock Typ				
		Cpx Lamp.	Quartz Lamp.	Ocellar Lamp.	Isotropic-base Lamp.	Amph Lamp.
1	1		1			
2	4		4			
3	5			4	1	
4	9			6	2	
5	2			2		
6	1				1	
7	4	2		2		
8	3	3				
9	3	1				1
10	4			2		2
11	3			3		

Table 3.9 Oxide Groupings from TWINSPAN Cluster Analysis of Coldwell Lamprophyre Data

Oxide	Group	Greatest Abundance Associated With High Low or Intermediate Numbered Specimen Groups, or No Clear Association
K2O	1	low
Na2O	2	high
FeO	3	high
CaO	4	intermediate
SiO2	5	none
Al2O3	5	none
Fe2O3	5	none
MnO	5	none
MgO	6	none
TiO2	7	high
P2O5	7	high

while K_2O behaves in the opposite sense. CaO is less abundant in the highest and lowest numbered specimen clusters than it is in the intermediate clusters. The remaining oxides display no clear preference; this includes SiO_2, which is somewhat suprising in view of the elevated SiO_2 content of the quartz lamprophyres relative to the other lamprophyre types. Therefore, FeO and, to a lesser extent, Na_2O, K_2O, TiO_2 and P_2O_5 are differential variables, as described above. The clustering scheme established by TWINSPAN is thus based primarily on the abundance of these oxides in the various specimens; it is tested for statistical significance in the following section by multivariate discriminant analysis.

Multivariate Discriminant Analysis

Mulitivariate discriminant analysis (MDA) is a statistical method whereby changes in m variables (oxides) in a given sample consisting of n cases (specimens) are examined simultaneously, in order to determine to what extent it is possible to distinguish between members of different groups or clusters in the specimens on the basis of the changes in the oxides (Le Maitre, 1982). MDA differs from cluster analysis, therefore, in that a prior knowledge of the clusters is required. Also, a basic underlying assumption is that the oxides are normally distributed, and that the groups

have equal variance-covariance matrices (Le Maitre, 1982), although this latter requirement may be offset by using a pooled within-groups covariance matrix (Klecka, 1975). Although a number of methods for carrying out MDA are available, the method utilized in this study involves the use of F-ratios (F=A/B, where A is the within-groups variance, and B is the between-groups variance) in order to determine which oxides have the greatest discriminating power (i.e. which variables account for the greatest variation between the groups) (Pearce, 1974). Calculated and empirical F-ratios are compared to determine if the null hypothesis (H_o) "that the means of each analysis are the same", can be rejected at the 0.01 significance level at a given number of degress of freedom (DF). If the calculated F-ratios exceed the empirical F-ratios for a given oxide, then that oxide is considered to have high discriminating power (Pearce, 1974). The method of Klecka (1975) determines which oxide maximizes the minimum F-ratio between pairs of groups. This oxide is then combined in turn with each remaining oxide to determine which new oxide in combination with the initial one, according to the F-ratio criteria, accounts for the greatest discriminating information. This pair of oxides is then combined with each remaining oxide in a similar manner to form an optimum triplet, and so on, until either no oxides remain, or until remaining oxides do not produce a minimum

level of improvement in the discriminating information accounted for. The method also excludes previously included oxides, if some new combination of oxides contains all of the information about group differences that was available in that oxide. The result of this stepwise procedure is a series of canonical discriminant functions containing the original variables which maximize the separation between the groups (Cooley and Lohnes, 1962; Klecka, 1975). Each succeeding canonical discriminant function accounts for less of the information regarding group differences than the preceding ones, in a manner analagous to the eigenvectors in PCA with regards to variance. The statistical significance of a given function is tested by means of Wilk's lambda (λ) and chi-square, both of which describe the amount of discriminating information unaccounted for by earlier functions at a given probability level; succeeding functions will exhibit higher Wilk's lambda, lower chi-square and higher probability level values; this latter reflects the likelyhood that the corresponding lambda value will occur due to the chances of sampling in the case of a random sample (Klecka, 1975). MDA further tests the grouping scheme by classifying each specimen according to the group to which it has the highest probability of belonging (Klecka, 1975); the percentage of specimens correctly classified is a measure of the significance of the groups. Graphically, since the

canonical discriminant functions are linear in nature, they may be plotted to portray the differences between the various groups. Within-group variation is represented by the distance between a given specimen and the centroid of the group with which it is associated; the centroid describes the location along the function in question of a typical specimen from that group (Klecka, 1975). The computer routine used to perform MDA upon the Coldwell lamprophyre data is part of the SPSS package, written by Klecka (1975).

For the purposes of this study, two methods of generating groups in the data for input into MDA were used. In the first method, the clusters produced by TWINSPAN cluster analysis were used, to assess the significance of the clustering scheme suggested by that procedure. The second method simply used the rock types, assigned by petrographic examination, as group delimiters. The results of each are discussed separately below.

Grouped by Cluster from Cluster Analysis

No consideration is given in this case to the distribution to the oxides, since, according to Marriott (1974) departures from normality are not too serious; the main purpose of MDA in this case is to assess the statistical

significance of the clusters generated by TWINSPAN. Inspection of Table 3.10a shows that two discriminant functions are required to represent effectively the discriminating information in the data; after the removal of function 1, 96% of the variation in the data is accounted for, and Wilk's lambda has a value of .846, which corresponds to a chi-square of 5.00 with a probability level of .7571. In terms of discriminating oxides, FeO and SiO2 are statistically the most useful for the Coldwell lamprophyres data when grouped by cluster analysis (Table 3.10b). However, Figure 3.15, a histogram showing the distribution of the groups along discriminant function 1, indicates that the various clusters are virtually indistinguishable. Only clusters 1 and 2, representing most of the quartz lamprophyres, are separated to any significant degree, although not from one another. The conclusion, therefore, is that the separation of the quartz lamprophyres by cluster analysis, achieved largely on the basis of FeO content, is statistically significant. All other clusters generated by TWINSPAN have no statistical significance, including those that apparently achieve some degree of separation of the cpx lamprophyres (clusters 7,8 and 9), so no distinction between the cpx, ocellar, isotropic-base and amphibole lamprophyres is possible on the basis of major and minor element chemistry by cluster analysis. This is emphasized by the

Table 3.10a Statistics of Canonical Discriminant Functions for MDA of Groups Generated by Cluster Analysis

Function	Eigenvalue	%Variance	Wilk's λ	Chi-square	Probability
0	0.0000	0.00	0.0209	116.05	0.0000
1	6.2933	96.06	0.8464	5.00	0.7571

Table 3.10b Summary of Wilk's λ and F-ratios for Oxides Involved in MDA of Groups Generated by Cluster Analysis

Oxide	Wilk's λ	F	Significance	Function 1
SiO2	0.9116	1.964	0.0632	1.6351
Al2O3	0.9654	0.659	0.6242	0.3254
Fe2O3	0.9875	0.365	0.8864	0.4217
FeO	0.8854	2.681	0.0111	2.1546
MgO	0.9325	0.876	0.1062	0.8324
CaO	0.9687	0.648	0.6631	0.5421
Na2O	0.9647	0.651	0.6524	0.5841
K2O	0.9783	0.421	0.7152	0.2149
MnO	0.9932	0.105	0.9562	-0.0214
TiO2	0.9865	0.234	0.9124	-0.1014
P2O5	0.9876	0.216	0.9331	0.3547

FIGURE 3.15- HISTOGRAM OF CANONICAL DISCRIMINANT FUNCTION 1 FOR CLUSTERS OF COLDWELL LAMPROPHYRES GENERATED BY CLUSTER ANALYSIS

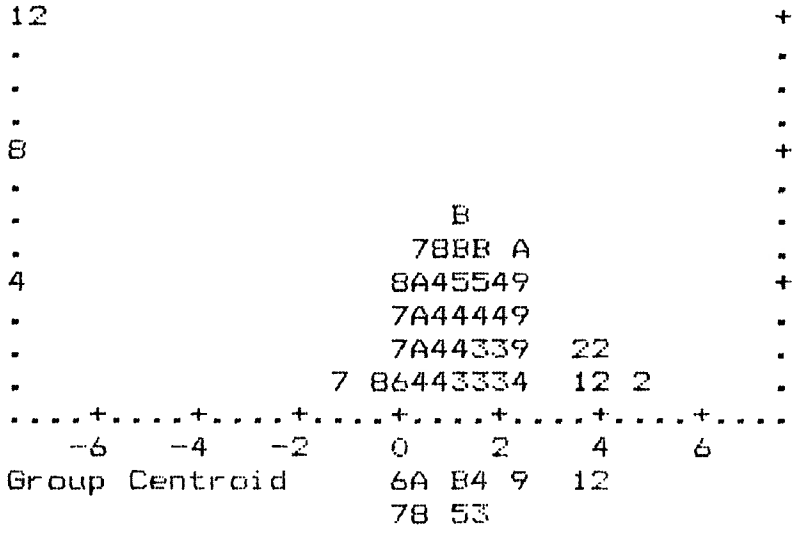

TABLE 3.11 CLASSIFICATION TABLE FOR GROUPS GENERATED BY CLUSTER ANALYSIS SHOWING CLASSIFICATION OF CASES IN EACH GROUP BY MDA

	1	2	3	4	5	6	7	8	9	A	B
1	100	0	0	0	0	0	0	0	0	0	0
2	25	75	0	0	0	0	0	0	0	0	0
3	0	0	75	0	0	0	0	0	0	0	25
4	0	0	0	44	34	0	0	0	0	0	22
5	0	0	0	100	0	0	0	0	0	0	0
6	0	0	0	0	0	0	100	0	0	0	0
7	0	0	0	0	0	0	50	25	0	25	0
8	0	0	0	0	0	50	50	0	0	0	0
9	0	0	0	0	0	0	0	0	100	0	0
A	0	0	0	0	0	0	25	25	50	0	0
B	0	0	33	0	0	0	0	0	0	0	67

Percentage of Cases Correctly Classified= 34%

classification procedure of MDA, in that only 34% of the cases were classified according to the same scheme generated by cluster analysis (see Table 3.11).

Grouped by Type from Petrographic Analysis

Although Marriott (1974) states that departure from normality by the variables (oxides) in MDA is not too serious, Le Maitre (1982) suggests that the optimim results will be achieved if the variables are normally distributed. Therefore, those oxides for which there was insufficient evidence to support the hypothesis of a normal distribution (SiO_2, MnO, TiO_2 and P_2O_5; see "Distribution of the Data" previously) were excluded from the MDA of the lamprophyre groups based on rock type, as determined by petrographic examination. The results are summarized in Table 3.12a and 3.12b. Inspection of the former table shows that after removal of the first three canonical discrminant functions, over 99% of the variation in the data is accounted for, while Wilk's lambda has a value of .950, corresponding to a chi-square of 1.650 at a probability level of .800. The 1st function accounts for most of the variance in the data (69%), while the second accounts for 20%. FeO and, to a lesser extent Al_2O_3, are the best discriminating oxides, as indicated in Table 3.12b. Figure 3.16 depicts the first two

Table 3.12a Statistics of Canonical Discriminant Functions for MDA of Groups Generated by Petrographic Analysis

Function	Eigenvalue	%Variance	Cum %	Wilk's λ	Chi-square	Probability
0	0.0000	0.00	0.00	0.0471	97.77	0.0000
1	4.3982	69.04	69.14	0.2543	43.82	0.0006
2	1.2855	20.18	89.22	0.5812	17.37	0.0667
3	0.6341	9.95	99.17	0.9497	1.65	0.7997

Table 3.12b Summary of Wilk's λ and F-ratios for Oxides Involved in MDA of Groups Generated by Petrographic Analysis

Oxide	Wilk's λ	F	Significance	Function 1	Function 2
Al2O3	0.1959	0.8796	0.1462	0.1589	0.0294
Fe2O3	0.0893	0.6915	0.6338	0.3798	-0.3358
FeO	0.2307	1.1964	0.0515	1.1451	-0.1067
MgO	0.6614	0.3162	0.5776	0.8338	-0.7684
CaO	0.0471	0.5192	0.8124	0.7779	0.5433
Na2O	0.1380	0.7757	0.5495	0.9326	0.6939
K2O	0.0745	0.5902	0.7354	0.1940	0.6017

TABLE 3.13 CLASSIFICATION TABLE FOR GROUPS GENERATED BY PETROGRAPHIC ANALYSIS SHOWING CLASSIFICATION OF CASES IN EACH GROUP BY MDA

	1	2	3	4	5
1	100	0	0	0	0
2	0	85	15	0	0
3	0	5	95	0	0
4	0	0	100	0	0
5	33	0	67	0	0

Percentage of Cases Grouped Correctly= 77%

canonical discriminant functions plotted against one another. Group 2, representing the quartz lamprophyres, is clearly separated from the other lamprophyre types, which are not separated, when viewed along the 1st function. This is in good agreement with the results of MDA on the cluster analysis generated groups above (i.e. that the quartz lamprophyres may be discriminated on the basis of FeO content). Examination of this function (see Table 3.12b) shows that all of the oxides behave in a positive sense, with strong contributions from Na_2O, MgO and CaO. The direct relationship between MgO and CaO is similar to that observed in the oxide-S.I. variation and PCA eigenvector diagrams (see above), however, the behaviour of Na_2O (i.e. directly related to MgO and CaO) is anomalous in this respect. As in the case of the earlier diagrams, the petrological significance of this function is unclear. Group 1, representing the cpx lamprophyres, shows some separation when the data is projected onto the 2nd discriminant function, while the other types are essentially unseparated. This function (see Table 3.12b) shows an inverse relationship between the ferro-magnesian components (FeO, Fe_2O_3 and MgO) and the other oxides. This may be related to the volumetric abundance of clinopyroxene phenocrysts in this rock type, however, the behaviour of CaO is not consistent with such an interpretation (i.e. an increase in the content of the

Figure 3.16

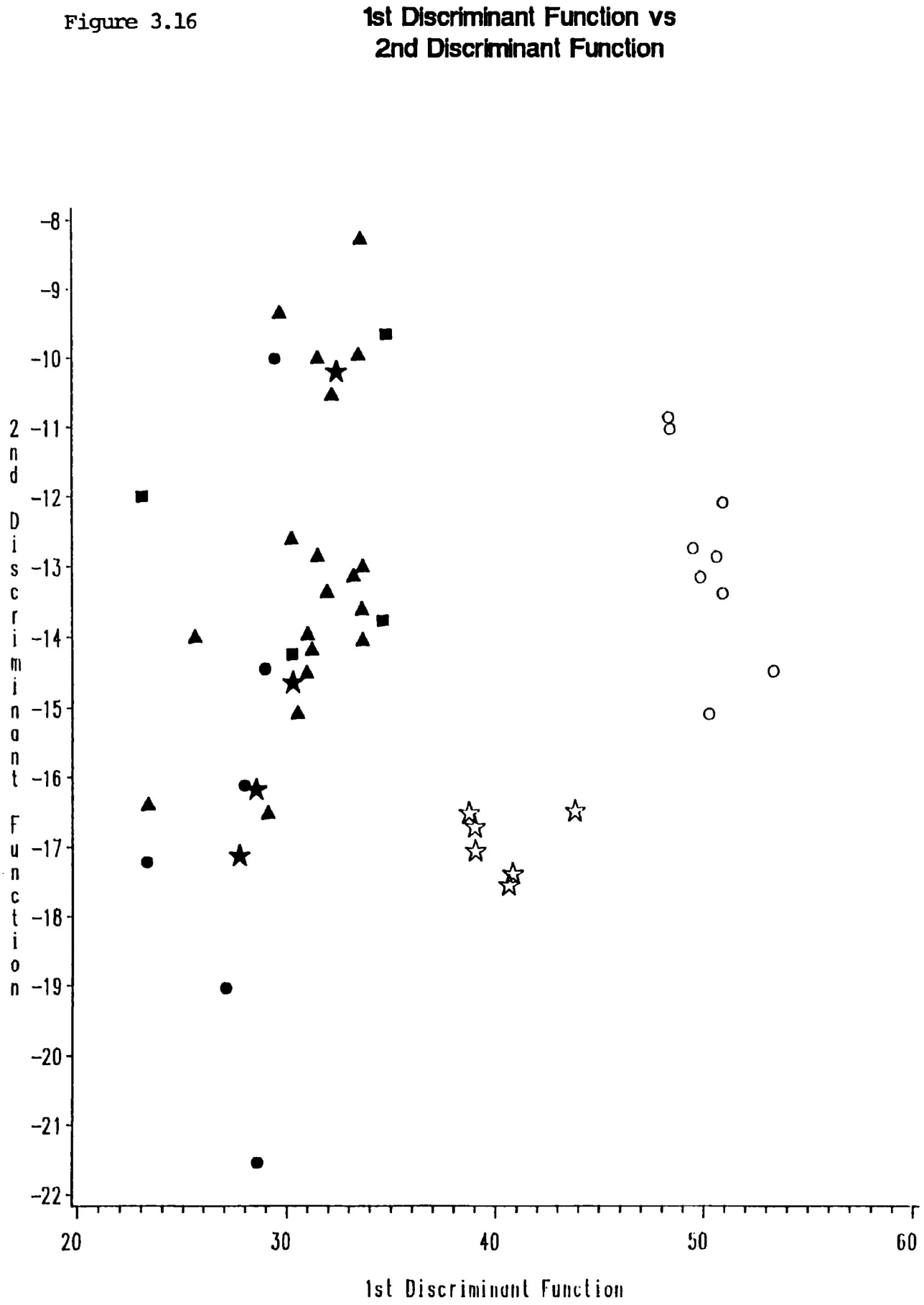
1st Discriminant Function vs
2nd Discriminant Function
2nd Discriminant Function
-8
-9
-10
-11
-12
-13
-14
-15
-16
-17
-18
-19
-20
-21
-22
20
30
40
50
60
1st Discriminant Function

ferro-magnesian components as a result of increased abundance of clinopyroxene should be accompanied by an increase in the CaO content), so this function may reflect a more complex mechanism. No separation is achieved by the 3rd function, in spite of its accounting for 9% of the variation in the data- since Fe_2O_3 and K_2O vary inversely with the other oxides, this function likely reflects changes in the various components brought about by alteration. 77% of the specimens were correctly classified according to the original grouping scheme (see Table 3.13).

Conclusions

The conclusion drawn in the previous section dealing with the oxide-S.I. variation diagrams and the PCA eigenvector diagrams, that the quartz lamprophyres form a distinct group from the other lamprophyre types, is confirmed by cluster analysis and MDA of the lamprophyre major and minor element data; it is possible to separate the quartz lamprophyres in a statisically significant manner on the basis of both SiO_2 and FeO contents. However, cluster analysis is not capable of making a statistically significant discrmination among the other lamprophyre types; this is confirmed by MDA of the groups representing those types produced by cluster analysis. Similarily, MDA of the groups

representing those types delimited by petrographic examination indicates that although a small degree of separation of the cpx-lamprophyres is achieved (by the 2nd canonical discriminant function), generally, the cpx, quartz, isotropic-base and amphibole lamprophyres can not be separated on the basis of major and minor element chemistry in a statistically significant manner.

CLASSIFICATION OF THE COLDWELL DYKE ROCKS

Classification schemes based on various parameters have been proposed for rocks which satisfy the general criteria required of lamprophyres by a number of authors, including Joplin (1966), Wimmenauer (1973, 1976), Sahama (1974) and others; these are summarized by Rock (1977), and, more recently, by Streckheisen (1978). The following sections summarize and discuss the application of these conventional classifications to the Coldwell lamprophyres. The tinguaites are adequately classified on the basis of previous work (Mitchell and Platt, 1977) (see Chapter 1).

Previous Work Concerning Lamprophyre Classification and Nomenclature

A detailed summary and discussion of much of the work concerning lamprophyre nomenclature and classification is given by Rock (1977). According to this author, four lamprophyre subgroups are recognized:

a) Shoshonitic lamprophyres, which are mildly potassic (Na<=K), intermediate and near-saturated, frequently occuring in association with post-orogenic granite;

b) Leucite lamproites, which are extremely rare, ultra-potassic glassy extrusives which have often been described as lamprophyric because of their porphyritic character and contain large phlogopite phenocrysts. Note that Mitchell (1985) and Bergman (1986) do not believe that lamproites are members of the lamprophyre group;

c) Alkaline lamprophyres ("anchibasaltic" lamprophyres of Wimmenauer (1973)) which are alkaline basaltic or basanitic in composition, although with a higher volatile content (i.e. containing primary amphibole and/or biotite), undersaturated, and are normally associated with sodic

alkaline rocks such as nepheline syenite/gabbro complexes; and

d) Ultrabasic lamprophyres, which are distinguished from the alkaline lamprophyres by their lower SiO_2 content, the presence of perovskite and melilite, a higher K/Na ratio, and an association with carbonatites.

The alkaline and shoshonitic sub-groups are by far the most widespread of the lamprophyre types (Rock, 1977). The IUGS has adopted a similar classification scheme to that outlined above, however, lamproites are not included (Streckheisen, 1978).

Application of the Rock's (1977) classification scheme to the Coldwell lamprophyres suggests that these are alkaline lamprophyres, since they are closely associated with the sodic alkaline rocks (nepheline syenites and gabbros) of the Coldwell Complex. This conclusion is supported by a more detailed application of the various criteria given by Rock (1977) in the following section. The general characteristics of the alkaline lamprophyres as distinct from those listed above are given in Table 3.14. This sub-group encompasses three important rock types (camptonite, monchiquite and sannaite) and one rare type (tannbuschite), which are

Table 3.14 General Characteristics of the Alkaline Lamprophyres (Summarized from various sources by Rock, 1977)

1. Association

Sodic alkaline rocks, particularily alkali basalts, gabbro-syenite complexes, and, to a lesser extent, carbonatites.

2. Nomative Character

93% of analyses in the literature have normative nepheline; more would if unoxidised, and some have normative kalsilite.

3. Megacrysts/xenoliths

Alkali feldspar (high/medium T structures) common; augite, kaersutite and apatite megacrysts less common; lherzolite xenoliths very rare.

4. Ocelli

Extremely common, containing feldspathoids and/or carbonate minerals

5. Petrogenesis

Generally considered to be volatile enriched basaltic magmas; $^{87}Sr/^{86}Sr$ ratios generally indicate a mantle origin (i.e. no involvement of crustal material)

Table 3.15 Mineralogical Distinction of Types of Alkaline Lamprophyres (After Rock, 1977)

Rock Type	Feldspar Mineralogy	Mafic Mineralogy
Camptonite	Plag(Lab/And)>Akf	Amph+Bio±Ti±Ol
Sannaite	Akf>Plag	Amph+Bio±Ti±Ol
Monchiquite	None(isotropic-base in groundmass with with microlititic Fsp,Fsptd,etc.)	Amph+Bio±Ti±Ol
Tannbuschite	Fsptd(Ne)>Fsp	Amph+Bio±Ti±Ol

Key

Plag=plagioclase, Lab=labradorite, And=andesine, Amph=barkevekite or kaersutite, Bio=biotite, Ti=titanaugite, Ol=olivine, Akf=alkali feldspar, Fsp=feldspar, Fsptd=feldpspathoid, Ne=nepheline

Table 3.16 Chemical Screen for Alkaline Lamprophyres (After Rock, 1977)

Major and Minor Element Criteria

Oxide	Weight %
SiO_2	38-47
TiO_2	<6
Al_2O_3	8-20
Total Fe	<15
Alkalis (each)	<6
P_2O_5	<3
Volatiles	no restriction

Normative Criteria

Normative Parameter	Weight %
Ne	>0
Or	20-25
Ol	20-25
C and Wo	0
He	no restriction (should be 0)
An/(Ab+An)	no restriction

distinguished largely on the basis of differences in felsic mineralogy, as shown in Table 3.15. Essentially, in the case of camptonites, plagioclase dominates over alkali feldspar while in the case of sannaites the reverse is true. Monchiquites contain little or no primary feldspar at all and they are characterized by a groundmass with a glassy (i.e. optically isotropic) base (see below). Tannbushcites contain feldspathoids (i.e. nepheline) which dominate, in terms of abundance, over feldspar. The mafic mineralogy of the various types is more difficult to characterize, largely due to inconsistencies in descriptions given by previous authors; Rock (1977) gives the important obervations concerning the mafic mineralogy of the alkaline lamprophyres as summarized in Table 3.15, and described below:

a) Olivine is reported only as a phenocryst phase, and is commonly resorbed;

b) Orthopyroxene is not an equilibrium phase;

c) Olivine, biotite and clinopyroxene are more abundant in monchiquites than camptonites, while in the case of amphibole the opposite is true; and

d) Although a sub-type of monchiquite lacking primary olivine called fourchite is described in the literature, its use is superfluous (i.e. the type monchiquite is olivine-free); the terms camptonite and monchiquite are

therefore adequate regardless of the presence or absence of olivine. Note, however, that Streckheisen (1978) has retained the term fourchite. This latter author has developed a version of the QAPF diagram which distinguishes the various types of alkaline lamprophyres, as well as lamprophyre types from the calc-alkaline sub-group, on the basis of modal abundance of quartz, alkali and plagioclase feldspar and feldspathoids (see Figure 3.17).

In terms of their chemistry, a screen for the alkali lamprophyres has been proposed by Rock (1977), which incorporates both whole rock major and minor element abundances and normative information (see Table 3.16). No such screen exists to distinguish between the various alkaline lamprophyre types because of the considerable overlap in chemical composition among them. This is emphasized by the work of Rock (1977), which employs discriminant analysis in an attempt to separate the various alkaline lamprophyres in general, and camptonites and monchiquites in particlular, on the basis of major and minor element chemistry. Due to the chemical similarity of the various types, no such separation proved possible given the available data (Rock, 1977). Therefore, while it is possible to distinguish the alkaline lamprophyres from the other sub-groups on the basis of chemistry, it is not possible to

make a similar distinction between the different types of alkaline lamprophyres.

Application of the Conventional Classification to the Coldwell Lamprophyres

An empirical classification according to the general criteria of Rock (1977) of the Coldwell lamprophyres suggests that they are members of the alkaline sub-group for the following reasons:

a) The lamprophyres are closely associated with the sodic alkaline rocks (nepheline syenites and gabbros) of the Coldwell complex.

b) According to Rock (1977), the alkaline lamprophyres are compositionally equivalent to alkali basalts or basanites. Analysis 13 in Table 3.1 is a typical alkali basalt from Carmichael et al (1974). Comparison of the various analyses of Coldwell lamprophyres in Table 3.1 with this alkali basalt shows the following:

i) With the exception of the quartz-bearing variety, the various Coldwell lamprophyres are similar to the alkali basalt in terms of SiO_2 content. The former type is strongly

enriched in silica due to the presence of free quartz.

ii) The Coldwell lamprophyres are enriched in terms of K_2O, P_2O_5 and volatile compenents (CO_2 and H_2O), and slightly depleted in terms of MgO and TiO_2, relative to the alkali basalt.

iii) The other oxides are generally similar in content among the Coldwell lamprophyres and the alkali basalt.

The enrichment in terms of volatile components of the Coldwell lamprophyres relative to the alkali basalt noted in (ii) above is in good agreement with the observations of Rock (1977); this author suggests that lamprophyres may represent basaltic magmas which did not undergo volatile loss during evolution and emplacement. The relative variation in terms of K_2O, P_2O_5 and MgO contents suggest that the lamprophyres may be evolved assemblages in comparison to the alkali basalt. Otherwise, the correspondence between the major element chemistry of the Coldwell lamprophyres and the alkali basalt is reasonably close, which is in good agreement with the observations of Rock (1977).

c) Application of the major and minor element data for the lamprophyres to the chemical screen given in Table 3.16

(Rock, 1977) shows that, generally, the chemistry of the clinopyroxene, ocellar, amphibole and isotropic-base lamprophyres satisfies the listed criteria such that the hypothesis that these rocks are alkaline lamprophyres seems reasonable. Deviations from this are as follows:

i) Of the 33 compositions involved, 14 exceed the value given by Rock (1977) for the SiO_2 criteria; however, the excess is, in 7 of those 14 cases less than 1%, and in only 2 cases exceeds 2%. Since Rock's (1977) screen is based largely on previous work, it is inferred that the Coldwell lamprophyres are slightly more silica-rich than previously analysed examples.

ii) 3 of the 33 analyses exceed the total Fe criteria; however, only in one case is this excess greater than 1%.

The quartz lamprophyres do not fulfill the criteria for SiO_2 and normative nepheline, as would be expected for a rock containing free quartz. However, all of the other conditions of the screen are satisfied for these rocks. Therefore, it is reasonable to consider these rocks also to be alkaline lamprophyres.

Figure 3.17 is the modified QAPF diagram of Streckheisen (1978), on which the appropriate data for the Coldwell lamprophyres is plotted. This diagram shows that the various rock types distinguished on the basis of petrographic analysis form coherent clusters of points, suggesting the following conventional nomenclature:

a) The clinopyroxene lamprophyres plot as sannaites, due to the dominance of modal alkali feldspar over plagioclase.

b) The ocellar and amphibole lamprophyres plot as camptonites (or monchiquites), due to the virtual lack of modal alkali feldspar in these types. However, classifying these types as monchiquites is ruled out on the basis of oberved petrography (i.e. lack of an isotropic constituent dominating the groundmass mineralogy).

c) The isotropic-base lamprophyres can not be plotted directly on Figure 2.17, due to the virtual lack of modal feldspar. However, the presence of the isotropic base in the groundmass suggests that these are monchiquites, since they are known to be alkaline lamprophyres.

d) The quartz lamprophyres plot on an anomalous portion of the diagram as a result of the abundance of modal quartz

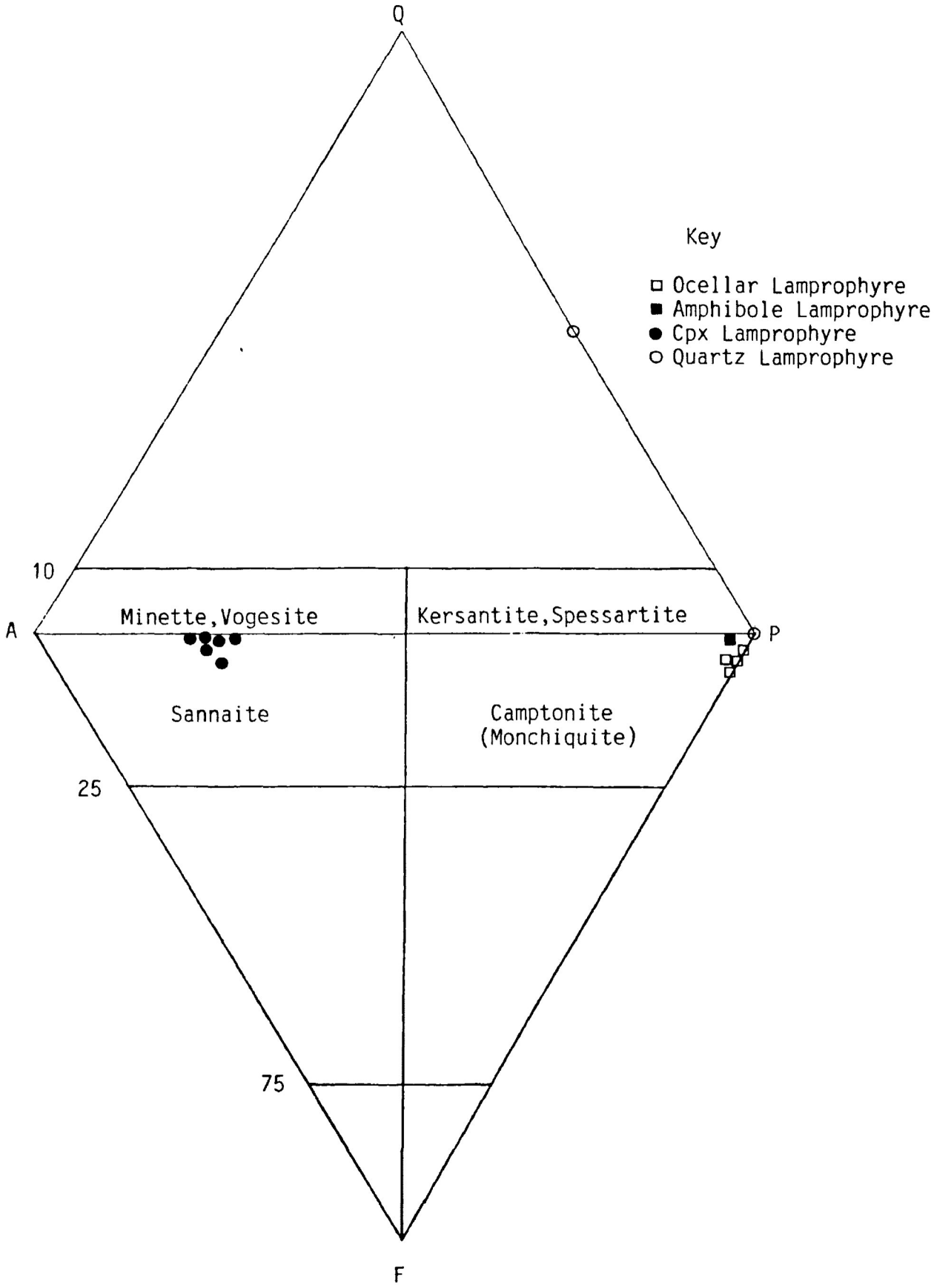

Figure 3.17 QAPF Diagram for Lamprophyres after Streckheisen (1978) with data for Coldwell lamprophyres plotted

in this rock type. However, the quartz lamprophyres fulfill all of the various mineralogical and chemical criteria to be classified as alkaline lamprophyres (see above), so that if the quartz is ignored, and these rocks are plotted onto Figure 3.17 only on the basis of modal feldspar abundance, then they plot as camptonites.

The poor separation among the various types of alkaline lamprophyres, especially camptonites and monchiquites, on the basis of their chemistry (Rock, 1977) has already been noted. With application of conventional nomenclature to the Coldwell lamprophyres (see above), similar conclusions to those of Rock (1977) are drawn, in that no reliable separation is achieved among the various Coldwell camptonites and monchiquites by MDA (see the preceding section dealing with MDA).

CHAPTER 4- MINERALOGY

CLINOPYROXENE

Paragenesis

Table 4.1 summarizes the optical and physical properties of the clinopyroxene occurring in each type of dyke rock. In the lamprophyres, it occurs as both a phenocryst and a groundmass phase. Phenocrysts are large, ranging from 2.0mm to 15.0mm in the sannaites, and from 1.0mm to 3.0mm in the other lamprophyres; they are typically subhedral to euhedral. In the case of the sannaites, clinopyroxene phenocrysts are distinctly zoned or mantled, in that a subhedral to rounded anhedral colourless or pale-brown core is surrounded and embayed by a euhedral, slightly pleochroic green (alpha=green, beta=gamma=pale green or colourless) or non-pleochroic pink-brown rim. The embayment may represent resorption of the core material (Scott, 1980; Clarke et al, 1983). The rim zone, in turn, commonly displays a complex pattern of small scale (0.05mm to 0.1mm) oscillatory zoning resulting from rhythmic changes in the shade of the green colour. The reverse situation, in which a pale green core is surrounded and embayed by a colourless rim, is also observed, commonly in phenocrysts from the same rock. Rarely, a

Table 4.1 Optical and Physical Properties of Clinopyroxenes

Rock Type	Size Range	Mean Size	Colour	Pleochroism	Twinning	2V
Sannaite						
Phenocryst	5-15mm	7mm	core:colourless	none	(100)	55-60
			rim:pale green	weak	(100)	50-56
Groundmass	0.2-2mm	0.8mm	pale green	nil-weak	none	
Ocellar Lamprophyre						
Phenocryst	1-5mm	3mm	core:variable	none	(100)	52-55
			rim:green,pink	nil-weak	(100)	52-57
Groundmass	0.1-0.5mm	0.2mm	pale green,pink	nil-weak	none	
Monchiquite						
Phenocryst	1-3mm	1mm	core:variable	none	(100)	54-57
			rim:green,pink		(100)	52-62
Groundmass	0.3-0.5mm	0.4mm	pale green,pink	nil-weak	none	
Amphibole Lamprophyre						
Phenocryst	1-6mm	4mm	core:variable	none	(100)	57-63
			rim:green,pink	nil-weak	(100)	56-66
Groundmass	0.1-0.5mm	0.4mm	pale green,pink	nil-weak	none	
Quartz Lamprophyre						
Phenocryst	1-5mm	3mm	core:variable	none	(100)	51-54
			rim:pink,brown	none	(100)	52-54
Groundmass	0.1-0.4mm	0.3mm	pale brown,pink	none	none	
Tinguaite						
Groundmass	0.1-0.2mm	0.2mm	deep green,yellow	strong	none	

concentric oscillation of zones with one repetition of the above cycle is observed. Similar patterns of zoning are observed in clinopyroxenes from lamprophyres from Ubekendt Ejlend (Clarke et al, 1983) and the Gran region, Norway (Scott, 1980). In the other lamprophyres, clinopyroxene phenocrysts similar to those observed in the sannaites are occasionally noted. These most commonly are unzoned and colourless, grey, pale green, or, rarely, pale pink or brown (particularily in the case of the clinopyroxene phenocrysts occurring in the quartz camptonites), or display only a thin, unzoned, colourless or pleochroic pale green (alpha=pale green, beta=gamma=colourless) rim around a subhedral to euhedral core. In a few instances, a dark green (alpha=dark green, beta=gamma=green or pale green) or pale pink rim is observed. In all cases, contacts between zones are sharp. Hourglass zoning is sometimes superimposed upon the concentric colour zoning, particularily in the case of large (2.0-10.0mm) crystals. Twinning is common parallel to (100), and less common parallel to (110).

Groundmass clinopyroxene in all lamprophyres consists of small (0.1mm to 0.5mm) subhedral to anhedral crystals generally similar in appearance to the rim zones of corresponding phenocrysts; i.e. generally colourless or pale to medium green grains, the green-coloured variety being

slightly pleochroic (alpha=green, beta=gamma=colourless or pale green). Measurement of the optical properties of groundmass clinopyroxene is made difficult by the small grain size and commonly advanced state of alteration (see below).

Clinopyroxene in the tinguaites occurs exclusively in the groundmass, as pleochroic dark green or blue-green acicular crystals 0.1mm or less in size, either individually or as fine aggregates intersitital to the phenocryst phases. Rarely, crystals as long as 1.0mm are observed. Pleochroism is intense (alpha=deep green-blue, beta=pale green or green, gamma=colourless or yellow). No twinning or zoning is observed in these crystals, and optical properties are difficult to quantify as a result of the generally small grain size and strong absorption colours.

Composition

Table 4.2 lists representative compositions of clinopyroxenes from Coldwell dyke rocks. All data utilized in this study are given in Appendix B. Compositions were determined by electron microprobe analysis as outlined in Appendix A. The Fe3+ content of the pyroxenes was estimated from the microprobe data using the method of Hamm and St

Table 4.2 Representative clinopyroxene analyses

Rock Type	Sannaite				Ocellar Camptonite					Amphibole Camptonite			
	normal zoning			ground-	normal zoning		reversed zoning		ground-	normal zoning			ground-
Oxide Wt%	core		rim	mass	core	rim	core	rim	mass	core		rim	mass
SiO2	53.51	52.91	51.68	51.42	49.14	45.13	49.73	48.08	48.52	48.62	48.86	48.28	48.67
Al2O3	2.18	2.62	4.21	3.38	5.87	8.72	4.28	6.46	6.45	6.38	6.33	5.88	6.68
TiO2	0.14	0.15	0.39	0.08	0.92	2.67	1.23	0.46	1.40	1.03	1.10	1.22	1.41
Fe2O3	1.72	2.59	5.17	4.40	3.38	6.17	4.18	3.92	4.49	4.03	3.65	3.64	3.77
FeO	1.08	0.14	2.17	3.81	2.17	2.59	8.99	3.05	3.03	4.46	1.59	4.21	3.67
MgO	17.98	17.59	12.94	12.89	14.44	11.44	9.46	13.40	13.01	12.30	14.03	12.69	13.00
CaO	22.60	22.09	21.76	21.93	22.02	22.10	20.75	21.90	21.07	21.25	22.51	21.91	22.09
Na2O	0.28	0.34	1.54	1.25	0.60	0.58	1.43	0.72	0.85	0.94	0.31	0.59	0.51
K2O	0.02	0.02	0.05	0.04	0.00	0.00	0.00	0.00	0.00	0.00	0.00	0.05	0.00
MnO	0.05	0.07	0.22	0.23	0.09	0.12	0.43	0.28	0.16	0.00	0.07	0.00	0.00
Cr2O3	0.84	1.59	0.87	0.04	0.35	0.03	0.04	0.07	0.04	0.00	1.01	0.00	0.05
Sum	100.40	100.11	101.00	99.47	98.98	99.55	99.82	98.97	99.02	99.01	99.46	98.47	99.85
Structural Formula Based On 6 Oxygens													
Si	1.937	1.922	1.904	1.916	1.833	1.709	1.902	1.807	1.810	1.833	1.815	1.824	1.813
Al(iv)	0.063	0.078	0.096	0.084	0.167	0.291	0.098	0.193	0.190	0.168	0.185	0.176	0.187
Al(vi)	0.030	0.034	0.097	0.064	0.091	0.098	0.095	0.093	0.095	0.116	0.092	0.086	0.106
Ti	0.004	0.004	0.011	0.022	0.026	0.076	0.013	0.035	0.040	0.029	0.031	0.035	0.040
Fe3+	0.043	0.079	0.159	0.137	0.105	0.196	0.134	0.123	0.000	0.127	0.113	0.115	0.117
Fe2+	0.042	0.004	0.067	0.119	0.068	0.082	0.288	0.096	0.236	0.141	0.049	0.149	0.114
Mg	0.970	0.953	0.711	0.716	0.803	0.646	0.539	0.751	0.727	0.691	0.777	0.715	0.722
Ca	0.877	0.860	0.859	0.875	0.880	0.897	0.850	0.882	0.872	0.853	0.896	0.887	0.882
Na	0.020	0.024	0.110	0.090	0.043	0.043	0.106	0.050	0.062	0.069	0.022	0.043	0.037
K	0.001	0.001	0.002	0.002	0.000	0.000	0.000	0.000	0.000	0.000	0.000	0.002	0.000
Mn	0.002	0.002	0.007	0.007	0.003	0.004	0.014	0.004	0.005	0.000	0.002	0.000	0.000
Cr	0.039	0.039	0.025	0.001	0.010	0.001	0.001	0.003	0.001	0.000	0.030	0.000	0.002

Table 4.2 (Continued)

Rock Type	Monchiquite			Quartz Camptonite		
	Normal Zoning			Normal Zoning		
Oxide Wt%	core	rim	ground-mass	core	rim	ground-mass
SiO2	52.26	44.50	46.90	50.11	50.22	52.00
Al2O3	3.22	7.02	6.36	3.64	3.40	3.96
TiO2	0.19	2.42	1.48	0.56	0.57	0.37
Fe2O3	5.58	2.29	3.06	2.56	2.30	2.08
FeO	4.23	11.69	9.44	8.98	9.30	4.68
MgO	11.44	9.61	10.36	14.48	14.15	18.38
CaO	21.55	21.85	21.18	18.28	18.46	17.62
Na2O	0.91	0.37	1.03	0.67	0.55	0.38
K2O	0.00	0.00	0.00	0.00	0.00	0.00
MnO	0.57	0.19	0.14	0.22	0.18	0.18
Cr2O3	0.00	0.00	0.00	0.00	0.00	0.57
Sum	99.95	99.94	99.95	99.50	99.13	100.22
Structural Formula Based On 6 Oxygens						
Si	1.924	1.750	1.814	1.889	1.900	1.894
Al(iv)	0.076	0.250	0.186	0.111	0.100	0.106
Al(vi)	0.065	0.077	0.105	0.051	0.052	0.064
Ti	0.005	0.071	0.043	0.016	0.016	0.010
Fe3+	0.171	0.076	0.101	0.081	0.073	0.634
Fe2+	0.130	0.386	0.297	0.283	0.294	0.143
Mg	0.626	0.566	0.602	0.814	0.798	0.998
Ca	0.850	0.921	0.879	0.738	0.748	0.688
Na	0.066	0.028	0.015	0.049	0.040	0.027
K	0.000	0.000	0.000	0.000	0.000	0.000
Mn	0.018	0.006	0.005	0.007	0.006	0.006
Cr	0.000	0.000	0.000	0.000	0.000	0.160

Figure 4.1a

CPX in Sannaites

Wo-En-Fs after Poldervaart and Hess (1951)

Di=Diopside
Hd=Hedenbergite
Sa=Salite
Au=Augite
Wo=Wollastonite
En=Enstatite
Fs=Ferrosilite

circles- phenocryst cores

triangles- phenocryst rims

crosses- groundmass grains

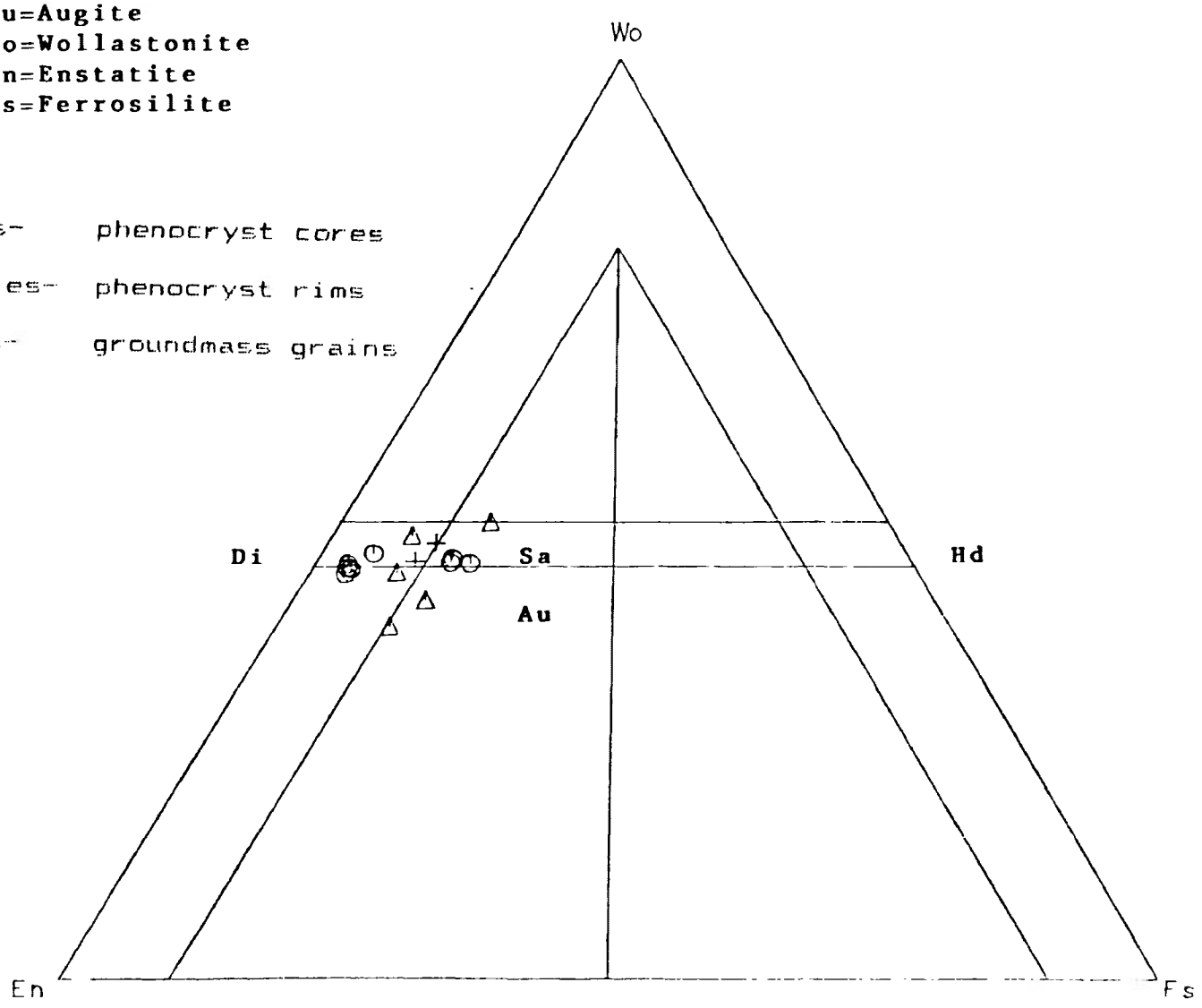

Figure 4.1b

CPX in Sannaites

Di=Diopside
Hd=Hedenbergite
Ac=Acmite

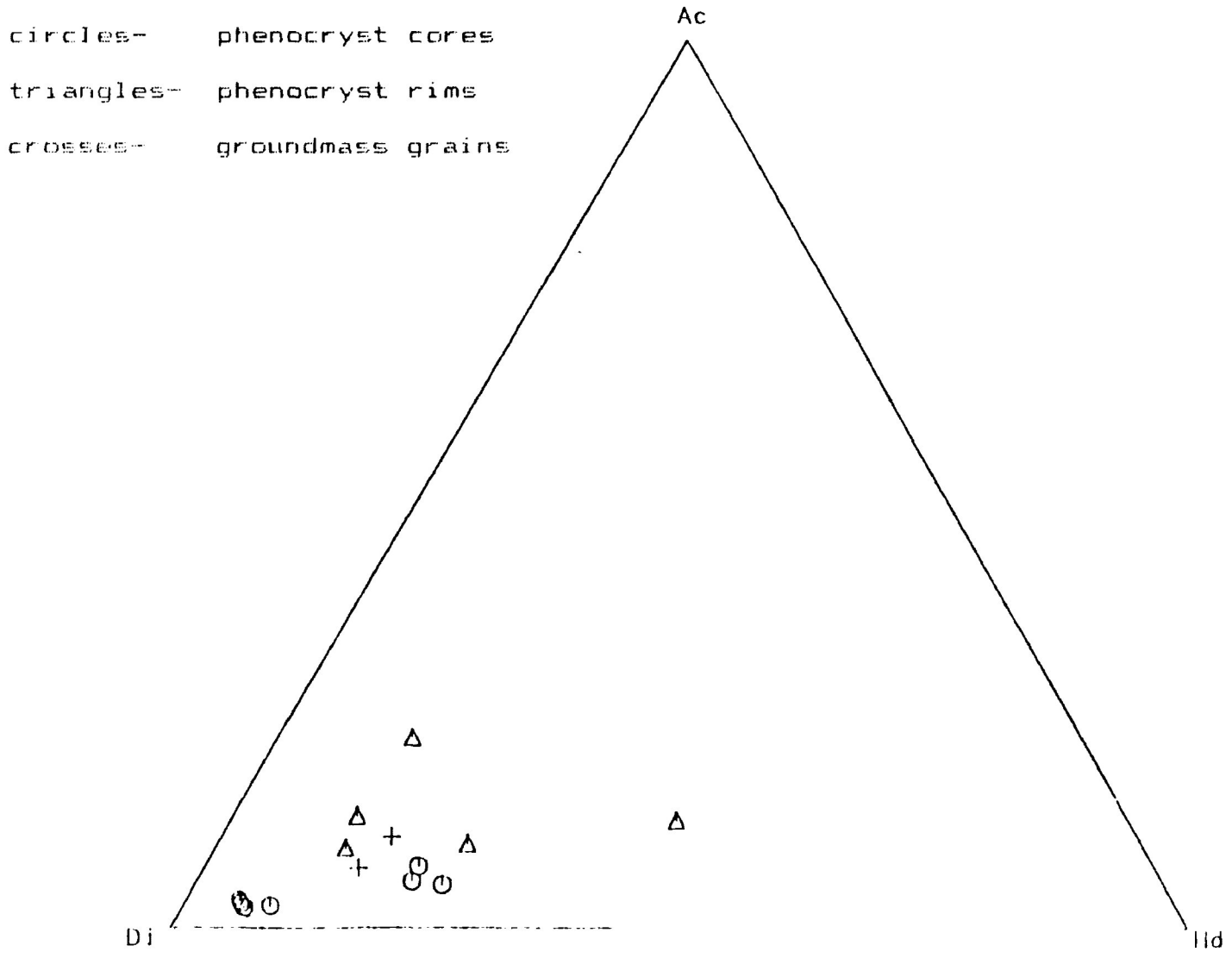

Figure 4.6a Total Fe vs Mg in Clinopyroxene Sannaites

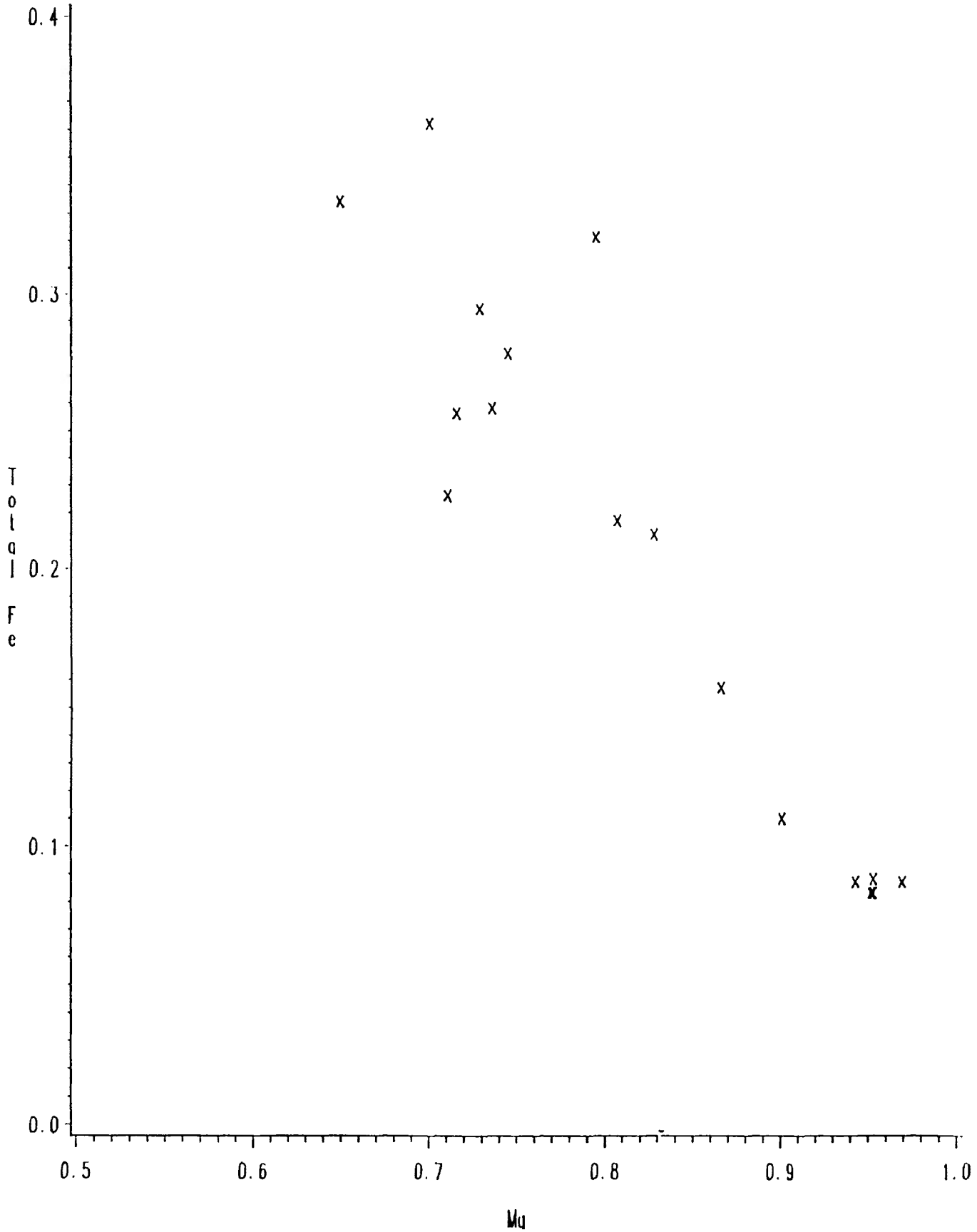

Figure 4.6b **Total Fe + Ti vs Mg in Clinopyroxene Sannaites**

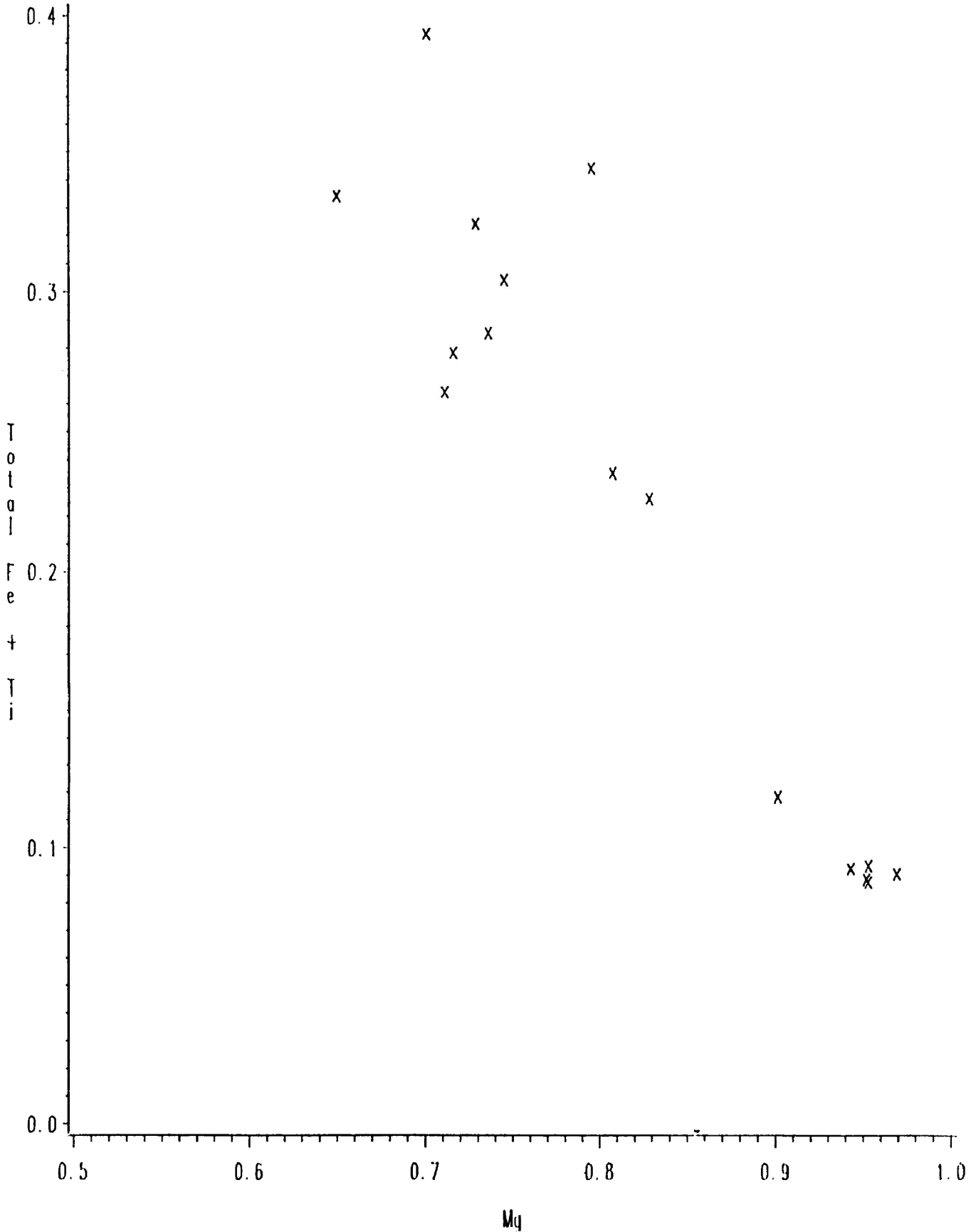

Figure 4.7a **Ti vs Total Al in Clinopyroxene Sannaites**

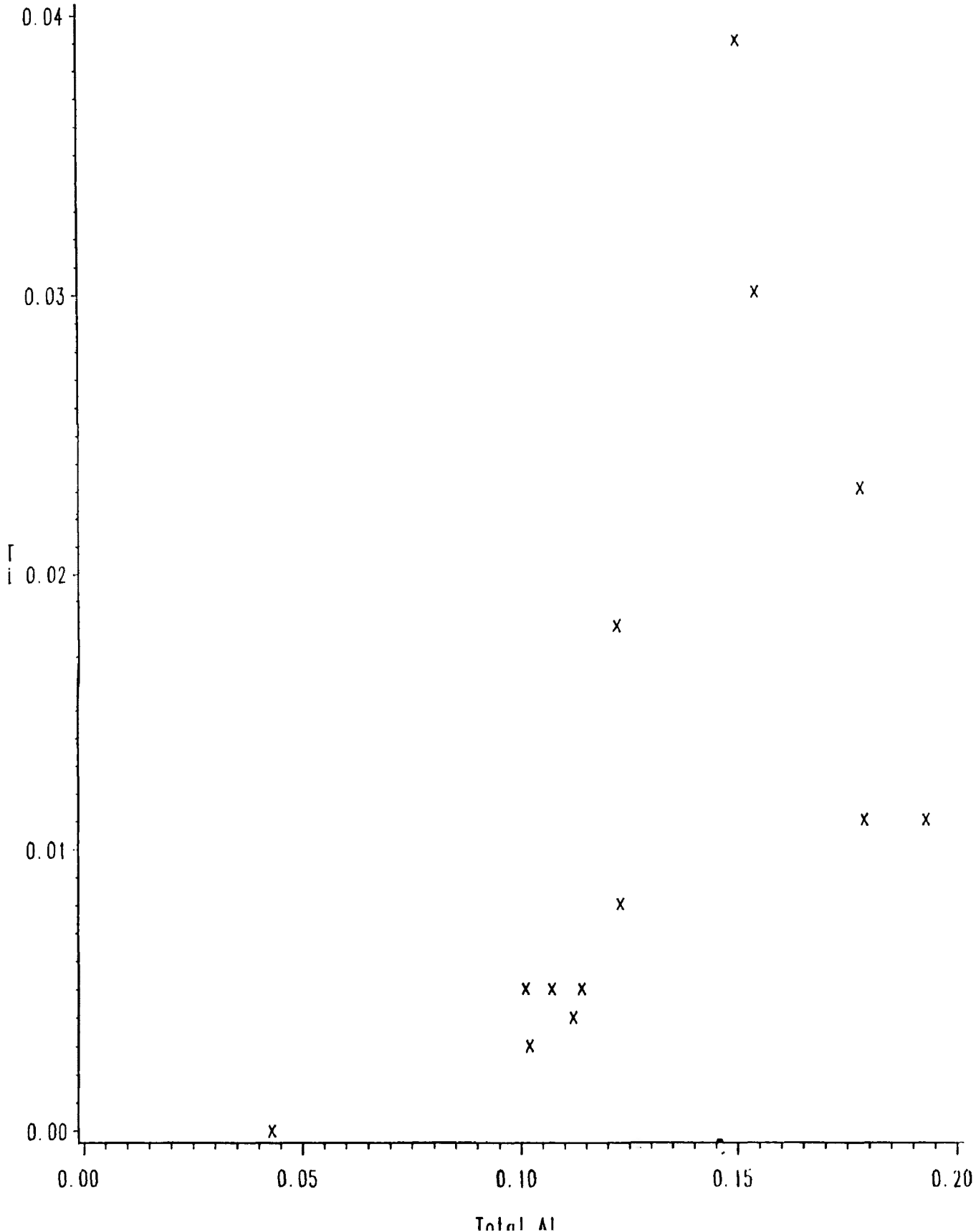

Figure 4.7b **Ti vs Al(iv) in Clinopyroxene Sannaites**

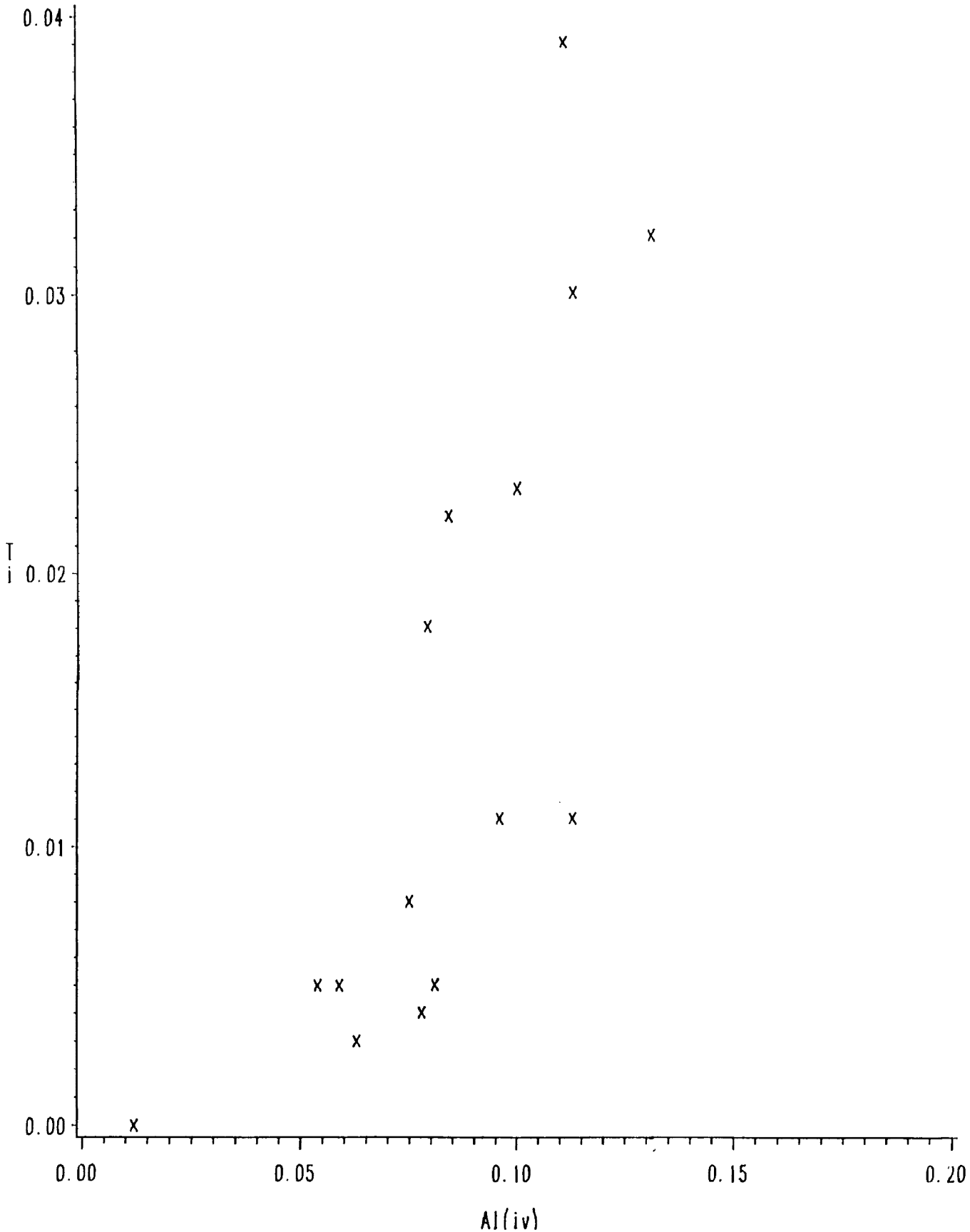

Vieten (1971) as summarized by Edwards (1976) (See Appendix A).

In Figures 4.1a to 4.5a representative pyroxene data for each type of lamprophyre are plotted in the ternary system $CaSiO_3$ (wollastonite)-$MgSiO_3$ (enstatite)-$FeSiO_3$ (ferrosilite) of Poldervaart and Hess (1951); in figures 4.1b to 4.5b data for the same clinopyroxenes are plotted in the ternary system $CaMgSi_2O_6$ (diopside)-$CaFeSi_2O_6$ (hedenbergite)- $NaFeSi_2O_6$ (acmite). Figure 4.1a shows that in the case of the sannaites, colourless or pale brown phenocryst cores are generally diopsidic ($Ca_{47}Mg_{45}Fe_8$), with pale green rims and groundmass grains tending towards salitic compositions ($Ca_{38}Mg_{44}Fe_{18}$). In Figure 4.6a total Fe is plotted against Mg (atoms per formula unit) for these pyroxenes in the manner of Scott (1980). Since the majority of the points approximate a straight line with a slope of 1, a simple substitution of Fe for Mg (in terms of end-member molecules, $CaFeSi_2O_6$ substituting for $CaMgSi_2O_6$) between the zones in these pyroxenes is sufficient to, for the most part, explain the mineralogical changes noted above. Since Ti and Al are observed to increase concurrently with Fe, while Si decreases (see Table 4.1), an additional component of the substitution may involve the hypothetical $CaTiAl_2O_6$ molecule (Scott, 1980), in conjunction with $CaFeSi_2O_6$. This coupled

substitution would be significant for those points which fall well below the line of unity slope on Figure 3.6a, as the addition of Ti to Fe on this plot will translate these points close to the line. This, however, causes the trend defined by all of the points to deviate from the line, worsening the fit (see Figure 4.6b). However, as noted by Scott (1980), not all of the Al involved in this substitution will necessarily be accounted for by $CaTiAl_2O_6$, as demonstrated in Figure 4.7a; an excess of Al over that required to satisfy the 2Al:1Ti ratio implicit in $CaTiAl_2O_6$ exists, of which a part is in tetrahedral coordination, as shown in Figure 4.7b. This likely reflects additional substitution of Tschermak's molecule ($CaAl_2SiO_6$) (Scott, 1980), which increases slightly as $CaTiAl_2O_6$ increases. Therefore, in these pyroxenes, $CaFeSi_2O_6$ plus varying but generally small amounts of $CaTiAl_2O_6$ and $CaAl_2SiO_6$ substitute for $CaMgSi_2O_6$ in the rim zones of normally zoned crystals. Figure 4.1b indicates that for the same phenocrysts, rims are also more acmitic than corresponding cores; groundmass grains are similarily acmitic. Increasing acmite ($NaFe^{3+}Si_2O_6$ end-member molecule) content is reflected in increasing abundances of Na and Fe^{3+} (see Table 4.2). Cr content is variable among phenocrysts, although in the case of individual phenocrysts in the sannaites it may approach 2% Cr_2O_3 by weight (i.e. 1.59 weight % Cr_2O_3 in a chrome-diopside phenocryst core in

specimen C1). Mn content is generally low, and, like Cr content, does not correlate well with any of the above chemical trends between zones of phenocrysts. K is not normally detected or is only present in trace amounts. Note that in those phenocrysts in which the colour zoning is reversed, the above compositional patterns are also reversed.

The clinopyroxenes of the ocellar camptonites, and those of the monchiquites, exhibit broadly similar behaviour to those of the sannaites in terms of compostional zoning, in that phenocryst rims and groundmass grains are generally more salitic and acmitic than phenocryst cores, which are usually diopsidic, or, in several cases, endiopsidic or augitic (see Figures 4.2 and 4.3 for plots of clinopyroxene analyses of ocellar camptonites, and monchiquites respectively). As noted above, rim zones tend to be narrower and more homogeneous than those of the sannaite clinopyroxenes. Rare pale pink or violet grains and phenocryst rim zones are titanaugite. In Figures 4.8 and 4.10, total Fe, and total Fe+Ti is plotted against Mg (atoms per formula unit) for the ocellar camptonites and monchiquites, as described for the sannaites above. Unlike the sannaites, however, in each case the addition of Ti to total Fe results in a better fit of the trend defined by the points to a line of unity slope. This suggests that a significant amount of $CaTiAl_2O_6$ is involved

Figure 4.2a
CPX in Ocellar Camptonites
Abbreviations as per Figure 4.1a

circles- phenocryst cores

triangles- phenocryst rims

crosses- groundmass grains

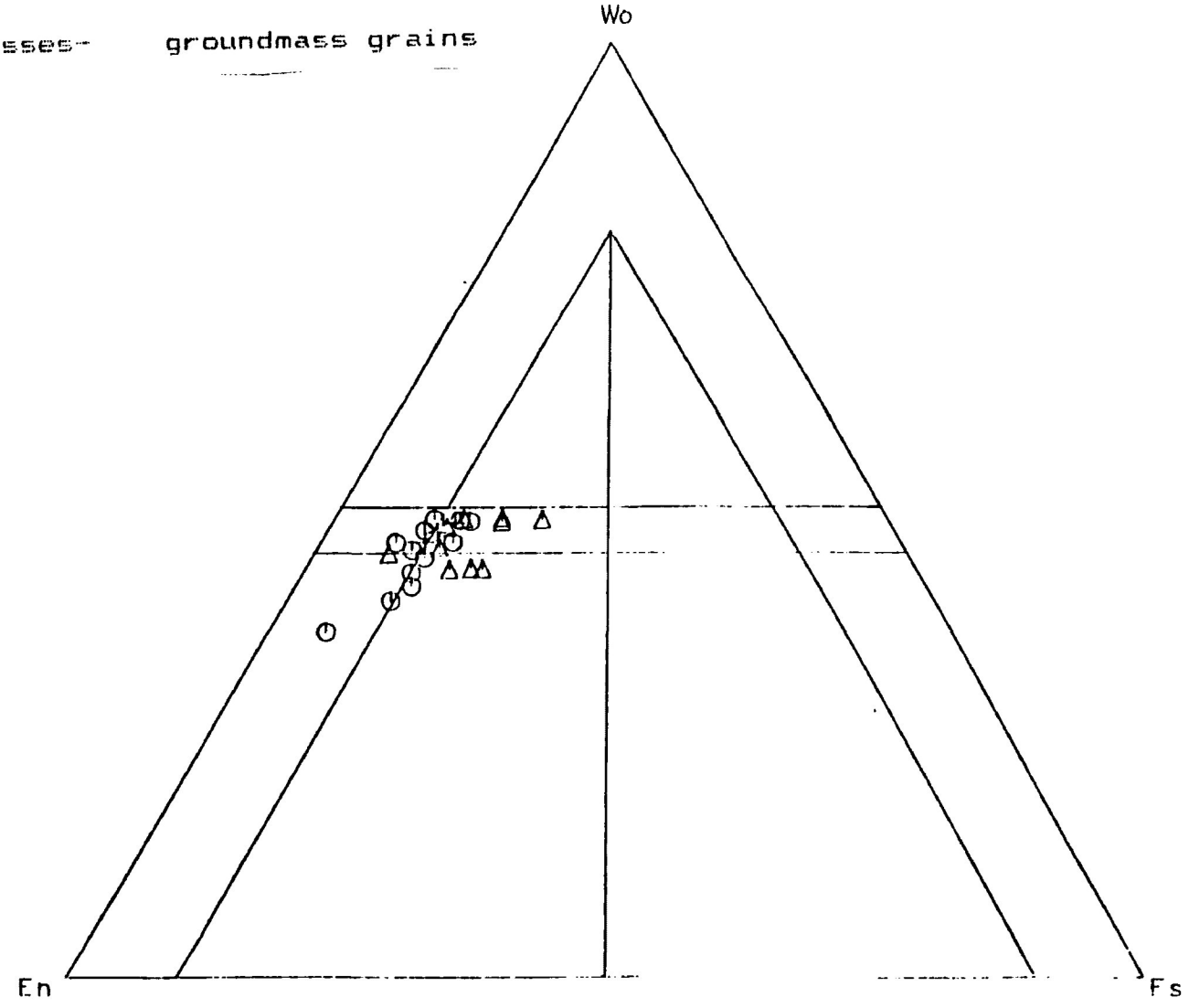

Figure 4.2b

CPX in Ocellar Camptonites

Abbreviations as per Figure 4.1b

circles- phenocryst cores

triangles- phenocryst rims

crosses- groundmass grains

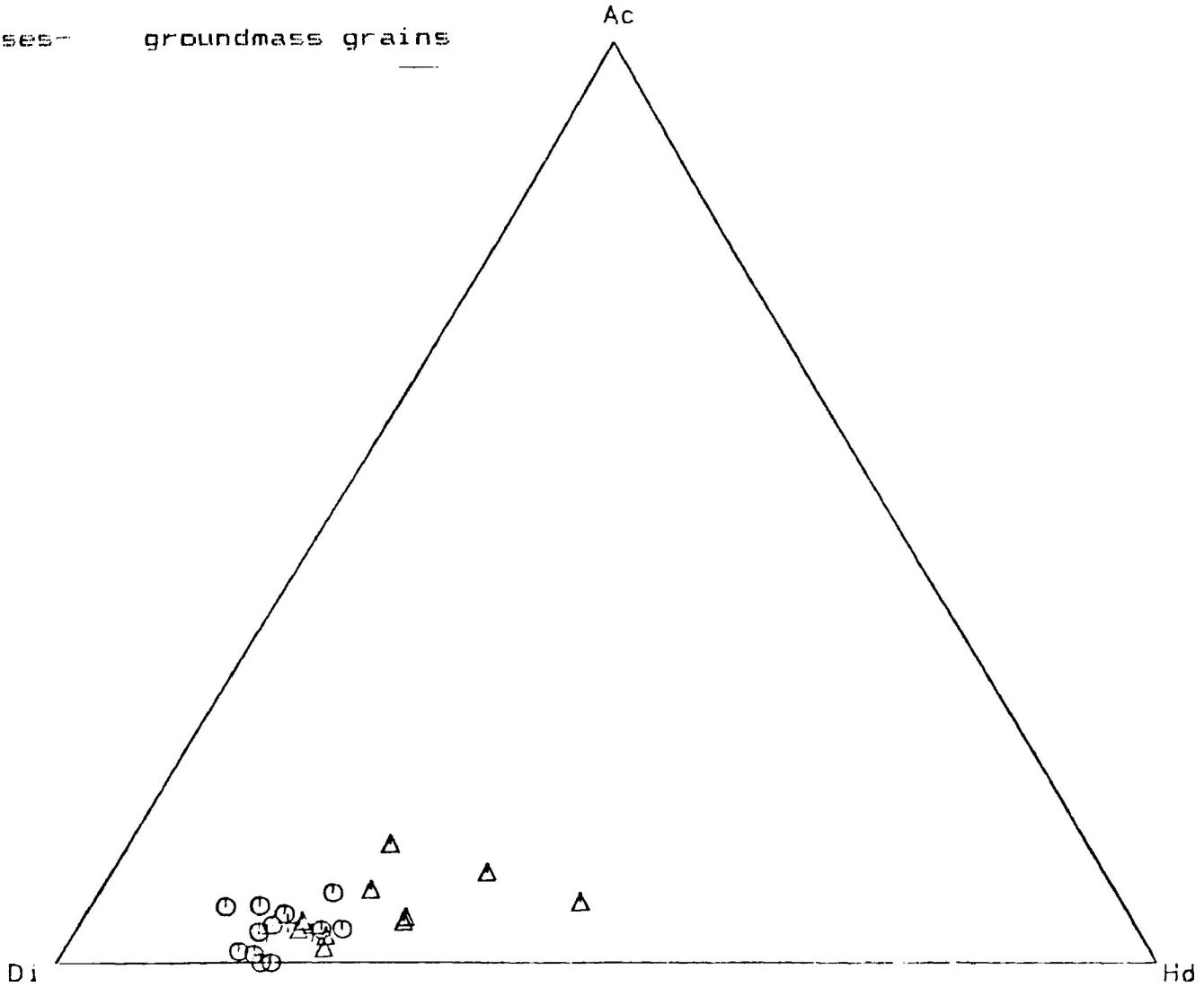

Figure 4.8a **Total Fe vs Mg in Clinopyroxene Ocellar Camptonites**

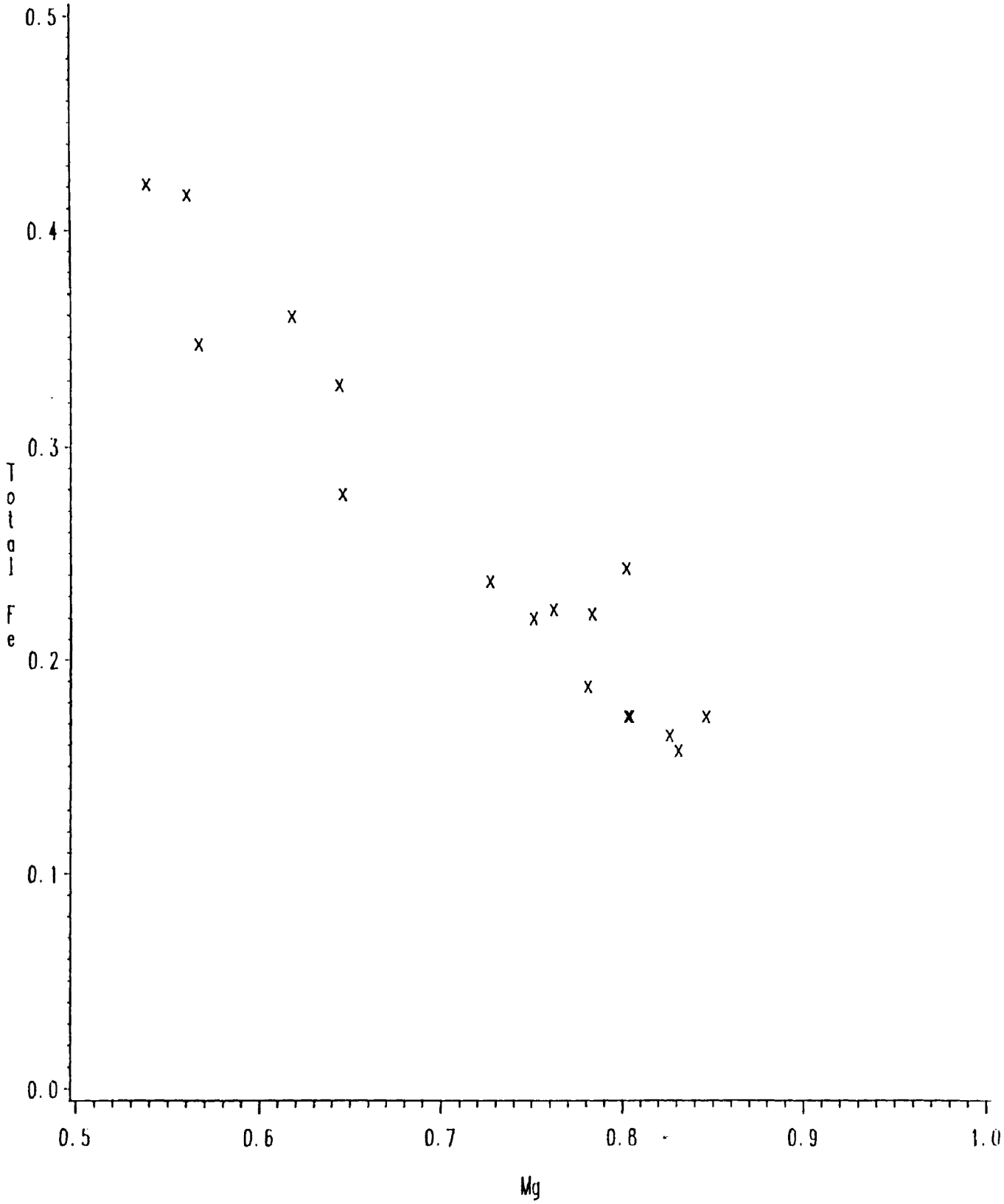

Figure 4.8b **Total Fe + Ti vs Mg in Clinopyroxene**
Ocellar Camptonites

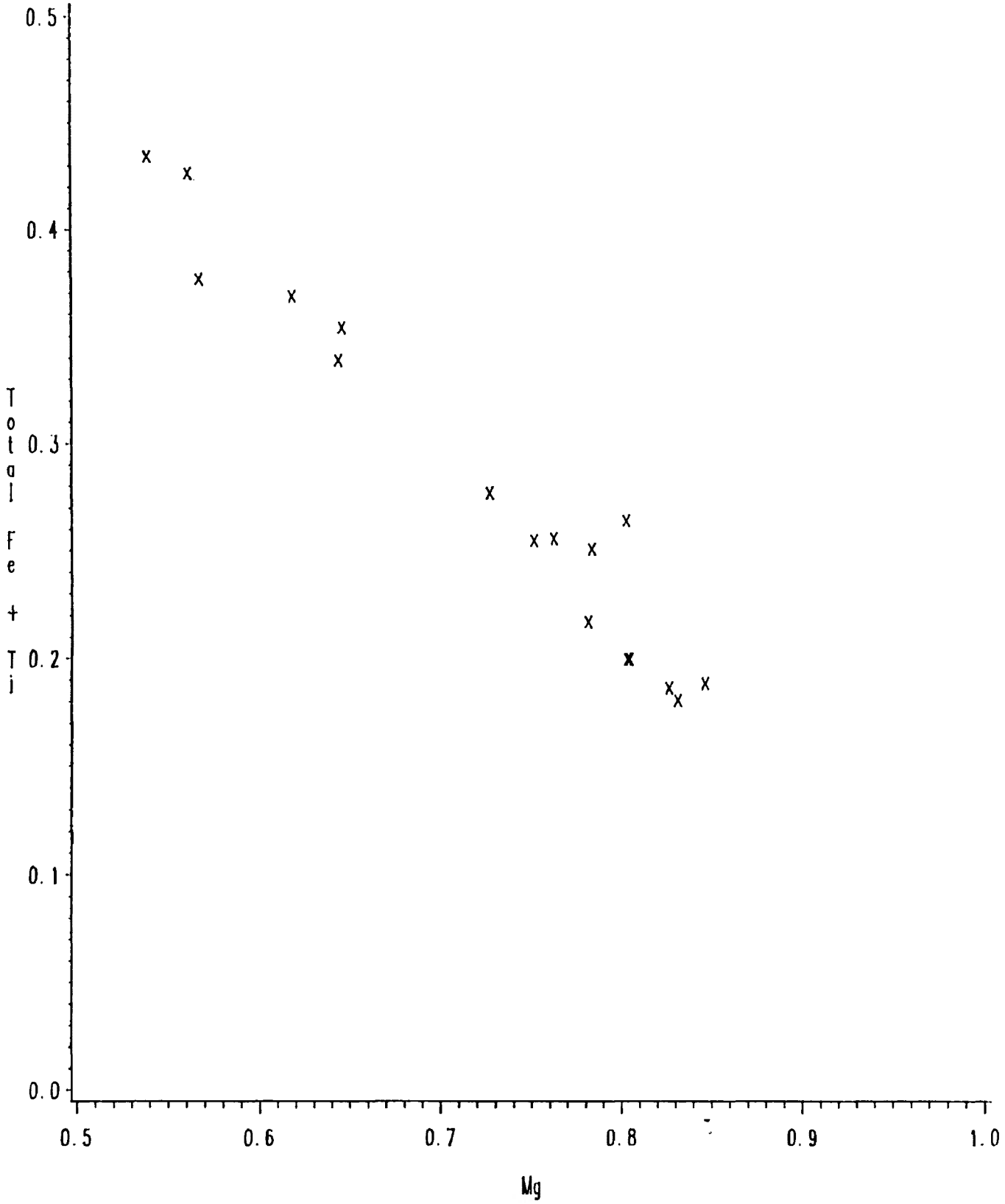

Figure 4.9a **Ti vs Total Al in Clinopyroxene Ocellar Camptonites**

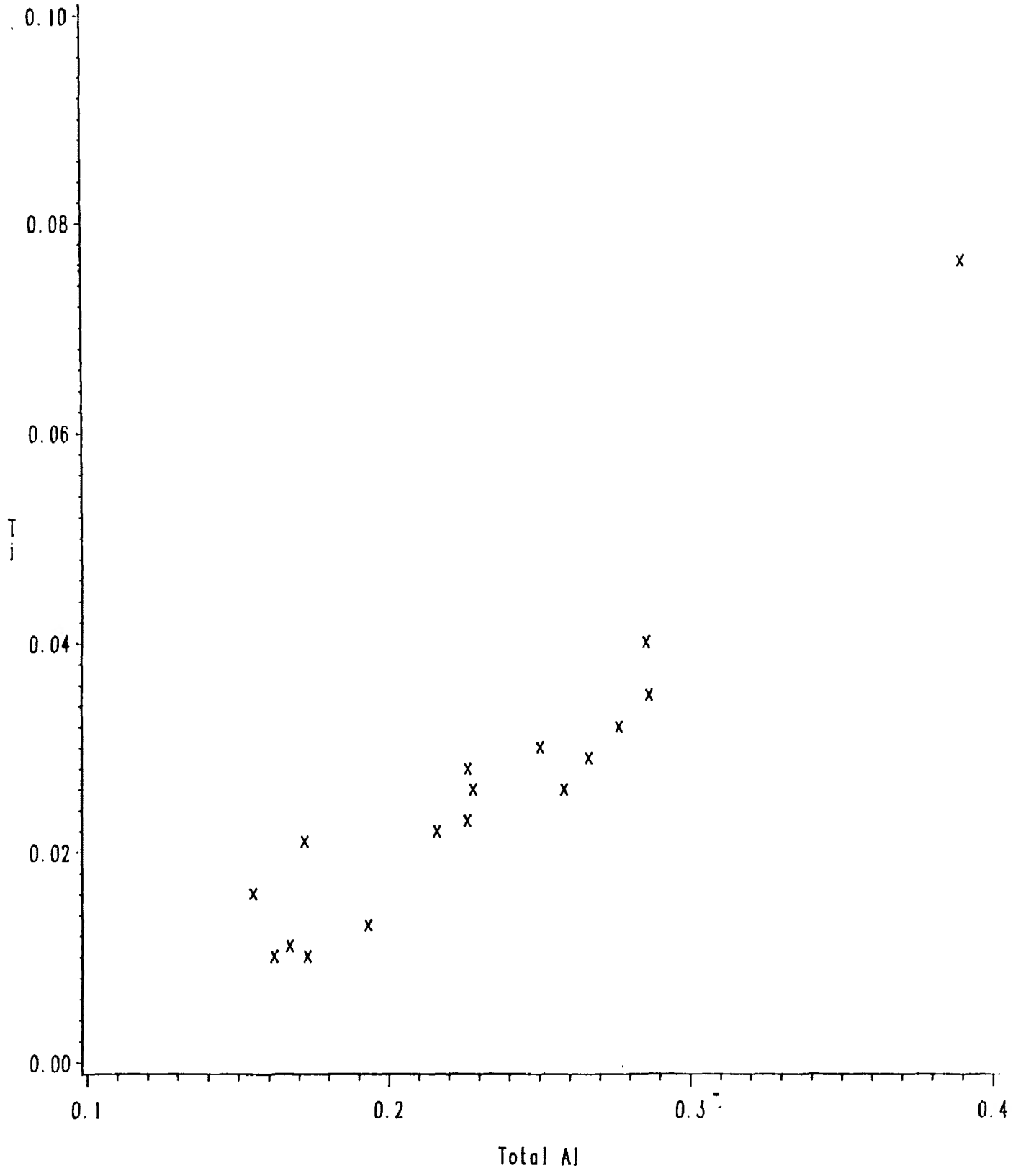

Figure 4.9b Ti vs Al(iv) in Clinopyroxene
Ocellar Camptonites

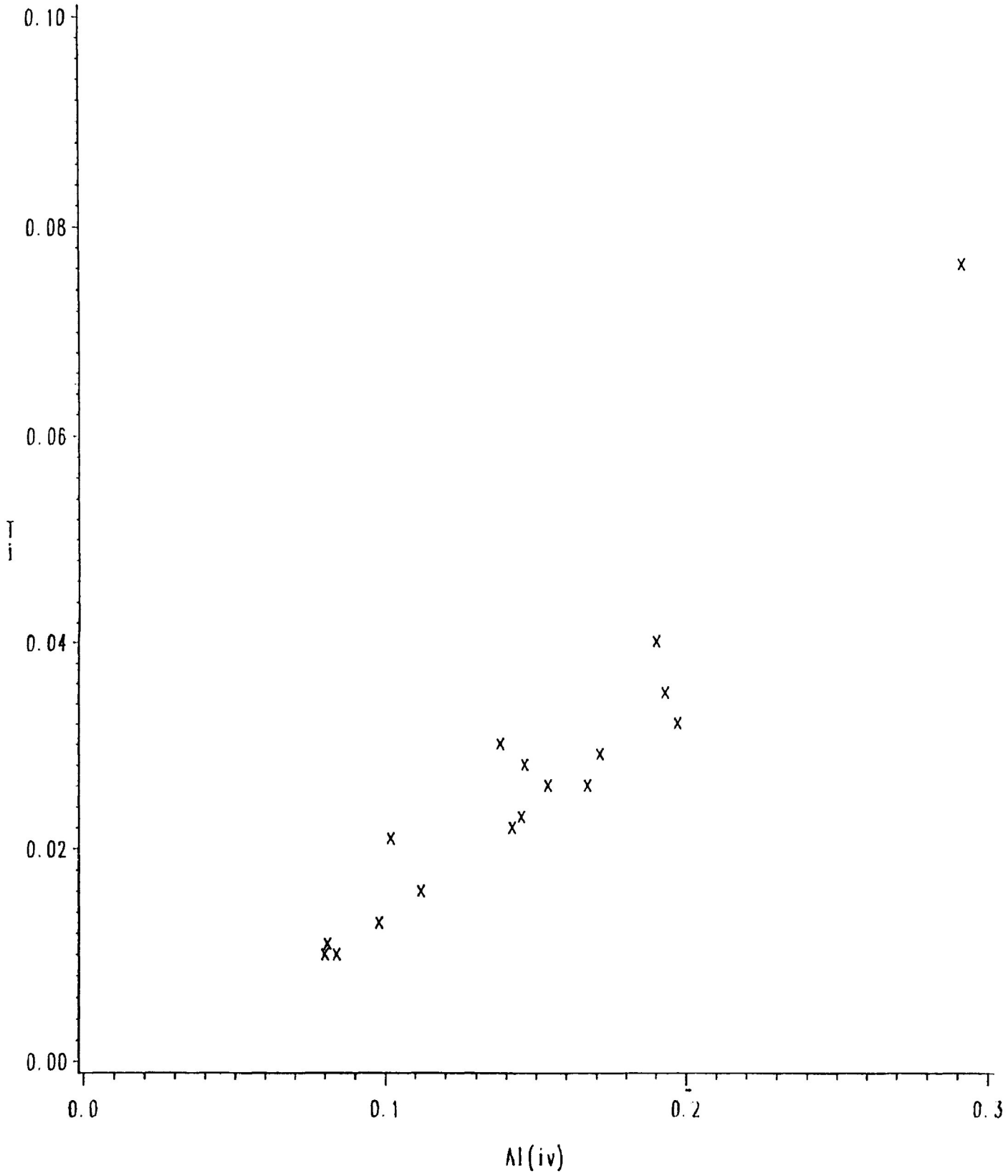

Figure 4.3a

CPX in Monchiquites

Abbreviations as per Figure 4.1a

circles- phenocryst cores

triangles- phenocryst rims

crosses- groundmass grains

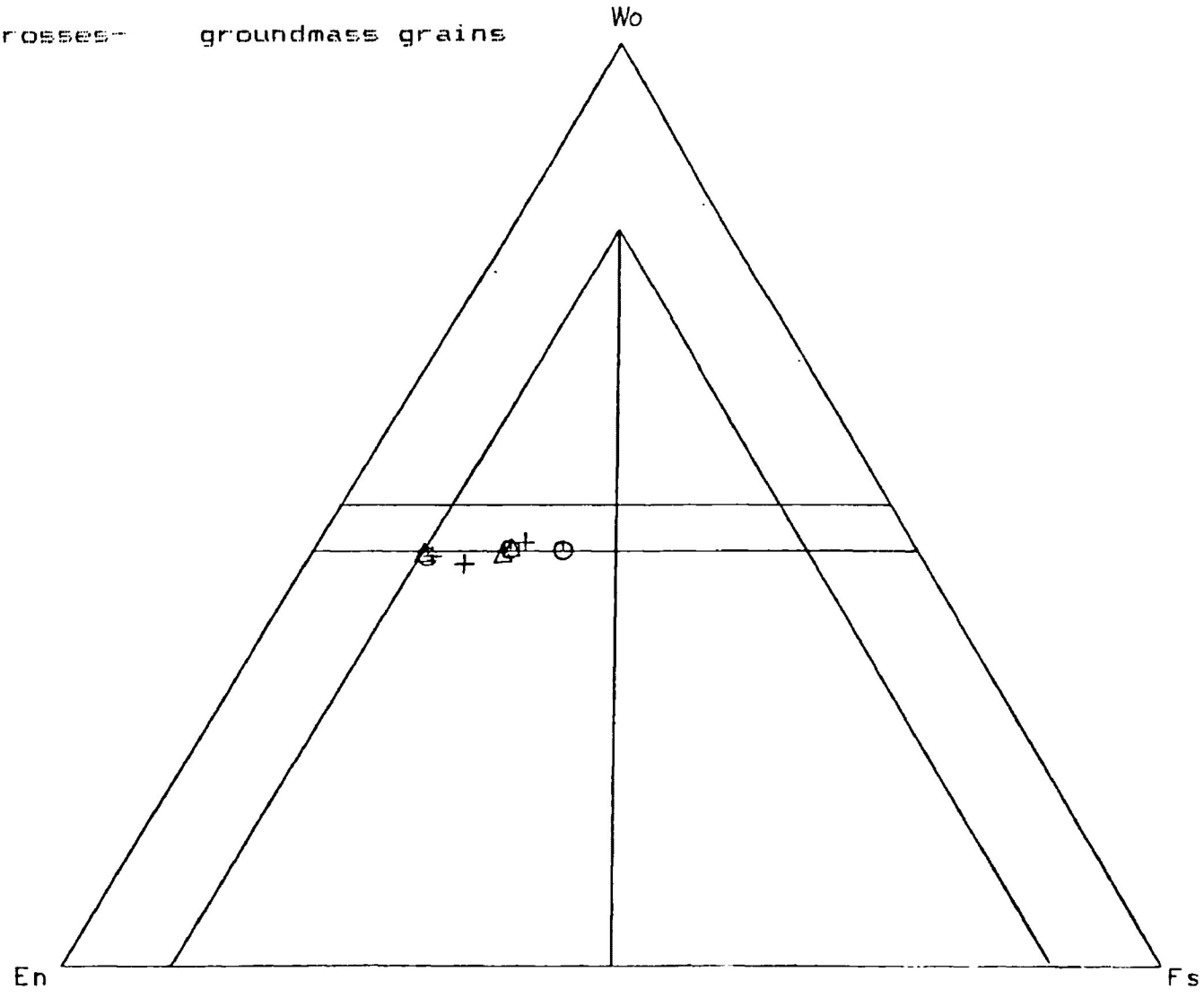

Figure 4.3b

CPX in Monchiquites

Abbreviations as per Figure 4.1b

circles- phenocryst cores

triangles- phenocryst rims

crosses- groundmass grains

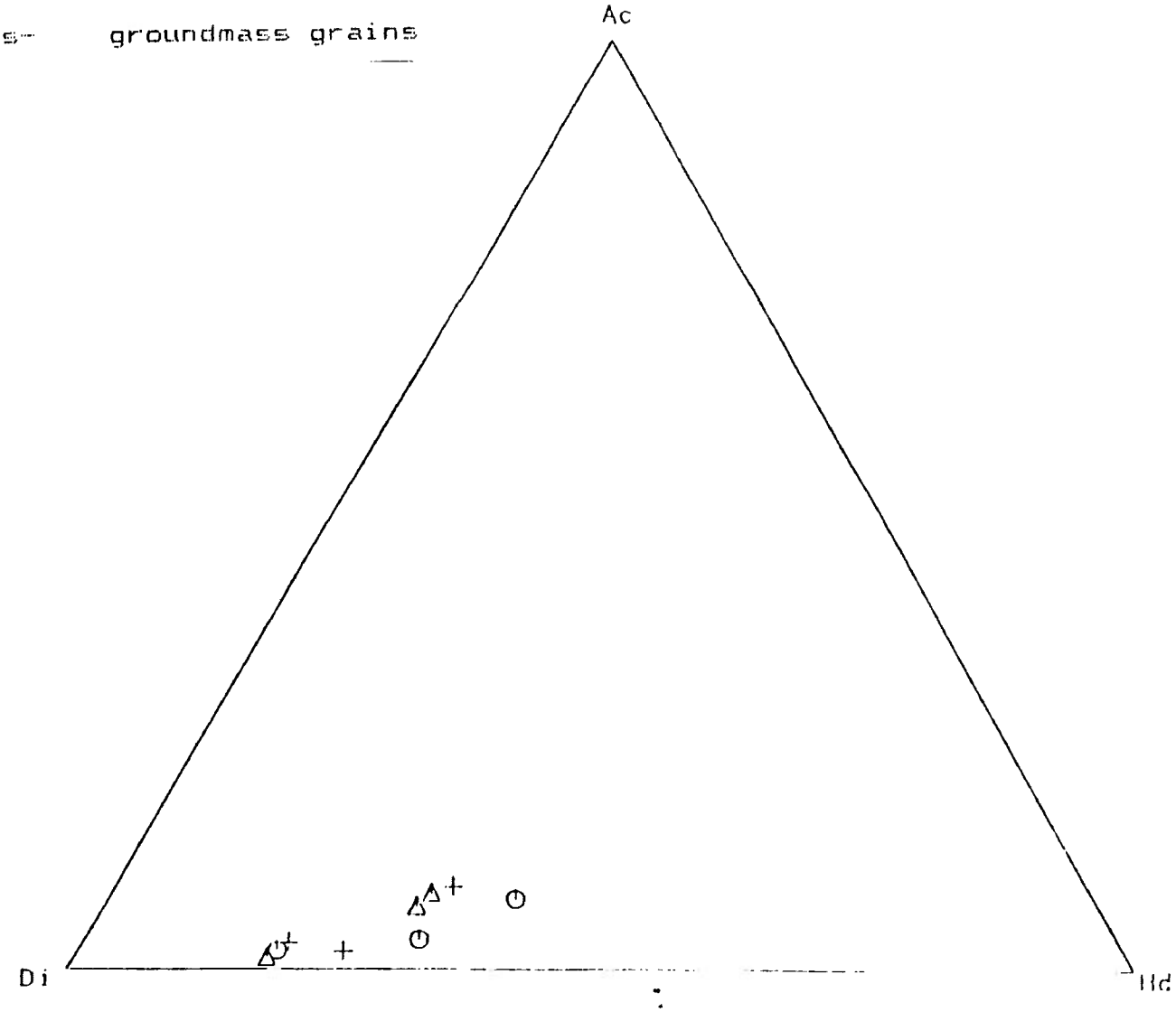

Figure 4.10a **Total Fe vs Mg in Clinopyroxene**
Monchiquites

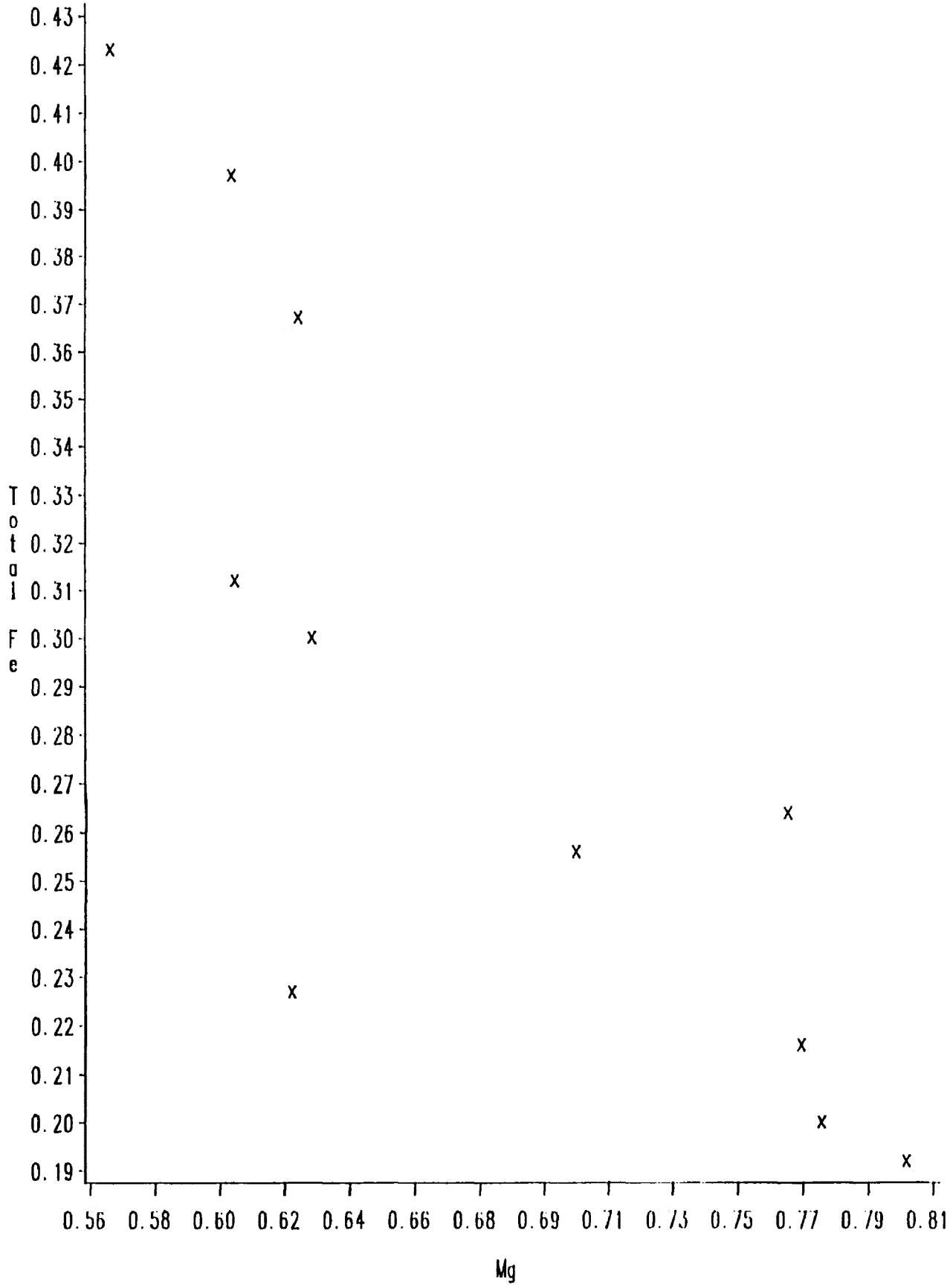

Figure 4.10b **Total Fe + Ti vs Mg in Clinopyroxene Monchiquites**

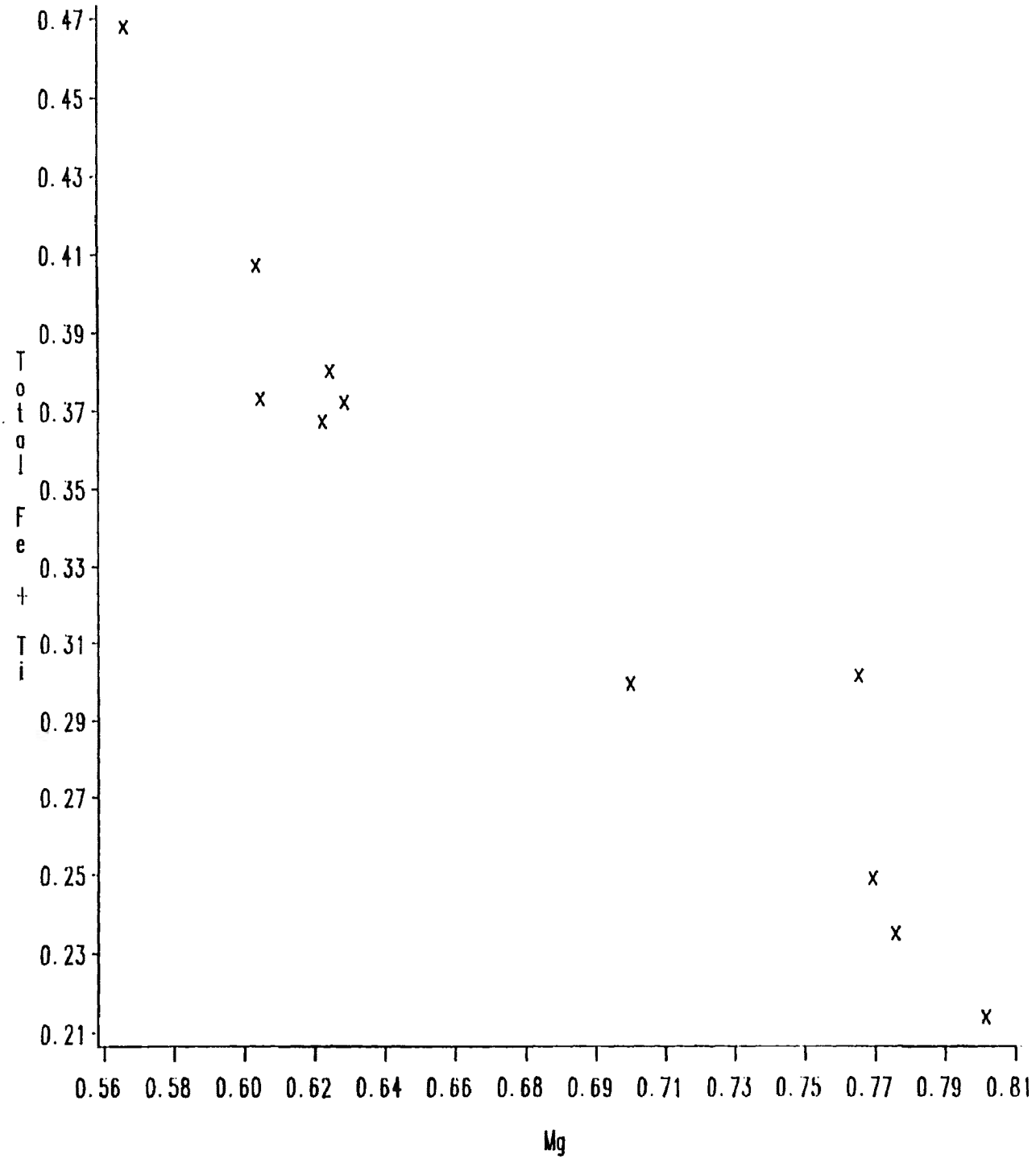

Figure 4.11a **Ti vs Total Al in Clinopyroxene**
Monchiquites

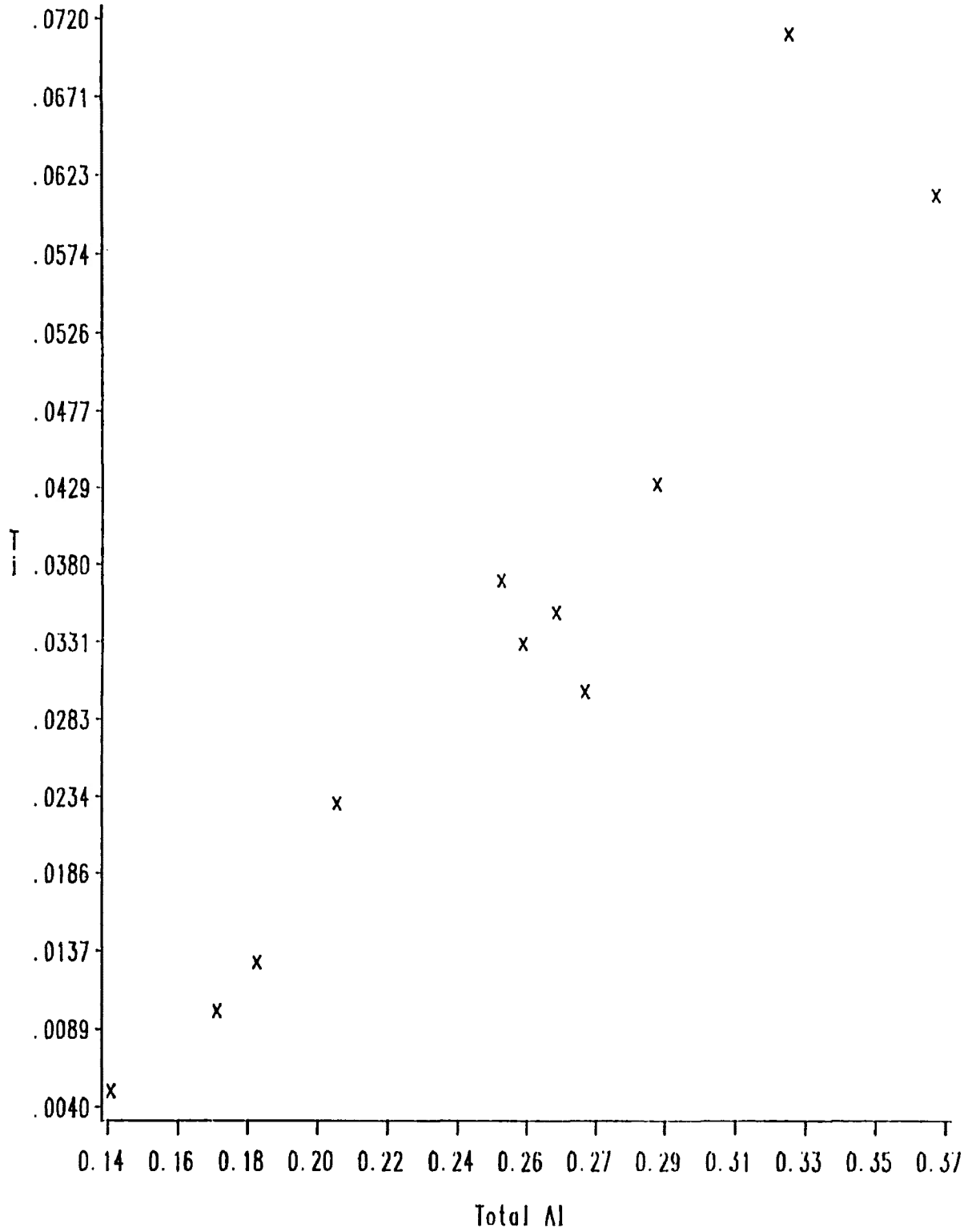

Figure 4.11b **Ti vs Al(iv) in Clinopyroxene Monchiquites**

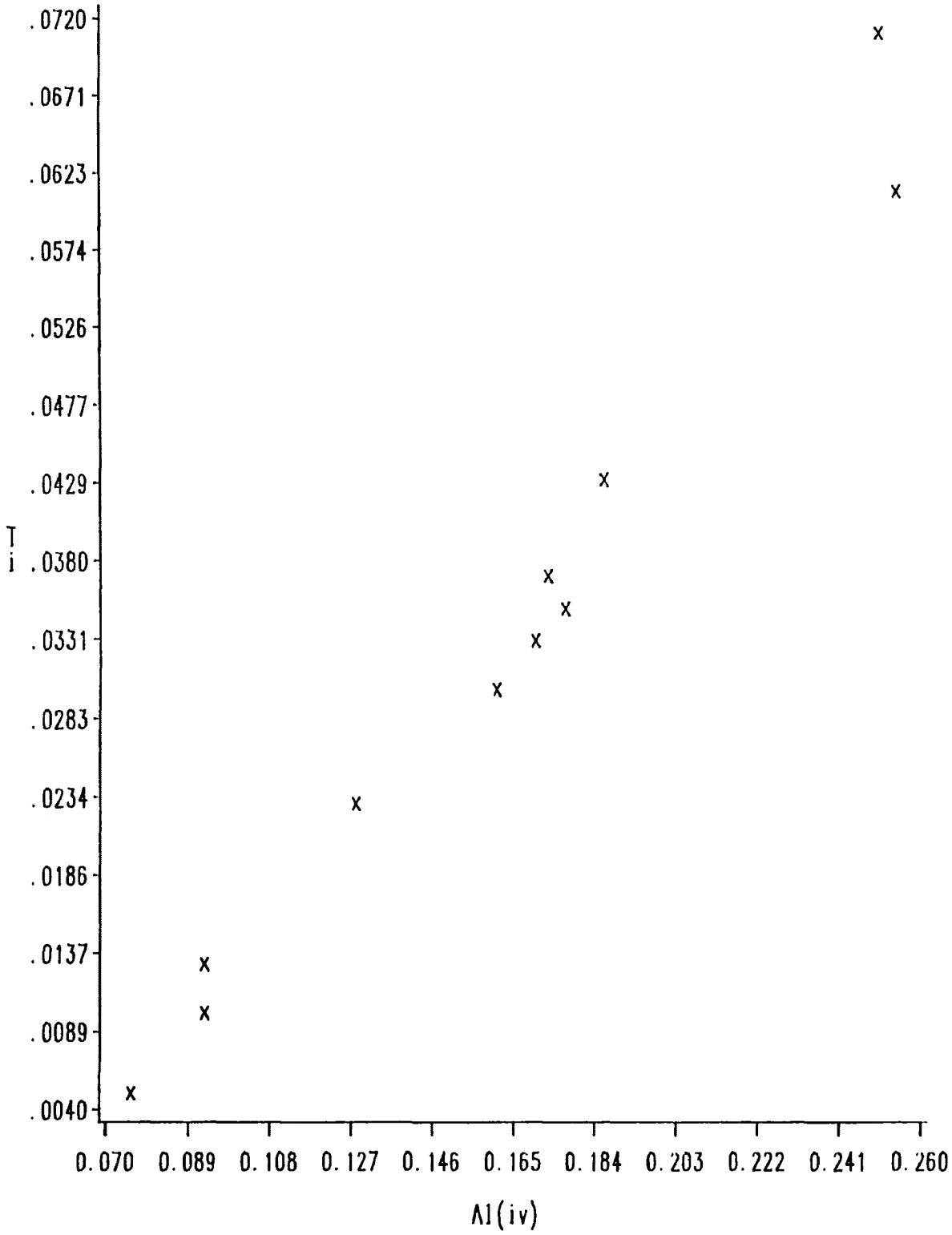

in a coupled substitution with $CaFeSi_2O_6$ for $CaMgSi_2O_6$ in the rims of normally zoned crystals. Excess Al, some of which is tetrahedrally coordinated, is also present, as depicted in Figures 4.9 and 4.11, indicating the involvement of $CaAl_2SiO_6$. This is in good agreement with the changes in the abundances of various components in Table 4.2, in that Fe, Al and Ti increase as Mg and Si decrease, similar to the sannaites. This is emphasized by the Ti content of some rim zones, which may be in excess of 2 weight % TiO_2 (i.e. 2.67 weight % TiO_2, in the case of a titansalite rim in specimen C26b). The contents of Fe^{3+} and Na tend to increase (e.g. increasing acmite content) with increasing Fe, Al and Ti as well. Cr and Mn contents are generally low and vary irregularly among phenocryst zones and groundmass grains; K is normally not detected or is present only in trace amounts. Therefore, the chemical changes between zones in clinopyroxene phenocrysts in these rock types, are similar to those that occur in the sannaites, although the substitutions are more complex than the simple covariance of Fe and Mg generally observed in the clinopyroxenes of that rock type, in that they involve greater amounts of Ti and Al. Again, in those cases in which the colour zoning is reversed, the above chemical and mineralogical trends are also reversed. These observations are similar to those made on clinopyroxenes occurring in camptonites from the Oran region, Norway,

(Scott, 1980) and in other camptonites (Brookes and Rucklidge, 1973; Brooks and Platt, 1975) and alkali basalts (Le Maitre, 1969; Scott, 1976).

As shown in Figure 4.4a, the clinopyroxenes from the amphibole camptonites occupy a restricted compositional range relative to the other lamprophyres, primarily in the salitic and augitic fields (or titansalitic and titanaugitic fields, considering the relatively high Ti content of these clinopyroxenes i.e. normally in excess of 1.0 weight % TiO_2, as shown in Table 4.2), although two core analyses plot as diopside. There is, therefore, a trend, albeit a weak one compared to that previously noted, from diopsidic cores to titansalitic or titanaugitic rims in phenocrysts. The acmite content increases slightly in rim zones of normally zoned phenocrysts, and in groundmass grains, relative to phenocryst cores, as shown in Figure 4.4b. In terms of the chemical changes associated with the above mineralogical changes, Figure 4.12a depicts the covariance of Fe and Mg; as in the other lamprophyres, involvement of Ti ($CaTiAl_2O_6$) and excess Al ($CaAl_2SiO_6$) with Fe in the substitution is suggested (Figure 4.12b and Figure 4.13), although the extent of the replacement of Mg is considerably less than that previously observed. The Na and Fe^{3+} contents change slightly in response to the slight increase in acmite content from cores

Figure 4.4a

CPX in Amphibole Camptonites

Abbreviations as per Figure 4.1a

circles- phenocryst cores

triangles- phenocryst rims

crosses- groundmass grains

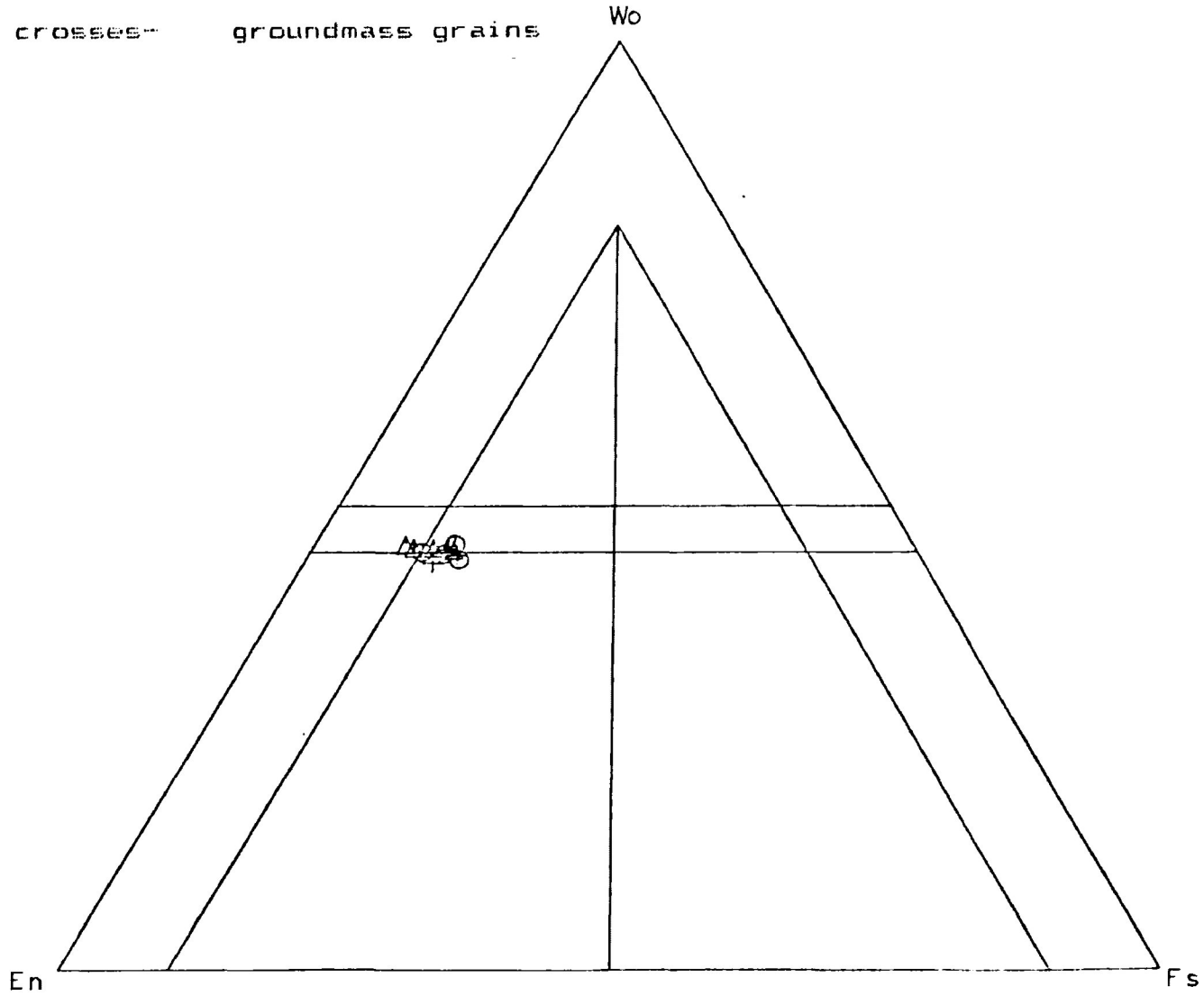

Figure 4.4b

CPX in Amphibole Camptonites

Abbreviations as per Figure 4.1b

circles- phenocryst cores

triangles- phenocryst rims

crosses- groundmass grains

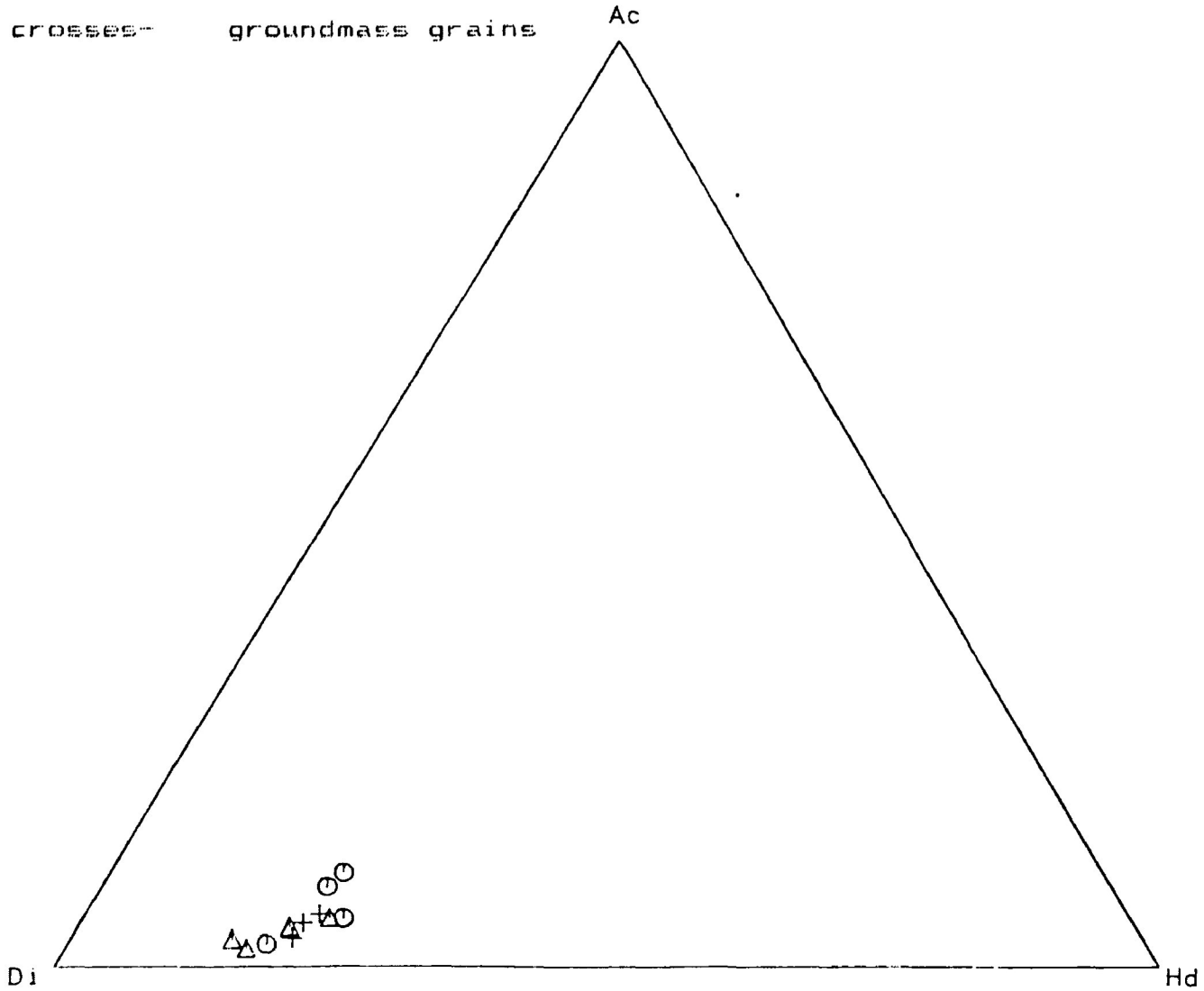

Figure 4.12a **Total Fe vs Mg in Clinopyroxene Amphibole Camptonites**

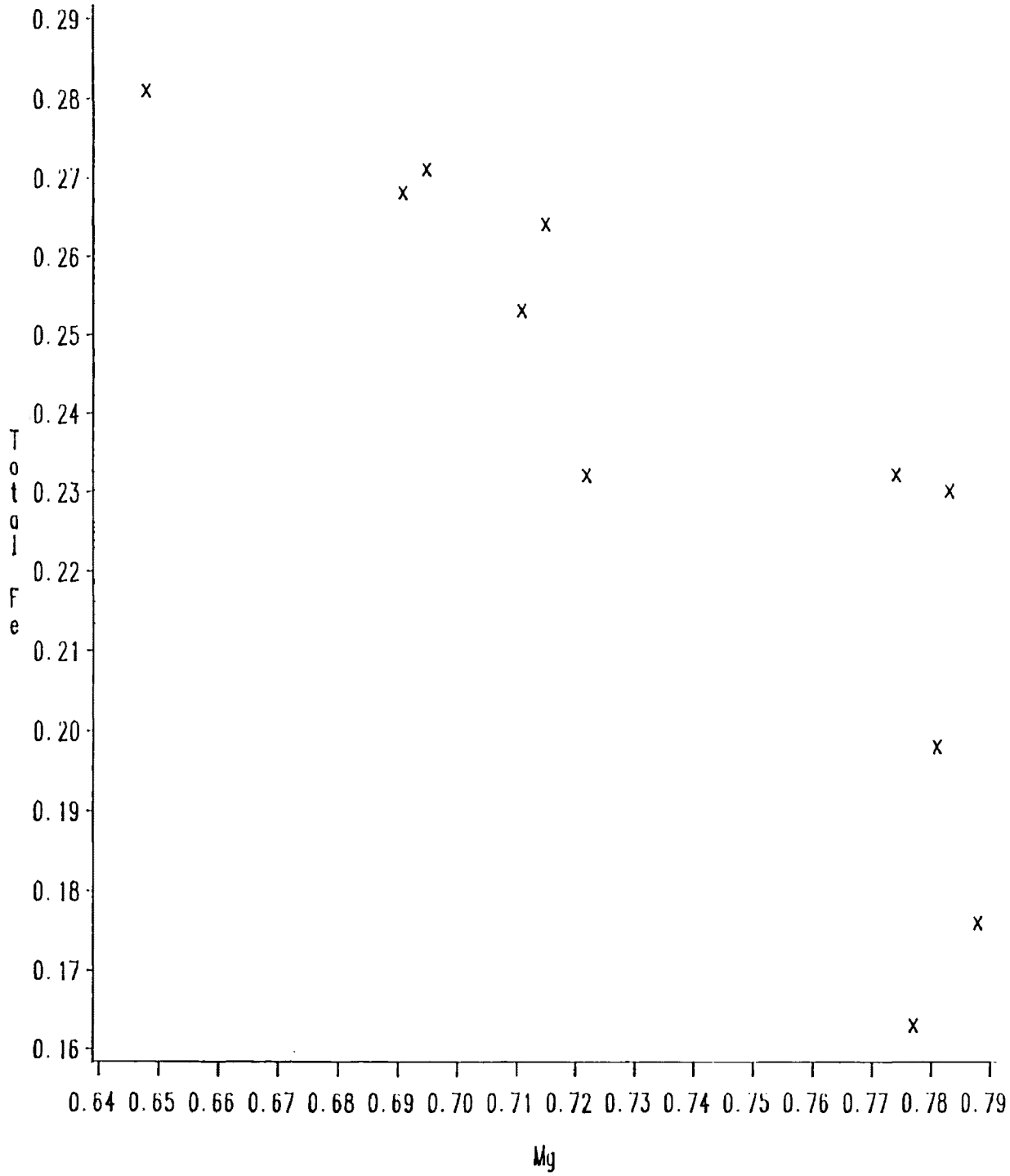

Figure 4.12b **Total Fe + Ti vs Mg in Clinopyroxene Amphibole Camptonites**

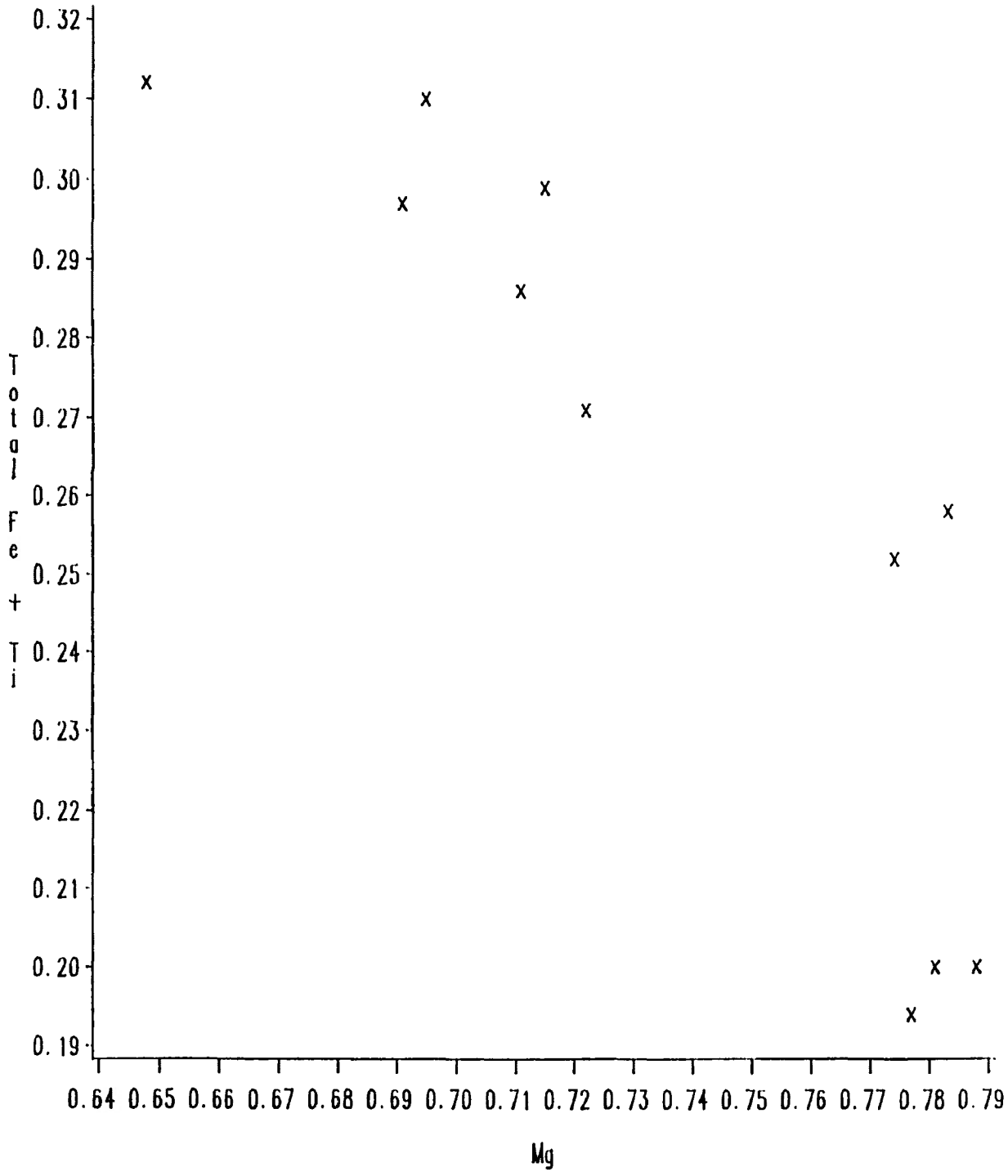

Figure 4.13a **Ti vs Total Al in Clinopyroxene Amphibole Camptonites**

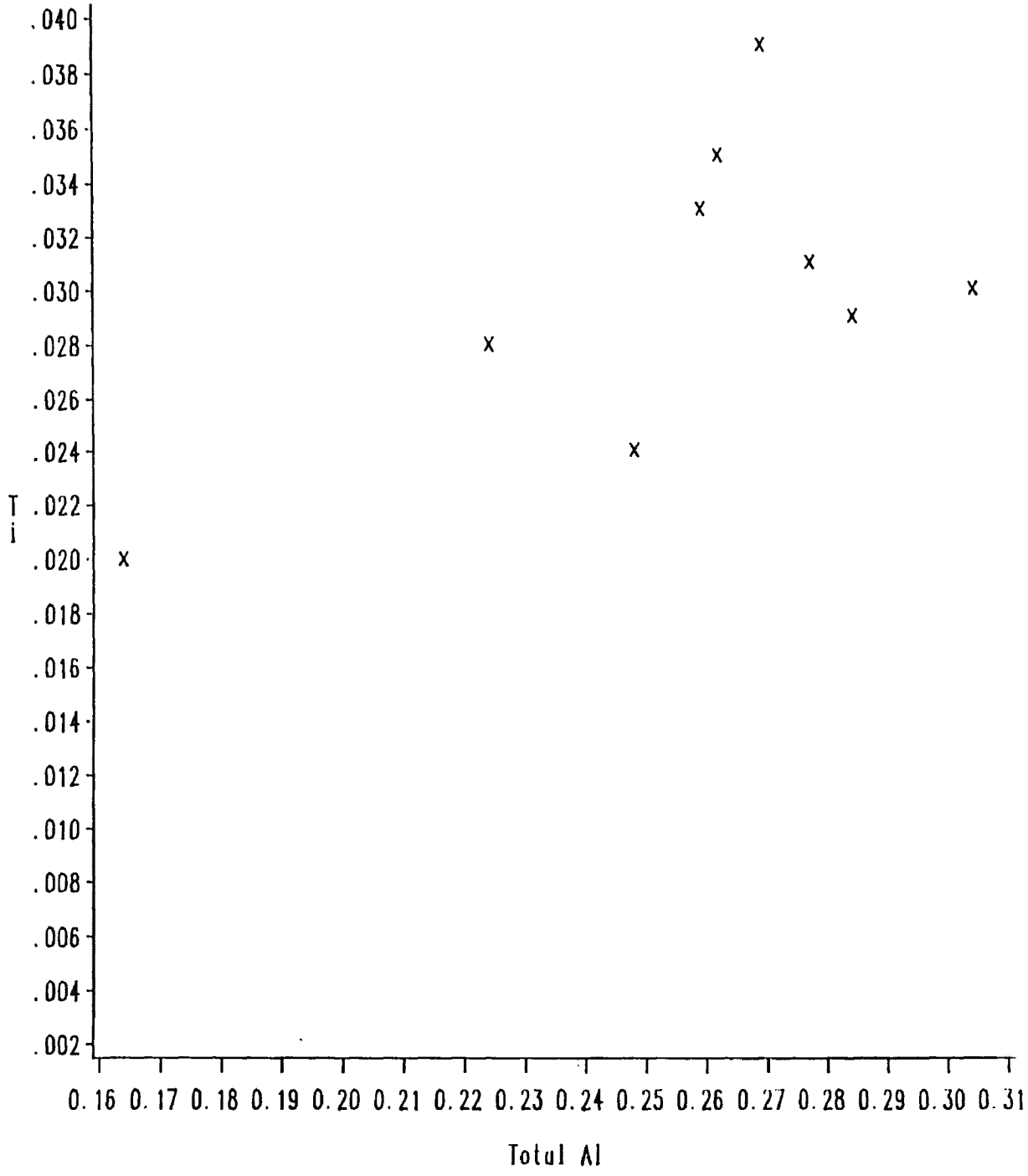

Figure 4.13b **Ti vs Al(iv) in Clinopyroxene Amphibole Camptonites**

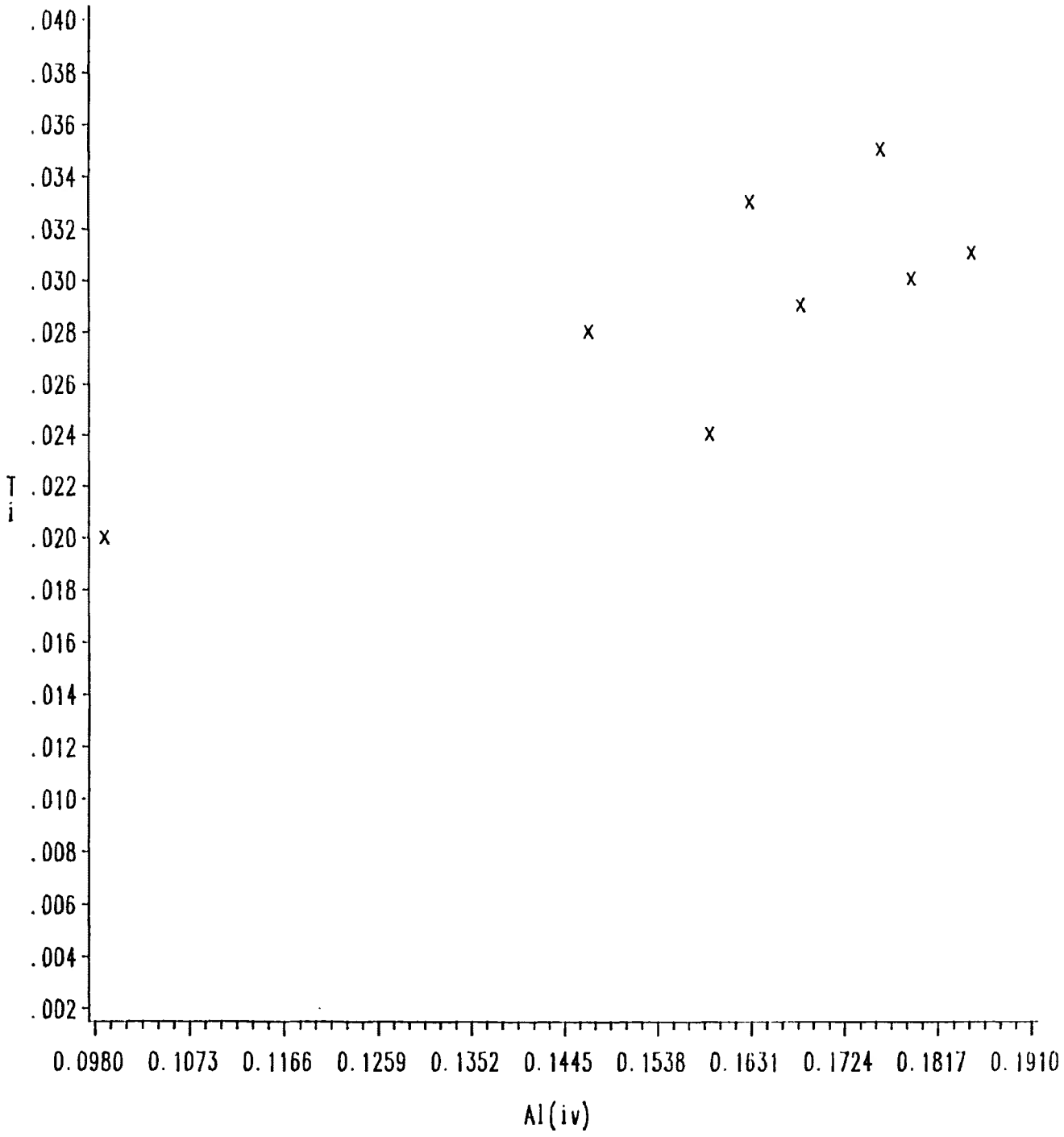

to rims and groundmass grains. The K, Mn and Cr abundances, where detected, are generally low, except in the case of one phenocryst, in which a Cr_2O_3 concentration of 1.01 weight % is observed.

Figure 4.5a indicates that the clinopyroxene compositions of the quartz camptonites occupy a limited range in the augite field (or titanaugite, since in many cases the abundance of TiO_2 approaches 2.0 weight %, as exhibited in Table 4.2), with only a weak tendency towards more diopsidic compositios in phenocryst rims and groundmass grains. This reflects both a widespread compositional homogeneity among phenocrysts and groundmass grains, and a generally lower CaO content in these pyroxenes relative to those occuring in the other lamprophyre types (see Table 4.2). Therefore, little variation in the abundance of the various components is observed, except, as noted above, a covariance of Mg and Fe, such that $CaMgSi_2O_6$ substitutes for $CaFeSi_2O_6$; this is apparently independant of other substitutions, as illustrated by the good fit of the trend defined by the points in Figure 4.14 to a line with unity slope. The acmite, and therefore the Na and Fe^{3+} content of these pyroxenes is also constant, or decreases slightly in groundmass grains and rim zones in phenocrysts, relative to phenocryst cores (see Fig 4.5b). Cr, Mn and K, where detected, tend to vary in concentration

Figure 4.5a

CPX in Quartz Camptonites

Abbreviations as per Figure 4.1a

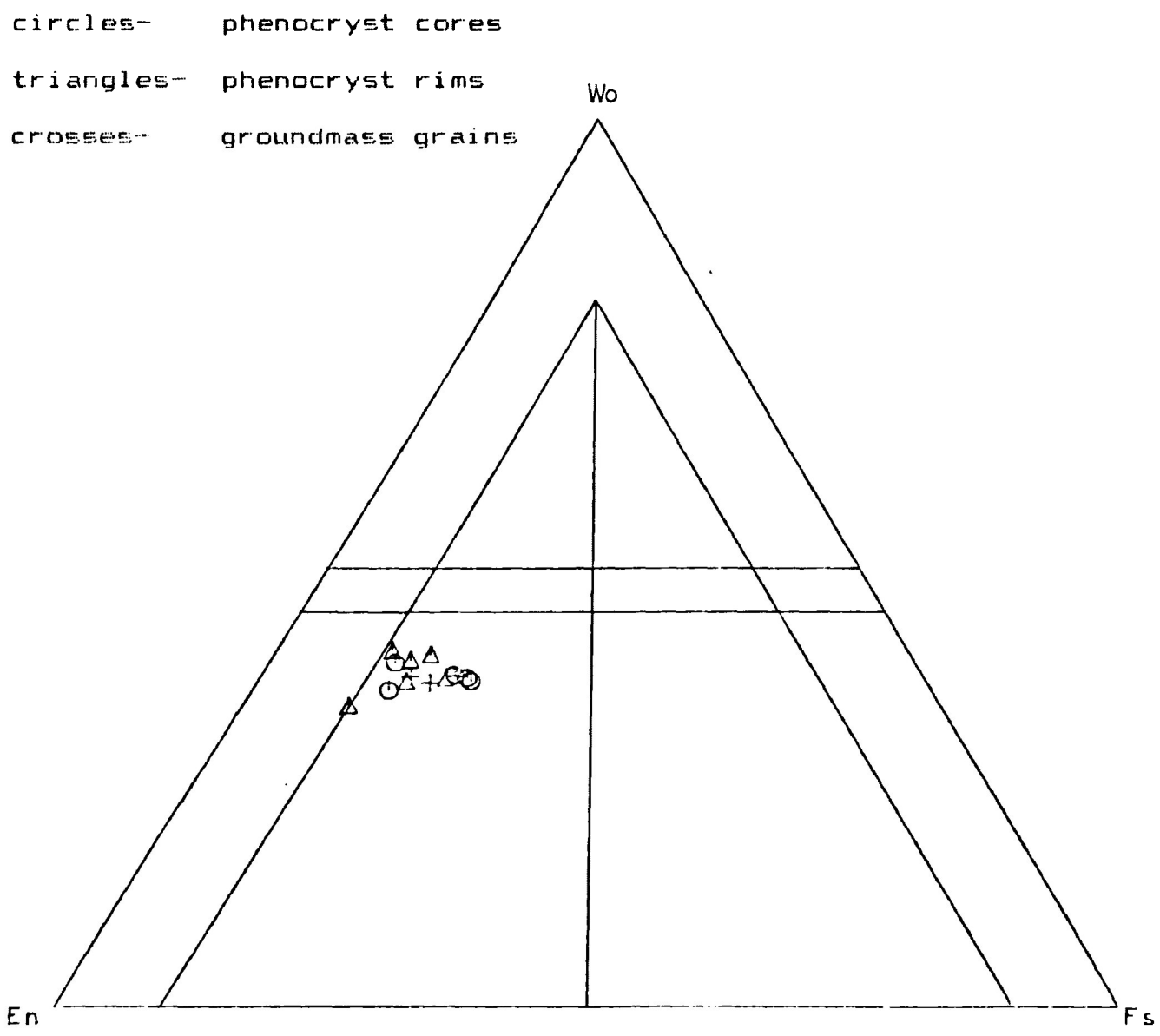

Figure 4.5b

CPX in Quartz Camptonites

Abbreviations as per Figure 4.1b

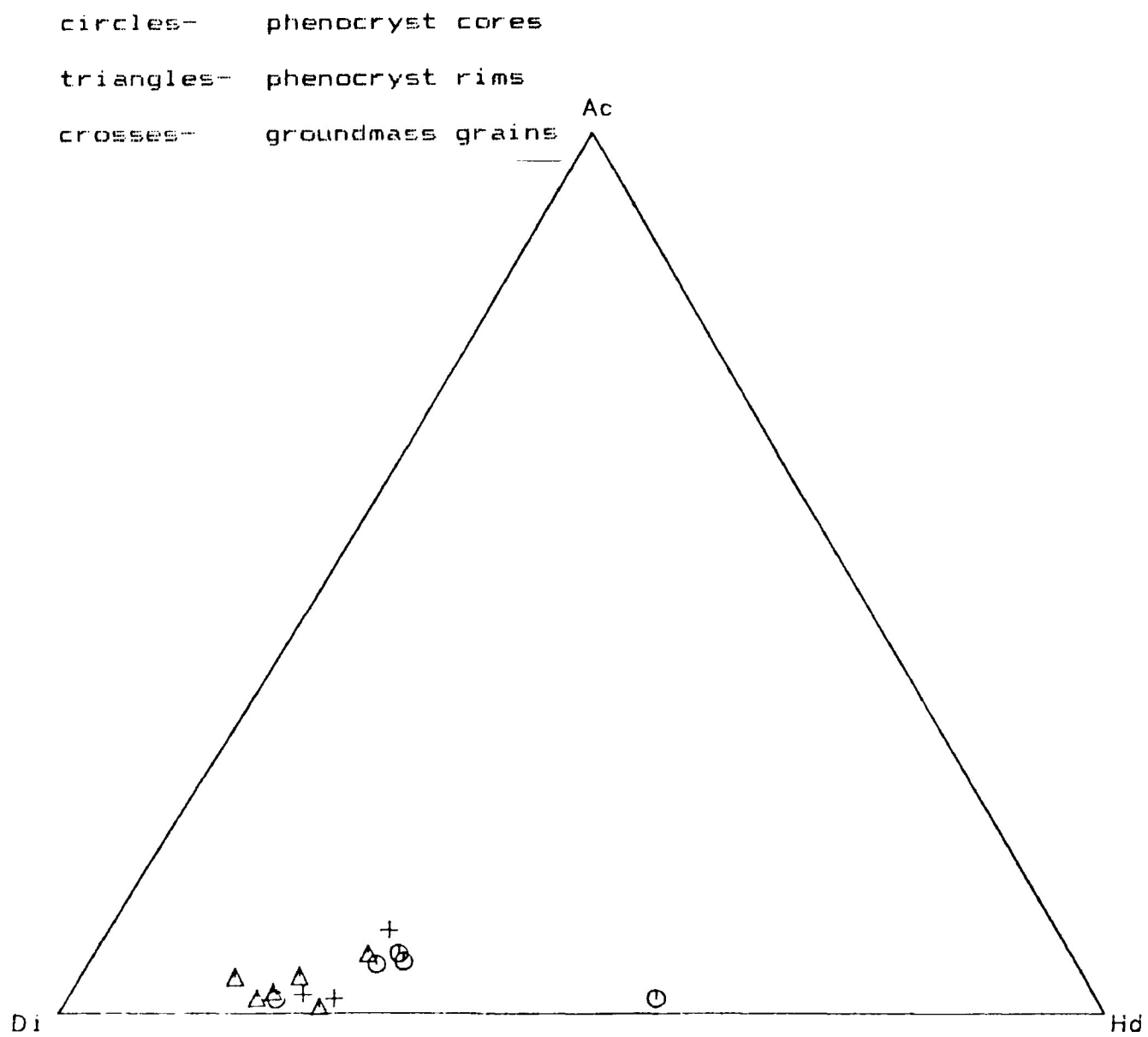

Figure 4.14a **Total Fe vs Mg in Clinopyroxene Quartz Camptonites**

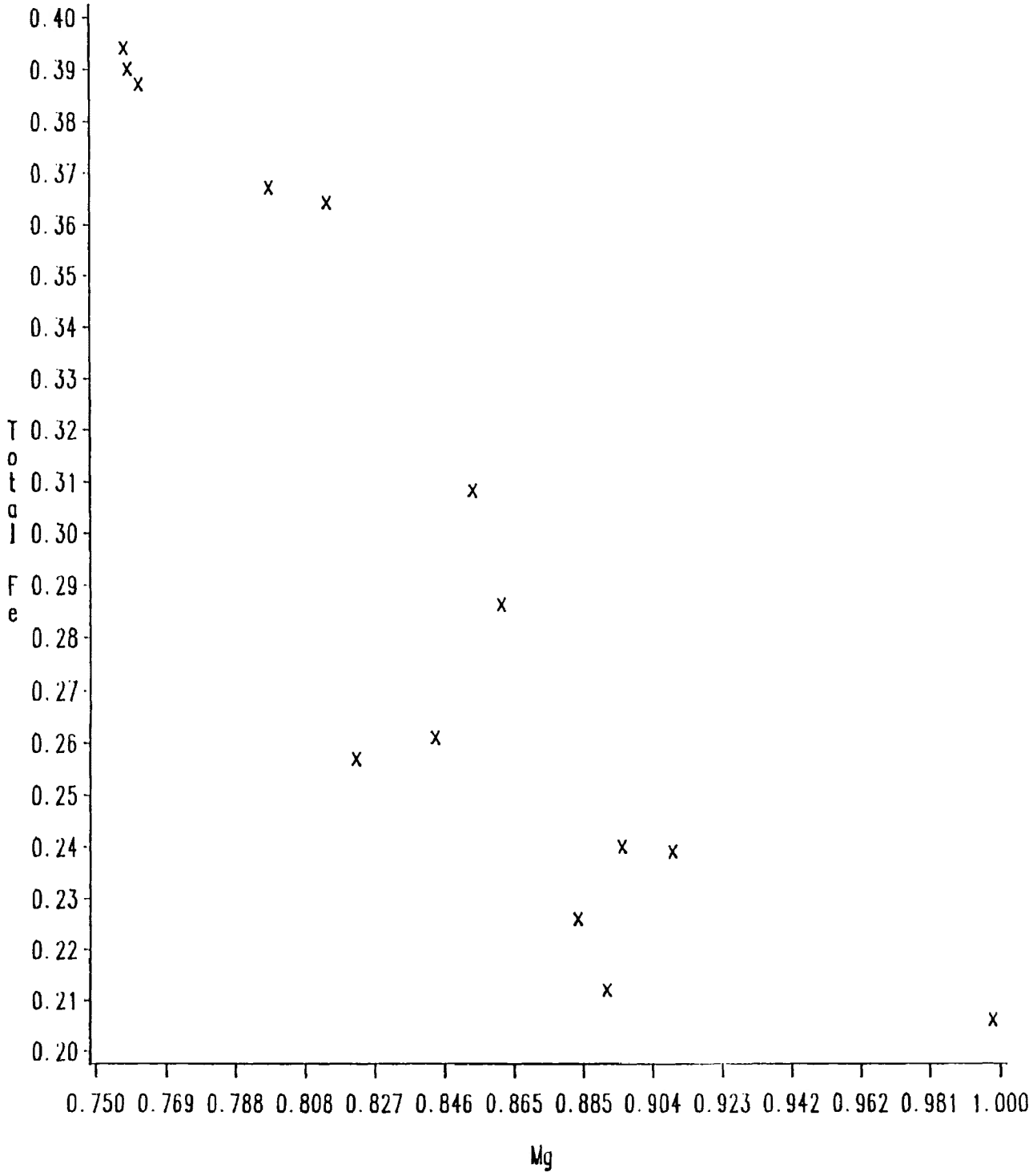

Figure 4.14b **Total Fe + Ti vs Mg in Clinopyroxene Quartz Camptonites**

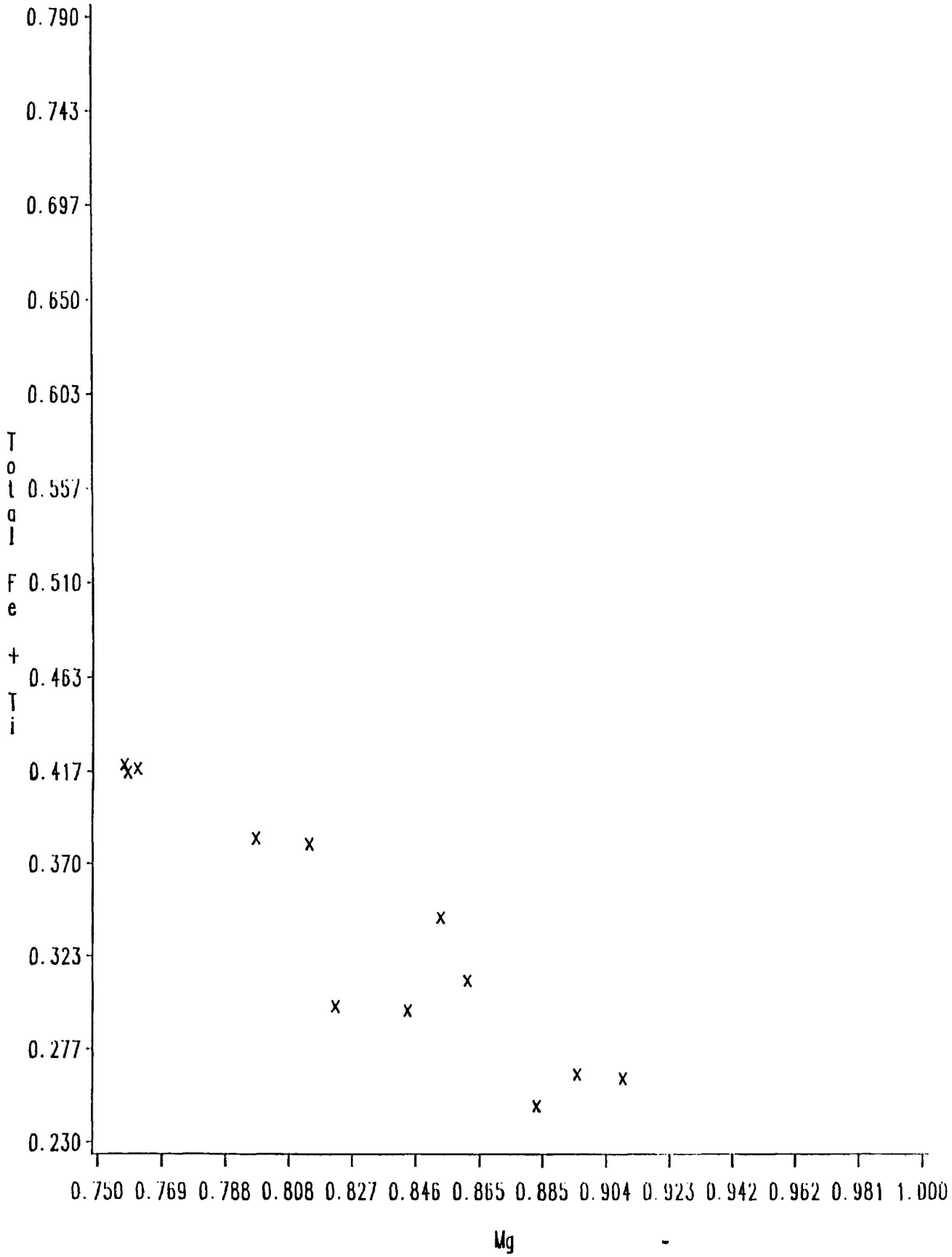

Figure 4.15a **Ti vs Total Al in Clinopyroxene**
Quartz Camptonites

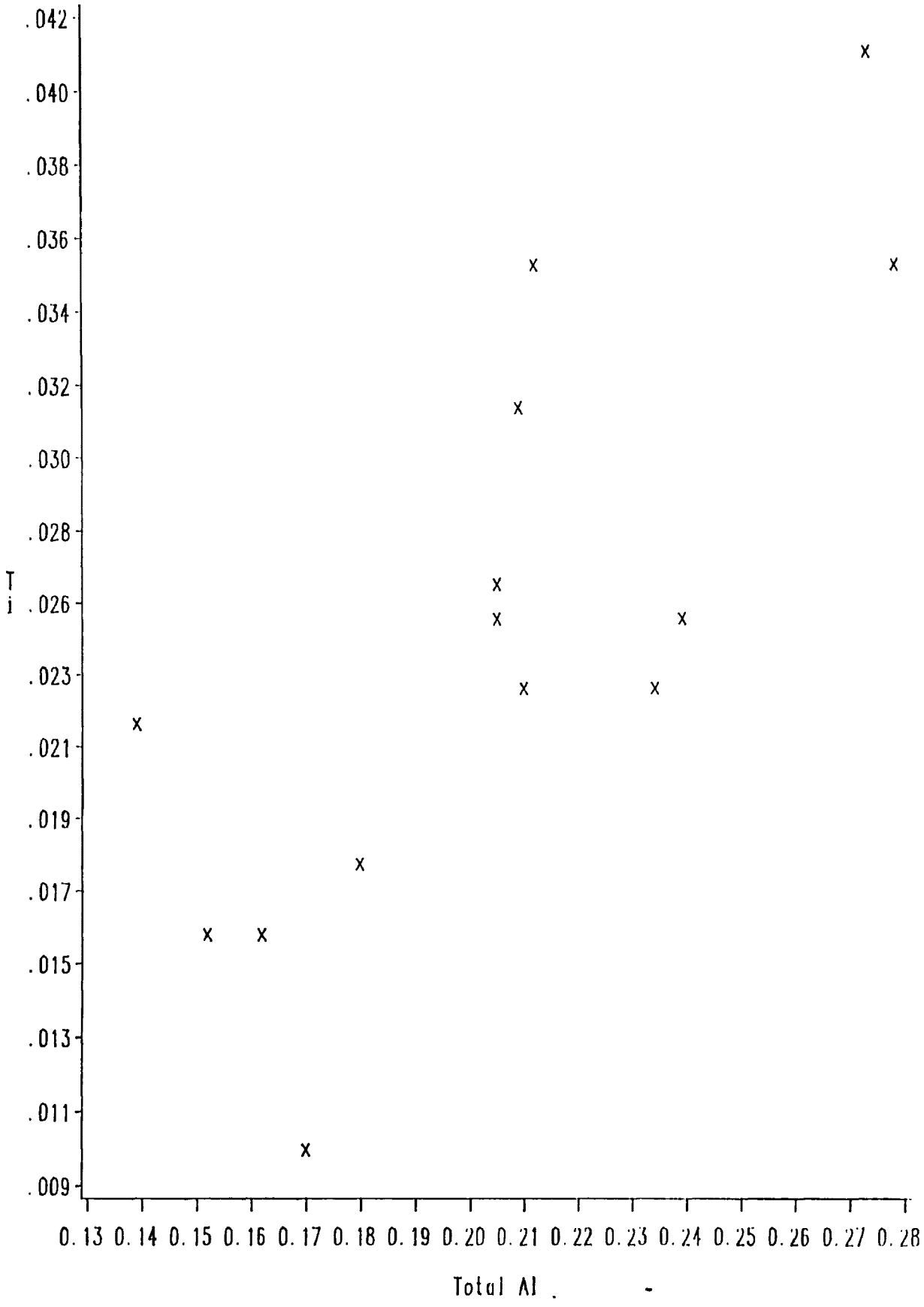

Figure 4.15b **Ti vs Al(iv) in Clinopyroxene**
Quartz Camptonites

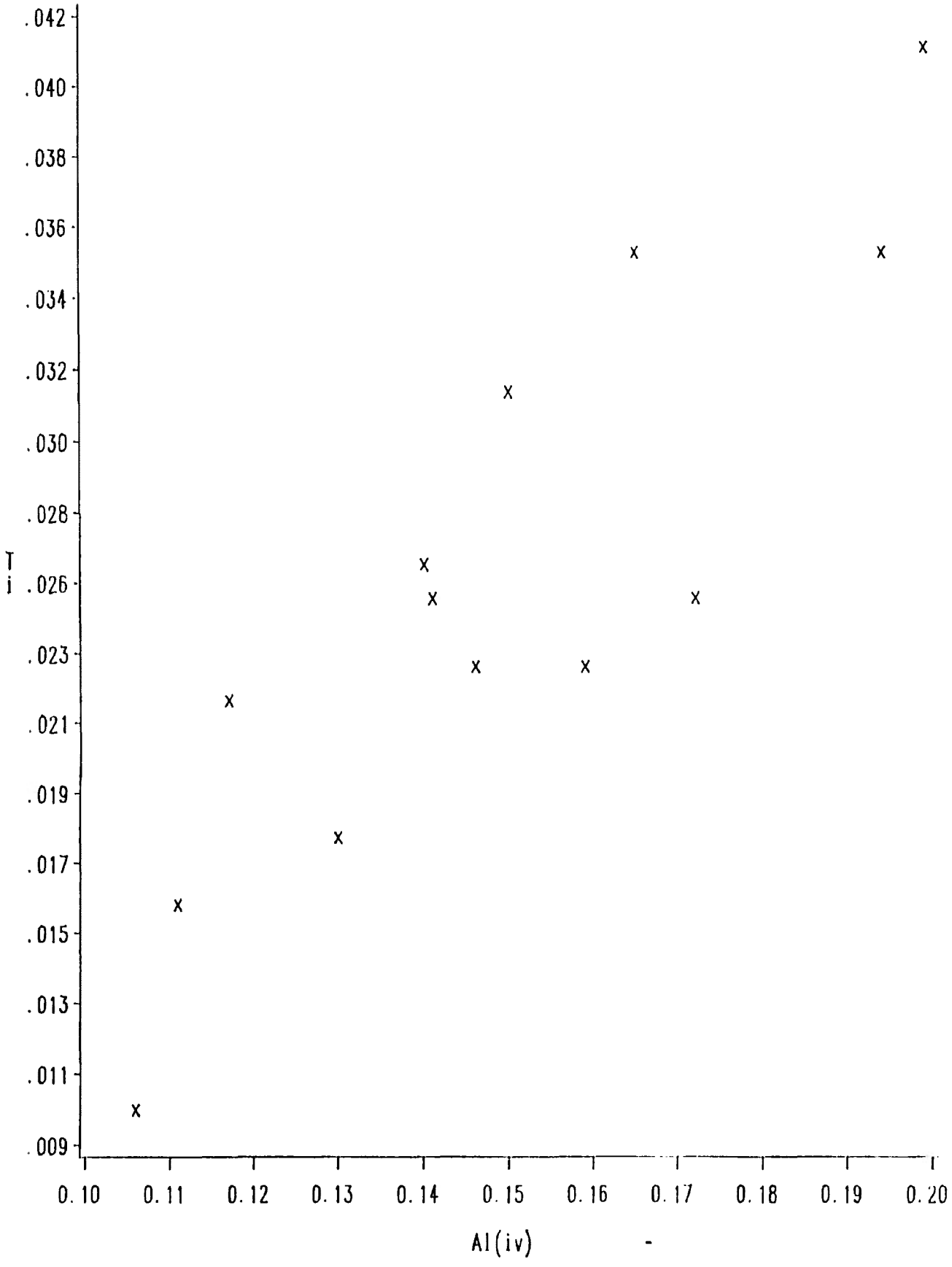

Table 4.3 Representative Clinopyroxene Analyses from Tinguaites

	Unzoned Aegerine		Unzoned Hedenbergite		Zoned Heden-bergite	Aegerine
Oxide Wt%	Core	Rim	Core	Rim	Core	Rim
SiO2	52.52	51.38	47.32	47.39	48.02	52.15
Al2O3	1.87	1.24	4.13	3.00	4.14	2.17
TiO2	3.84	3.89	1.53	1.14	1.27	3.51
FeO	22.21	23.38	16.87	16.98	14.30	22.77
MgO	0.22	0.30	6.12	6.16	7.88	0.24
CaO	1.27	2.18	20.90	21.33	21.35	1.18
Na2O	14.26	14.32	1.69	1.25	1.27	14.26
K2O						
MnO	0.63	0.56	0.61	0.74	0.38	0.57
Cr2O3						
Total	96.82	97.25	99.17	97.99	98.61	96.85

(see Table 4.2).

Clinopyroxenes occurring in the tinguaites exhibit three general compositional schemes (see Table 4.3):

a) A uniformly acmitic (i.e. aegerine) composition;

b) A uniformly hedenbergitic composition; and

c) An hedenbergitic core surrounded by an acmitic rim.

Therefore, clinopyroxenes occurring in the tinguaites are characterized by high Fe/Mg ratios, and, in the case of type (a) clinopyroxenes above, a high content of Na and Fe^{3+} (i.e. acmitic components). In the case of type (c) clinopyroxenes, the concentration of acmitic components increases from core to rim. Mn contents are variable, while K and Cr are generally not detected.

It is noteworthy that, as previously described, optical examination suggests that aegerine is the dominant type of clinopyroxene present in the tinguaites, and therefore does not indicate the presence of abundant hedenbergite. This apparent disparity between optical and compositional evidence suggests that more extensive study of the tinguaite

clinopyroxenes is required.

AMPHIBOLE

Paragenesis

Table 4.4 summarizes the optical and physical properties of the amphiboles which occur in the various dyke rocks. In the camptonites and monchiquites, primary amphibole occurs as both a phenocryst and a groundmass phase. In the former mode of occurence, it is subordinate only to clinopyroxene in abundance (see Table 2.1), except in the cases of the quartz camptonites, in which it is also subordinate to quartz, and the amphibole camptonites, in which it is the dominant phenocryst phase. In the groundmass, it is subordinate to feldspar and clinopyroxene. In all of these rock types, crystals are generally euhedral to subhedral and equant to elongated, in the case of phenocrysts; and subhedral in the case of the groundmass grains (see Plate 4.4). Pleochroic yellow-brown to brown (alpha=yellow-brown or pale brown, beta=gamma=brown, dark brown, green-brown or rarely olive-brown) grains are pargasitic or hastingsitic hornblende, based on petrographic and XRD analysis (see Table 4.4 and above). Less common red-brown phenocrysts (alpha=pale brown, beta=red-brown, gamma=dark red-brown or

Table 4.4 Optical and Physical Properties of Amphiboles

Rock Type	Size Range	Mean Size	Colour	Pleo-chroism	Twinning	2V
Sannaite						
Groundmass	0.3-1.0mm	0.7mm	brown	weak	none	51-56
Ocellar Camptonite						
Phenocryst	1-3mm	2mm	core:(red)brown	moderate	(100)	55-57
			rim:dk(red)brown	moderate	(100)	29-53
Groundmass	0.2-0.7mm	0.5mm	dark(red)brown	moderate	none	35-51
Monchiquite						
Phenocryst	1-2.5mm	1.5mm	core:(red)brown	moderate	(100)	56-61
			rim:dk(red)brown	moderate	(100)	45-52
Groundmass	0.1-0.5mm	0.4mm	dark(red)brown	moderate	none	41-58
Amphibole Camptonite						
Phenocryst	1.5-7.5mm	5mm	core:(red)brown	moderate	(100)	55-70
			rim:dk(red)brown	moderate	(100)	32-56
Groundmass	0.1-0.6mm	0.4mm	dark(red)brown	moderate	none	23-34
Quartz Camptonite						
Phenocryst	1-4mm	2.5mm	core:(red)brown	moderate	(100)	54-61
			rim:dk(red)brown	moderate	(100)	34-44
Groundmass	0.1-0.3mm	0.2mm	dark(red)brown	moderate	none	27-45
Tinguaite	1-3mm	3mm	deep blue,yellow	strong	none	66-76
Phenocryst						

brown) are kaersutite. Phenocrysts, and in a few cases, larger matrix grains, are zoned, with a subehdral or rounded core surrounded, and sometimes embayed by, a subhedral to euhedral outer zone which is characterized by darker and greener absorption colours. Rarely, fine concentric oscillations in the shade of the absorption colours of the outer zone are observed. Contacts between the zones are always sharp. Twinning parallel to (100) is often noted. Many of the phenocrysts incorporate fine disseminations of opaque or cryptocrystalline grains. Small groundmass grains are normally unzoned, and are similar in terms of optical properties to the outer zones of the phenocrysts.

In the case of the sannaites, primary amphibole occurs only in the groundmass, and then in small quantities (see Table 2.1). Crystals are typically unzoned, subhedral to anhedral tabular or lath shaped grains. Pleochroism tends to be weak (alpha=brown, beta=gamma=dark brown or rarely olive brown); the amphibole is pargasitic or hastingsitic hornblende based on optical properties.

In all of the lamprophyres, a secondary amphibole is commonly observed as an overgrowth on, or replacement of, primary amphiboles and clinopyroxenes. It normally occurs as massive or fibrous, weakly or non-pleochroic pale green or

grey-green (alpha=colourless or very pale green, beta=pale green, gamma=grey or grey green) patches along rims and cleavage surfaces of these minerals. Generally, the replacement is pseudomorphous. This amphibole may be tremolite, but, as noted by Deer et al (1966), the term uralite may be preferable to describe an ill-defined, secondary, fibrous, blue-green amphibole of undetermined composition.

Amphibole in the tinguaites occurs as phenocrysts. They are elongated, euhedral to subhedral pleochroic blue-green (alpha=black, deep blue or green-blue, beta=indigo blue, gamma=green or blue green) laths, which are riebeckite, based on petrographic analysis (Plate 2.12).

Composition

Table 4.5 gives representative compositions of amphiboles from the various types of dyke rocks; a complete list of data is given in Appendix B.

Figures 4.16a and 4.16b outlines the nomenclature of the amphiboles as described by Leake (1978) in terms of various chemical parameters. Inspection of this diagram shows that all amphiboles occurring in the lamprophyres are calcic. In

Table 4.5 Representative Analyses of Amphiboles

Rock Type	Sannaite		Ocellar Camptonite				Monchiquite	Quartz Camptonite	Amphibole Camptonite			Tinguaite	
Oxide Wt%	Small Crystal	Ground-mass Grain	Ground-mass Grain	Ground-mass Grain	Core	Rim	Large Crystal	Large Crystal	Core	Rim	Ground-Mass Grain	Small Lath	Small Lath
SiO2	38.42	38.74	40.04	40.23	38.76	39.67	40.43	40.47	39.86	40.23	39.32	48.98	49.36
Al2O3	15.02	16.17	11.77	11.61	14.01	11.69	9.80	12.54	13.08	12.77	12.54	0.74	1.19
TiO2	2.12	2.17	3.08	2.60	3.04	2.12	1.80	0.94	4.25	3.53	3.52	1.07	0.81
Fe2O3	3.37	2.75	2.54	1.75	2.18	2.48	4.19	2.44	1.07	2.91	2.17	10.12	9.81
FeO	13.33	13.48	18.14	18.33	11.61	17.69	19.28	15.41	10.74	12.34	16.45	24.93	23.79
MgO	9.04	8.93	8.14	8.42	10.88	7.78	6.82	9.66	12.95	11.22	9.02	0.68	3.09
CaO	11.49	11.76	11.45	11.47	11.68	11.35	10.50	11.55	11.78	11.48	11.28	1.31	5.56
Na2O	2.13	2.12	2.69	2.93	2.02	1.99	2.89	2.99	2.45	2.37	2.68	6.65	4.22
K2O	1.52	1.63	1.05	1.13	1.77	1.89	1.44	1.43	1.87	1.67	1.63	0.99	0.75
MnO	0.29	0.28	0.10	0.15	0.37	0.47	0.66	0.34	0.00	0.17	0.17	1.34	1.30
Cr2O3	0.01	0.00	0.00	0.00	0.00	0.11	0.00	0.00	0.00	0.00	0.00	0.00	0.00
Total	96.74	98.02	99.00	98.62	96.32	97.24	97.81	97.77	98.05	98.69	98.78	96.80	99.88
Structural Formula Based on 23			Oxygens										
Si	5.867	5.751	6.086	6.139	5.898	6.162	6.307	6.163	5.918	5.990	5.979	7.836	7.606
Al(iv)	2.133	2.249	1.914	1.861	2.102	1.838	1.693	1.837	2.082	2.010	2.021	0.140	0.216
Al(vi)	0.570	0.654	0.194	0.226	0.410	0.302	0.108	0.413	0.207	0.230	0.215	0.000	0.000
Ti	0.243	0.249	0.352	0.298	0.348	0.248	0.211	0.108	0.474	0.395	0.400	0.140	0.094
Fe3+	0.387	0.315	0.291	0.201	0.249	0.290	0.492	0.280	0.120	0.326	0.247	1.218	1.138
Fe2+	1.702	1.717	2.306	2.339	1.477	2.297	2.515	1.963	1.333	1.537	2.081	3.334	3.065
Mg	2.058	2.029	1.844	1.915	2.468	1.802	1.586	2.193	2.866	2.490	2.035	0.162	0.710
Ca	1.880	1.920	1.864	1.875	1.904	1.889	1.755	1.884	1.874	1.831	1.828	0.225	0.917
Na	0.631	0.626	0.793	0.867	0.596	0.599	0.874	0.883	0.705	0.684	0.786	2.026	1.261
K	0.296	0.317	0.204	0.220	0.344	0.374	0.287	0.278	0.354	0.317	0.315	0.202	0.147
Mn	0.038	0.036	0.013	0.019	0.048	0.062	0.087	0.044	0.000	0.021	0.022	0.181	0.170
Cr													

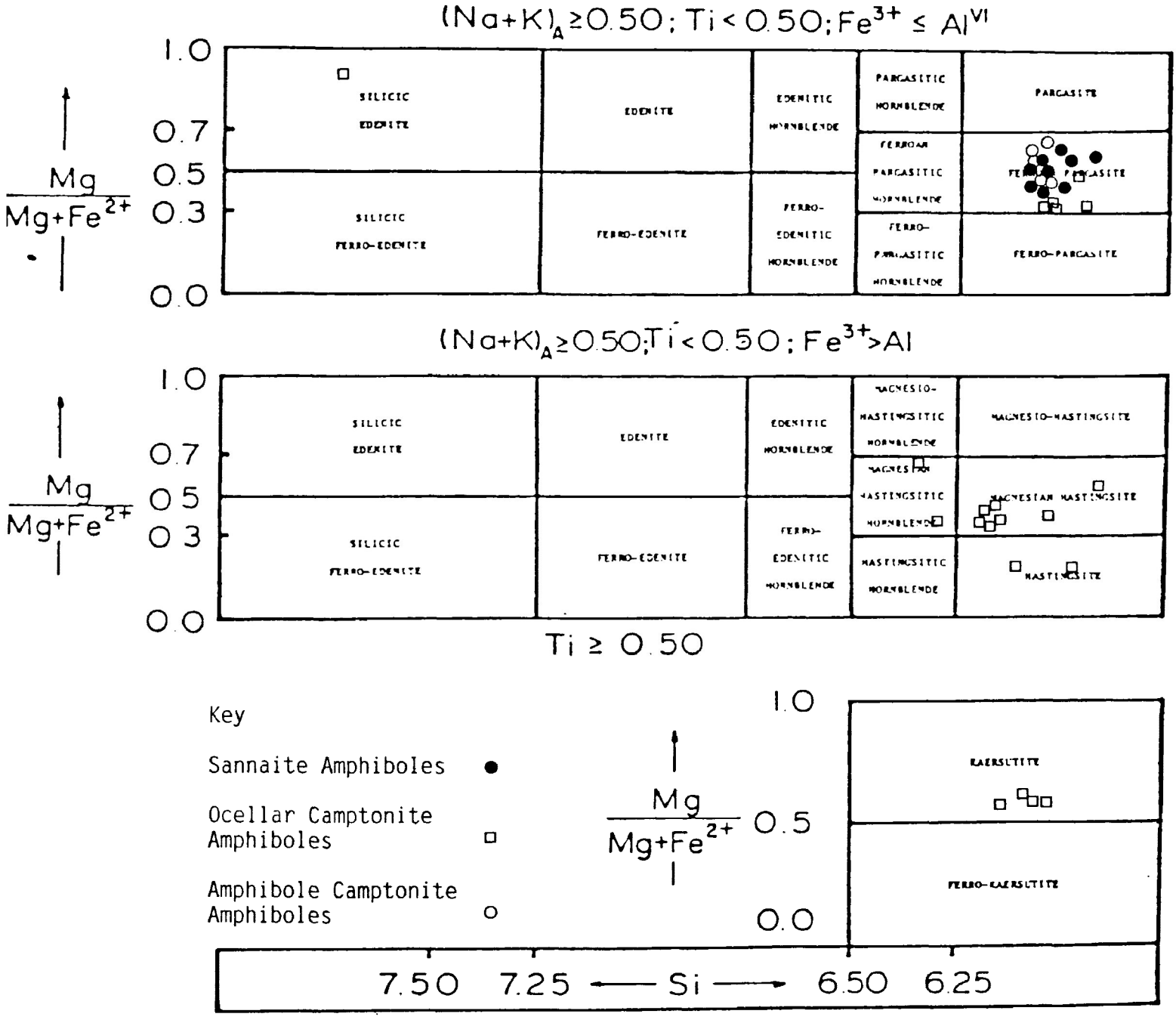

Figure 4.16a Amphibole nomenclature after Leake (1978) with data points for amphiboles from Coldwell lamprophyres plotted

the case of the sannaites and the amphibole camptonites, all amphibole analyses plot as ferroan pargasite, or titanian ferroan pargasite if Ti is in excess of 0.25 atoms per formula unit. The amphiboles of the other lamprophyres exhibit more compositional variation, with the brown-olive brown variety plotting as hastingsite, magnesian hastingsite, magnesian hastingsitic hornblende or ferroan pargasite (in many cases, these are titanian). The separation of the ferroan pargasites from the various hastingsitic analyses, however, is largely a function of the relative abundances of Al and Fe^{3+} being close in magnitude; in fact, inspection of Table 4.5 shows that the compositions of the brown amphiboles from all of the lamprophyres display little variation, with the exception of those of the amphibole camptonites, which tend to be somewhat more Ti-rich (3-4 weight % TiO_2 as opposed to 2-3 weight % for the other amphiboles). Red-brown amphiboles plot as kaersutites. One analysis of a colourless crystal plots as silicic edenite, although this may be a xenocryst or an effect of alteration.

In the case of the tinguaites, most amphibole analyses plot as riebeckite (see Figure 4.16b), with high Fe^{3+} relative to Mg, although one plots as arfvedsonite, due to an abundance of Na+K in the A site. Another is a sodic-calcic amphibole which plots in the ferro-richterite field.

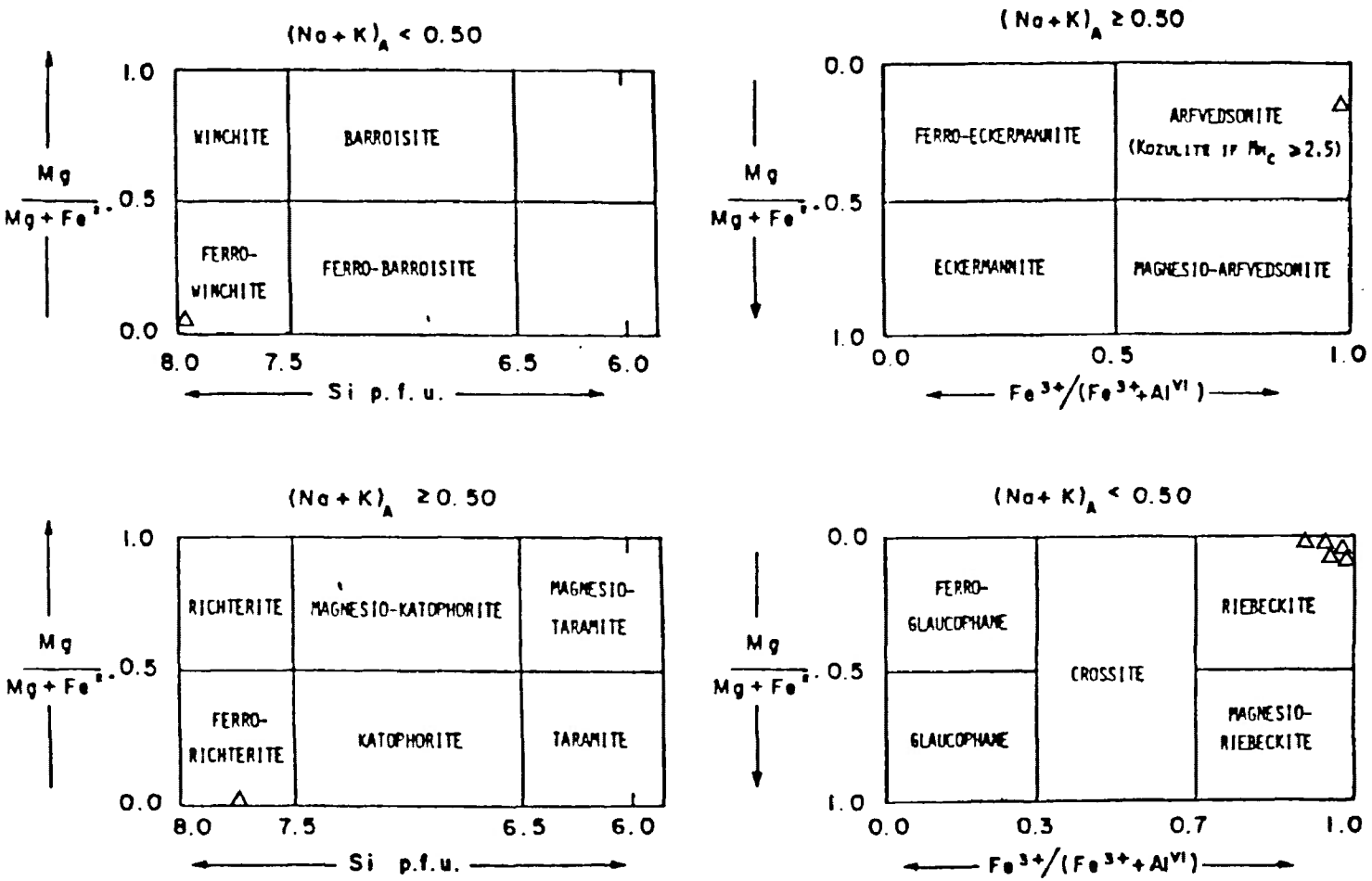

Figure 4.16b Amphibole nomenclature after Leake (1978) with data points for amphiboles from Coldwell tinguaites plotted

Figure 4.17 Total Fe vs Mg in Amphiboles
Sannaites

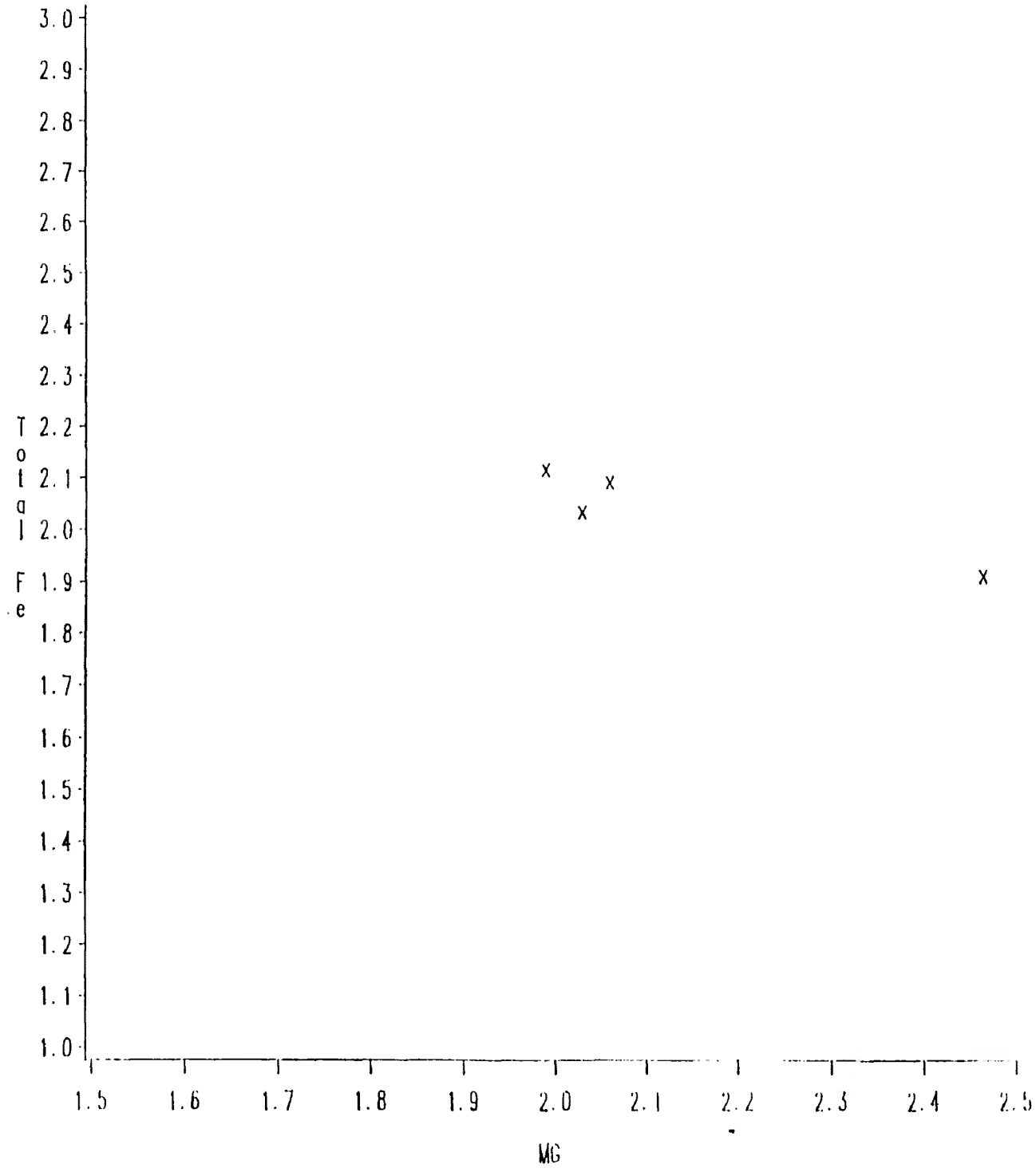

Figure 4.18 Total Fe vs Mg in Amphiboles
Amphibole Camptonites

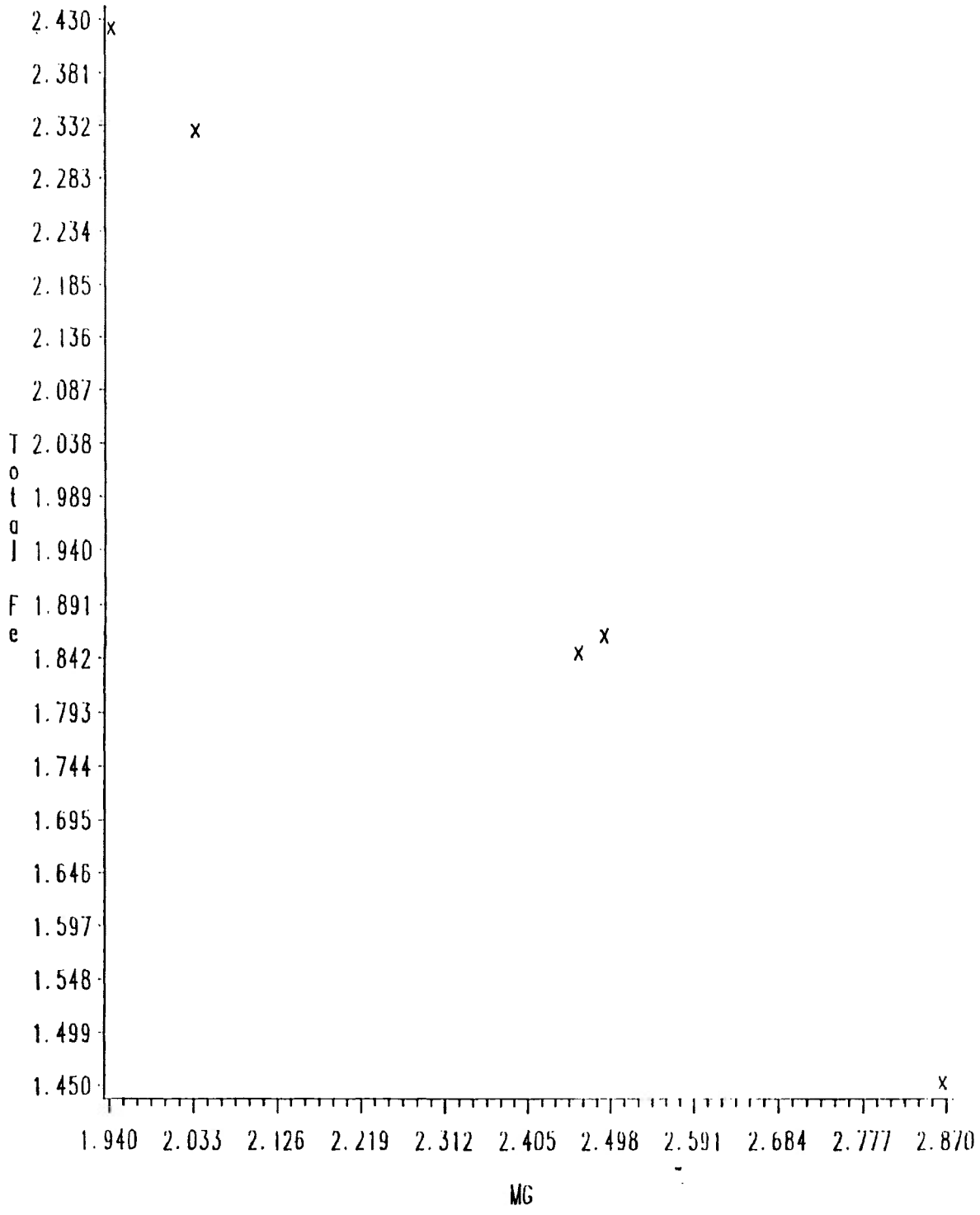

Figure 4.19 Total Fe vs Mg in Amphiboles
Ocellar Camptonites and Monchiquites

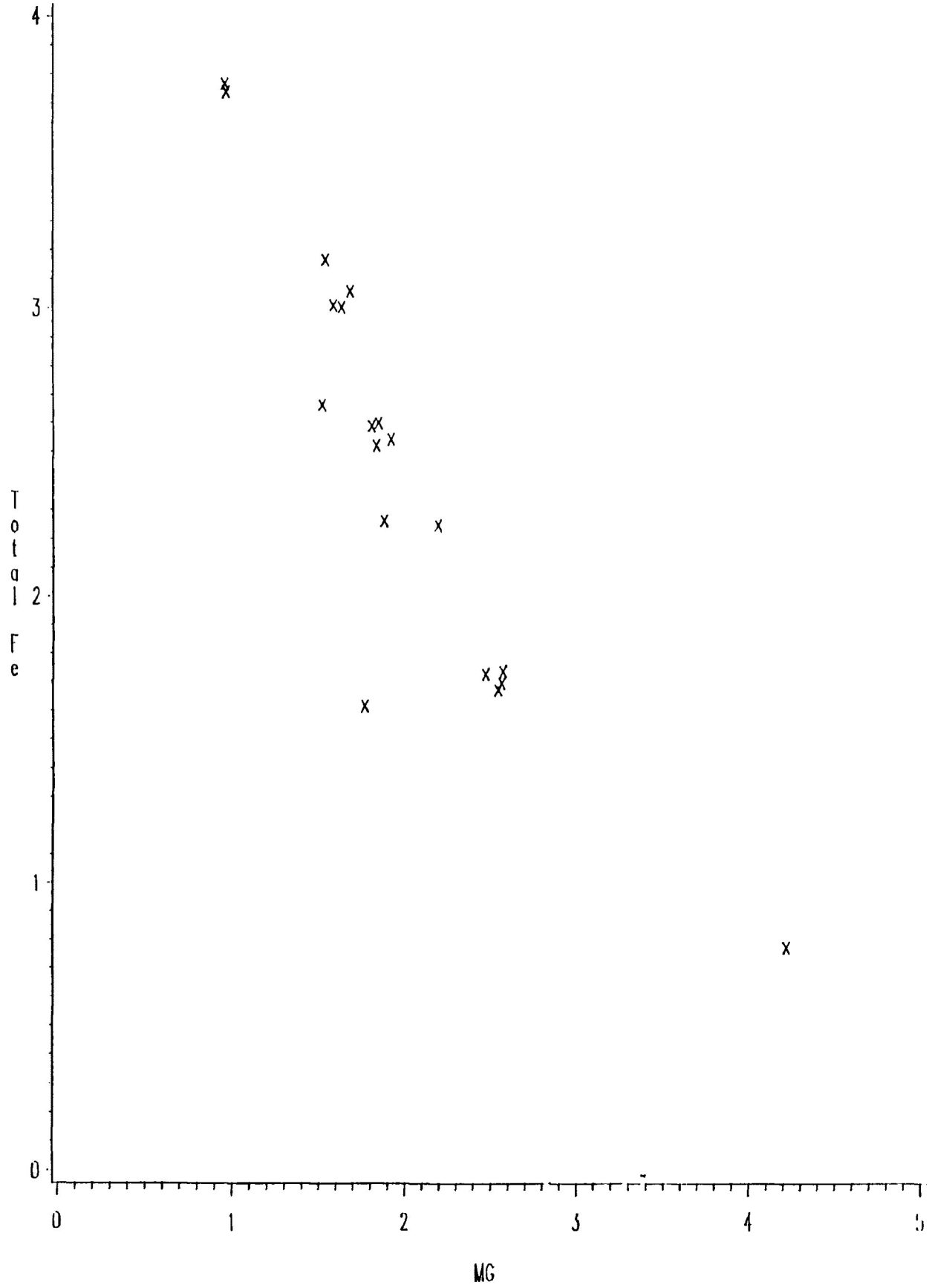

Figure 4.20 **Total Fe vs Mg in Amphiboles**
Quartz Camptonites

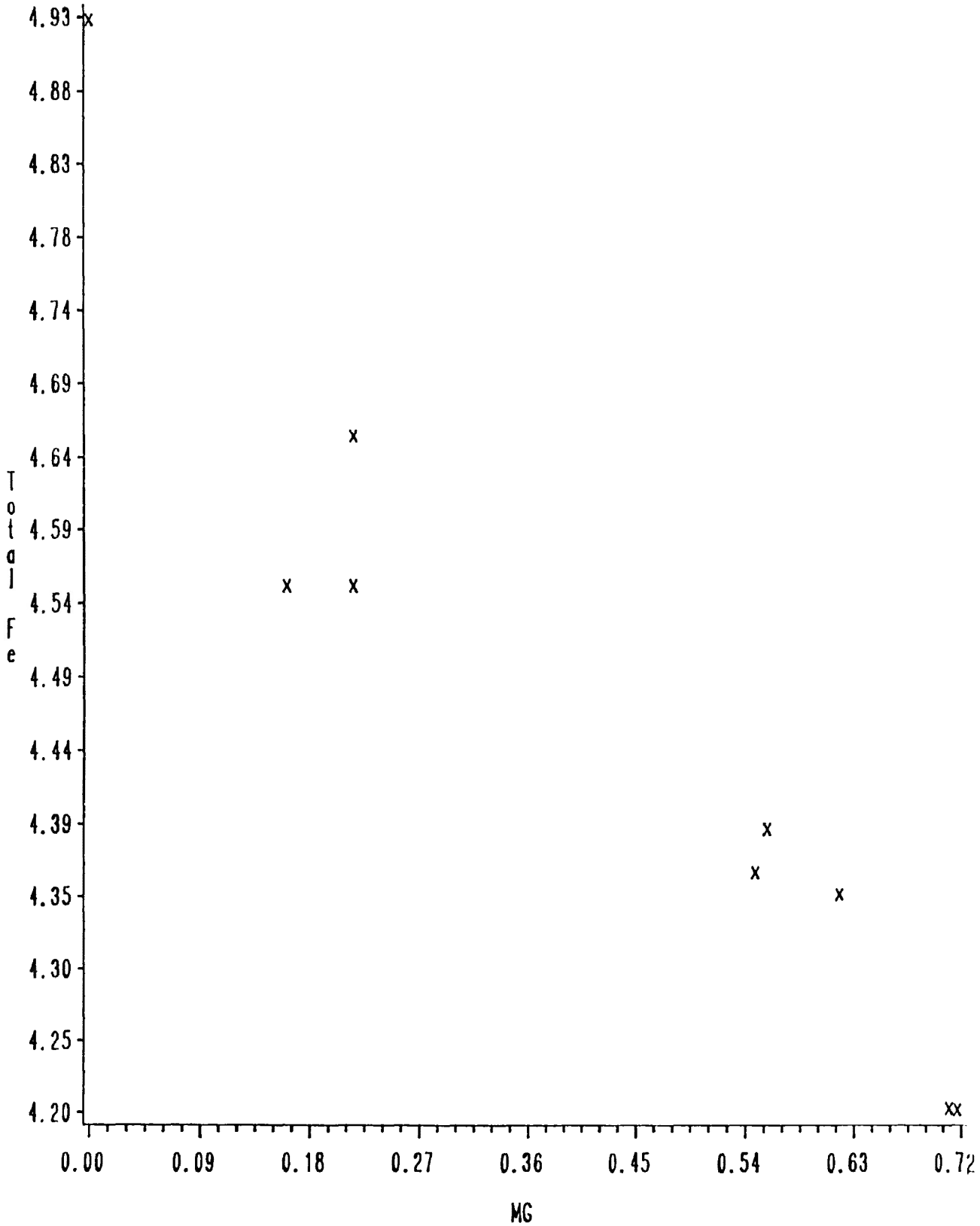

In terms of variations in the compositions of the various amphiboles, the dominant substitution involves the replacement of Mg with Fe (or in terms of end members, the replacement of pargasite with ferrohastingsite) in the outer zones of zoned phenocrysts and in groundmass grains, relative to phenocryst cores; this is also true in the kaersutites, although the extent of the replacement of Mg by Fe is less. This is demonstrated in Figures 4.17, 4.18, 4.19 and 4.20, for the sannaites, amphibole camptonites, and the other camptonites and the monchiquites respectively, since in each case Mg and Fe exhibit a negative covariance along lines with slopes close to unity. This is similar to the situation noted in the clinopyroxenes, although the amphibole replacements are apparently independant of other substitutions since no other plots of atomic proportions of elements result in distinct co-variations. A similar covariance of Fe and Mg is noted in amphiboles occuring in camptonites from the Gran region, Norway, by Scott (1980). No clear pattern of compositional variation is observed in the alkali and sodic-calcic amphiboles of the tinguaites.

FELDSPAR

Paragenesis

In the sannaites and camptonites, feldspar occurs primarily as subhedral or rounded, elongated laths 0.05-0.2mm in length throughout the groundmass. Most crystals are not twinned. Where twinning is observed, carlsbad twinning is most common, although albite twinning is occasionally observed; rarely, baveno twinning is noted. The difference in the degree of extinction between adjacent compositional units in the twinned crystals is often small, however. Feldspar crystals are normally altered to a fine granular assemblage of indeterminant composition, which may include sericite and clay minerals; epidote is occasionally observed replacing feldspar. The degree of alteration varies, and appears to extend from crystal margins inward, although many crystals exhibit fine disseminations of grains which may represent alteration of the interior of the crystal. The feldspars become increasingly turbid with these disseminations as the degree of alteration of the crystal margins increases. Although no definite identification of feldspar type is possible based on petrographic observation, due to small grain size and the commonly advanced degree of alteration, the types of twinning observed (see above)

suggest that plagioclase is more abundant than alkali feldspar, and that at least some of the plagioclase is albitic.

Feldspar also occurs in the sannaites and camptonites as megacrysts i.e. large, intensely altered, elongated laths up to 15mm long displaying well developed albite twinning, and in some cases combined carlsbad and albite twinning, although this type of occurence is very rare.

Feldspar occurs in the monchiquites only as rare, large (up to 10mm), elongated laths similar to the megacrysts described above. Otherwise, the groundmass is dominated by an isotropic material (see below). A similar material in monchiquites from other locations is described by Rock (1977) as being a glass which is feldspar-free or contains microlitic phases which may be incipient feldspar.

In the tinguaites, feldspar occurs as large (0.5mm to 1.5mm), subhedral to euhedral crystals exhibiting well developed carlsbad, or rarely baveno, twinning. Zoning and perthitic exsolution are not observed. Optical properties are more easily determined for these feldspars, although alteration is, in some cases, quite extensive. Crystals are normally altered along their margins, and along fracture

surfaces within the crystal, to fine grained aggregates of sericite, zeolites, calcite and possibly clay minerals. Determination of 2V values for 15 crystals gives a range from 45° to 65°, with a mean value of 53°; this corresponds to a composition of anorthoclase.

Composition

Table 4.6 lists representative compositions determined by electron microprobe analysis for feldspars from the various dyke rocks. In the case of the sannaites, feldspar compositions approximate $Ab_{45}An_{5}Or_{50}$ (microcline or anorthoclase), and $Ab_{95-100}An_{5-0}$ (see Figure 4.21). Rock (1977) states that sannaites are characterized by the presence of alkali feldspar, hence it is reasonable to assume that the former composition represents the primary feldspar of the sannaites, while the latter, albitic composition reflects secondary processes involving Na-somatism which has resulted in albitization of the primary feldspar. Note that this is supported by the information presented in Table 4.6, in that a clearly altered feldspar lath exhibits a very albitic composition, while a less altered lath displays a composition with a higher content of the orthoclase end-member. Furthermore, this is in good agreement with the findings of Spear (1980), who has studied the compositional

Table 4.6 Representative Feldspar Analyses

Rock Type	Sannaite		Quartz Camptonite		Ocellar Camptonite					Amphibole Camptonite		Tinguaites		
Oxide Wt%	altered grdmss. lath	grdmss. lath	grdmss. lath	altered large lath	altered grdmss. lath	grdmss. lath core	grdmss. lath rim	grdmss. lath	xeno. centre	altered grdmss. lath	grdmss. lath	phen. core	phen. rim	altered phen.
SiO2	68.94	55.88	54.39	62.95	64.73	52.05	65.47	54.74	52.02	68.47	57.58	65.05	65.22	66.28
Al2O3	19.55	27.06	28.50	23.92	21.04	30.14	21.14	27.66	29.77	19.28	25.28	17.99	17.83	21.09
TiO2	0.00	0.09	0.00	0.00	0.00	0.00	0.07	0.00	0.00	0.00	0.00	0.00	0.00	0.00
Fe2O3	0.00	0.00	0.00	0.00	0.00	0.00	0.00	0.00	0.00	0.00	0.00	0.00	0.00	0.00
FeO	0.00	0.85	0.68	0.23	0.20	0.27	0.17	0.87	0.24	0.00	0.68	0.00	0.08	0.25
MgO	0.05	0.46	0.12	0.00	0.01	0.00	0.00	0.00	0.00	0.00	0.00	0.00	0.00	0.00
CaO	0.00	0.64	11.30	4.96	2.29	12.13	1.96	10.29	8.47	0.00	7.36	0.00	0.00	0.55
Na2O	11.38	6.06	5.07	9.02	8.12	4.80	10.09	5.31	4.58	11.59	7.59	0.25	0.20	10.02
K2O	0.00	7.70	0.52	0.68	0.20	0.06	0.00	0.48	2.39	0.10	0.08	16.47	16.59	0.97
MnO	0.00	0.30	0.00	0.00	0.00	0.00	0.00	0.00	0.00	0.00	0.00	0.00	0.00	0.00
BaO	0.00	0.00	0.00	0.00	0.00	0.00	0.00	0.00	0.00	0.00	0.29	0.00	0.00	0.00
Structural Formula Based On 32														
Si	12.018	10.163	9.818	11.015	11.683	9.493	11.610	9.976	9.683	12.016	10.479	12.056	12.077	11.719
Al(iv)	0.000	0.000	0.000	0.000	0.000	0.000	0.000	0.000	0.000	0.000	5.424	0.000	0.000	0.000
Al(vi)	4.017	5.801	6.064	4.933	4.476	6.479	4.419	5.943	6.531	3.988	0.000	3.930	3.891	4.395
Ti	0.000	0.012	0.000	0.000	0.000	0.000	0.000	0.000	0.000	0.000	0.000	0.000	0.000	0.000
Fe3+	0.000	0.000	0.000	0.000	0.000	0.000	0.000	0.000	0.000	0.000	0.000	0.000	0.000	0.000
Fe2+	0.000	0.126	0.103	0.038	0.030	0.041	0.025	0.133	0.037	0.000	0.105	0.000	0.000	0.037
Mg	0.013	0.125	0.032	0.000	0.003	0.000	0.000	0.000	0.000	0.000	0.000	0.000	0.000	0.000
Ca	0.000	0.149	2.186	0.930	0.443	2.370	0.372	2.009	1.689	0.000	1.435	0.000	0.000	0.104
Na	3.847	2.137	1.775	3.060	2.842	1.698	3.469	1.876	1.653	3.944	2.678	0.090	0.072	3.435
K	0.000	1.501	0.120	0.152	0.046	0.014	0.009	0.112	0.568	0.022	0.019	3.894	3.919	0.219
Mn	0.000	0.046	0.000	0.000	0.000	0.000	0.000	0.000	0.000	0.000	0.000	0.000	0.000	0.000
Ba	0.000	0.000	0.000	0.000	0.000	0.000	0.000	0.000	0.000	0.000	0.022	0.000	0.000	0.000

Fig 4.21 Feldspars in Sannaite

circles- crystal cores

triangles- crystal intermediate regions

x's- crystal rims

crosses- groundmass grains

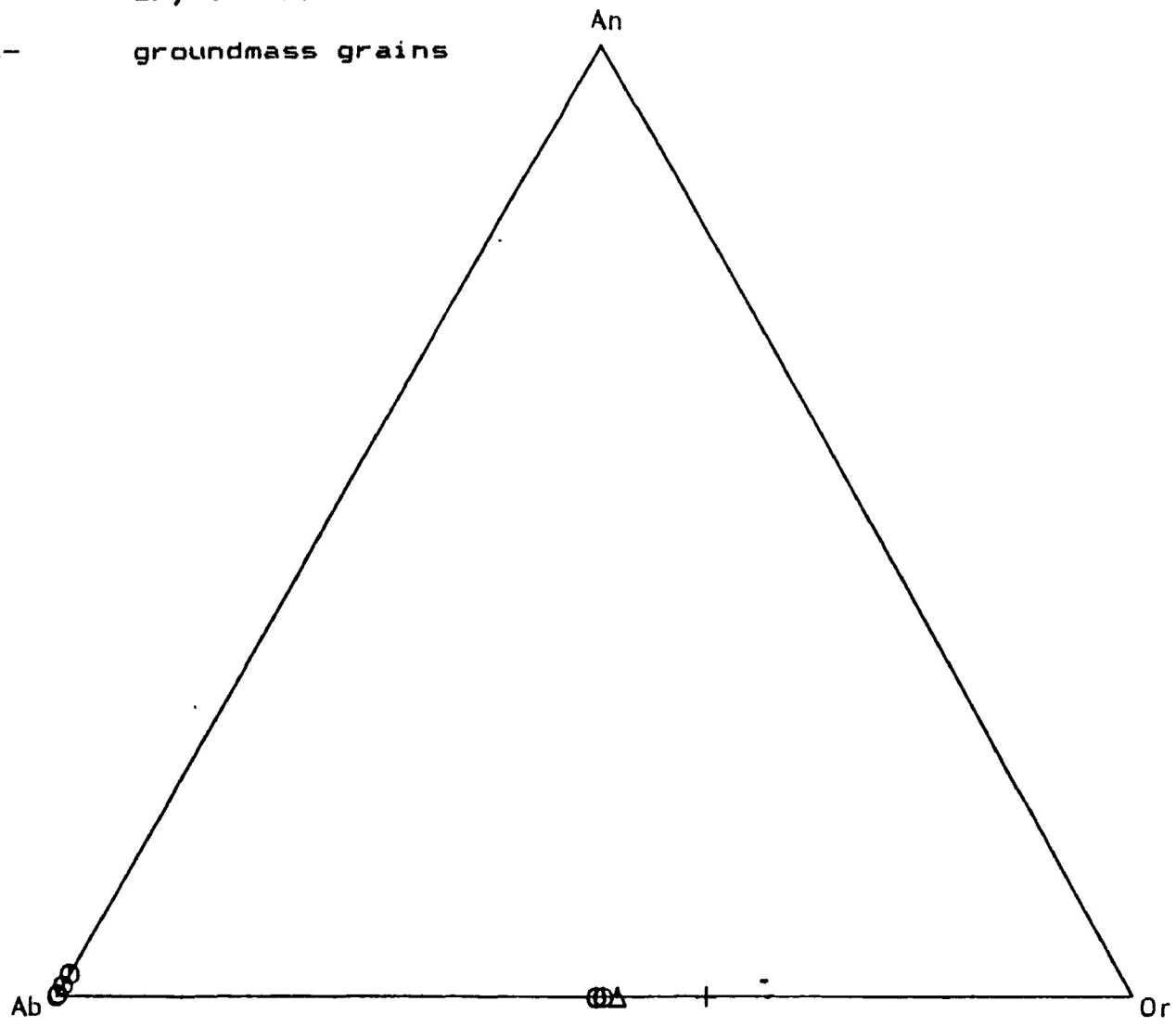

relationships between plagioclase and amphibole, and has found that Na-rich amphiboles coexist with Na-rich plagioclase. However, the amphiboles occuring in these rocks are not Na-rich. The apparent gap between the two above compositions is difficult to explain given the relatively small number of analyses, and therefore may be an artifact of sampling.

With respect to the remaining lamprophyres compositions span a range from almost pure albite in the case of the ocellar and amphibole camptonites, and $Ab_{90}An_{10}$ in the case of the quartz camptonites, to An_{60-70}(labradorite); Or content is generally quite low in the former rock types, rarely exceeding Or_2, while in the latter type it is generally higher, averaging Or_7 (see Figures 4.22, 4.23 and 4.24). No systematic variation in composition is noted between core, intermediate and rim regions in any of the crystals in which these were analyzed. For all of these analyses, those with the highest content of the albite end-member are those which exhibit the most advanced alteration (an exception is the case of one feldspar, occuring in a calcite-zeolite rich veinlet traversing the rock, which also exhibits a high albite content). As suggested for the sannaites, this is probably a result of secondary albitization of more calcic primary feldspar. The

Fig. 4.22 Feldspars in Quartz Camptonites

circles- crystal cores

triangles- crystal intermediate regions

x's- crystal rims

crosses- groundmass grains

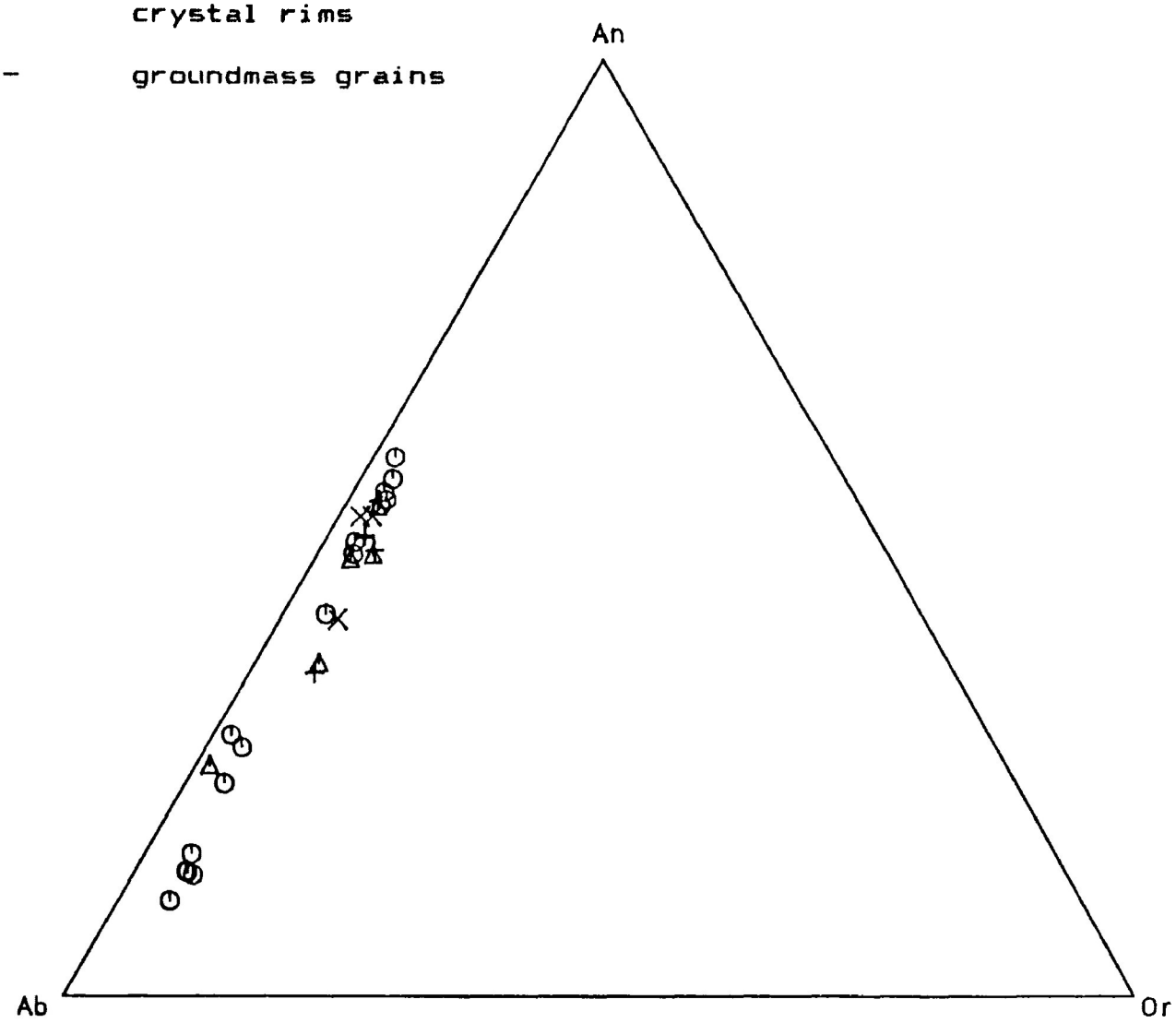

Fig 4.23 Feldspars in Ocellar Camptonite

circles- crystal cores

triangles- crystal intermediate regions

x's- crystal rims

crosses- groundmass grains

solid circle- megacryst

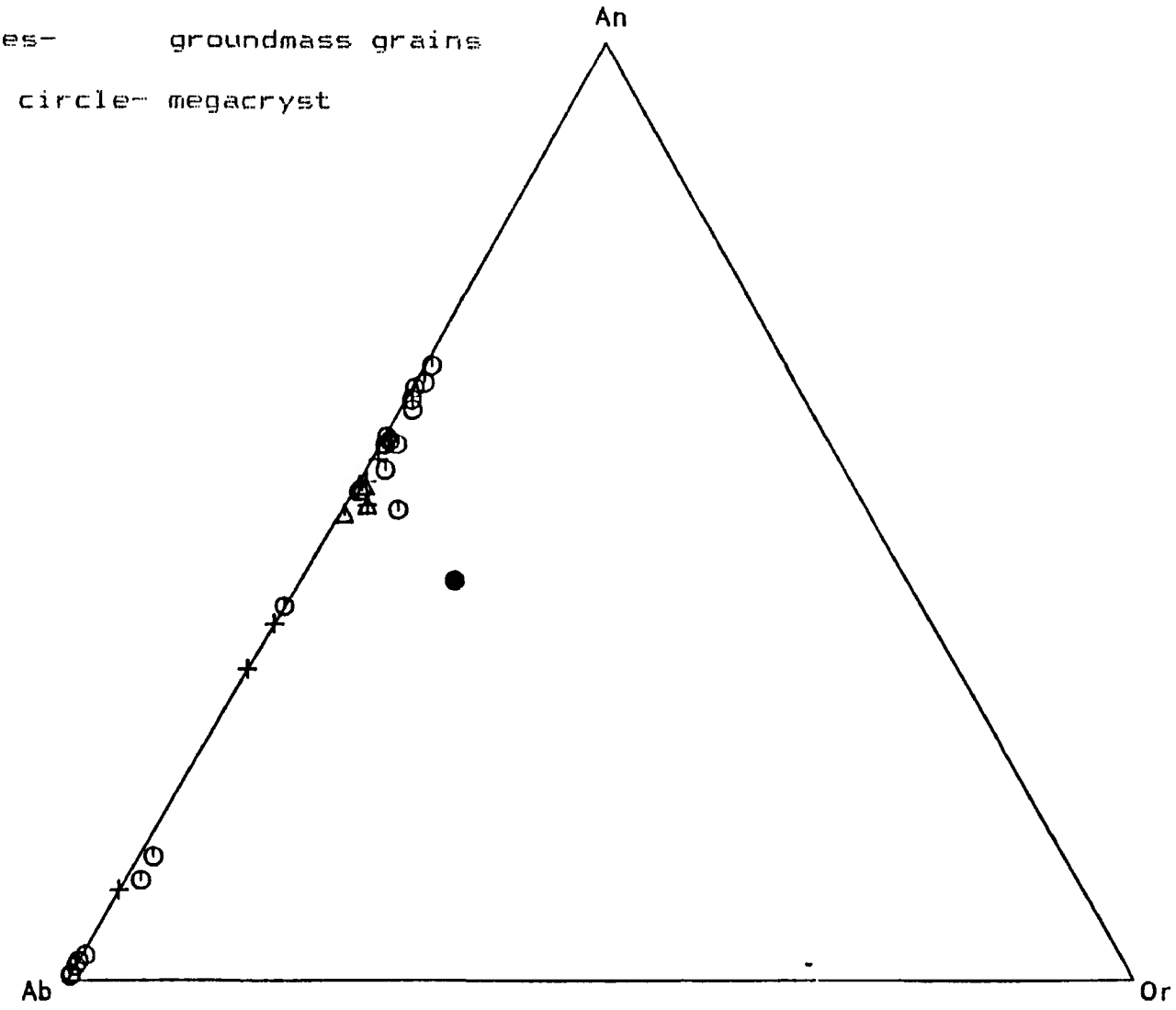

Fig.4.24 Feldspars in Amphibole Camptonite

circles- crystal cores

triangles- crystal intermediate regions

x's- crystal rims

crosses- groundmass grains

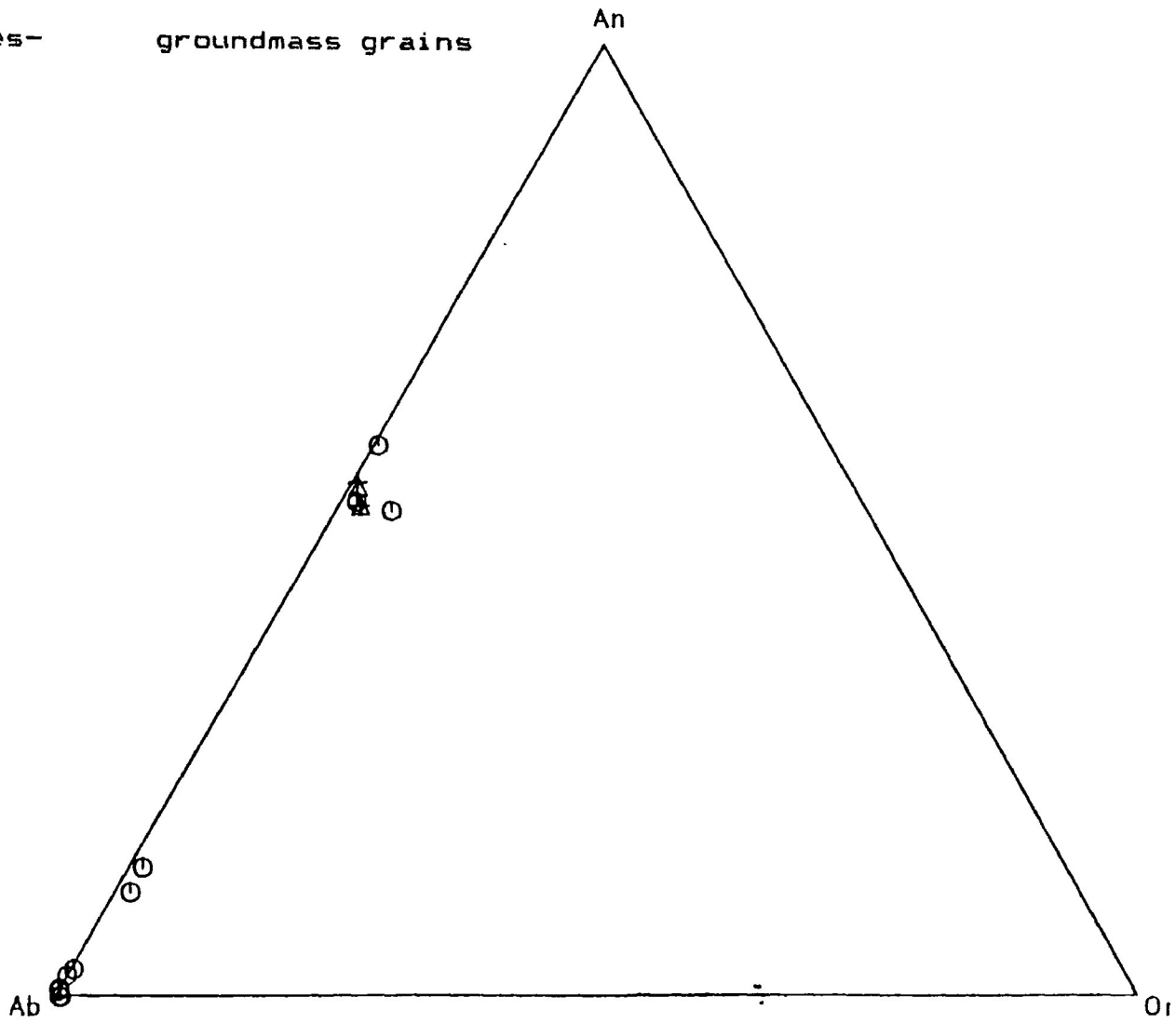

Fig.4.25 Feldspars in Tinguaites

circles- crystal cores

triangles- crystal intermediate regions

x's- crystal rims

crosses- groundmass grains

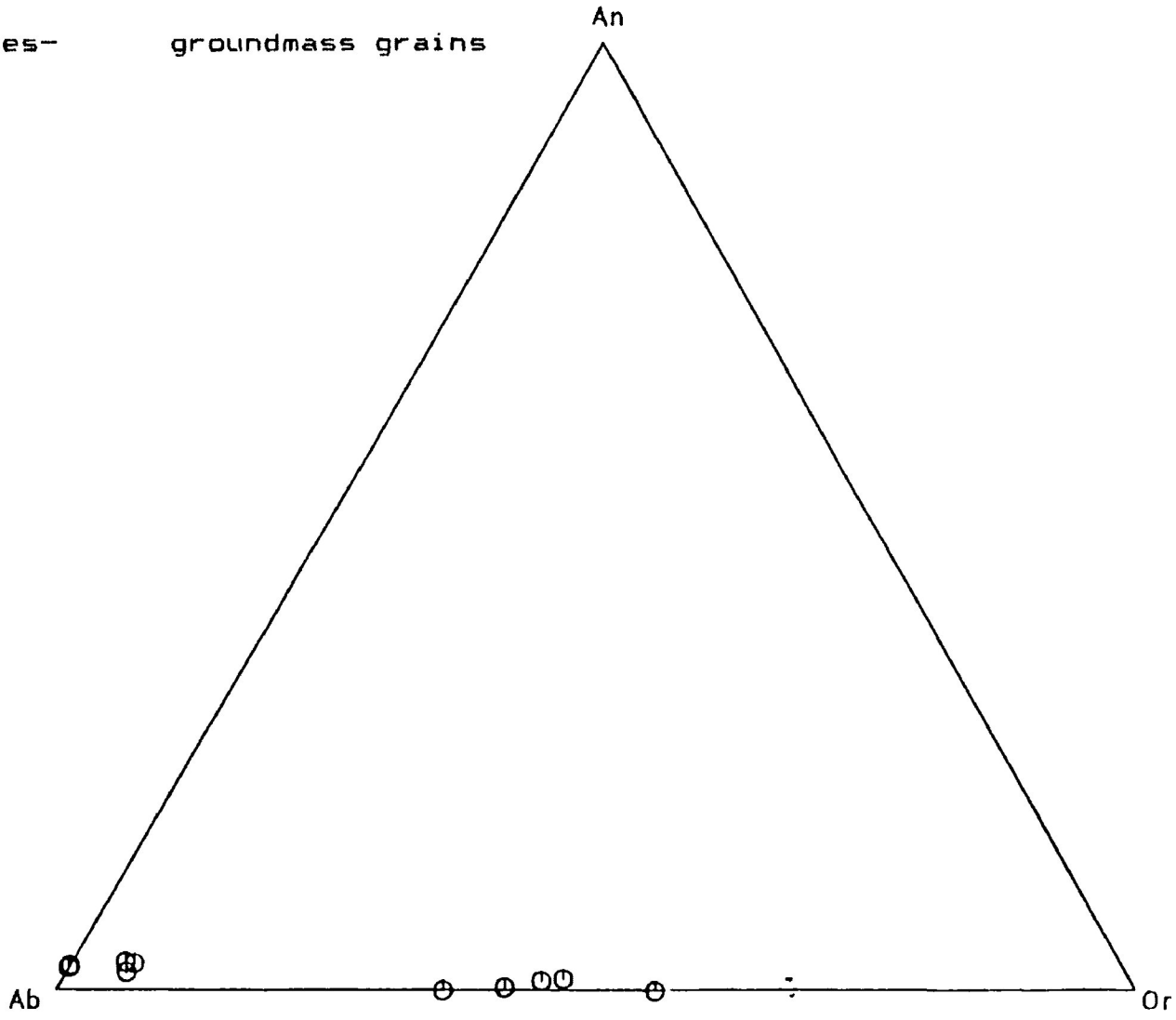

composition of a large feldspar lath which may be xenocrystic is also given in Table 4.6, and is plotted as a filled circle on Figure 4.23. This composition lies off of the main trend defined by the other feldspars occuring in the ocellar camptonites, a fact which suggests that the megacrysts are actually xenocrysts.

In the tinguaites, feldspar compositions range from $Ab_{98}An_2$ to $Ab_{45}An_0Or_{55}$, with an apparent gap (see Figure 4.25). Again, the more Or-rich compositions are believed to represent the primary feldspar, while the Ab rich analyses reflect Na-alteration, as shown in Table 4.6. The compositions of the primary feldspar as given in this table are in good agreement with the composition determined from petrographic analysis (i.e. anorthoclase).

BIOTITE

Paragenesis

Biotite occurs only in the lamprophyres, and only as a groundmass phase. It is considerably more abundant in the camptonites and monchiquites than in the sannaites (see Table 2.1), which are distinguished by a paucity of primary hydrous phases. Crystals are small (0.1mm or less) and anhedral, or

occasionally suhedral, and weakly to moderately pleochroic from brown (alpha) to dark brown (beta=gamma) in the case of the biotites occuring in the sannaites. In the camptonites and monchiquites, biotite crystals form relatively large (up to 1.0mm) subhedral to euhedral laths, which are normally moderately to strongly pleochroic (alpha=pale brown or yellow brown, beta=gamma=brown, dark brown or reddish-brown). Pleochroic haloes are occasionally observed in biotite crystals from all of the various dyke rocks, but are apparently less common in those of the quartz camptonites.

In all rock types, alteration of biotite results in the formation of chlorite, fibrous granular or felted aggregates which may include clay minerals and sericte, opaque phases and rarely calcite. These secondary phases form along cleavage surfaces within the biotite grains, along grain margins, and especially at the terminations of laths. In some cases, biotite grains are completely pseudomorphed by these phases.

Composition

Representative compositions of biotite from the various dyke rocks are given in Table 4.7. In the case of the sannaites and the ocellar camptonites, biotites span a

Table 4.7 Representative Biotite Analyses

Rock Type	Sannaite		Quartz Camptonite	Ocellar Camptonite			Monchiquite	Amphibole Camptonite
Oxide Wt%	grdmss. lath	grdmss. lath	grdmss. lath	grdmss. lath	grdmss. lath	grdmss. lath	grdmss. lath	grdmss. lath
SiO2	35.86	39.72	32.52	32.35	31.08	37.78	31.51	31.27
Al2O3	15.41	10.10	15.25	15.23	17.28	14.78	15.71	17.43
TiO2	2.42	0.48	3.36	7.19	2.72	0.85	0.10	2.82
Fe2O3								
FeO	19.04	8.80	22.58	20.77	19.82	16.30	23.74	19.02
MgO	12.57	22.42	8.57	9.44	10.81	14.50	11.64	11.08
CaO	0.02	0.18	0.39	0.00	0.07	2.33	0.31	0.10
Na2O	0.08	0.35	0.16	0.51	0.48	0.62	0.13	0.50
K2O	9.24	8.26	7.20	6.99	7.12	7.36	5.45	7.34
MnO	0.27	0.18	0.33	0.29	0.29	0.24	0.37	0.28
Cr2O3	0.03	0.02	0.00	0.00	0.00	0.13	0.00	0.00
Sum	94.94	90.51	90.36	92.77	89.67	94.89	88.96	89.84
Structural Formula Based On 22 Oxygens								
Si	5.497	6.036	5.333	5.117	5.072	5.678	5.183	5.706
Al(iv)	2.503	1.809	2.667	2.839	2.928	2.322	2.817	2.294
Al(vi)	0.281	0.433	0.280	0.000	0.395	0.286	0.229	1.045
Ti	0.279	0.055	0.414	0.855	0.334	0.096	0.123	0.344
Fe2+	2.441	1.118	3.097	2.748	2.705	2.049	3.266	2.582
Mg	2.872	5.078	2.095	2.226	2.629	3.249	2.854	2.681
Ca	0.003	0.029	0.067	0.000	0.012	0.375	0.055	0.017
Na	0.024	0.103	0.051	0.156	0.152	0.181	0.042	0.157
K	1.807	1.601	1.506	1.411	1.482	1.411	1.144	1.520
Mn	0.035	0.023	0.046	0.039	0.040	0.031	0.052	0.039
Cr	0.004	0.002	0.000	0.000	0.000	0.015		0.000

compositional range based largely on the covariance of Fe^{2+} and Mg (in terms of end-member components, annite and phlogopite). Ti appears to be coupled with Fe^{2+} in this substitution (Deer et al, 1966). Note that those biotites with the highest Ti content (i.e. 7.19 weight % TiO_2 in one biotite from an ocellar camptonite, as shown in Table 4.7) exhibit the reddest absorption colours.

Biotites are apparently more compositionally uniform in the other rock types, tending to be annitic. Replacement of K by Na in biotites in these rocks rarely exceeds 0.2 atoms per formula unit, and K by Ca 0.05 atoms per formula unit, with the notable exception of one analysis (see Table 4.7) of a biotite crystal in an ocellar camptonite, in which CaO constitutes 2.33 weight %. The relatively low K_2O content of the biotite composition from the monchiquite in Table 4.7 is probably an effect of alteration (Mitchell, personal communication).

OLIVINE

Paragenesis

Olivine occurs in only a small number of lamprophyres (2 ocellar lamprophyres- C87 and C577- and 2 monchiquites- C560

and C586), and only as a volumetrically minor phenocryst phase. In all cases the crystals are large (2.0mm to 7.0mm), colourless or pale yellow-green and subhedral. Normally, alteration is extensive, particularily along grain margins and fractures within the crystals. Alteration and replacement products include chlorite, calcite, iddingsite, granular and felted cryptocrystalline aggregates which may include serpentine minerals, and opaque phases. The latter are both disseminated as fine grains, or occur as coarser aggregates along rims of and fractures within olivines. In many cases, olivine phenocrysts are completely pseudomorphed by these phases, and normally, only small amounts of relict olivine remain. No zoning is observed in any of the olivine phenocrysts.

Occasionally, a rim or corona, apparently distinct from the products of the alteration described above, comprising fine grained clinopyroxene and very fine grained opaque phases is seen to partially or completely encircle an olivine phenocryst. Rarely, the clinopyroxene occurs as sub-radially oriented laths. The width of this rim is variable. Rounded, fine grained masses of nearly cryptocrystalline material in part resembling this clinopyroxene are also observed, and may represent complete replacement of olivine phenocrysts by the rim-forming clinpyroxene. Similar rims are observed in

association with other occurences of olivine (Deer et al, 1966), resulting from the reaction of olivine and plagioclase at upper greenschist-lower amphibolite facies conditions, in the presence of water. However, Rock (1979) observes similar clinopyroxene-bearing rims around olivine phenocrysts (or xenocrysts) in lamprophyres in the Serra del Monchique alkaline complex, Portugal, and interprets them to be the result of resorption by the host magma. Given the complete lack of plagioclase in the monchiquites of the Coldwell complex (in which corona-bearing olivines occur) and the lack of evidence for upper greenschist-lower amphibolite facies metamorphic conditions post-dating the Coldwell dykes, the former interpretation (Deer et al, 1966) appears unlikely. Therefore, such rims, in the case of the Coldwell dykes, are interpreted to represent resorption such as that noted by Rock (1979).

In several olivines occuring in a monchiquite (C560), inclusions of a fine grained opaque phase are noted within unaltered olivine.

Composition

Table 4.8 gives representative compositions of olivine phenocrysts. Although, as noted above, no optical zoning is

Table 4.8 Representative Olivine and Spinel Analyses

Rock Type	Ocellar Camptonite				Monchiquite			
Oxide Wt%	remnant olivine phen. w corona	phen. core	phen. rim	small phen.	altered phen. core	altered phen. rim	remnant small phen.	small spinel inc. in olivine
SiO2	33.84	39.74	39.12	38.97	39.81	38.63	39.76	
Al2O3	0.00	0.10	0.10	0.08	0.00	0.00	0.00	15.56
TiO2	0.00	0.00	0.02	0.00	0.00	0.00	0.00	1.38
Fe2O3								
FeO	43.99	10.74	16.61	14.16	11.07	18.71	12.79	26.91
MgO	21.48	48.26	43.46	45.50	47.47	41.20	46.99	11.15
CaO	0.00	0.33	0.61	0.45	0.27	0.19	0.23	
Na2O	0.09	0.04	0.04	0.05	0.00	0.00	0.00	
K2O	0.00	0.00	0.00	0.00	0.00	0.00	0.00	
MnO	1.50	0.18	0.39	0.27	0.06	0.21	0.11	0.22
Cr2O3	0.00	0.06	0.00	0.02	0.00	0.00	0.00	44.98
Sum	100.90	99.45	100.35	99.50	98.68	98.94	99.88	100.20
Structural Formula Based On 4 Oxygens								*
Si	0.982	0.986	0.989	0.983	0.995	0.999	0.990	
Al(iv)	0.000	0.003	0.003	0.002	0.000	0.000	0.000	
Al(vi)	0.000	0.000	0.000	0.000	0.000	0.000	0.000	4.8466
Ti	0.000	0.000	0.000	0.000	0.000	0.000	0.000	0.2743
Fe3+								1.8114
Fe2+	1.068	0.223	0.351	0.299	0.232	0.405	0.266	4.1361
Mg	0.929	1.785	1.684	1.711	1.769	1.588	1.745	5.2137
Ca	0.000	0.009	0.017	0.012	0.007	0.005	0.006	
Na	0.005	0.002	0.002	0.002	0.000	0.000	0.000	
K	0.000	0.000	0.000	0.000	0.000	0.000	0.000	
Mn	0.037	0.003	0.008	0.006	0.001	0.005	0.002	0.0384

observed, for larger phenocrysts occuring in both the ocellar camptonites and the monchiquites the Fe (and Mn) content increases while Mg content decreases in rims relative to cores. In terms of end-members components, phenocryst cores approximate $Fo_{90}Fa_{10}$, while rims are $Fo_{81}Fa_{18}Tp_{01}$. Smaller crystals have compositions intermediate to these values. This is noteworthy, since in the case of other phenocryst phases, such as clinopyroxene and amphibole, small crystals normally have compositions similar to phenocryst rims; the inference is that different olivines may have nucleated and begun to crystallize at different times. A remnant olivine phenocryst with a corona such as that described above gives a composition of $Fo_{46}Fa_{52}Tp_{2}$ (see Table 4.8); this represents an extreme example of Fe+Mn substitution for Mg, such that this may represent a relatively late-crystallizing olivine.

Table 4.8 also includes an analysis of an opaque grain occuring within unaltered olivine in a monchiquite. This is a spinel with a composition dominated by the chromite, $spinel_{ss}$ and, to a lesser extent, magnesiochromite end-members. Note that all such spinels analysed have very similar compositiitons.

NEPHELINE

Paragenesis

Nepheline occurs in all of the various types of dyke rocks, although in the lamprophyres it is present only as a minor groundmass phase (see Table 2.1). In the tinguaites, it forms an important phenocryst phase (see Table 2.2).

Determination of the optical properties of nepheline occurring in the lamprophyres is difficult i.e. crystals are normally very small (0.1mm or less), and alteration is extensive. The common alteration products are cryptocrystalline granular aggregates, zeolites, analcite and carbonate minerals. Rarely, pale yellow-orange cancrinite is recognizeable. It is difficult to distinguish positively nepheline from alkali feldspar (Kerr, 1977), especially in the case of small crystals, so that nepheline may be mis-identified in some cases, and is therefore under-represented in Table 2.1. Generally, where postively identified, nepheline occurs as anhedral, or occasionally subhedral, colourless and frequently turbid grains.

In the case of the tinguaites, determination of the optical properties and positive identification of nepheline

is facilitated by the relatively large grain size (up to 1.5mm). Crystals are subhedral to euhedral, and are normally turbid with disseminated fine-grained inclusions. Zoning is not observed. In the tinguaites, nepheline is distinguished from alkali feldspar (anorthoclase) by a lack of twinning, low birefingence and by a negative uniaxial interference figure. Alteration products include the zeolites natrolite and stilbite, carbonate minerals, pale yellow or yellow cancrinite, analcite, and rarely sericite. The analcite, which is abundant in many of the Coldwell tinguaites, may be commonly derived from nepheline (see below).

Composition

Representative compositions of nepheline are given in Table 4.9. The nephelines occuring in the various camptonites are quite uniform in composition being approximately $Ne_{76}Ks_{23}Q_1$. Note that the Ks content of these nephelines is somewhat higher than that observed for nephelines occurring in other lamprophyres (ie. Rock, 1978). No compositions were determined for nepheline occurring in the sannaites and monchiquites.

In the tinguaites, compositions were determined for

Table 4.9 Representative Nepheline and Analcite Analyses

Rock Type	Lampro-phyre	Tinguaite	Tinguaite
	grdmss. nepheline	nepheline phenocryst	analcite
Oxide Wt%			
SiO2	41.88	44.65	54.73
Al2O3	32.99	32.03	23.65
TiO2	0.03	0.00	
FeO*	0.74	0.59	0.09
MgO	0.00	0.00	
CaO	0.78	0.71	
Na2O	16.11	17.25	11.15
K2O	6.82	3.66	0.09
MnO			
Sum	99.35	98.89	89.71
Structural Formula Based On 32			Based On 7
Si	8.179	8.585	2.362
Al(iv)	7.595	7.361	
Al(vi)			1.203
Ti	0.005	0.000	
Fe2+	0.109	0.085	0.003
Mg	0.000	0.000	
Ca	0.163	0.147	
Na	6.098	6.428	0.933
K	1.699	0.897	0.005
Mn			

* Total Fe as FeO

three nepheline phenocrysts; these are all close to $Ne_{62}Ks_{13}Q_5$.

ANALCITE

Paragenesis

Analcite occurs in all types of dyke rocks, but is volumetrically abundant only in the tinguaites (see Tables 2.1 and 2.2), in which it occurs as phenocrysts.

In the lamprophyres, analcite is observed most commonly in ocelli, where it is closely associated with carbonate minerals. It occurs as coarse (0.1mm to 0.8mm), colourless, anhedral grains of low relief, which are characteristically isotropic. Normally, analcite is confined to the margins of the ocelli, but, in some cases, is observed to occur throughout; such a paragenesis is common (e.g. Philpotts, 1974; Foley, 1984; Strong and Harris, 1974). The nature and origin of the analcite occuring in the ocelli will be discussed in detail below.

In the case of groundmass and vein occurences, the crystals tend to be smaller (less than 0.1mm), occuring singly or as irregular aggregates. Groundmass grains are

normally interstitial to other phases, and in rare instances, appear to replace various primary phases, (e.g. nepheline and feldspar) in conjunction with other zeolites, calcite, and cryptocrystalline phases (possibly clay minerals and sericite).

It is difficult, therefore, to determine whether any of the groundmass analcite is primary, since at least some is noted to be secondary, and, with respect to the remainder, Deer et al (1966) note that the distinction between magmatic (primary) and hydrothermal (secondary) analcite is not easily made when it occurs as interstitial grains. However the occurence of primary analcite is possible in rocks such as these (Deer et al, 1966; Kerr, 1973). Note, however, that the P-T range in which analcite plus melt is a stable assemblage is quite limited (i.e. 5-13 kb and 600°-640°C in the systems Ne-Ab-H_2O and Ne-Or-Ks-H_2O; Gibbs and Henderson, 1977), and may be well below the solidus for mafic rocks such as these lamprophyres (Gibbs and Henderson, 1977, 1983), although this does not consider the depression of the solidus with respect to T brought about by increased P_{H2O}. Nevertheless, this would appear to indicate that a primary origin for this analcime is unlikely, and therefore that it represents an alteration of a primary phase such as nepheline, in a manner similar to that observed by Gibbs and

Henderson (1983) in the Dippin Sill, Isle of Arran, Scotland. Such alteration may be related to the presence of a Na-rich solution, which may also be related to the formation of albite-rich rims on feldspar crystals (Gibbs and Henderson, 1977). More detailed analyses of the felsic phases occuring in the lamprophyres in the manner of Gibbs and Henderson (1983) may resolve this question conclusively.

Analcite in veinlets is secondary (e.g of hydrothermal origin), occuring as aggregates of fine (0.1mm or less) anhedral or subhedral grains intimately intergrown with other veinlet-forming phases (i.e. calcite, other zeolites, prehnite, pectolite, epidote and chlorite- see Chapter 2).

The isotropic material forming much of the groundmass of monchiquites in other locations has been identified as analcite (Pirsson, 1896; Evans, 1901). This is discussed with reference to the Coldwell monchiquites in detail in a later section dealing with the isotropic base of these rocks.

Analcite in the tinguaites normally occurs as large (0.2mm to 1.5mm), clear or slightly turbid, subhedral or rarely euhedral crystals interstitial to the alkali feldspar and nepheline phenocrysts which comprise the bulk of the rock. It is commonly closely intergrown with anhedral

carbonate minerals. It is also sometimes observed as irregular patches apparently replacing nepheline, however, it is almost always in sharp contact with the feldspar. Rarely, it occurs in veinlets traversing the rock, where it occurs with other zeolites and carbonate minerals.

Although it is clear that analcite replacing nepheline and occuring in veinlets is secondary, resulting from the action of hydrothermal solutions at sub-solidus temperatures, the origin of the interstitial analcite is more problematical. As noted previously, analcite plus melt is stable under limited conditions in Ne-Ab-H_2O and Ne-Or-Ks-H_2O, both of which systems are relevant to the tinguaites. Therefore, a secondary origin may be more realistic for the interstitial analcite in the tinguaites, as discussed previously in the case of the lamprophyres. However, the tinguaite solidus may approach the relatively low temperatures defined by the above systems, so that a primary origin for this analcite is conceivable. Webb (1971) considers analcite occuring with calcite in lenses which are continuous with the groundmass of phonolite flows from the South Turkana region of the Kenya rift valley to be primary, representing crystallization of a late stage residuum.

Composition

A representative composition of a an interstitial analcite crystal from a tinguaite is given in Table 4.9. No CaO was detected in this specimen, which, as Gibbs and Henderson (1983) suggest may represent a recrystallized earlier-formed analcite. Such are characterized by higher CaO content.

QUARTZ

Paragenesis

Quartz is confined almost entirely to the quartz-bearing camptonites, in which it occurs as an important phenocryst (or xenocryst) phase. It occurs very rarely in the ocelli of a few of the other camptonites.

In the quartz camptonites, quartz occurs as isolated anhedral (i.e. rounded), or rarely subhedral or euhedral (i.e. sub-hexagonal to hexagonal) crystals which are generally large, but exhibit considerable variation in size (1.0mm to 10.0mm). Extinction is characteristically uniform throughout a given crystal, and crystals are normally relatively free of inclusions, although in some instances

isolated opaque grains are present. Invariably, quartz crystals occurring in the quartz camptonites are surrounded by narrow (0.1mm or less) rims of cryptocrystalline melanocratic material. Positive identification of this material is difficult, although detailed examination shows that in some instances, elongated mafic laths are arranged sub-radially around the quartz crystal. Donaldson (1905), performing experiments to determine the rate of dissolution of quartz in a basaltic magma, observed the formation of rims of elongate pigeonite crytals around the quartz grains, while Nicholls et al (1973) state that quartz crystals occurring in some basic lavas are surrounded by coronae of pyroxene grains. Therefore, it is possible that similar mafic laths around quartz crystals in the Coldwell quartz camptonites are clinopyroxene. In the example of sub- and euhedral quartz grains, such rims often do not completely surround the crystal, but dark bands at the interface of a crystal face and the groundmass may represent incipient clinopyroxene rims. Where rims are present, they appear to have formed at the expense of quartz, in that the euhedral outlines of crystals are slightly rounded. Such rims, therefore, represent resorption of the quartz by the host magma. This is a clear indication of disequilibrium between the quartz and the magma, which may indicate a xenocrystic origin for quartz. This is observed by Bacon and Carmichael (1975) in

basalts from the San Quintin region of Baja, California, since these authors determined that a pressure of 52 kb was required to precipitate quartz from these basalts. In this example, however, the basalts intruded a sandstone, which provided an abundant supply of rounded quartz grains. At the Coldwell Complex, only small volumes of highly evolved Centre 1 rocks containing quartz could supply such material to these dykes, unless a quartz-bearing source which is currently not exposed or is external to the complex (i.e. the Archean terrain) is invoked. There is little evidence to support either of the latter sources. A xenocrystic origin for the quartz is therefore believed to be unlikely. Nicholls et al (1973) determined that quartz crystals occurring in basic lavas from Lassen Peak, California and Talasea, New Britain, are cognate in origin, crystallizing directly from magmas, at 14.3 kb (Lassen Peak) to 16.0 kb (Talasea), assuming a quenching temperature of approximately 1000° C. A cognate origin is therefore suggested for the quartz crystals occuring in the Coldwell quartz camptonites; this is supported by the occurence of euhedral quartz grains, which may represent crystals which have undergone little resorption, perhaps as a result of local conditions in the magma, such as a local elevation in the silica activity, which would serve to inhibit the dissolution of quartz (Donaldson, 1985).

Rarely, quartz occurs as an ocellar phase. The crystals tend to be small (less than 0.2mm) and anhedral, and generally form aggregates of interlocking grains usually located along the periphery of the ocelli in which they occur. In a few instances, larger single grains are observed in ocelli. In either case, quartz crystals normally exhibit uniform or weakly undulose extinction, and a complete lack of inclusions. The absence of quartz-bearing veinlets, and silicification of the groundmass, associated with quartz-bearing ocelli indicates that the quartz is primary with respect to the ocelli. This suggests that at least some of the ocellar material, which is silica-oversaturated, represents a separate system with respect to the host groundmass, which is normally silica undersaturated (i.e. precipitates primary nepheline).

ISOTROPIC MATERIAL

Paragenesis

The isotropic material described in this section refers to that comprising most of the groundmass of the monchiquites. This is a low relief material, normally pale grey-brown, or less commonly deep brown, red-brown or

colourless. It is dark, or displays a slight mottling of neutral colours throughout an extinct background, under cross-polarized light. No distinct features (e.g. cleavage, form, etc.) are observed, although a granular appearance is common. Indeterminant dark-coloured streaks, patches and feathery structures are also noted. Microlitic grains and needles are abundant; dark coloured types may include clinopyroxene, amphibole, biotite and accessory phases such as zircon, sphene and Fe-Ti oxides, while neutral or colourless microlites may be feldspar and nepheline. The brown colour of the isotropic material is likely at least in part due to inclusion of these microlites.

The presence of an isotropic constituent in the groundmass of monchiquites is characteristic of this type of rock (Rock, 1977,1978,1979,1981). The exact nature of this material has been the subject of some debate, in that early workers (e.g. Pirrson, 1896), concluded that it was analcite, while more recently (e.g Rock, 1977,1979), glass has been considered a more realistic alternative. Analcite may, however, be an alteration product of glass.

In the Coldwell monchiquites, the complete lack of a distinct analcite pattern in the powder x-ray spectrum generated by x-ray diffraction analysis of this rock type

indicates that the presence of analcite is unlikely. Therefore, the isotropic material forming the base of the groundmass in the Coldwell monchiquites is probably a glass whose exact composition has not been determined. However, as noted in Chapter 3, the major element chemistry of the monchiquites is essentially indistinguishable from that of the ocellar camptonites, and the mafic mineralogy of these two rock types is much the same. Therefore, it is reasonable to infer that the composition of the glass in the monchiquite groundmass will be close to that of the feldspars (and nepheline- Rock, 1977) occuring in the ocellar camptonites (see Feldspar, previously). Note that according to Rock (1977), this glass occurs in place of feldspar in the monchiquite groundmass. The microlitic phases observed may represent, at least in part, incipient feldspar formation.

ACCESSORY PHASES

Accessory phases include sphene, apatite, zircon, aenigmatite, magnetite, titanmagnetite, ilmenite and sulphide phases. Each of these is described in the following sections. Some of the minerals occuring in the ocelli may also be primary (see Chapter 4), however, these are dealt with in a subsequent section.

Sphene

Sphene occurs as small (0.05mm or less), generally euhedral grains in the groundmass of many of the camptonites and monchiquites, and less commonly in the tinguaites. Normally, it is deep brown or black; according to Deer et al (1966) such dark colouration in sphene reflects a high Fe content. This is in good agreement with the analysis given in Table 4.10. No pleochroism is evident. In one instance, a pale yellow alteration product is probably leucoxene. Sphene is notably absent from the sannaites.

Apatite

Apatite is ubiquitous in the Coldwell dyke rocks. It occurs as small (0.05mm or less), colourless, subhedral to euhedral grains confined to the groundmass of the various dyke rocks. Fine microlitic needles associated with the glassy component of the monchiquite groundmass may be apatite as well.

Zircon

Although very small (0.03mm or less), euhedral grains of zircon are commonly observed in all of the lamprophyres,

Table 4.10 Representative Analyses of Accessory, Secondary, and Ocellar Minerals

	Accessory Minerals		Carbonate Minerals			Scapolite		Epidote	
	sphene	magnetite	grdmss. carbonate	ocellus carbonate	veinlet carbonate	scapolite rep. feldspar	ocellus scapolite	grdmss. epidote	ocellus epidote
Oxide Wt%									
SiO2	30.23	0.31	0.01	0.00	0.01	55.01	53.92	38.37	37.59
Al2O3	1.97	4.23	0.03	0.00	0.00	22.89	24.30	26.37	25.22
TiO2	34.63	0.05	0.00	0.00	0.00			0.47	0.02
FeO*	1.67	95.60	0.05	2.67	0.03	0.18	0.15	7.39	10.64
MgO		0.06	0.06	1.26	0.05				0.11
CaO	27.55	0.02	54.14	54.82	54.23	7.38	8.30	23.59	20.78
Na2O			0.01	0.00	0.00	8.06	8.38		3.10
K2O			0.00	0.00	0.00	0.90	0.65		0.00
MnO			0.15	1.47	0.25			0.21	0.05
Cr2O3			0.01	0.00	0.00				0.00
BaO									
CO2#			45.54	39.78	45.43				
Total	96.05	100.27	100.00	100.00	100.00	94.42	95.70	96.40	95.51

* Total Fe as FeO

CO2 in carbonate minerals calculated by summation to 100%

Table 4.10 (Cont)

Zeolites				Chlorite		Veinlet Minerals	
grdmss. zeolite	ocellus zeolite	ocellus zeolite (natro-lite)	ocellus zeolite (thom-sonite)	grdmss. chlorite	ocellus chlorite	veinlet prehnite	veinlet pecto-lite
46.68	63.79	51.95	36.32	28.99	29.60	43.49	53.02
32.41	18.35	24.35	30.45	15.77	15.89	23.85	
	0.11		0.00				
0.79	0.05		0.00	25.98	25.21		
	0.03		0.01	15.20	16.20		
1.04	0.07	0.88	13.00	0.48	0.43	27.07	33.70
3.66	0.08	12.59	3.25				8.94
5.99	15.98	0.13	0.01				
	0.05	0.11	0.00	0.33	0.40		
	0.00		0.01				
0.66							
91.23	98.51	90.01	83.05	86.75	87.73	94.41	95.66

this mineral is most abundant in the tinguaites (see Table 2.2), where it occurs with acicular aegerine in the interstices between phenocrysts. Zoning is not observed, and crystals are normally a pale neutral brown. That zircon occurs as inclusions in the major phases is evidenced by the presence of pleochroic haloes in biotite crystals, therefore, it is reasonable to assume that some of the fine included minerals in many of the other phases, such as clinopyroxene and amphibole, may also be zircon.

Aenigmatite

Pleochroic brown or red-brown (alpha=beta=brown, gamma=deep red or red brown) aenigmatite is occasionally identified in the tinguaites, where it occurs as small subhedral grains (0.05mm, and rarely up to 0.1mm) in the groundmass. Aenigmatite is not observed in the lamprophyres.

Magnetite

Magnetite occurs in all of the various types of dyke rocks in varying abundance, although it is more abundant in the lamprophyres than it is in the tinguaites (see Tables 2.1 and 2.2). In the lamprophyres, it forms widely disseminated subhedral to euhedral grains of varying size (0.01mm to

0.1mm, although rarely crystals may be as much as 0.5mm in size) throughout the groundmass. In reflected light crystals are dark grey, with occasional light grey or pinkish grey exsolution lamellae of ilmenite, particularily in larger crystals. This suggests that the Ti content of some of the magnetite is quite high (i.e. titanomagnetite). Occasionally, exsolution lamellae of haematite are observed; this mineral is distinguished in reflected light by moderate reflection pleochroism from pale grey or white to dark grey, and occasional deep red reflections.

Magnetite in the tinguaites forms widely disseminated, small (less than 0.05mm), generally subhedral grains. Exsolution of ilmenite is not observed. An analysis of a magnetite crystal with a low Ti content is given in Table 4.10.

Magnetite also occurs in the lamprophyres as a secondary phase, in that it is associated with the alteration of mafic phases, particularily olivine and clinopyroxene, and, to a lesser extent, amphibole and biotite. Magnetite is itself altered to ill-defined granular opaque material, and to red-brown haematite; the latter phase both replaces it, particularily along grain margins, and stains the surrounding crystals.

Ilmenite

Besides its occurence as an exsolution product in magnetite, ilmenite is occasionally observed (see Table 2.1) to occur in the lamprophyres as small (0.05mm or less), isolated subhedral crystals. These tend to be very pale pink-brown or grey under reflected light, and occasionally exhibit alteration to pale grey or yellow leucoxene.

Haematite

Haematite occurs largely as a result of the alteration of magnetite in the lamprophyres. Very rare, small (0.1mm or less) haematite crystals are observed in the groundmass of some lamprophyres. These are distinguished by deep red margins in an otherwise opaque crystal in transmitted light, and by moderate reflection pleochroism from pale grey to dark grey in reflected light. It is noted, however, that some such crystals approximate cubic form, and may therefore simply be pseudomorphous after magnetite.

In the tinguaites, haematite very rarely forms distinct crystals, but rather appears to stain most other phases, so that tinguaites are typically pink or orange-pink in hand

specimen, while most constituent phases of these rocks exhibit pale pink-brown colour in thin section. Rarely, translucent deep-red brown haematite is observed to occur along grain boundaries.

Sulphide Minerals

Rare, isolated, generally anhedral grains and irregular masses of sulphide minerals are observed in the lamprophyres. These are recognized by white or yellow metallic lustres under reflected light, and are generally small (0.05mm or less, with the exception of one large grain in an ocellar camptonite, C144, which is 1.5mm in size). Optical studies using reflected light suggests that pyrite is most common, with occasional deeper yellow grains probably being chalocpyrite.

Commonly, however, sulphide grains exhibit alteration which has resulted in the production of haematite, suggesting that many such sulphide minerals have a high Fe content. More detailed study is required to characterize conclusively the sulphide phases occurring in these rocks.

SECONDARY AND OCELLAR PHASES

Secondary and ocellar phases are considered together in the following section, in order to facilitate comparison, since a number of minerals are observed in both occurrences. There is considerable evidence, however, presented below and in Chapter 5, that ocellar phases are actually primary.

Calcite

Calcite is widespread in all of the various types of dyke rocks. Normally, it occurs, in approximate order of abundance, in lamprophyre ocelli, in marginal segregations closely associated with both lamprophyres and tinguaites, as a groundmass phase in lamprophyres, as a groundmass phase and occasionally as a pseudomorph of phenocrysts in the tinguaites, and in small veinlets traversing all rock types.

Ocellar calcite occurs as coarse (0.1mm to 0.5mm) aggregates of anhedral to subhedral, or rarely euhedral crystals, which are normally confined to the center of the ocellus. Occasionally, a single, large, optically continuous crystal occupies most or all of an individual ocellus. In all cases, crystals are colourless, or rarely pale pink-brown, and often exhibit twin lamellae parallel to

(0112) and (0001). Scapolite is frequently intimately associated with calcite, apparently replacing it around ocellar margins.

Calcite in marginal segregations is distinguished by its close association with haematite, other opaque phases, small amounts of chlorite and occasionally quartz. The size of calcite grains ranges from as much as 0.2mm, in which case grains are generally euhedral, to a very fine grained variety. Colloform texture is characteristic, and haematite staining, resulting in a pale yellow-brown to red-brown colour is common.

Calcite occurring as a groundmass phase in lamprophyres typically forms small (0.1mm or less), colourless, anhedral grains which generally fill the interstices between other, primary groundmass phases such as clinopyroxene, amphibole and feldspar. Crystals are usually shaped to accomodate these interstices, therefore, it is apparent that calcite in this occurence is secondary (i.e deposited by late-stage or secondary fluids). In some cases, calcite-bearing veinlets traversing the rocks are closely associated with, and even grade into groundmass calcite. This suggests that such veinlets may act as "feeder" veins for groundmass calcite. Groundmass calcite grains often contain abundant

cryptocrystalline inclusions.

Calcite is a common interstitial phase in the tinguaites, forming small (0.1mm or less), colourless anhedral crystals, where it is associated with aegerine, nepheline, aenigmatite and zircon; however, as in the case of groundmass calcite in the lamprophyres, crystals are normally anhedral and accomodate the available interstitial volumes. Occasionally, larger (up to 1.0mm) anhedral to subhedral grains are observed interstitial to nepheline and alkali feldspar phenocrysts; these appear to be larger versions of the typical groundmass calcite. Twin lamellae are generally uncommon. Calcite in the tinguaites is apparently secondary, and is analagous to secondary calcite in the lamprophyres.

Calcite in veinlets usually occurs as fine (0.05mm or less), colourless, anhedral crystals intimately associated with zeolites, chlorite, prehnite, pectolite and occasionally epidote. As noted earlier, such veinlets commonly grade into similar groundmass phases, and therefore apparently represent conduits for the movement of mineralizing fluids.

Composition

Table 4.10 gives representative compositions of calcite

from various occurences, and shows that calcite occuring in a lamprophyre groundmass, in a veinlet traversing a lamprophyre, and in a tinguaite, are all similar in composition. Generally, all are close to pure calcite in composition, with only small quantities of the siderite ($FeCO_3$), magnesite ($MgCO_3$) and rhodochrosite ($MnCO_3$) end-members being present. This suggests that such calcite formed at temperatures less than 500°C or less, since Goldsmith (1983) notes that at this temperature, about 5 mol% magnesite is soluble in calcite, while less than 1 mol% magnesite is observed. Such a temperature range of formation is consistent with a late-stage (i.e. hydrothermal) origin for this calcite.

The calcite occurring in the ocelli is compositionally distinct from the calcite in other occurrences. The amounts of the siderite, magnesite and rhodochrosite end-members are significantly higher in this type. This latter constituent may account for the pink or pink-brown colour (Deer et al, 1966) observed in some of the Coldwell ocellar calcite. Such a composition (i.e. particularily a higher content of magnesite in solid-solution) argues for a higher temperature of origin for ocellar calcite relative to groundmass calcite (Goldsmith, 1983). The ocellar phases are discussed in more detail in Chapter 6.

Scapolite

Scapolite occurs only in the lamprophyres, primarily as an ocellar phase but occasionally in the groundmass as well. In both cases, they resemble feldspar, and in the latter occurence are difficult to distinguish from that phase, hence many groundmass scapolite grains may be mis-identified. Identification of scapolite is facilitated by the absence of lamellar twinning, and by its uniaxial interference figure. Ocellar scapolite forms scaly or columnar aggregates of small (0.1mm or less), subhedral crystals, generally along ocellar margins, and in close association with calcite. In some cases, scapolite appears to replace calcite. Low birefringence (interference colours up to low second order, but generally first order grey) suggests a low meionite (Ca-scapolite end-member) content (Deer et al, 1966). Groundmass scapolite is similar in terms of optical properties, although crystals are generally anhedral, and smaller (less than 0.05mm). Crystals are commonly associated with calcite and plagioclase.

Composition

Compositions of scapolite from an ocellus and from a

lamprophyre groundmass are given in Table 4.10. In both cases, compositions reflect approximately 35% of the meionite component, which is in good agreement with the low to moderate birefringence noted above (Deer et al, 1966). Little replacement of Na by K is noted. Scapolite likely forms as a result of the reaction of solutions rich in Na, Cl and CO_2 with feldspar and calcite (Deer et al, 1966).

Epidote

Epidote occurs in the lamprophyres as an ocellar phase, a groundmass phase, and, occasionally, as a constituent of veinlets traversing the various dykes, including the tinguaites. In all occurences, it occurs as granular aggregates of small (0.1mm or less), or individual elongated laths and columnar aggregates (0.1mm or more), this latter occurence being restricted to ocelli. Crystals are generally pale yellow or yellow-green, and are slightly to moderately pleochroic (alpha=beta=pale yellow, gamma=yellow-green or pale green). In ocelli it is associated with scapolite in ocellar margins, while in groundmass occurences, it is commonly associated with plagioclase. The colour and pleochroism suggest that the mineral is dominantly epidote$_{ss}$ (Kerr, 1973; Deer et al, 1966).

Composition

Compositions of epidote from an ocellus and a lamprophyre groudmass are given in Table 4.10. These compostitions are similar to one another, and to published analyses of epidote$_{ss}$ (Deer et al, 1966). Such a composition is in good agreement with that suggested by optical properties above. Epidote in the groundmass is probably the result of saussuritization of plagioclase by late-stage or secondary fluids, although Deer et al (1966) note that it may occur as a late magmatic mineral. Epidote occurring in the veinlets has a hydrothermal origin, being associated with calcite, chlorite and other vein phases. The origin of epidote in the ocelli is problematical and is discussed in more detail in Chapter 6.

Chlorite

Chlorite is a major alteration product of all of the primary mafic phases occurring in the various dyke rocks. In the lamprophyres, it is the dominant secndary phase in the groundmass, replacing clinopyroxene and, to a lesser extent, amphibole and biotite. Typically, chlorite occurs as fibrous or scaly aggregates of crystals of varying size (dominantly fine grained, 0.05mm or less, although indivdual crystals up

to 0.3mm are rarely observed), exhibiting characteristic pleochroism (alpha=beta=green, gamma=pale green or yellow-green), and occasionally anomalous deep blue interference colours. Chlorite replacements are sometimes pseudomorphous, but more often form irregular patches and stringers, and lenticular masses, particularily in groundmass occurences. Where chlorite coexists closely with serpentine minerals, as in some altered olivine phenocrysts, it is sometimes difficult to distinguish positively between them, although the latter tends more towards cryptocrystallinity. Chlorite occasionally replaces aegerine in the tinguaites, in which case it is strongly pleochroic (alpha=beta=dark green or olive green, gamma=pale yellow), as a result of a high Fe^{3+} content (Deer et al, 1966).

Chlorite also occurs in ocelli, and as a common phase in veinlets. In both cases, it is unlikely to represent an alteration of a pre-existing phase; in the case of veinlet chlorite, it is probably an infilling. The origin of chlorite in the ocelli is discussed in more detail in Chapter 4. In both cases, the chlorite exhibits similar physical and optical properties to that occuring in the lamprohyre groundmass, although crystals tend to be better defined in the case of veinlet chlorite.

Compositions of chlorite occurring in the groundmass of a lamprophyre, and in an ocellus, are given in Table 4.10. Examination of these data shows that the compositions of both chlorites are similar, such that both are unoxidized chlorites, specifically ripidolite, as defined by Hey (1954). The weak pleochroism is an indication of the low Fe^{3+} content (Deer et al, 1966). Although no chlorite replacing aegerine in the tinguaites was analysed, the high Fe^{3+} content inferred from the strong pleochroism may result in chlorite in this occurrence being an oxidized type (e.g. thuringite, chamosite or delessite, depending on Si content- Hey, 1954).

Fluorite

Fluorite occurs only as a rare ocellar phase, and then only in relatively few ocelli (see Table 2.1). It forms small (0.05mm or less), isolated, anhedral crystals which range in colour from pale to deep violet, and exhibit characteristic isotropy in cross-polarized light. Normally, fluorite occurs near the margins of ocelli, where it is usually associated with scapolite. If, as noted previously, scapolite forms as a result of the interaction of Na-Cl bearing solutions on calcite, then fluorite may be similarily formed if F is a consituent of these solutions as well.

Cancrinite

Pale yellow cancrinite is occasionally observed as a groundmass phase in lamprophyres and less commonly as an ocellar phase; rims of colourless or pale yellow cancrinite commonly partially or, in rare cases, completely surround nepheline phenocrysts in some tinguaites.

In the lamprophyre groundmass occurences, cancrinite crystals are anhedral and generally small (0.1mm or less, although one crystal 0.5mm in size was observed). Although it is inferred to be an alteration product of nepheline, in no case is cancrinite actually seen to be replacing nepheline.

Ocellar cancrinite is optically similar, however, crystals are smaller (0.05mm or less), and sometimes occur as aggregates; in this occurence it is normally associated with scapolite. As noted above, cancrinite in the tinguaites replaces nepheline along rims, and less commonly along fractures within nepheline phenocrysts. In the tinguaites, it is commonly colourless, and is recognized by the difference in optical properties (e.g. extinction) relative to the nepheline it is replacing.

In tinguaite and lamprophyre groundmass occurences, cancrinite is probably a replacement of primary nepheline, resulting from the interaction of this latter phase with residual or secondary CO_2-bearing fluids (Deer et al, 1966). It is reasonable to assume, therefore, that crystals are dominantly cancrinite$_{ss}$ (CO_3-cancrinite); Cl-cancrinite (microsommite) may be present as well, if such fluids also contained Cl (see Scapolite). The nature and origin of the cancrinite in the ocelli is less clear, however, since nepheline has not been observed as an ocellar phase. It is possible that minor amounts of ocellar calcite have been replaced by cancrinite, or that a more complex, poorly-understood reaction involving ocellar material and later-stage fluids occurred.

Other Secondary and Ocellar Phases

Abundant, ill-defined granular and fibrous material occurs in the groundmass of most of the lamprophyres; in some cases, such as specimen C80, in which the degree of alteration is highly advanced, such material may dominate the groundmass. Due to its cryptocrystalline nature, however, it is difficult to identify this material by optical methods, and X-ray diffraction studies add little information. Possible constituents include very fine grained chlorite,

serpentine minerals and secondary amphiboles such as tremolite or uralite, resulting from the alteration of primary groundmass mafic phases, and clay minerals, very fine grained zeolites, sericite and epidote, resulting from the decomposition of groundmass feldspars. Furthermore, secondary minerals deposited by deuteric or later-stage fluids, such as zeolites and calcite may be included as well. Such a diverse range of potential minerals may result in the strong background spectrum noted in many of the X-ray diffraction patterns obtained; this poor response would be enhanced by the potential for secondary absorption and the tendency for many of the platy minerals to exhibit a strong preferred orientation with respect to XRD analysis.

Microlitic phases are frequently observed in the ocelli, consisting of fine grains and needles of indeterminant composition. Fine rounded and irregular inclusions may be fluid inclusions.

CONCLUSIONS

A number of conclusions concerning the descriptions and discussions of the various minerals comprising the Coldwell dyke rocks are given in the following sections.

a) By their presence as phenocrysts, it is suggested that clinopyroxene, amphibole and to a lesser extent biotite were early crytallizing phases in the lamprophyres. Olivine was present as an early crystallizing phase in at least some lamprophyres, but apparently underwent extensive resorption. Small quantities of a spinel phase crystallized in association with olivine, as evidenced by spinel inclusions in unaltered relict olivine. Quartz was an early crytallizing phase in the quartz camptonites, but later in the history of these rocks ceased to be an equlibrium phase, as evidenced by resorption rims around phenocrysts.

b) Feldspar (dominantly anorthoclase- $Ab_{45}An_5Or_{50}$- in the sannaites, and dominantly labradorite- An_{60-70}- in the other lamprophyres) is abundant in the groundmass of the lamprophyres, with the exception of the monchiquites, but does not form phenocrysts. This is probably a reflection of the order of crystallization of the primary liquidus phases i.e. feldspar is a late liquidus phase in these rocks relative to the mafic phases described in (a) above.

c) Because feldspar crystals, or rims of feldspar crystals, with the most albitic compositions are generally those displaying the most advanced alteration, it is suggested that the relatively high albite content of some

feldspars is a result of metasomatic reactions between feldspar crystals and late-stage or secondary fluids. Rock (1977) notes that large volumes of alkali-rich fluids are associated with the emplacement of an alkaline intrusion. Such an origin may be applicable to the Coldwell Complex.

d) It is apparent that considerable differences exist between the clinopyroxenes occurring in the quartz camptonites, and those occurring in the other lamprophyres. Most notably, the zoning evident in the clinopyroxene phenocrysts of the latter rocks indicates that conditions in the magma from which these crystallized changed with respect to time, while, conversely, the general lack of zoning in clinopyroxene phenocrysts of the quartz camptonites suggests that conditions in the magma from which these crystallized remained relatively unchanged. Furthermore, these clinopyroxenes are compositionally distinct from those occurring in the other lamprophyres (i.e. generally lower Ca/Ca+Mg ratio, reflected in the relative paucity of the wollastonite end-member, and less overall compositional variation). The inference is that the clinopyroxenes occurring in the quartz camptonites crystallized at a higher temperature than those in the other lamprophyres.

e) In the clinopyroxene phenocrysts occurring in the

sannaites, compositional variation among the zones is best explained by a simple substitution of Fe (hedenbergite end-member) for Mg (diopside end-member) from core to rim in a normally zoned phenocryst, with little or no involvement of Ti and Al. In the clinopyroxenes of the other lamprophyres, however, considerable amounts of Ti and Al are involved in the substitution. The overall Ti content of these clinopyroxenes is also relatively high compared to that of the sannaitic clinopyroxenes as well. Since the solubility of $CaTiAl_2O_6$ in diopside decreases with increased pressure (Scott, 1980), this suggests that the sannaitic clinopyroxenes crystallized at relatively high pressure, and that these high pressure conditions remained constant, or decreased only slightly, for the duration of this crystallization; this is exemplified by the low content of Ti and Al in the rim zones and groundmass grains, which represent the most recently crystallized material. The zoning thus reflects changes in the Fe/Mg ratio, most likely brought about by changing composition of the magama from which the clinopyroxene was crystallizing. That such changes may have been discontinuous is evidenced by the frequently rounded and embayed phenocryst cores. Magma mixing, appearance of a new liquidus phase such as amphibole (Scott, 1980- see below) or some similar mechanism may have altered the composition of the magma such that phenocryst core

material was placed into a state of disequilibrium with it, resulting in partial resorption. Minor zoning which is sometimes observed to occur in phenocryst rims may represent smaller-degree fluctuations in magma composition (Scott, 1980).

f) In the case of the clinopyroxenes occurring in the ocellar and amphibole camptonites and the monchiquites, crystallization took place at lower pressures, as evidenced by the higher Ti and Al contents; furthermore, pressure decreased somewhat as crystallization proceeded, since phenocryst rims and groundmass grains tend to be enriched in Ti and Al relative to the cores (Yagi and Onuma, 1967). This pressure decrease must have been abrupt, such as that resulting from an eruption from a greater depth to a lesser, since contacts between core zones and rim zones tend to be sharp; the lack of resorption of the core material, demonstrated by the lack of rounding or embayment of phenocryst cores, suggests that this pressure change was not accompanied by a disequilibrium between the clinopyroxene and the coexisting magma. The lack of zoning within cores and rims suggests that, otherwise, conditions in the magmas were stable or varied only slightly. Note that the similar overall compositions and intra-crystal patterns of compositional variation, and apparently similar

crystallization histories may indicate that the magmas from which these clinopyroxenes crystallized were related (i.e. comagmatic and cogenetic).

g) Reversed zoning in the clinopyroxenes of the various lamprophyres, , with the exception of those occurring in the quartz camptonites, may be a result of the addition of liquids approximating an earlier composition of the host magma (Scott, 1980), resulting in the formation of rims with more Mg-rich compositions over relatively Fe-rich cores, which had themselves nucleated later than the earliest clinopyroxene. Resorption of amphibole as a result of a decrease in P_{H_2O} may also give rise to a reversal in zoning (see below).

h) In all cases, the Na (acmite end-member) content increases in phenocryst rims relative to cores, although this increase is slight in the case of the clinopyroxenes occurring in the quartz camptonites. This reflects the normal evolution trend of pyroxenes in alkaline rocks towards acmite (Mitchell, personal communication).

i) The occurrence of hedenbergite along with aegirine in the tinguaites is probably a result of variations in f_{O_2}. Aegirine is stable at relatively high oxygen fugacities (i.e.

equivalent to the haematite-magnetite buffer, and descending as low as the FMQ buffer) which favour the oxidation of iron to form Fe^{3+} (Brousse and Rancon, 1984). Since aegirine is observed to form rims on hedenbergite, the implication is that f_{O_2} increased during the crystallization of the tinguaite magma, stabilizing Fe^{3+} relative to Fe^{2+} in the melt. The presence of groundmass aenigmatite, which is characterized by stability at relatively low oxygen fugacities (i.e. equivalent to the iron-wustite buffer, and as high as the FMQ buffer) (Scott, 1976), therefore probably crystallized early relative to the aegerine. This suggests that there may have been a considerable change in the f_{O_2} conditions (i.e. from as low as those represented by the iron-wustite buffer to as high as those represented by the haematite-magnetite buffer) during the crystallization of the tinguaites.

j) Amphiboles occurring in the lamprophyres exhibit little compositional variation. In cases where amphibole phenocrysts are zoned, the only clear change between zones is a general replacement of Mg by Fe from core to rim in normally zoned phenocrysts, which is a similar trend to that observed in the clinopyroxenes in general, and those occurring in the sannaites in particular. As in the lamprophyres, this increase in the Fe/Mg ratio likely

reflects a changing composition in the magma from which the amphiboles were crystallizing.

k) The paucity of primary hydrous phases in general, and amphibole in particular, in the sannaites, suggests that the sannaitic magma was relatively anhydrous compared to the other lamprophyres throughout its crystallization history.

l) Rounded and embayed cores observed in many amphibole phenocrysts suggests that resorption has occurred. This is probably a result of a large decrease in P_{H_2O}, perhaps brought about by eruption (Scott, 1980). Brooks and Rucklidge (1973) postulate that amphibole resorption may give rise to a reversal in the zoning of clinopryoxene, as noted above. Minor zoning observed in phenocryst rim zones is probably in response to smaller changes in P_{H_2O}, magma composition and/or temperature (Scott, 1980).

m) In the absence of zoning in biotite, it may be inferred from the pattern of compositional variation noted among zones in other mafic phases (e.g. clinopyroxene and amphibole), that more Fe-rich (i.e. annitic) crystals formed later than Mg-rich (i.e. phlogopitic) crystals, where the two types coexist, reflecting changes in the Fe/Mg ratio of the magma.

n) The pattern of zoning observed in olivine, from Mg-rich cores (Fo_{90}) to relatively Fe-rich rims (Fo_{82}) is consistent with the increase in Fe/Mg exhibited by the other mafic phases.

o) Where present, olivine has undergone extensive resorption. It is possible that some completely pseudomorphed phenocrysts in various lamprophyres represent completely resorbed olivine, so that this phase may have originally crystallized in abundance. As a result of changes in temperature, pressure and/or magma composition, olivine ceased to be an equilibrium liquidus phase and underwent resorption. The extent of the resorption may be a result of extreme disequilibrium brought about by a high degree of undersaturation of the coexisting liquid with respect to olivine components (Donaldson, 1971), although the exact mechanism (e.g. change in temperature, pressure and/or composition) causing this is not clear.

p) Quartz is a primary phase in the quartz camptonites. As noted in Chapter 3, these rocks are distinct from the other lamprophyres in terms of their whole rock major element chemistry, and, as noted previously in this section, are also distinguished on the basis of their clinopyroxene composition. The presence of primary quartz in these

lamprophyres further supports the suggestion that they are genetically distinct, although the mechanism by which the silica activity was elevated sufficiently to allow the precipitation of primary quartz is problematical. This is discussed further in Chapter 8.

q) Quartz in the quartz camptonites has undergone varying degrees of resorption. Narrow rims of clinopyroxene may be a result of a decrease in pressure. Nicholls et al (1971) state that quartz in basic magmas may be stable at elevated pressures (e.g. 14.3 to 16.0 kb in the case of the Lassen Peak and Talasea lavas respectively assuming 1000°C quenching temperature). The apparently small degree of quartz resorption may be a function of elevated silica activity in the coexisting magma, resulting in only a slight effective undersaturation of the liquid with respect to quartz components (i.e. SiO_2); polymerization of the melt as plagioclase becomes a stable phase, and formation of the clinopyroxene reaction rim, may further inhibit the resorption process (Donaldson, 1985).

r) Nepheline occurring in the quartz camptonites crystallized after the primary quartz ceased to be an equilibrium phase.

s) The isotropic base of the monchiquites is composed primarily of glass whose composition is believed to approximate that of the feldspar and nepheline occurring in the ocellar camptonites. Abundant colourless microlitic phases probably represent incipient feldspar. Analcite is an alteration product. Irregular dark patches and streaks are devitrification products of indeterminant composition.

t) Analcite in other lamprophyres is also a secondary phase, resulting from the alteration of nepheline. A primary origin is unlikely because of the restricted range of P-T conditions under which analcite plus melt is a stable assemblage (Gibbs and Henderson, 1977, 1983).

u) Late-crystallizing phases include clinopyroxene and amphibole with compositions similar to that of corresponding phenocryst rims, apatite, sphene, aenigmatite, zircon, Fe-Ti oxides and sulphide minerals. As noted previously, feldspar crystallized late, and was therefore confined to the groundmass.

v) The types and compositions of secondary phases provide information concerning the nature of late- and/or post-magmatic processes which occurred in the Coldwell dyke rocks. It is apparent that such processes were dominated by

CHAPTER 5- TRACE ELEMENT CHEMISTRY

WHOLE ROCK TRACE ELEMENT CHEMISTRY

A representative suite of the various types of dyke rocks was analysed to determine the abundance of 24 trace elements including 3 alkaline elements (Li,Rb,Cs), 2 alkaline earths (Sr,Ba), 10 transition elements (Sc,Cr,Co,Ni,Cu,Y,Ta Nb,Zr,Hf), 8 REE (La,Ce,Nd,Sm,Eu,Tb,Yb,Lu) and Th. Analytical methods are detailed in Appendix A. Table 5.1 presents representative compositions of each type; a full listing of these data is given in Appendix B. Table 5.2 lists descriptive statistics for the trace element compositions of each type of dyke.

Behaviour of Trace Elements

Prior to discussing the distribution of trace elements in the Coldwell dyke rocks, it is important to define the terminology employed below. Complete discussions are given in MacIntire (1963) and Arth (1976). In particular, trace elements tend to exhibit either compatible or incompatible behaviour, such that compatible elements tend to concentrate in the solid phase, and incompatible elements in the liquid phase, given a liquid from which solid phases

Table 5.1 Abundances of Trace Elements in a Representative Suite of Coldwell Dyke Rocks (All analyses in ppm)

Element	1	2	3	4	5	6	7	8	9	10	11	12
Li		24	12		90			7		52	12	
Rb	9	99	74	69	63	64	74	168	174	227	140	453
Cs	40		3			1		21		6	54	
Sc	44	23	18	15	19	27		19	19	13	0.12	0.13
Co	54	53	37	34	69	62		51	46	35	19	9
Cr	93	620	16	336		28		20	519	17	3	
Ni	210	250	155	111	106	98	130	64				6
Cu	55	71	63	50	100	97	101	49				18
Hf	4.45	4.96	3.81	6.02	4.93	3.98	5.08		5.40	5.22	22.55	31.70
Zr	182	270	206	224	226	213	232	167	403	557	1196	1732
Ta	3.92	9.48	7.43	9.49	7.49	4.42	10.27		7.88	8.52	33.32	32.10
Nb	56	176	85	95	123	72	126	54			143	487
Sr	670	1295	645	413	1854	1000	2532	670	1649	1806	265	27
Ba	335	1011	819	948	2403	1180	2894	929	2812	2538	655	132
Y	28	39	26	26	35	28	34	24	50	59	52	95
Pb		9	13	8	5	4	5					22
Th	5.75	16.80		19.44	15.54	9.89	12.30		15.77	11.33	54.77	133.24
La	75.80	128.33	64.05	68.26	154.96	88.44	163.43	76.08	159.75	185.49	202.83	602.91
Ce	122.98	228.42	158.51	132.66	291.41	172.41	328.61	139.95	255.60	236.45	341.40	887.92
Nd	86.82	167.98	48.88	77.14	100.21	105.00	94.63	45.85	139.34	82.40	156.44	541.39
Sm	11.76	21.25	7.49	9.77	16.87	13.67	16.31	9.19	17.24	13.83	20.99	74.64
Eu	3.38	5.86	2.41	2.41	5.35	3.61	4.56	2.60	5.32	3.36	5.93	4.58
Tb	1.17	1.92	0.95	0.92	1.03	1.37	1.76	0.85	1.60	0.73	2.59	10.40
Yb	1.89	2.98	2.89	2.74	2.45	2.81	2.37	1.93	2.51	1.82	7.51	9.72
Lu	0.28	0.39	0.44	0.37	0.31	0.39	0.29	0.26	0.36	0.30	0.96	1.84
La:Yb	40.1	43.1	22.2	24.9	63.2	31.5	69.0	39.4	63.6	101.9	27.0	62.0
Sum(REE)	304.08	557.13	285.62	294.27	572.59	387.70	611.96	276.71	581.72	524.38	738.65	2133.40

1 & 2- sannaites
3 & 4- quartz camptonites
5 & 6- ocellar camptonites
7 & 8- monchiquites
9 & 10- amphibole camptonites
11 & 12-tinguaites

Table 5.2 Descriptive Statistics for Trace Element Data

	Ba	Rb	Sr	Hf	Zr	Ta	Nb	Sc	Co	Cr	Ni	Cu	Pb	Li
Sannaites (6 specimens)														
Mean	665	43	1048	4.34	233	5.56	102	27	54	357	152	57	19	24
Standard Deviation	437	35	596	1.35	33	2.11	44	9	4	373	81	16	21	0
Quartz Camptonites (6 specimens)														
Mean	906	84	569	5.95	222	8.18	89	8	37	119	121	62	12	10
Standard Deviation	115	27	156	1.12	10	1.71	9	2	4	188	21	11	3	3
Ocellar Camptonites (19 specimens)														
Mean	1121	91	892	5.62	232	5.93	86	21	54	23	107	76	14	90
Standard Deviation	432	45	434	1.17	91	1.91	34	6	12	17	65	34	17	
Monchiquites (4 specimens)														
Mean	1629	99	1269	5.08	208	10.27	114	19	51	20	127	94	8	
Standard Deviation	893	46	880		30		55				45	31	6	
Amphibole Camptonites (5 specimens)														
Mean	2081	170	1390	6.22	364	8.72	122	13	46	179	28	90	1	67
Standard Deviation	712	48	396	1.58	149	0.96		7	12	295				21
Tinguaites (13 specimens)														
Mean	523	216	167	19.37	913	25.01	252	2	21	2	5	9	32	25
Standard Deviation	771	105	214	7.23	379	9.07	132	4	13	1	3	7	30	18

Table 5.2 (Cont.)

La	Ce	Nd	Sm	Eu	Tb	Yb	Lu	Th	Y
103.45	183.36	95.33	14.80	4.12	1.35	2.24	0.32	10.24	34
23.03	41.53	36.84	3.84	1.07	0.30	0.50	0.05	4.27	4
68.16	134.00	57.37	8.43	2.19	0.79	2.45	0.23	19.44	27
4.07	23.00	17.17	1.19	0.38	0.26	0.64	0.17		1
119.73	221.01	91.83	15.12	4.14	1.28	2.56	0.31	12.47	35
28.31	55.79	17.34	3.35	1.15	0.32	0.37	0.13	4.28	12
146.18	263.88	70.24	12.75	3.58	1.30	2.15	0.28	12.30	27
60.89	99.83	34.49	5.04	1.38	0.64	0.31	0.02		5
110.11	174.90	86.13	12.06	3.66	0.99	1.78	0.29	11.10	36
72.95	82.57	51.44	6.26	1.54	0.53	0.76	0.07	4.78	22
299.93	467.37	138.21	18.11	3.92	2.02	5.51	0.72	37.06	60
134.89	191.71	16.88	2.49	2.67	0.50	1.73	0.21	15.34	18

crystallizing (MacIntire, 1963). This behaviour is quantified by D, the distriution coefficient:

$$D = \frac{[i]_{solid}}{[i]_{liquid}}$$

where i is the element under consideration (Villemant et al, 1981). Incompatible elements have D values < 1, while compatible elements have D values > 1. An element which exhibits a D value << 1 throughout the crystallization of a magmatic series is termed hygromagmatophile (Treuil et al, 1979). However, the D value for a given element varies depending upon the mineral phase in question. The bulk distribution coefficient, D_b, which is a function of the D values of all coexisting phases for a given element, is given by:

$$D_b = x_1 D_1 + x_2 D_2 + \ldots + x_n D_n$$

where x_1 and D_1 are weight fraction of phase i and the D value of the element in question in phase i, x_2 and D_2 are similar values for phase j, and phase n is the last phase (Arth, 1976).

General Observations

A number of general observations concerning the whole rock trace element chemistry of the various dyke rocks are discussed in the following section:

a) Table 5.1 shows that the tinguaites are distinct from the lamprophyres on the basis of the abundance of virtually all trace elements. Specifically, the tinguaites are enriched in Rb,Hf,Zr,Ta,Nb,Th,Y and the REE, and depleted in Ba,Sr,Sc,Co,Cr,Ni, and, to a lesser extent, Cu and Pb, relative to the lamprophyres. Therefore, the tinguaites are enriched in terms of incompatible elements, and depleted in terms of compatible elements, relative to the lamprophyres.

b) There is no apparent systematic varation of Li and Cs among the various types of dyke rocks.

c) The quartz camptonites are depleted in terms of the LREE, as demonstrated by low La:Yb ratios, and, to a lesser extent MREE, and exhibit low total REE, relative to the other lamprophyres.

d) The amphibole camptonites tend to exhibit higher

total REE than the other lamprophyres.

e) There is considerable variation in the abundance of Ba, Cr, and, to a somewhat lesser extent Rb and Sr among individual specimens of each type of dyke.

f) In terms of their Sr content, tinguaites are of two distinct types- those represented by specimen 12 (see Table 4.1), which exhibit low Sr abundances (6 examples), and those represented by specimen 11, which have much higher Sr abundances (4 examples). Tinguaites displaying higher Sr abundances also tend to have low total REE, and vice versa.

Variation Diagrams

Variation diagrams are given for the trace elements in order to examine the behaviour of these elements among the various dyke rocks. Diagrams were constructed by plotting the logarithm of the concentration of each element against the logarithm of the concentration of a hygromagmatophile element (La).

Log Element-Log La Diagrams

Log-log variation diagrams portray the behaviour of

trace elements, so that relationships between the rocks in question may be examined, and major processes involved in the genesis of those rocks may be identified. Cocherie (1986) proposes a method whereby the log of the concentration of an element of relatively high D value ($D > 1$) is plotted against the log of the concentration of an element with $D << 1$. The relative behaviour of the two elements will indicate what relationships may exist among the rocks in question, such that:

a) A rapid decrease in the concentration of the compatible element, accompanied by a correspondingly small increase in the concentration of the incompatible element, suggests a crystallization process.

b) A rapid increase in the concentration of the incompatible element, accompanied by a correspondingly small decrease in the concentration of the compatible element, suggests a fusion process.

Each of these two general processes represents an infinite range of specific processes between the extremes of perfect equilibrium crystallization or fusion to fractional crystallization or fusion. Straight lines on such a diagram suggest the fractionation situation (Cocherie, 1986). Magma

mixing is indicated by a concave downward curve (Cocherie, 1986). Villemant et al (1981) use similar log-log diagrams to define the various stages in the crystallizaton sequence of the volcanic rocks of the Chaine de Puys, France, such that distinct breaks in the slope of the lines on the diagrams are observed, corresponding to changes in the type and abundance of crystallizing phases. These changes in slope reflect changes in the D_b for the various elements observed. Other authors (e.g. Treuil and Varet, 1973; Allegre et al, 1977) have used log-log diagrams for similar purposes.

In order to examine the relationships among the various Coldwell dyke rocks, and to infer possibly something of the processes which may have operated during their genesis, log-log diagrams have been constructed (see Figures 5.2 to 5.24), in which the logarithm of the concentration of each trace element is plotted against the logarithm of the concentration of an index element which is assumed to exhibit nearly hygromagmatophile behaviour, and will therefore function as an indicator of the degree of crystallization or fusion if these rocks are related as one or more magmatic series. La is chosen as the index element, for the following reasons:

Table 5.3 Correlation Statistics for Trace Element Variation Diagrams

Element	Pearson's r	Standard Error of Estimate	Slope	Intercept
Li	0.113	0.62	-6.32	5.43
Rb	0.649	0.45	0.87	0.74
Sc	-0.585	0.22	-3.54	2.34
Co	-0.531	0.54	-0.94	2.13
Cr	-0.602	0.49	-10.42	9.43
Ni	-0.545	0.47	-4.11	5.88
Cu	-0.464	0.52	-0.74	2.39
Hf	0.765	0.34	1.24	0.85
Zr	0.737	0.15	1.13	0.11
Ta	0.801	0.04	4.67	0.02
Nb	0.943	0.05	1.03	0.96
Ba	-0.453	0.73	-2.30	4.96
Sr	-0.476	0.64	-3.60	6.84
Th	0.623	0.42	1.21	-0.21
Y	0.758	0.44	0.88	-0.11
Pb	0.277	0.61	4.52	-1.46
Ce	0.984	0.02	1.02	1.29
Nd	0.725	0.06	2.13	1.05
Sm	0.784	0.05	1.34	-0.12
Eu	0.568	0.09	0.63	-0.79
Tb	0.636	0.09	0.67	-1.27
Yb	0.671	0.11	0.89	-1.19
Lu	0.533	0.17	1.96	-2.89

a) La will tend to be incorporated into crystallizing apatite. However, this phase is not volumetrically important in the Coldwell dyke rocks (see Chapter 2 and Table 2.1), and does not occur as phenocrysts, so there is little evidence to suggest that either phase has controlled fractionation to any significant degree. It is reasonable to assume that La was not significantly fractionated as no other minerals for which D_{La} is close to or greater than 1 are observed. Thus, La behaved as a hygromagmatophile element in all of the Coldwell dyke rocks.

b) La correlates well with a number of other trace elements. Table 5.3 lists correlation statistics for the various trace element-La correlations. Examination of this table shows that La exhibits strong linear relationships with Ce, Nb, and to a lesser extent Sm, Nd, Y, Ta, Zr, Th, Tb and Eu.

c) Since Ce, Nb, and Th have been observed to exhibit hygromagmatophile behaviour (Allegre et al, 1977; Villemant et al, 1981; Cocherie, 1986), the strong linear relationships between these elements and La, with slopes close to unity (see Table 5.3), noted in (b) above, indicate that the ratio of the concentrations of these elements to the concentration of La is nearly constant throughout the

evolution of the various dyke rocks. Therefore, this supports the suggestion that La is hygromagmatophile in the case these rocks.

d) La is generally immobile during secondary processes, including hydrothermal (Michard and Albarede, 1986; Sturchio et al, 1986) and low temperature (Michard and Albarede, 1986) alteration. Therefore, the observed La abundances are likely representative of the original concentrations. Use of La as the index variable, therefore, will, to some extent, offset the effects of secondary processes.

A number of general observations are made concerning these diagrams:

a) The logarithms of the concentrations of Ba, Sr, Sc, Co, Cr, Ni, Cu and Li exhibit negative correlations with the logarithm of the concentration of La. The strength of the relationship varies from very weak to moderate (see Table 5.3). With the exception of Li and Cr, for which there is no clear pattern, the lamprophyres are enriched in these elements relative to the tinguaites. Of these elements, Sc, Co, Cr and Ni (and Ba and Sr during the crystallization of feldspar) are compatible (Arth, 1976).

KEY TO FIGURES 5.2 TO 5.24

Coldwell Dyke Rocks

filled circles-	sannaites
open stars-	quartz camptonites
filled triangles-	ocellar camptonites
filled stars-	monchiquites
filled squares-	amphibole camptonites
open circles-	tinguaites

Fig. 5.2 Log Ba vs Log La

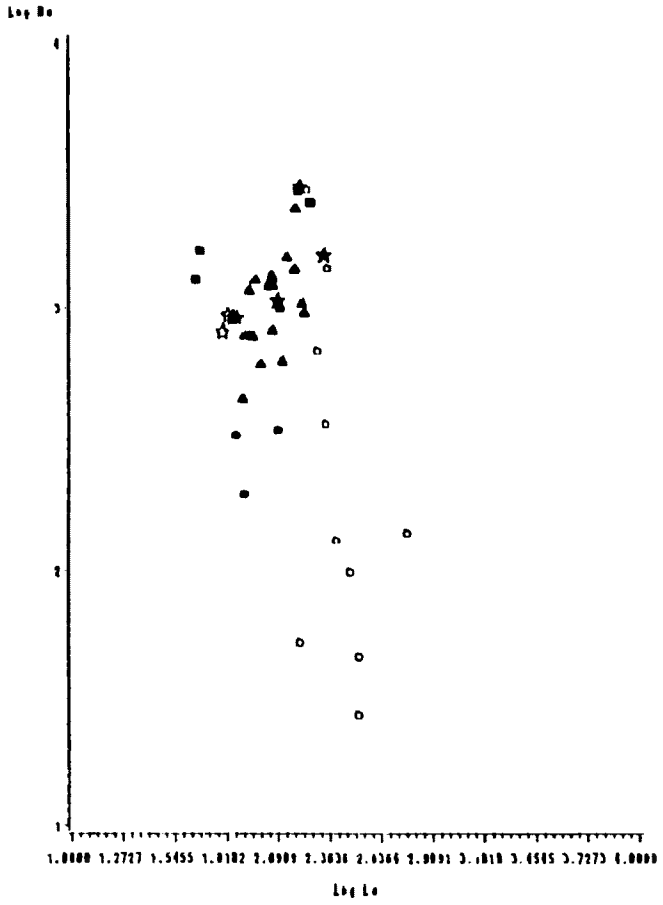

Fig.5.3 Log Rb vs Log La

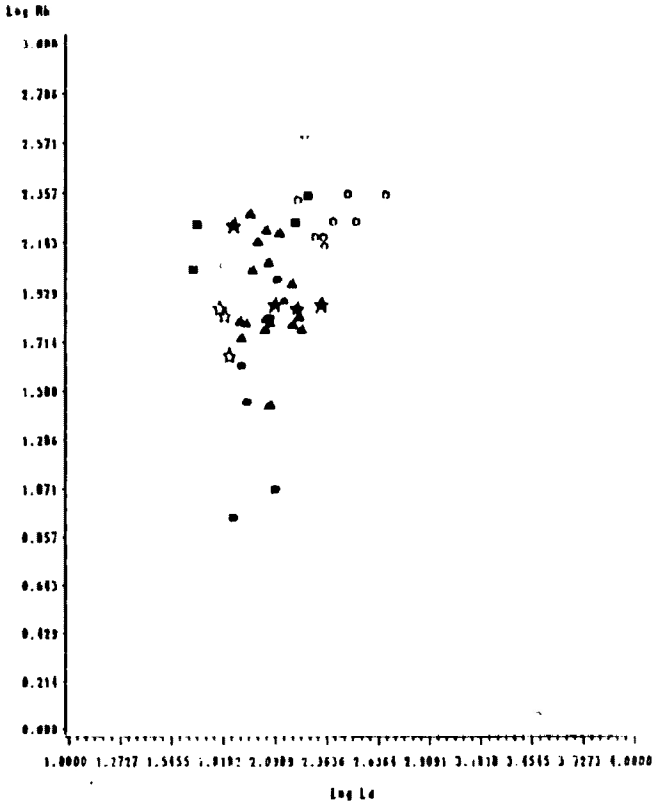

Fig. 5.4 Log Sr vs Log La

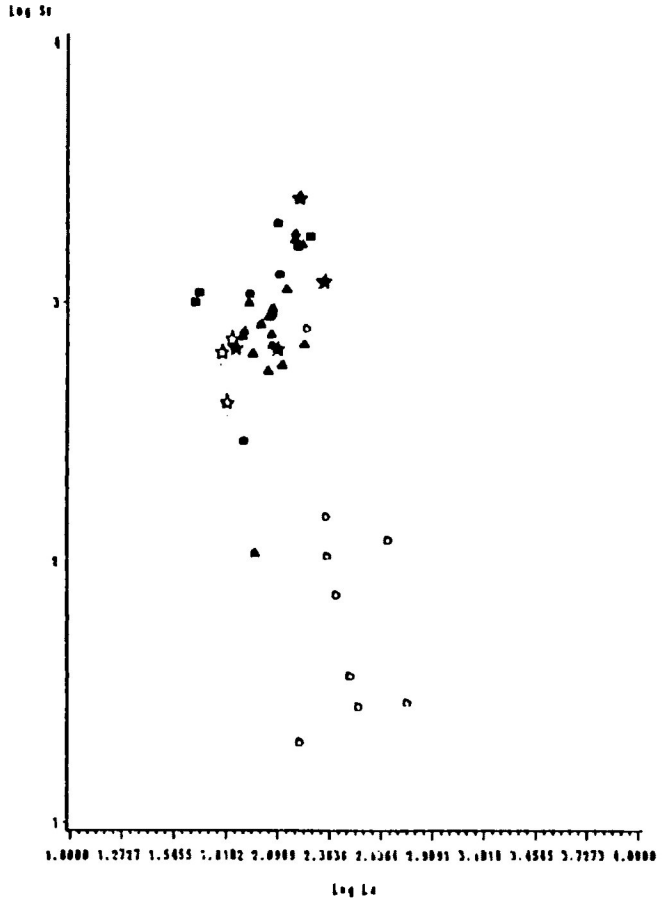

Fig. 5.5 Log Zr vs Log La

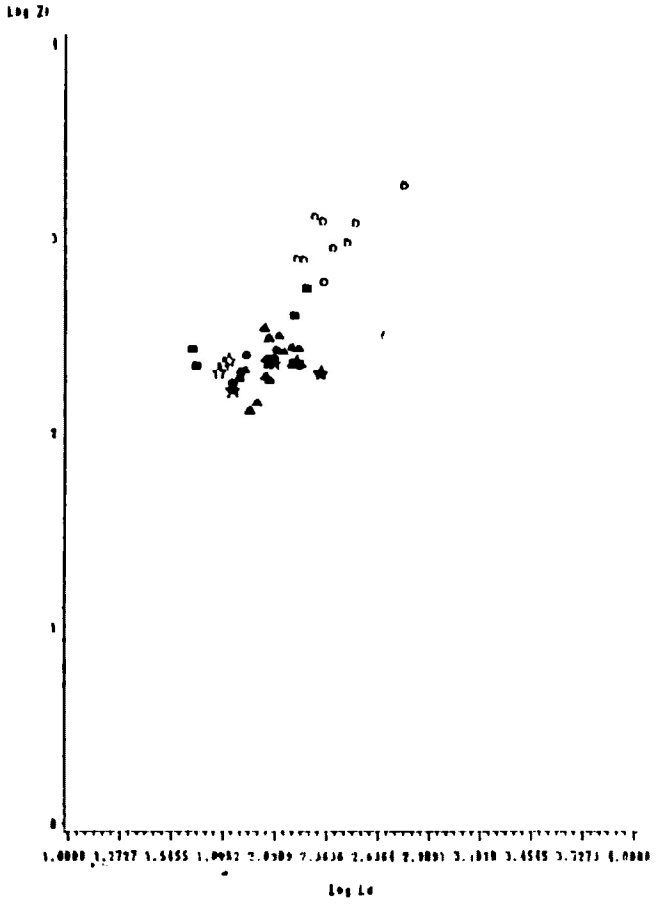

Fig. 5.6 Log Hf vs Log La

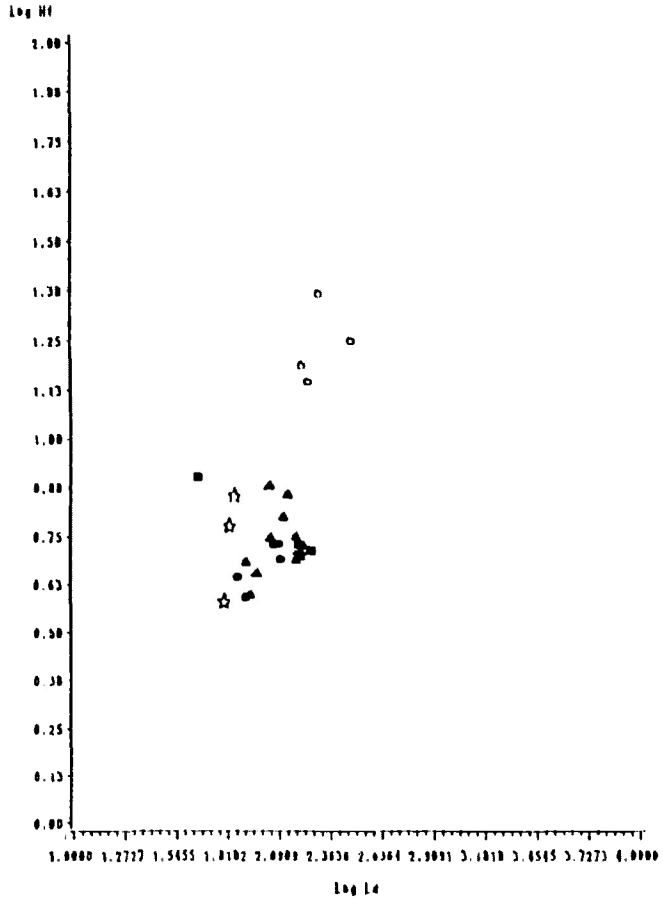

Fig. 5.7 Log Ta vs Log La

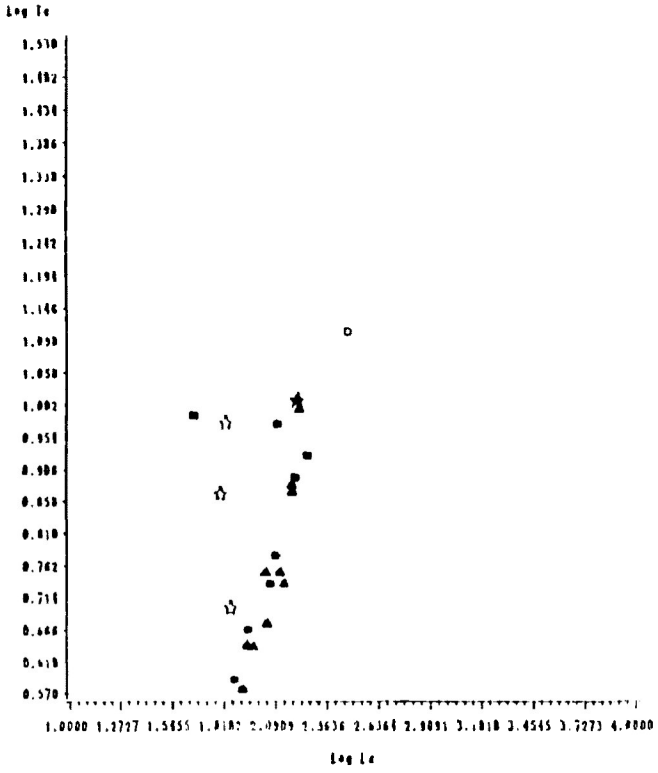

Fig. 5.8 Log Nb vs Log La

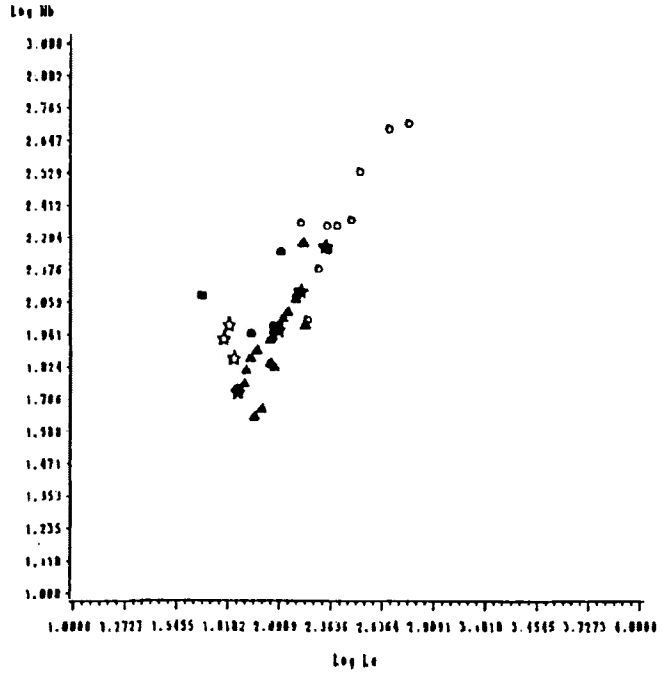

Fig. 5.9 Log Sc vs Log La

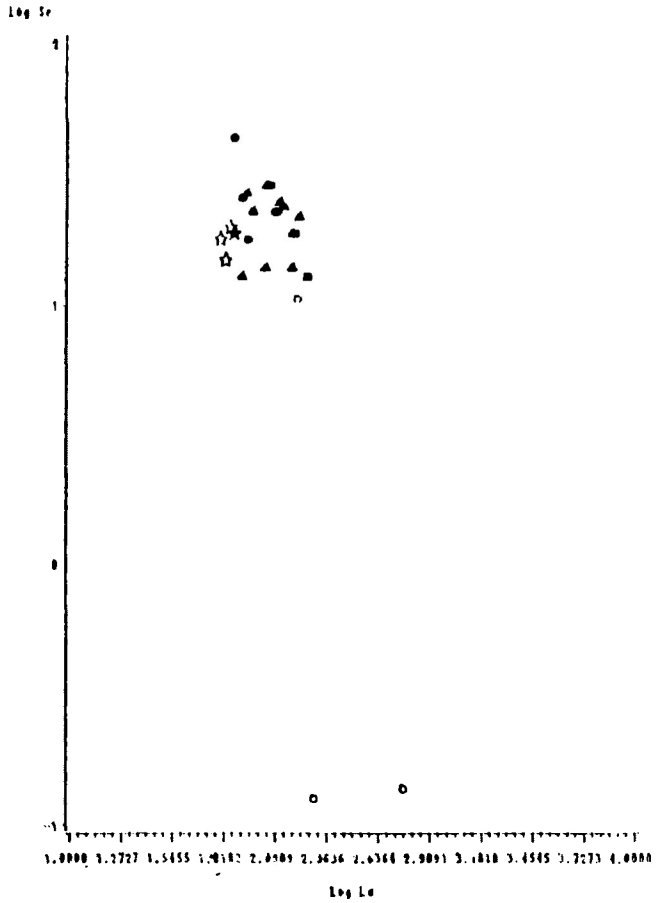

Fig. 5.10 Log Co vs Log La

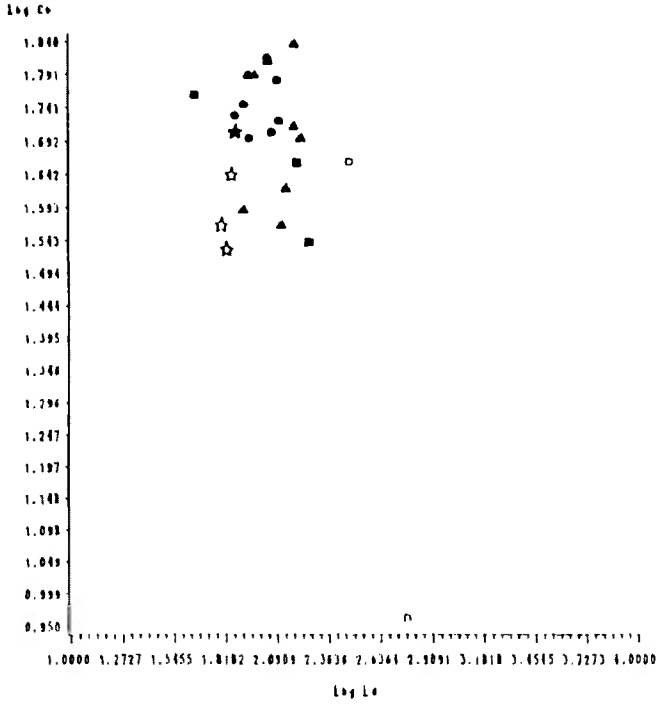

Fig. 5.11 Log Cr vs Log La

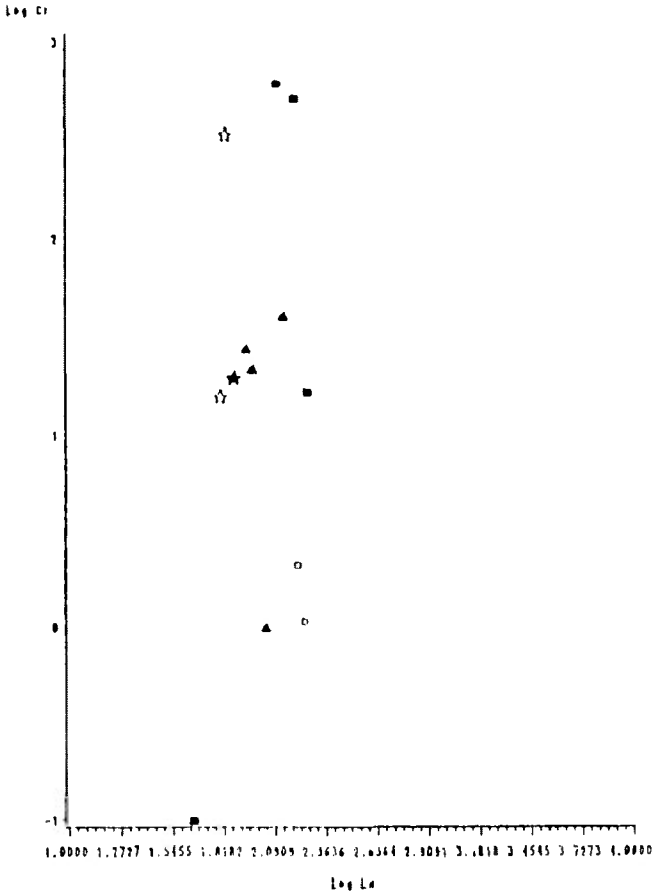

Fig. 5.12 Log Ni vs Log La

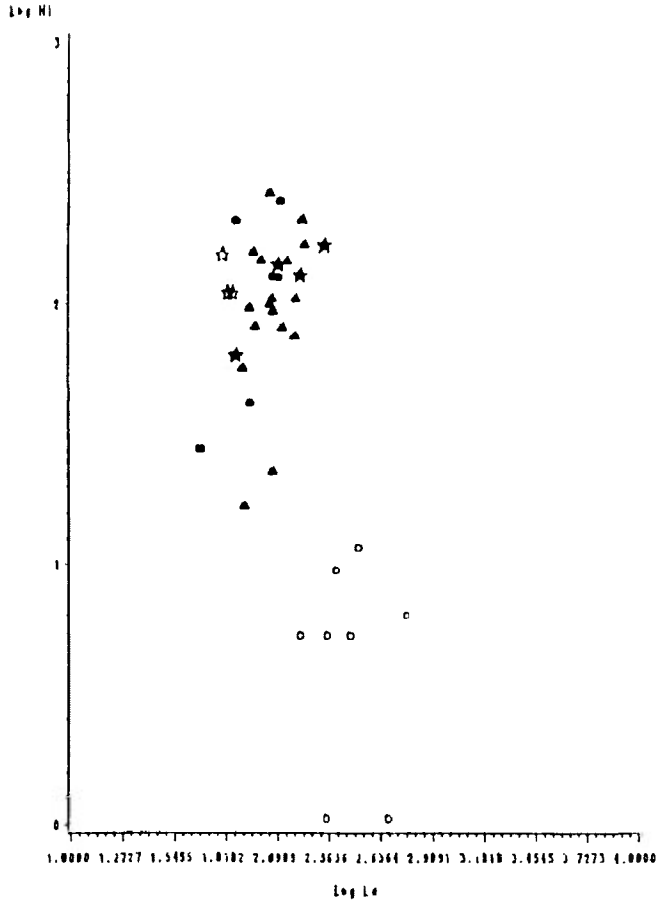

Fig. 5.13 Log Cu vs Log La

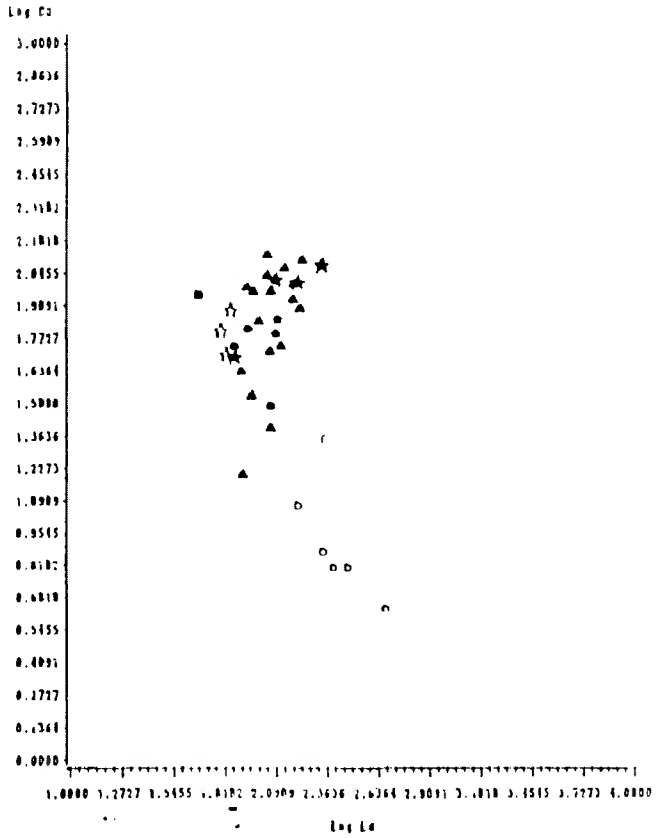

Fig. 5.14 Log Pb vs Log La

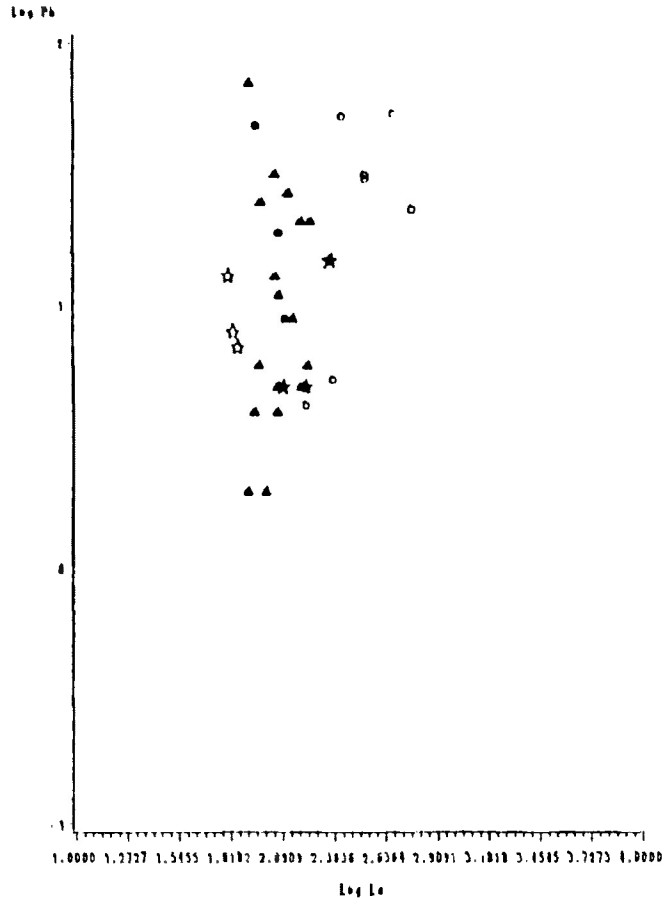

Fig. 5.15 Log Li vs Log La

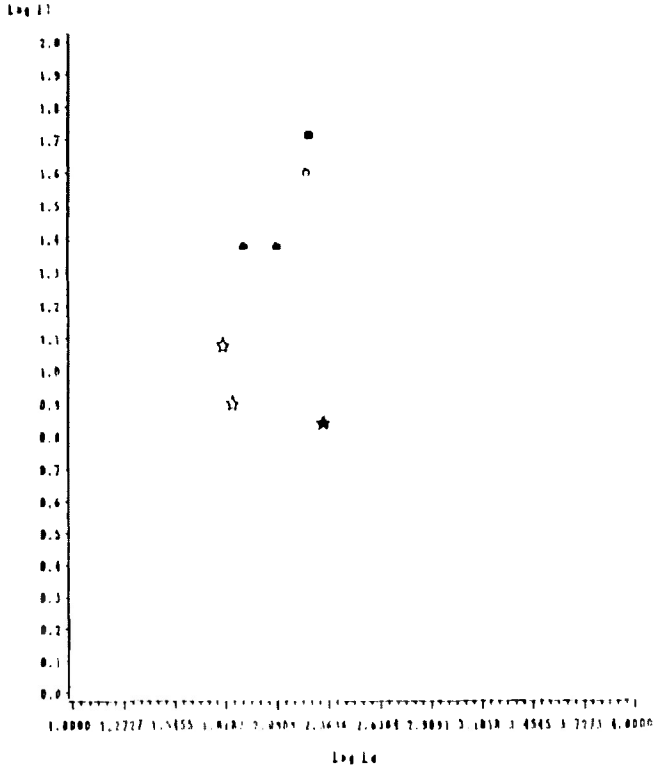

Fig. 5.16 Log Ce vs Log La

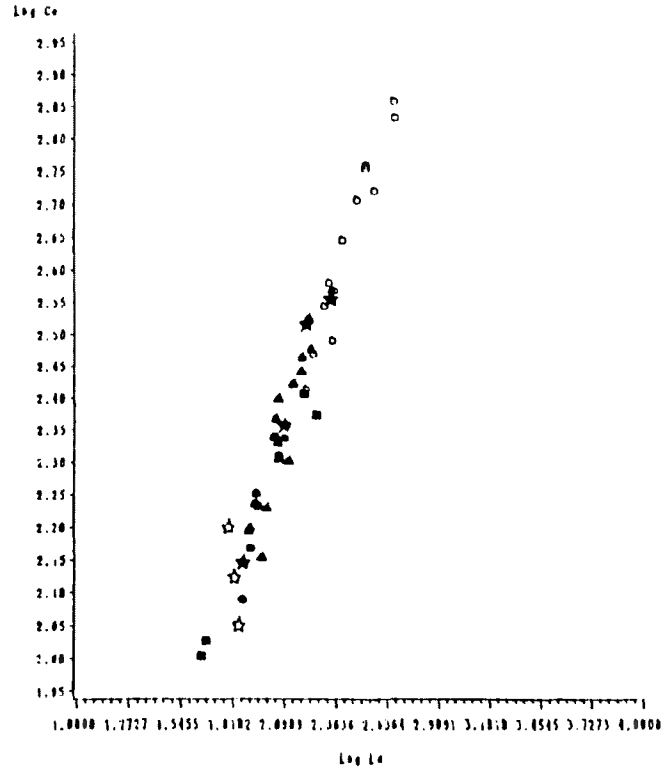

Fig. 5.17 Log Nd vs Log La

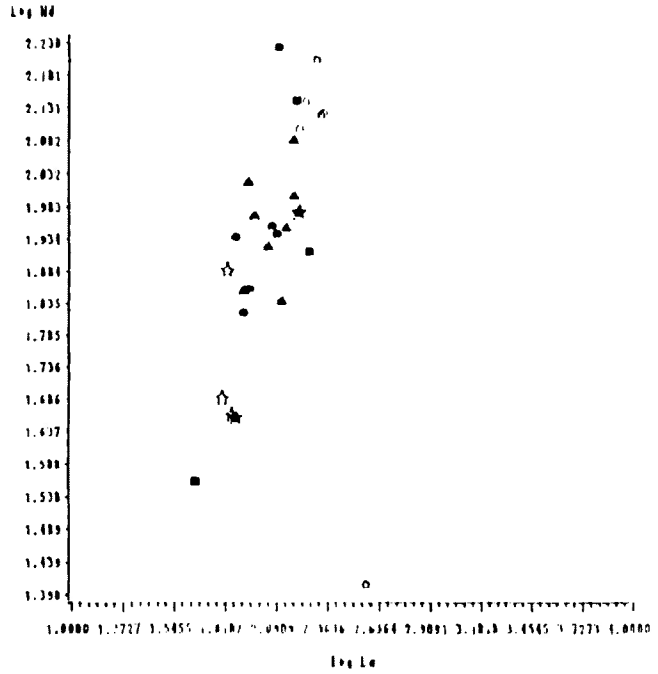

Fig. 5.18 Log Sm vs Log La

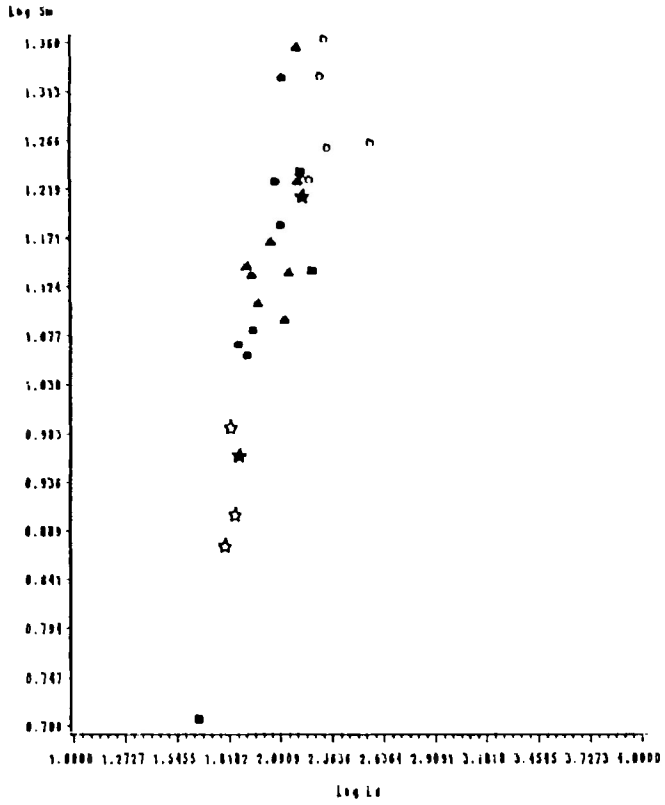

Fig. 5.19 Log Eu vs Log La

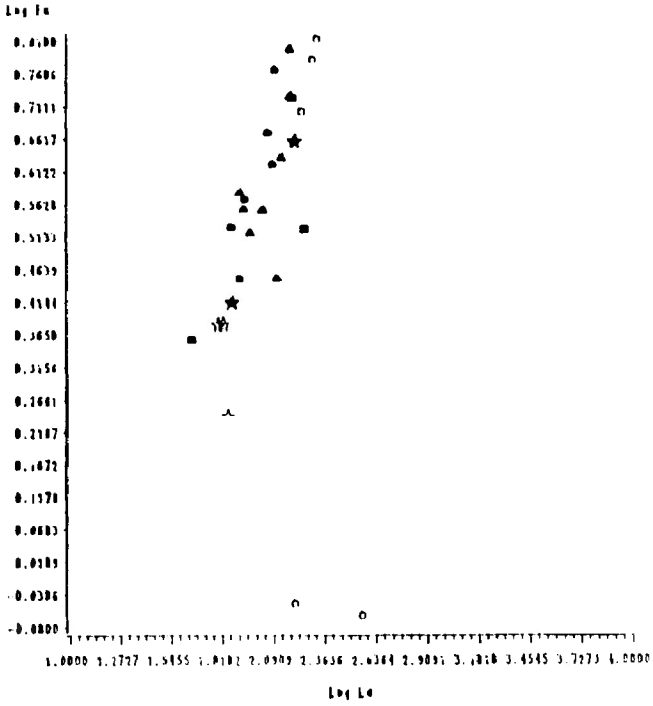

Fig. 5.20 Log Tb vs Log La

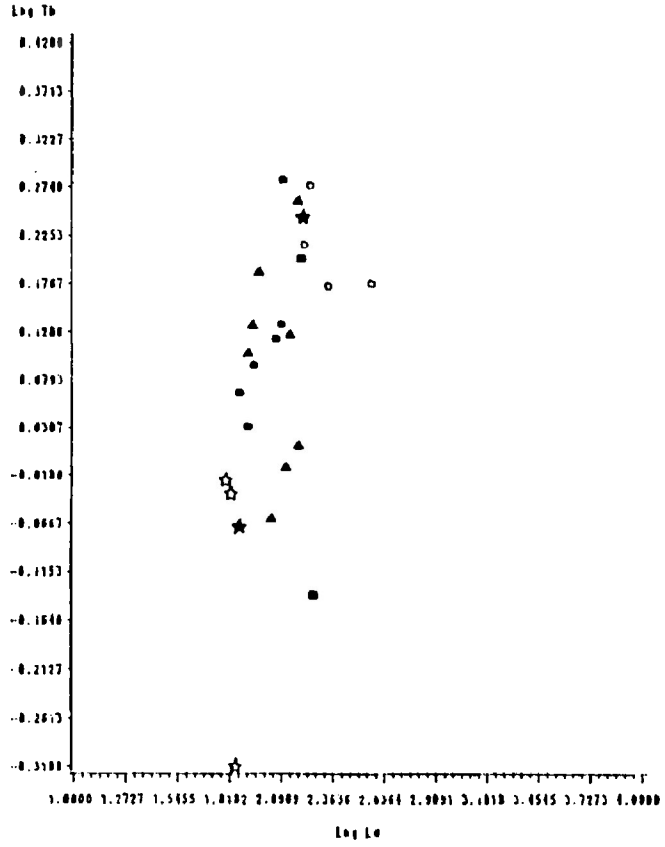

Fig. 5.21 Log Yb vs Log La

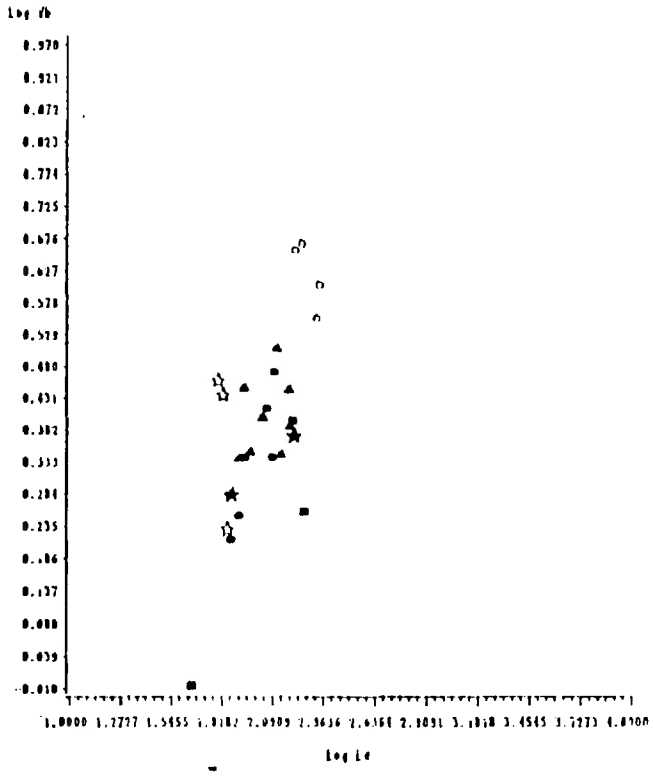

Fig. 5.22 Log Lu vs Log La

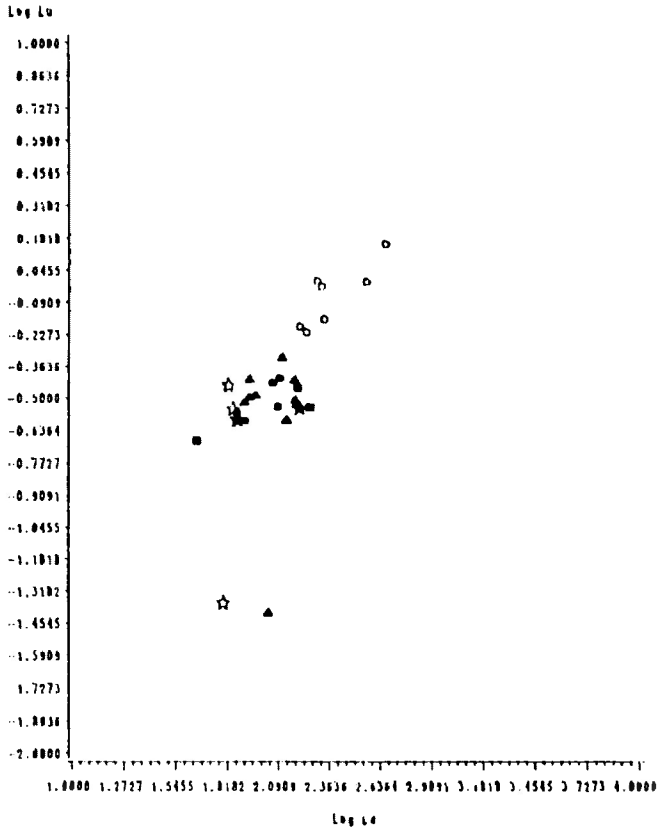

Fig. 5.23 Log Th vs Log La

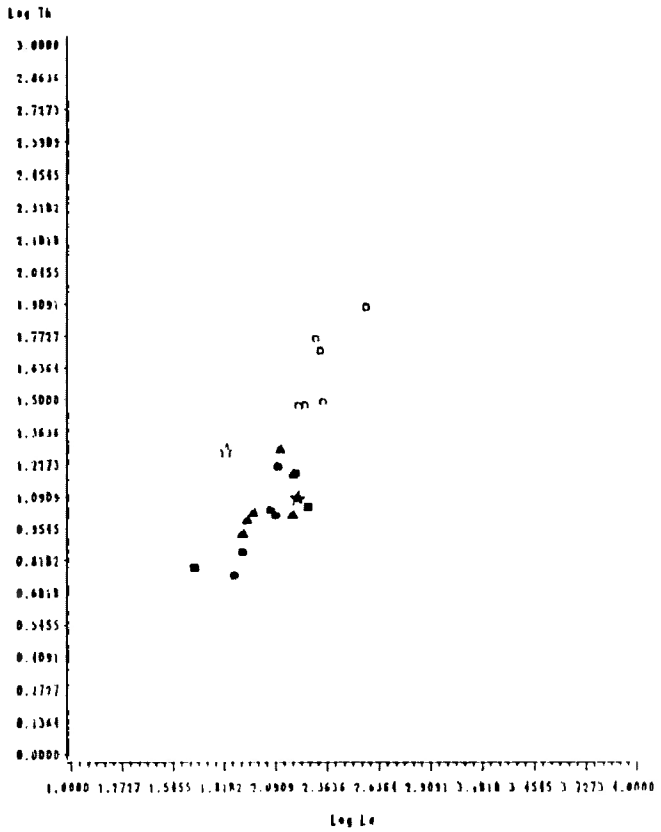

Fig. 5.24 Log Y vs Log La

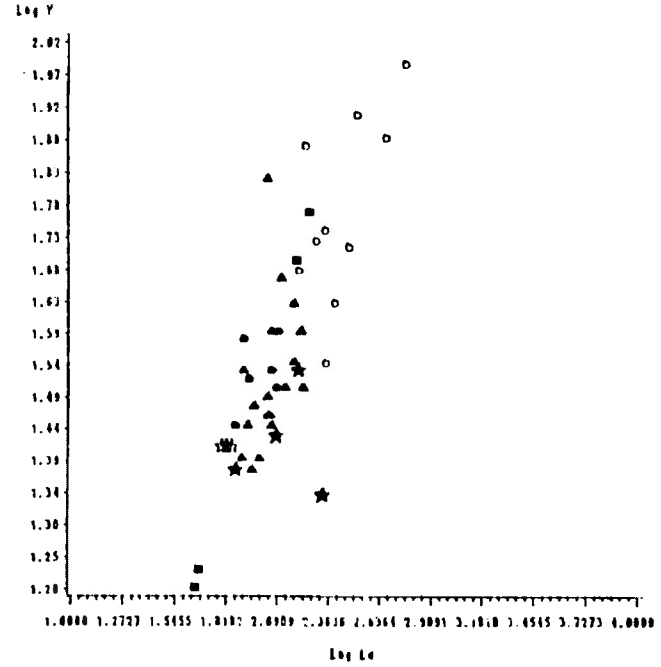

b) The logarithms of the concentrations of Rb, Zr, Hf, Ta, Nb, Pb, the REE, Th and Y exhibit positive correlations with the logarithm of the concentration of La. The strength of the linear relationship varies from weak to strong (see Table 5.3). With the exception of Pb, Eu, and, to a lesser extent, Nd, for which elements there is no clear pattern, the tinguaites are enriched in these elements relative to the lamprophyres. All of these elements are generally incompatible (Arth, 1976).

c) The points representing the quartz camptonites generally tend to fall off of or deviate from the trend defined by the other data points on the various diagrams. This is most evident on those diagrams for which the linear relationship is strong (i.e. Log Ta vs Log La, Log Nb vs Log La, Log Ce vs Log La). In the case of other diagrams which exhibit a higher degree of scatter of the data points, this deviation is still observed, although the exact nature of the deviation is less certain. This deviation is, at least in part, attributable to the low La content of these rocks relative to the other lamprophyres.

These observations suggest the following:

a) The general strength of the linear relationships

noted above suggests that the various types of dyke rocks may represent a single series, or several similar series. This is reinforced by the relative behaviour of La and Th, both of which are hygromagmatophile elements and should therefore maintain a nearly constant ratio during liquid evolution. The slope of the line defined by the log-log plots of these elements, therefore, should be close to unity; Table 5.3 shows that it is actually 1.2 for these rocks. The quartz camptonites may not be related to the other rock types.

b) The enrichment of the tinguaites in terms of incompatible elements, and depletion in terms of compatible elements, relative to the lamprophyres, suggests that the tinguaites are more evolved rocks than are the lamprophyres.

c) The decrease in concentration of the compatible elements, and the increase in concentration of the incompatible elements, relative to an element with low D_b, suggests that fractional crystallization was the dominant mechanism operating during the formation of the one or more series represented by the Coldwell dyke rocks. Note that while no distinct breaks in the slope of the trends defined by the points, such as those described by Villemant et al (1981) are observed, it is possible that such features may be camouflaged by the scatter exhibited by the trends on most of

the diagrams.

d) Consideration of the behaviour of various trace elements will indicate which phases may have reasonably been involved in this fractional crystallization mechanism. Depletion of the tinguaites relative to the lamprophyres in terms of Ni and Cr suggests the involvement of olivine, while similar depletion of Cr and Sc indicates the removal of clinopyroxene. The depletion of Co, Ba and Sc in the tinguaites relative to the lamprophyres suggests that amphibole underwent fractional crystallization. The depletion of the tinguaites in terms of Ba and Sr may be the result of the removal of alkali feldspar or plagioclase. Note that similar patterns of behaviour among various trace elements suggests that biotite and Fe-Ti oxides may have been involved as well, but the enrichment of the tinguaites in terms of Rb (in the case of biotite) and Zr (in the case of Fe-Ti oxides) is not consistent with the fractionation of these phases.

Figures 5.25 to 5.30 are chondrite-normalized plots (Haskin et al, 1971) of the abundance of the REE in each of the various types of dyke rocks. Representative examples of each type are superimposed in Figure 5.31. A number of observations may be made concerning these diagrams:

a) Figures 5.25 to 5.31 emphasize the general depletion of the HREE relative to the LREE, as noted previously, exemplifed by the downward trend of the curves (see La:Yb ratios in Table 5.1).

b) Inspection of Figure 5.31 emphasizes the enrichment of the tinguaites, and the depletion of the quartz camptonites in terms of the REE relative to the other lamprophyres. Considerable overlap exists among the other lamprophyres, although there is a slight tendency for the sannaites to have lower values. This is expressed in total REE content (see Table 5.1).

c) Some of the tinguaites display negative Eu anomalies, as shown in Figures 5.30 and 5.31.

The LREE

As shown in Figures 5.25 to 5.30, the LREE are generally enriched relative to the MREE and HREE in all of the dyke rocks (La:Yb ratios are given in Table 5.1 for each rock type). There is generally little decrease in terms of concentration among the LREE for the sannaites and the ocellar camptonites, so that generally the REE distribution

Figure 5.25 **Chondrite Normalized REE Patterns of Sannaites**

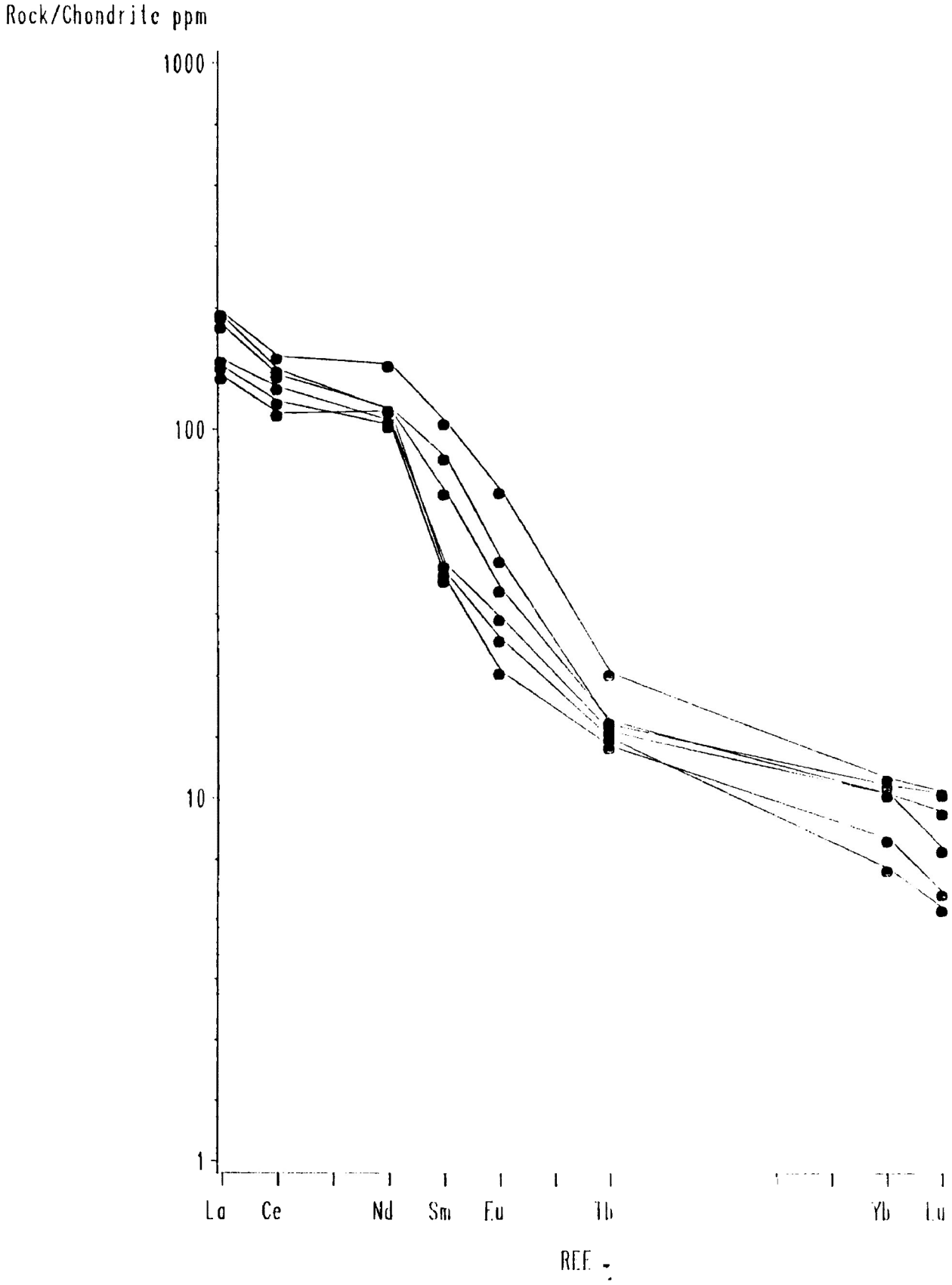

Figure 5.26 **Chondrite Normalized REE Patterns of Quartz Camptonites**

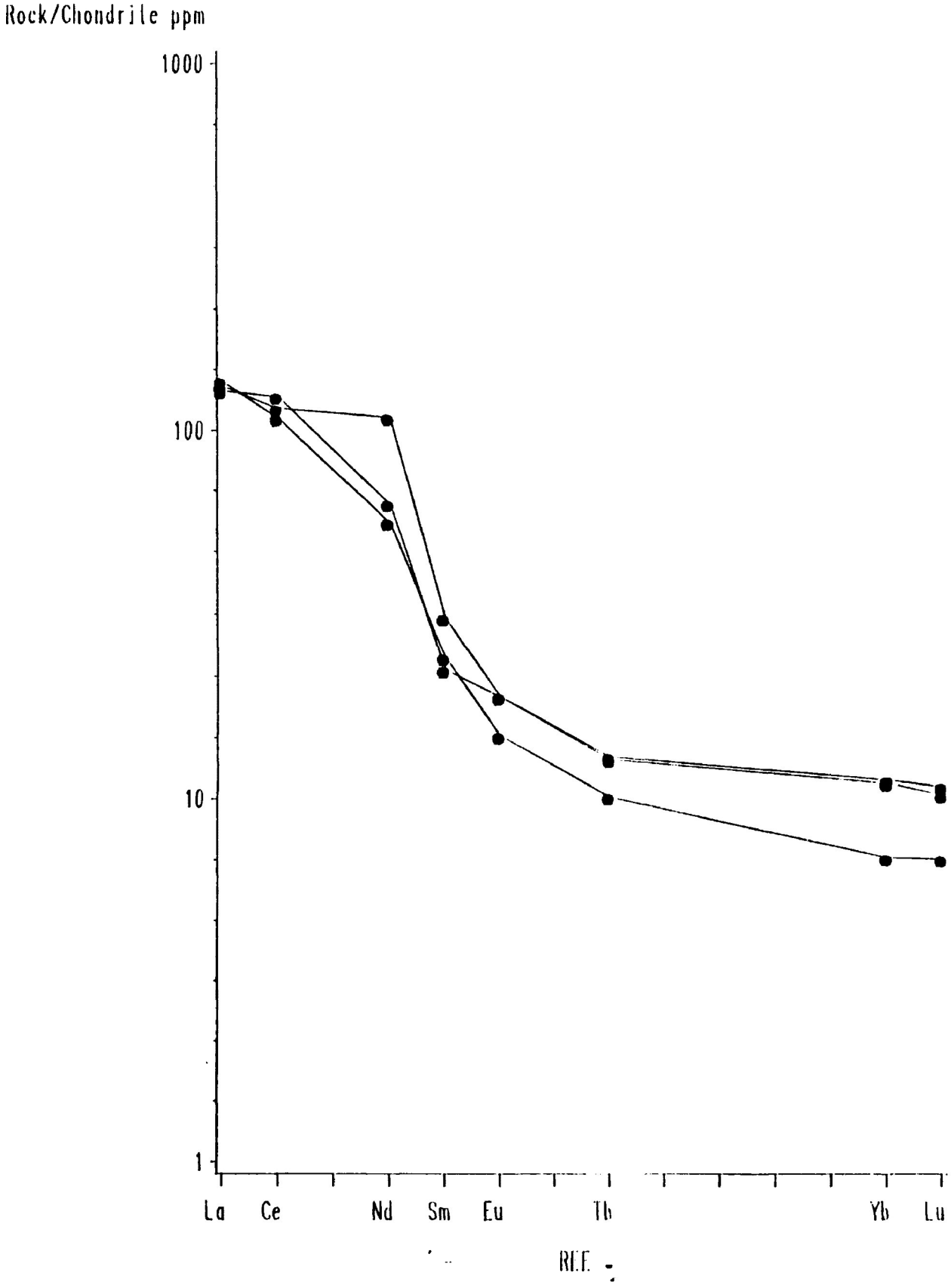

Figure 5.27 **Chondrite Normalized REE Patterns of Ocellar Camptonites**

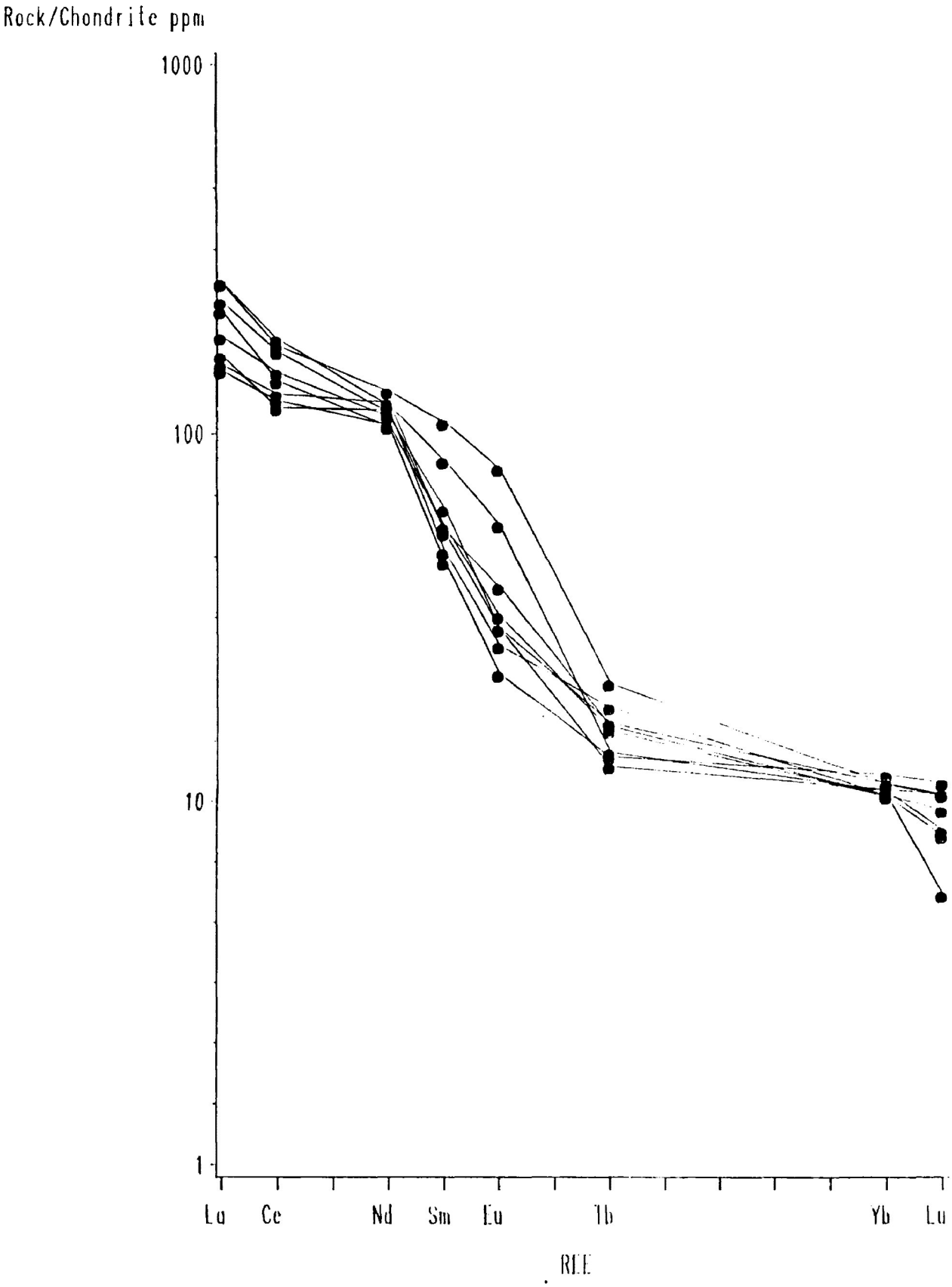

Figure 5.28 **Chondrite Normalized REE Patterns of Monchiquites**

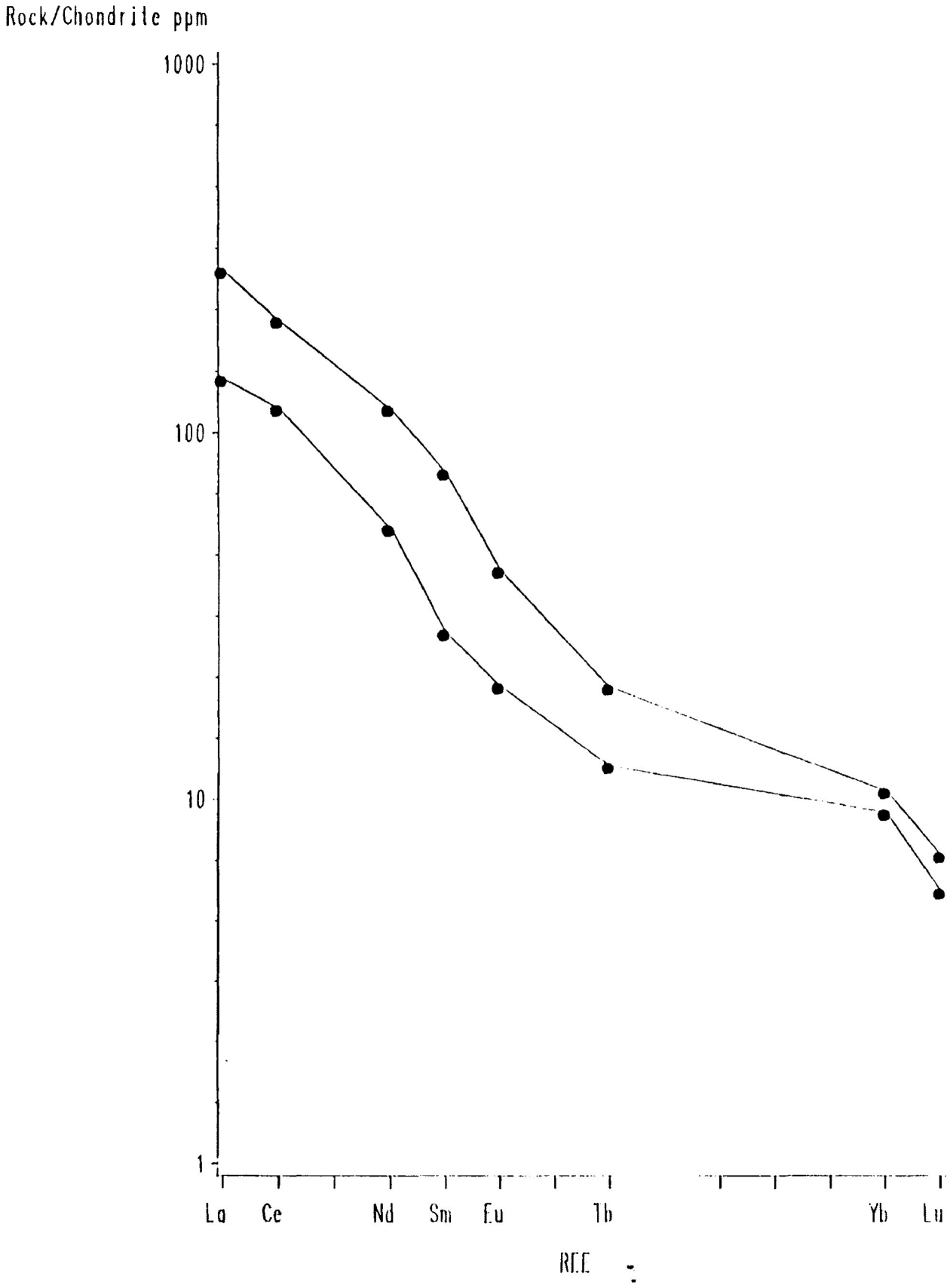

Figure 5.29 **Chondrite Normalized REE Patterns of Amphibole Camptonites**

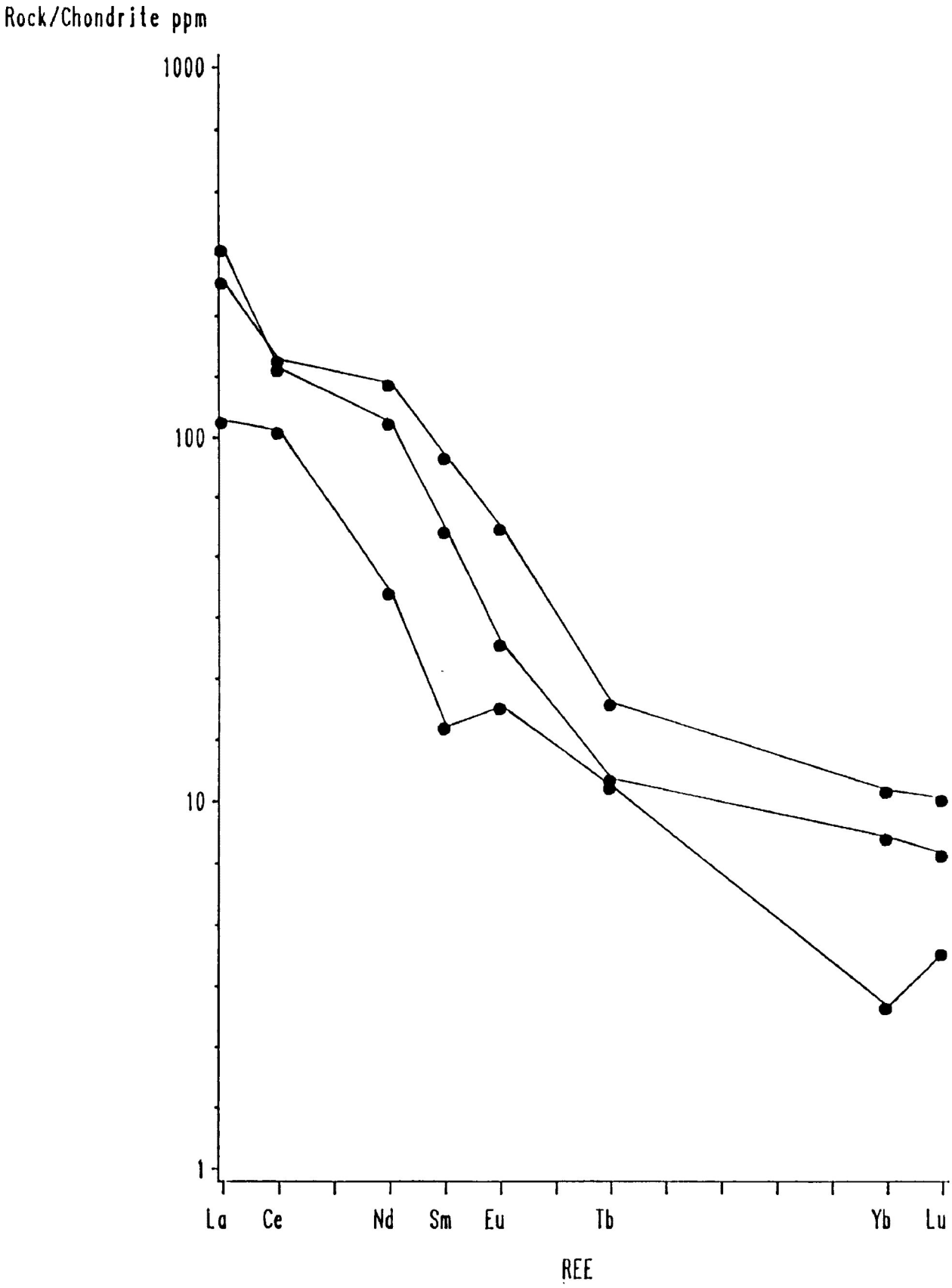

Figure 5.30 **Chondrite Normalized REE Patterns of Tinguaites**

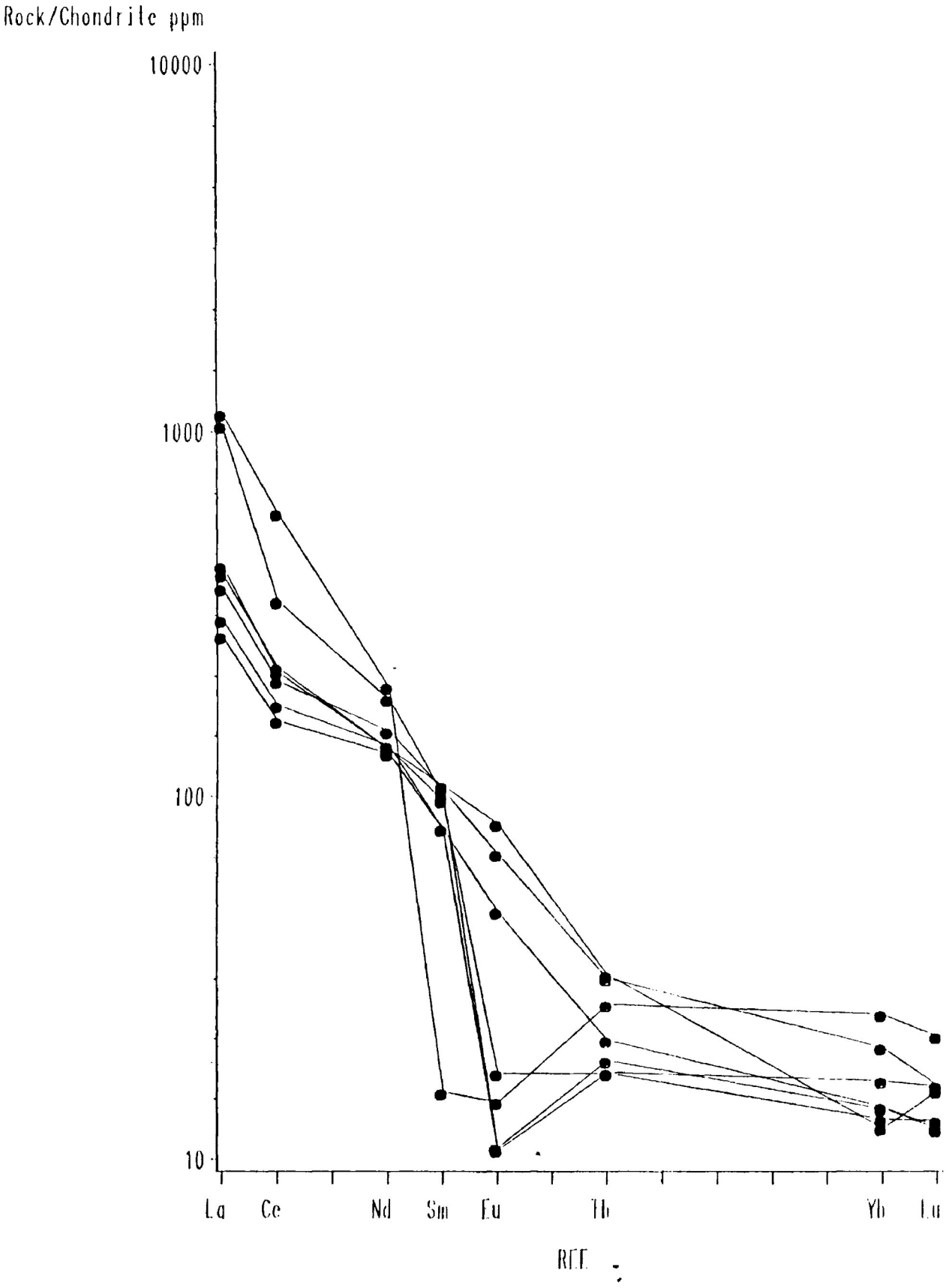

Figure 5.31 **REE DISTRIBUTION PATTERNS OF A REPRESENTATIVE SUITE OF DYKE ROCKS**

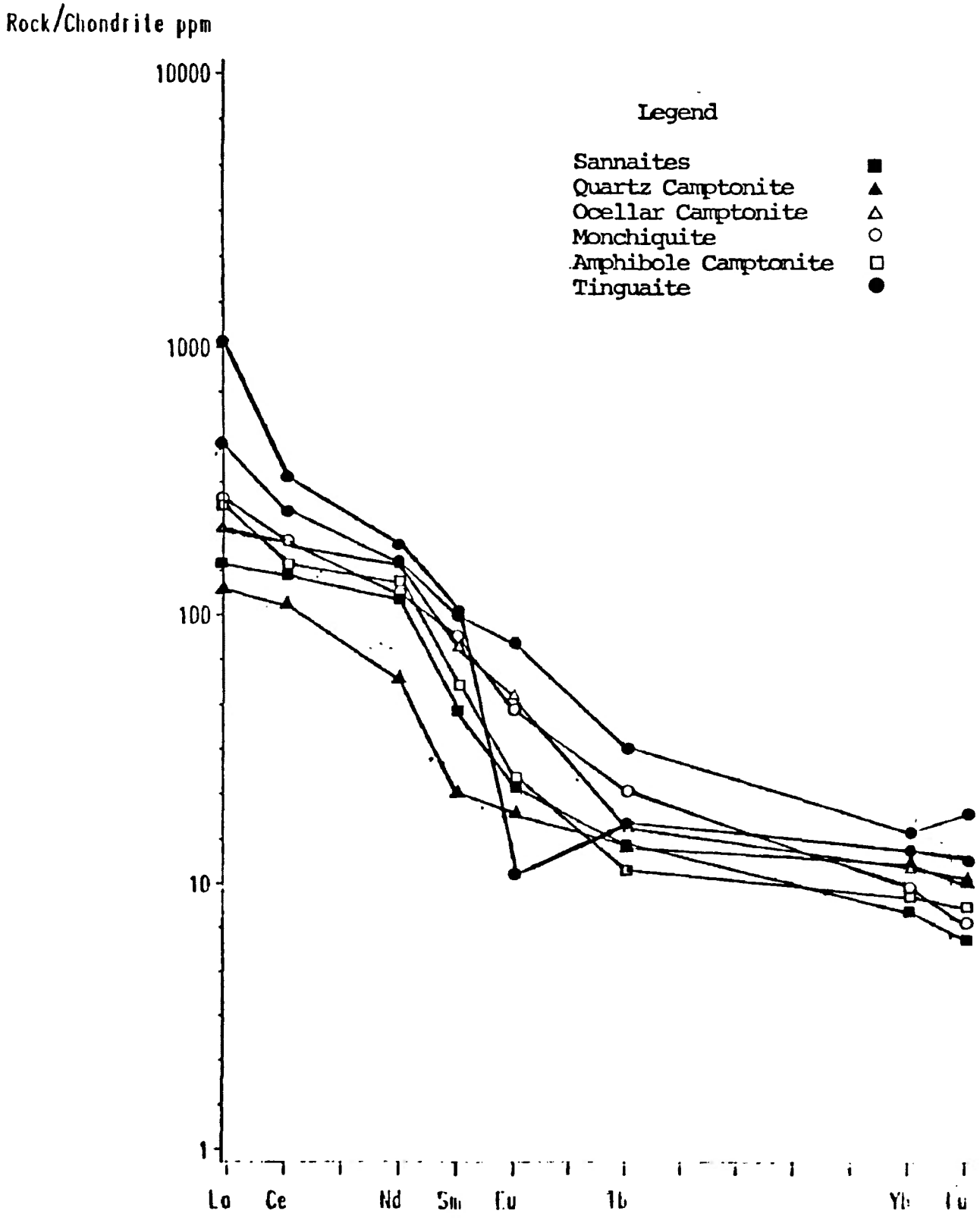

patterns for these rock types are relatively flat from La to Nd. The tinguaites generally exhibit higher abundances of the LREE than the lamprophyres. However, some overlap between the two rock types are noted, particularily in the case of two tinguaites in terms of their Nd content (see Figure 5.17); the reason for this Nd depletion is unclear, since no mechanism which fractionates Nd exclusively is known, but may result from redistribution of the REE by secondary processes; alternatively, it may be a spurious datum point. Among the lamprophyres, as noted previously, no clear pattern of distribution is observed, although one amphibole camptonite consistently displays very low values, and the quartz camptonites exhibit low values, particularily in terms of La and Ce (see Figures 5.16 and 5.26) , relative to the other lamprophyres. Inspection of Figure 5.16 also shows the deviation of the quartz camptonites from the trend defined by the other dyke rocks, noted previously, suggested by the distribution of the data points. Otherwise, considerable overlap exists among the ocellar and amphibole camptonites, the monchiquites and the sannaites in terms of their LREE abundances.

The MREE

The general fractionation trend of the REE (i.e.

enrichment of the LREE over the MREE and HREE) is reflected by the MREE, in that, generally, [Sm] > [Eu] > [Tb], while the MREE as a group are enriched relative to the HREE in each type of dyke rock (see Figures 5.25 to 5.30). As shown in Figures 5.18 and 5.20, the tinguaites are generally enriched in terms of Sm and Tb relative to the lamprophyres, although some overlap is noted. The case of Eu in the tinguaites is discussed below. Among the lamprophyres, there is no clear pattern to the distribution of the various types, so that considerable overlap exists, although the quartz camptonites exhibit relatively low values for all of the MREE, while the same amphibole camptonite exhibiting low values for the LREE has a very low Sm content.

The HREE

Examination of Figures 5.25 to 5.31 shows that all of the various types of dyke rocks are strongly depleted in terms of the HREE relative to the other REE. Generally, however, the REE distribution patterns depicted in these diagrams are relatively flat among the REE, so that generally [Yb] is only slightly greater than [Lu] for each rock type. As shown in Figures 5.21 and 5.22, the tinguaites are enriched in the HREE relative to the lamprophyres. Again, among the lamprophyres, no clear pattern to the distribution

of the various types is recognized, although the same amphibole camptonite exhibiting low concentrations of the LREE and MREE displays a very low Yb content, while one quartz camptonite and one ocellar camptonite have anomalously low Lu contents.

Based on the preceding observations, a number of conclusions may be drawn concerning the REE in the various dyke rocks:

a) As shown in Figure 5.19, several tinguaites display low Eu contents relative to the other tinguaites. These low Eu abundances are reflected in Figure 4.30 as negative Eu anomalies in the chondrite-normalized REE distribution patterns. Note, however, that other tinguaites do not exhibit such anomalies; the mechanism involved in Eu fractionation affected only some of the tinguaites. Therefore, these rocks represent at least two distinct sets of evolutionary conditions. Such Eu depletion may be a result of fractionation of plagioclase (D=0.5 to 3.0), or, to a lesser extent, alkali feldspar (D=1.2) (Villemant et al, 1981). In order to test the possibility that Eu depletion is at least in part a function of plagioclase and/or alkali feldspar fractionation, Eu is plotted against Sr in Figure 5.32. Sr has high D values for plagioclase, and

Figure 5.32 Sr vs Eu in Tinguaites

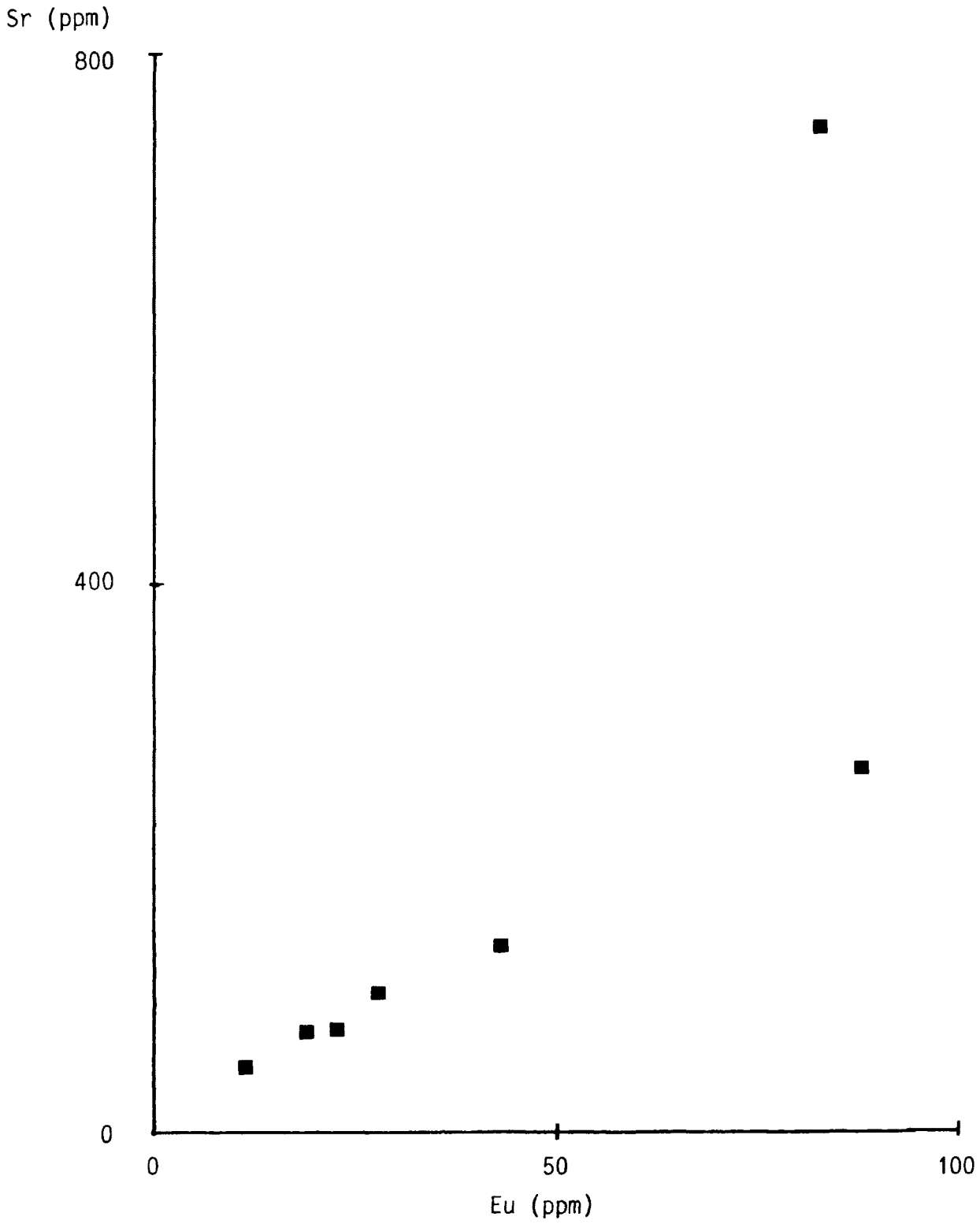

particularily for alkali feldspar, and therefore will act as an indicator of removal of these phases. This diagram shows that there is a positive correlation between these two elements, although the strength of the linear relationship is reduced by the specimen which displays an anomalously high concentration of Sr (i.e. 749 ppm); otherwise the correlation coefficient is 0.98. This strong positive correlation between Eu and Sr in the tinguaites suggests that Eu depletion is, at least in part, a result of feldspar fractionation. There is no evidence to indicate that plagioclase has fractionated extensively, therefore removal of alkali feldspar appears to be a more important mechanism in producing negative Eu anomalies. Note that the effects of other factors, such as melt structure, temperature and volatile components are probably important as well (Moller and Muecke, 1984), but since quantification of these parameters is beyond the scope of the present work, their exact effects are impossible to determine. However, changes in these parameters will contribute significantly to the Eu depletion (e.g. increasing water content would result in depolymerization of the melt and subsequent stabilization of Eu^{2+} in crystallizing feldspars (Moller and Muecke, 1984)). Indeed, the close inter-relationship of these parameters (Moller and Muecke, 1984; Lemarchand et al, 1987) allows that variable degrees of fractionation of alkali feldspar among

the tinguaites may themselves be a result of changes in these factors during the genesis of some of these rocks.

b) Enrichment of the LREE over the HREE will result from one or more of the three following fundamental types of mechanisms:

i) A mechanism which will remove HREE, such as fractional crystallization of garnet, which has high D values for the HREE (e.g. D^{garnet}_{Yb}=11.5 to 39.9, D^{garnet}_{Lu}=11.9 to 29.6 (higher values from Schnetzler and Philpotts, 1970; lower values from Arth, 1976);

ii) A mechanism which will add LREE, such as addition of a CO_2-rich vapour phase, since such a phase will itself tend to be preferentially enriched in the LREE (Clarke et al, 1983; Wendlandt and Harrison, 1979); and

iii) Partial melting of a LREE enriched source to produce a LREE enriched parental magma.

Clarke et al (1983), in their study of the alkaline lamprophyres of Ubekjendt Eiland, West Greenland, invoke the first mechanism (specifically, eclogite fractionation) to explain the depletion of HREE relative to the LREE observed in those rocks; they acknowledge that the second mechanism

(specifically, involvement of a CO_2-rich vapour phase) may have had some unquantified effect on the REE distribution patterns. In the case of the Coldwell dyke rocks, there is no evidence beyond the relative depletion of the HREE to suggest that garnet was a fractionating phase (i.e. garnet is not observed to occur in any of the dyke rocks), unless garnet fractionation was involved in the formation of the liquids which were parental to the Coldwell dyke rocks; this is impossible to determine definitely, but such a mechanism cannot, at this point, be ruled out. However, there is ample evidence to suggest that a CO_2-rich vapour phase was present during the formation of the various dyke rocks (e.g. presence of abundant carbonate minerals (see Chapter 4), especially in ocelli (see Chapter 6) in the various dyke rocks). Therefore, it is suggested that the relative LREE enrichment observed in the various dyke rocks is a result of the presence of this vapour phase; involvement of garnet fractionation is not necessary, but is acknowleged as a possible factor.

c) Evidence from the REE support the suggestion that the quartz camptonites are distinct from the other dyke rocks, which, as previously suggested, are members of a magmatic series. Specifically, the quartz camptonites display low total REE, and low La:Yb ratios, relative to the other

lamprophyres. Furthermore, the REE distribution patterns depicted in Figure 5.26 are distinctly concave, suggesting depletion of the MREE by some mechanism (see below).

d) There is considerable overlap among the lamprophyres, excepting the quartz camptonites, in terms of their REE distribution patterns (see Figure 4.31), although there is a slight tendency for the sannaites to exhibit relatively low abundances of the REE, and total REE (see Table 4.1). Furthermore, there are no distinct changes in the shape of the curves on Figure 4.31, with the exception of the development of negative Eu anomalies among some of the tinguaites, which, as noted above, are probably the result of alkali feldspar fractionation, and the concave shape of the quartz camptonite curves, so that any genetic mechanism (or mechanisms) has apparently simply translated the curves upwards on the diagram (i.e. from the lamprophyres to the more evolved tinguaites). According to Clarke et al (1983), gabbro fractionation will result in such an upward translation, although, as noted, there is no evidence to suggest that plagioclase has fractionated extensively. However, fractionation of olivine, which has very low D values for all of the REE (Schnetzler and Philpotts, 1970; Arth, 1976; Villemant et al, 1981) will result in a general upward translation. Fractionation of hornblende, and, to a

slightly lesser extent, clinopyroxene, which are suggested by evidence from other trace elements (see, for example, the preceding section dealing with Sc) will tend to fractionate the MREE, however, the magnitude of the differences between D clinopyroxene$_{MREE}$ and D clinopyroxene$_{LREE \text{ and } HREE}$ are small (i.e. less than 0.1), and are only slightly greater in the case of hornblende (i.e. 0.4 or less) so that the magnitude of relative MREE depletion will probably be minor. Overall, D values for the REE in both phases are small (i.e. 0.6 or less) (Schnetzler and Philpotts, 1970; Arth, 1976). Therefore, fractionation of clinopyroxene and amphibole will generally result in an upward translation of the pattern. However, development of the concavity exhibited by the quartz camptonite curves may be related to more extensive fractionation of clinopyroxene and/or amphibole i.e. of sufficient extent to cause a significant depletion of the MREE in spite of the above.

Conclusions

A number of significant conclusions may be drawn from the preceding discussion of trace element geochemistry of the Coldwell dyke rocks:

a) Based on Ni and Cr contents, none of the lamprophyres

represent primitive magma compositions, and therefore have all undergone some degree of evolution from a parental liquid.

b) The sannaites, the ocellar and amphibole camptonites, the monchiquites and the tinguaites are members of a comagmatic series. Alternatively, they may represent several series which have evolved along similar paths on the various preceding diagrams.

c) The tinguaites are the most evolved members of the series. Determination of the most primitive member of the series is more problematical, however. REE contents suggest, albeit with considerable uncertainty, that the sannaites are the most primitive members. Evidence from other data (i.e. Log Ce, Log Y and Log Nb vs Log La) indicate that specimens of amphibole or ocellar camptonite may be more primitive, however.

d) The tinguaites represent two distinct sets of evolutionary conditions, exemplified by the occurrence of negative Eu anomalies in some specimens of this rock type, but not in others. The exact mechanism for this is not, at this point, clear, but it is probably some combination of fractionation of alkali feldspar and changes in melt

structure brought about by changing volatile content, oxygen fugacity and temperature.

e) The quartz camptonites are not members of the series defined by the other types of dyke rocks. This is exemplified by the deviation of this rock type from the trend defined by the other types on the various log-log diagrams, and by significantly different REE distribution patterns.

f) The dominant mechanism responsible for the evolution of the various dyke rocks is fractional crystallization, as evidenced by the observed enrichments and depletions of compatible and incompatible elements respectively relative to an element of low D (i.e. La).

g) The only phases which, fractionating, satisfy the observed patterns of trace element variation, as well as petrographic evidence, are clinopyroxene, amphibole (generally hornblende), olivine and alkali feldspar.

The success of any petrogenetic model will be determined by how well it can take the above, as well as conclusions from petrographic and major element analysis, into account.

CHAPTER 6- OCELLI

INTRODUCTION

Ocelli occur in varying abundance in all types of lamprophyres (see Table 2.1). They are described in detail in terms of their form and constituent mineralogy in Chapter 2; in summary, they comprise three distinct types, in order of abundance:

a) globular or irregular lobate segregations composed primarily of calcite, with lesser amounts of scapolite, chlorite, epidote, zeolites, cancrinite, quartz and fluorite;

b) globular or irregular lobate segregations of a similar composition to type (a) above, but in which the silicate phases in general, and zeolites (e.g. stilbite, thompsonite and analcite) in particular, predominate; and

c) irregular lobate segregations of felsic silicate phases including alkali feldspar, plagioclase and nepheline; only one example of this type has been found.

The optical, physical and compositional details of the phases occurring in each are presented in Chapter 4.

In order to determine compositional relationships between ocelli and the corresponding host rock, samples of each type of material were separated from specimens of three lamprophyres containing ocelli, including two ocellar camptonites (C26b and C88) containing silicate-carbonate and carbonate ocelli, and one monchiquite (C560), the latter exemplifying silicate ocelli (type (c) above). Both ocellar and corresponding matrix material were analysed to determine the abundance of 15 trace elements, including Ba,Sc,Cr,Co,Ta,Hf,La,Ce,Nd,Sm,Eu,Tb,Yb,Lu and Th. In the case of the pink silicate ocelli occurring in specimen C560, sufficient material was available to determine the major element composition. Analytical methods are detailed in Appendix A. Data are given in Table 6.1.

PREVIOUS WORK

Ocelli are a common feature of alkaline lamprophyres and are known from: Callander Bay, Ontario (Ferguson and Currie, 1971); the Beemerville Carbonatite-Alkaline Complex, New Jersey (Maxey, 1976); Aillik Bay, Labrador (Foley, 1984; Malpas et al, 1986); Central Newfoundland (Strong and Harris, 1974); Serra del Monchique, Portugal (Rock, 1979); Monteregian Hills, Quebec (Eby, 1980); West Otago, New

Table 6.1 Chemistry of Ocelli and Coexisting Host Rock

Element	C26b Ocelli	C26b Host Rock	C88 Ocelli	C88 Host Rock	C560 Ocelli	C560 Host Rock
SiO2	nd	nd	nd	nd	54.58	45.46
Al2O3	nd	nd	nd	nd	19.78	14.15
Fe2O3	nd	nd	nd	nd	2.16	4.69
FeO	nd	nd	nd	nd	1.76	5.64
MgO	nd	nd	nd	nd	0.81	7.35
CaO	nd	nd	nd	nd	4.41	9.94
Na2O	nd	nd	nd	nd	8.57	3.40
K2O	nd	nd	nd	nd	1.28	2.52
MnO	nd	nd	nd	nd	0.09	0.20
TiO2	nd	nd	nd	nd	0.18	1.65
P2O5	nd	nd	nd	nd	0.04	1.20
CO2	nd	nd	nd	nd	1.83	0.62
H2O	nd	nd	nd	nd	4.32	3.33
Ba	3385	1682	455	1256	2011	2585
Sc	1	19	1	16	1	20
Cr	8	289	3	298	8	420
Co	3	40	3	38	55	101
Ta	7	5	1	11	11	10
Hf	1	5	0	4	4	3
La	344.12	164.58	158.12	32.53	163.52	80.03
Ce	454.11	238.40	228.72	53.79	328.59	166.72
Nd	226.01	115.79	117.06	16.68	34.63	58.69
Sm	31.01	18.57	18.77	3.38	16.31	10.40
Eu	7.22	5.09	1.48	5.11	4.65	2.98
Tb	1.99	1.54	1.68	0.37	1.76	1.11
Yb	2.06	2.33	2.49	0.61	2.37	2.17
Lu	0.27	0.35	0.35	0.05	0.29	0.33
Th	11	17	10	25	31	15

nd = no data

Zealand (Cooper, 1979); and others. Rock (1977), compiling some 350 descriptions of alkaline lamprophyres, notes that 40% are ocellar. In terms of their constituent mineralogy, three general categories of ocelli are recognized:

a) ocelli composed entirely of silicate minerals (e.g. Foley, 1984);

b) ocelli composed entirely of carbonate minerals (predominantly calcite) (e.g. Cooper, 1979); and

c) ocelli composed of both silicate and carbonate minerals (e.g. Ferguson and Currie, 1971).

Note that in terms of detailed mineralogy in general, and silicate mineralogy in particular, considerable variation exists. Glass is also sometimes observed as an ocellar constituent (Upton and Wadsworth, 1968). Although category (a) ocelli are most common at other occurrences, category (c) ocelli are most abundant in the Coldwell lamprophyres, with lesser amounts of category (b) ocelli, and, as noted previously, few examples of category (a) ocelli, being observed.

Various mechansims have been proposed to explain the

origin of ocelli. These include:

a) silicate-silicate or silicate-carbonate liquid immiscibility (e.g. Ferguson and Currie, 1971; Philpotts, 1976; Rock, 1977);

b) segregation of late-stage fluids into earlier formed vesicles by filter pressing, or pressure differentials resulting from contraction of cooling vesiclar gas (e.g. Smith, 1967; Upton and Wadsworth, 1971);

c) segregation of late-stage (i.e. pegmatitic) fluids (Bogoch and Margaritz, 1983);

d) incomplete assimilation or replacement of included material (Bogoch and Margaritz, 1983);

e) deposition of secondary phases into vesicles by the action of hydrothermal or meteoric water (e.g. Horne and Thompson, 1967); and

f) formation in-situ, at some nucleation site , by spherulitic or orbicular crystallization (e.g. Carstens, 1982).

OBSERVATIONS

A number of observations may be made concerning the ocelli occurring in the Coldwell dyke rocks:

a) Ocellus-matrix contacts are typically sharp, suggesting that little or no diffusion across the interface has occurred.

b) Ocelli exhibit features suggestive of a discrete fluid phase (i.e. gas or liquid) occurring in a second fluid medium (i.e. tangential arrangement of elongate crystals around the ocellus, deformation where impinged upon by a larger crystal, elongation parllel to the direction of flow, and coalescence of ocelli to form complex lobate patterns).

c) Calcite occurring in the ocelli exhibits a composition distinct from that occurring in the coexisting matrix of the rock (i.e. ocellar calcite is enriched relative to matrix calcite in terms of the siderite, magnesite and rhodochrosite end member molecules). This suggests that ocellar calcite has an origin distinct from that of matrix calcite.

d) Table 6.1 shows that the ocellar material occurring

in specimens C26b and C88 are depleted in terms of Sc, Co and Cr relative to the matrix material. Note, however, that this material is also depleted in terms of Th, and, to a lesser extent, Hf, relative to the host rock. Ba and Ta do not exhibit any clear pattern to their distribution between ocellar and host rock material.

e) Figure 6.1 is a chondrite normalized REE plot of silicate-carbonate ocellar material and corresponding host rock from two ocellar lamprophyres. This diagram shows that ocellar material is enriched in terms of LREE and MREE in the case of C88, and all REE in the case of C26b, relative to the coexisting host rock.

f) Where silicate phases (e.g. scapolite, epidote, chlorite, analcite and zeolites) and fluorite occur in ocelli with calcite, the former phases are apparently replacing calcite. In some instances, this replacement is complete, or nearly so i.e. in specimen C80, an ocellar camptonite in which normally observed patterns of alteration are extremely advanced, ocelli are almost completely replaced, or in some cases are completely replaced, by stilbite.

g) The various silicate phases comprising the ocelli occurring in specimen C560 (e.g. alkali feldspar, nepheline

Figure 6.1 Chondrite Normalized REE Patterns of Ocellar Material vs Matrix Material

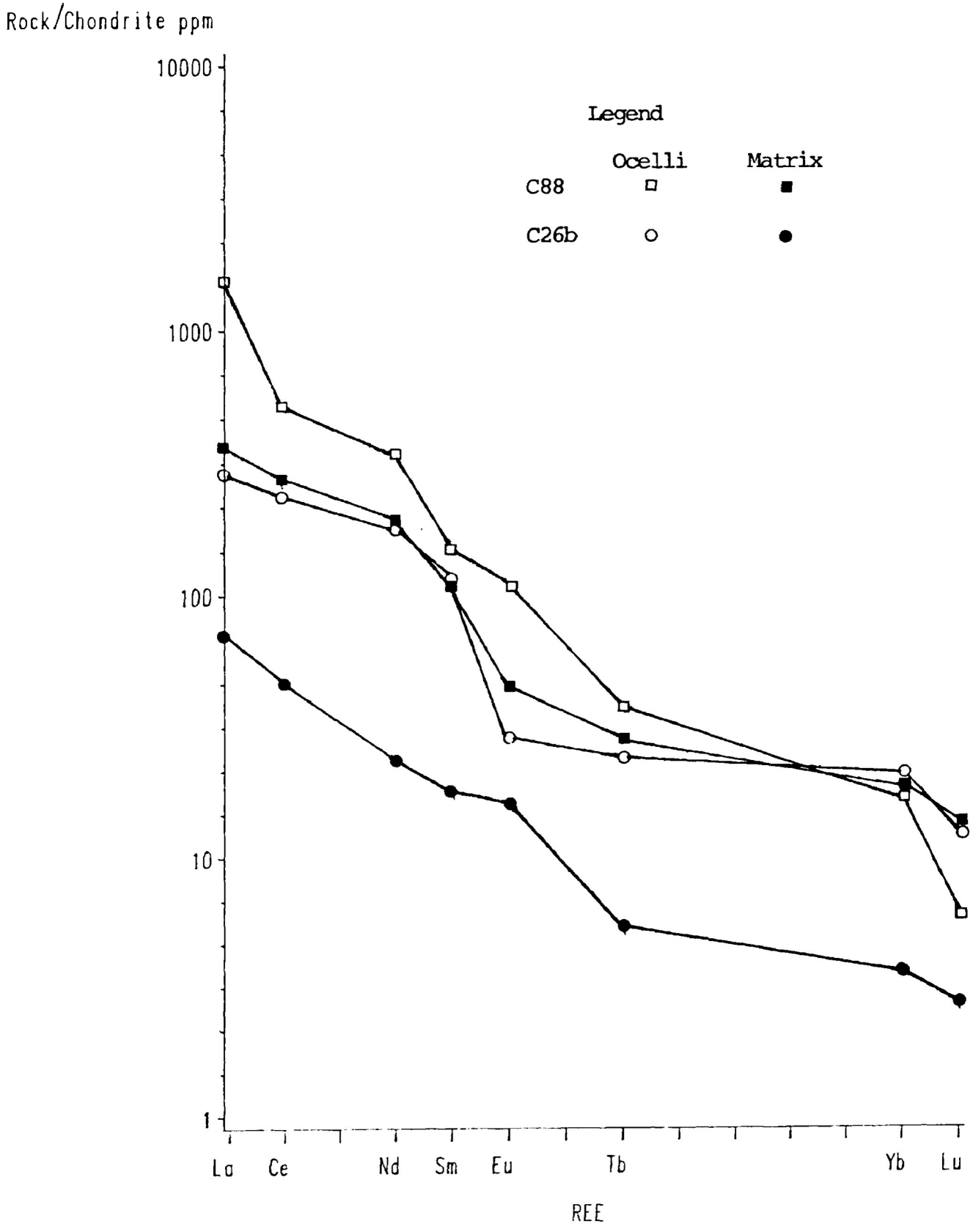

and analcite) are similar to the constituent minerals of the tinguaites.

h) Table 6.1 shows that in the case of the silicate ocelli occurring in specimen C560, ocellar material is enriched in terms of SiO_2, Al_2O_3 and Na_2O, and depleted in terms of all other oxides relative to the coexisting host rock. This pattern of major and minor element enrichment and depletion is similar to that observed in the case of tinguaites relative to lamprophyres (see Chapter 3), although the degree of SiO_2 enrichment is smaller, and the behaviour of K_2O is anomalous. Likewise, the ocellar material is depleted in terms of Sc, Cr, Co, enriched in terms of Th, and slightly enriched in terms of Ta and Hf, relative to the coexisting host rock. This pattern of incompatible element enrichment and compatible element depletion is also consistent with the pattern observed in the case of tinguaites relative to lamprophyres (see Chapter 5).

i) Figure 6.2 is a chondrite normalized REE plot of silicate ocellar material and corresponding host rock from a monchiquite (C560). This diagram shows that with the exception of Nd (the depletion of which is probably a result of analytical error, rather than real Nd fractionation), and to a lesser extent Lu, ocellar material is enriched in terms

Figure 6.2 Chondrite Normalized REE Patterns of Ocellar Material vs Matrix Material

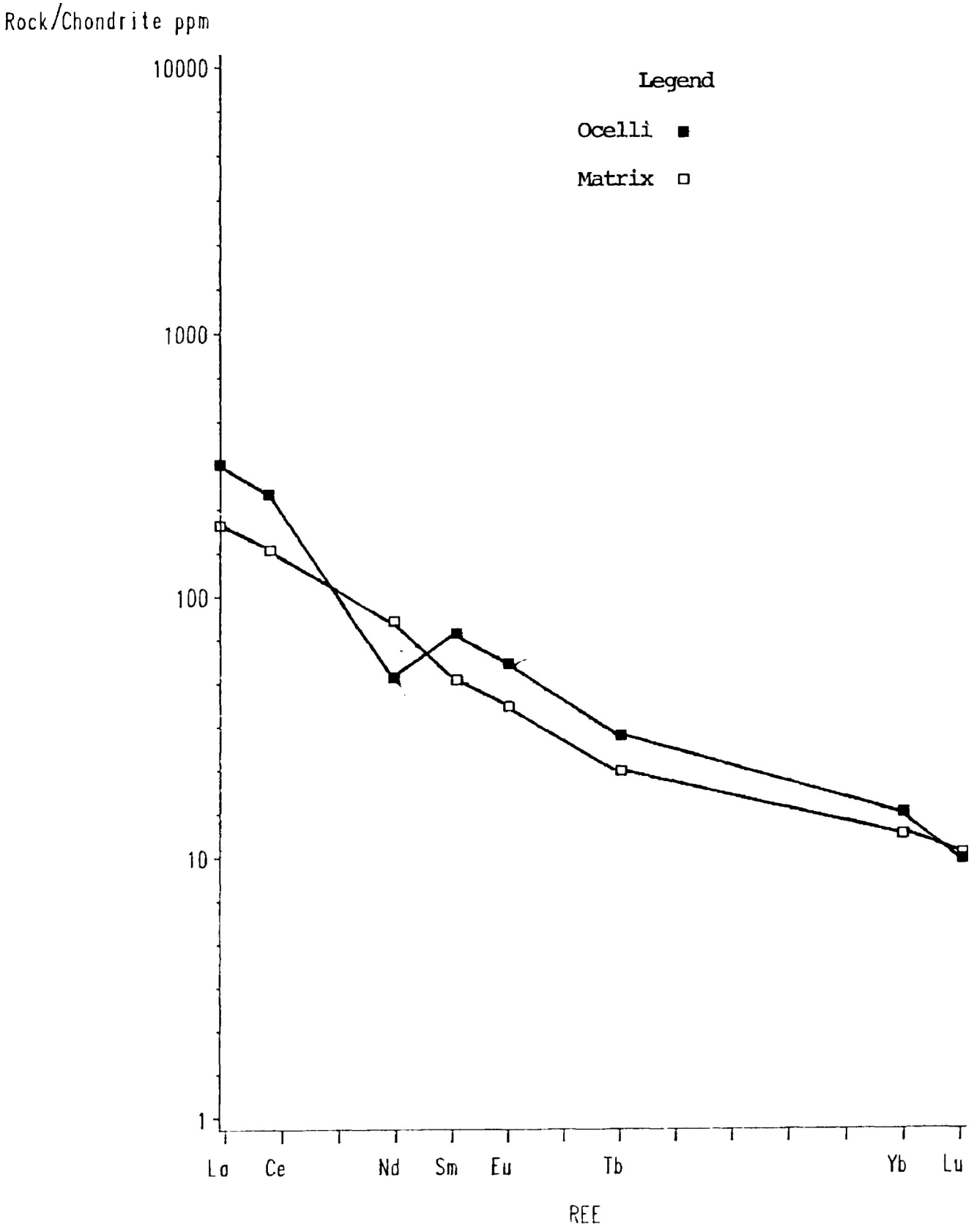

of all REE relative to the coexisting host rock.

CONCLUSIONS

Consideration of the above observations allows conclusions to be drawn concerning the origin of the ocelli:

a) There is no evidence to suggest that the carbonate-bearing ocelli represent incompletely assimilated inclusions, since the various dyke rocks do not intrude calcite-rich material, unless such material is not presently exposed.

b) Observations (a) and (b) suggest that the ocelli originated as distinct segregations of a fluid phase (i.e. liquid droplets or vesicles). Likewise, they would appear to rule out in-situ (i.e. spherulitic or orbicular) crystallization (in which case fluid behaviour is not expected), and late pegmatitic segregations (which have diffuse boundaries (Ferguson and Currie, 1972)).

c) If the ocelli did originate as vesicles, and were subsequently filled with secondary minerals (i.e. if the ocelli are amygdules) then it would be reasonable to expect that the ocellar calcite would be similar to calcite

occurring in veinlets transecting the dykes (i.e. secondary calcite). However, observation (c) shows that this is not the case. Alternatively, ocellar calcite may represent a late-stage (i.e. carbonatitic) melt, which was segregated into the ocelli by some mechanism, and which is therefore compositionally distinct from secondary calcite.

d) Wendlandt and Harrison (1979), studying the partitioning of REE between immiscible carbonate and silicate liquids, determined that at 5 kb and 20 kb, the carbonate liquid was enriched in terms of all REE relative to the silicate liquid, and that this enrichment increased with increasing atomic number. Observation (d) suggests that the Coldwell ocelli represent a similar situation (i.e. droplets of an immiscible carbonate liquid coexisting with the silicate magma from which the various lamprophyres crystallized). However, this enrichment is not observed to increase with increasing atomic number, as noted above, but rather the opposite is true. It is possible that this results from the influence of a CO_2-rich vapour phase which coexisted with the immiscible carbonate liquid phase. Such a vapour will be further enriched in terms of the LREE relative to the coexisting carbonate liquid (Wendlandt and Harrison, 1979). Alternatively, there is evidence that subsequent to their formation, the ocelli were affected by secondary

processes which introduced new components (see below). Therefore, the apparent depletion of the ocellar material in HREE may be a result of these secondary processes. Otherwise, observations (a) and (b) above are in good agreement with a liquid immiscibility origin, while the occurrence of siderite, magnesite and rhodochrosite end-members in ocellar calcite may be explained by the incorporation of these components into the carbonate liquid at the onset of its immiscibility with the mafic silicate (lamprophyric) magma.

e) As suggested by observation (f), the occurrence of silicate phases in many of the carbonate-bearing ocelli is probably a result of late-stage and secondary processes. Phases such as scapolite and fluorite may form in response to the effect of deuteric and/or secondary fluids containing Na, Cl, F and CO_2 on calcite. Formation of cancrinite, analcite, chlorite, epidote, zeolites and quartz probably involve more complex reactions which required the addition of other components including FeO, MgO and SiO_2; the exact nature of such reactions is problematical and requires further study. The thermodynamic requirements of these reactions may have been at least in part fulfilled by thermal energy related to the Centre 2, and subsequent Centre 3 magmatic activity in the Coldwell Complex.

f) The silicate ocelli occurring in specimen C560 are distinct in terms of their composition and constituent mineralogy from the more common carbonate and silicate-carbonate ocelli. Observations (g), (h) and (i) indicate that the material comprising these ocelli has a composition approaching that of the tinguaites i.e. a more evolved silicate liquid than that represented by the lamprophyres. Nevertheless, observations (a) and (b) are true for these ocelli, suggesting that they may represent an immiscible felsic silicate liquid fraction in a mafic silicate liquid host.

From the above, it is concluded that the carbonate, and the silicate-carbonate ocelli occurring in the Coldwell lamprophyres originated as a result of immiscibility between coexisting silicate and carbonate liquids. This resulted in the formation of carbonate-liquid droplets in the lamprophyric magmas. As noted by Rock (1977), such a process may in part be a reflection of the hydrous state of the lamprophyres, since increasing P_{H_2O} will expand the size of the immiscibility field inherent in alkaline melts. This would explain why the sannaites, which are distinguished by a paucity of primary hydrous minerals exhibit few ocelli relative to the other lamprophyres, in which primary hydrous

phases are more abundant (see Chapter 2, and Table 2.1). Irvine (1975) suggests that CO_2 may also be effective in promoting immiscibility, although Eby (1980) observes that this has not been adequately evaluated. The lack of HREE enrichment in the ocelli may be evidence of the presence of a CO_2 rich vapour phase during crystallization, therefore, silicate-carbonate liquid immiscibility may also reflect an increased P_{CO_2}.

The origin of the silicate ocelli occurring in specimen C560 is somewhat more problematical. As suggested above, they may reflect a felsic silicate-mafic silicate liquid immiscibility mechanism based on textural evidence, however, there is no compelling compositional evidence for this. Eby (1980) has described, and has discussed the nature of, the partitioning of various minor and trace elements between immiscible felsic silicate ocelli and mafic silicate matrix in lamprophyres from the Monteregian Hills. While the observed distributions given in Table 6.1 are in good agreement with this author's results, it is difficult to separate the effects of partitioning according to Eby's (1980) criteria from a distribution resulting from enrichments of incompatible elements and depletions of compatible elements due to evolution of the felsic liquid. It is suggested, therefore, that the felsic ocelli in

specimen C560 did not result from the spontaneous splitting of a single magma into two immiscible fractions, but rather that a felsic differentiate which approaches a tinguaite composition was combined with the lamprophyric magma by some mechanism, and the compositional distinction in concert with the prevailing physical conditions (e.g. P, T, P_{H2O}, etc.) resulted in the two liquids being immiscible. This felsic liquid may therefore represent residue from ongoing fractional crystallization of a lamprophyric magma (see Chapter 8), which was sampled by the liquid which formed C560 as it was extracted from the magma chamber. Note that such mixing of magmas by simultaneous withdrawl from different locations within a magma chamber is feasible (Spera et al, 1986).

CHAPTER 7- DYKE MARGIN-CENTRE RELATIONSHIPS

INTRODUCTION

As noted in Chapter 2, many of the Coldwell dyke rocks exhibit marginal features such as aphanitic or chilled margins, potential reactions with adjacent wall rock, and concentration of phenocrysts and ocelli into dyke centres. In order to determine the extent to which the development of such features may have altered the composition of the dykes, and to determine what compositional variations, if any, exist across their width, specimens of material from the margins and corresponding centres of examples of each type of dyke rock were analysed for major elements and trace elements including Li, Rb,Ba,Sr,Sc, Cr, Co, Y, Zr, Ta, Nb, Zr, Hf, Th and the REE. Analytical methods are detailed in Appendix A. The major element data are presented in Table 7.1, and the trace element data in Table 7.2.

TEXTURAL OBSERVATIONS

Plates 7.1 and 7.2 are photomicrographs of the centre and the margin, respectively, of a sannaite dyke which, in hand specimen, shows the development of a chilled marginal assemblage. These plates show that the marginal assemblage

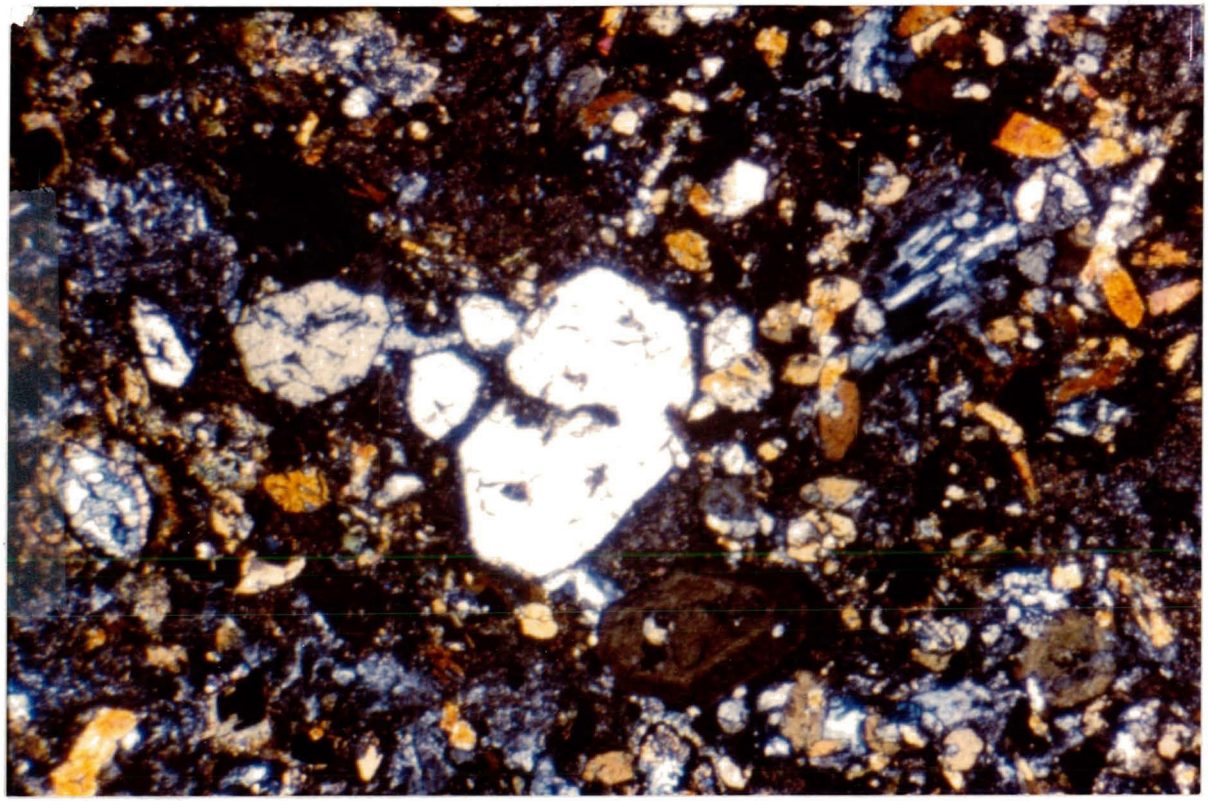

Plate 7.1 Sannaite dyke centre; note abundance of phenocrysts (fov 9.5mm; xpl).

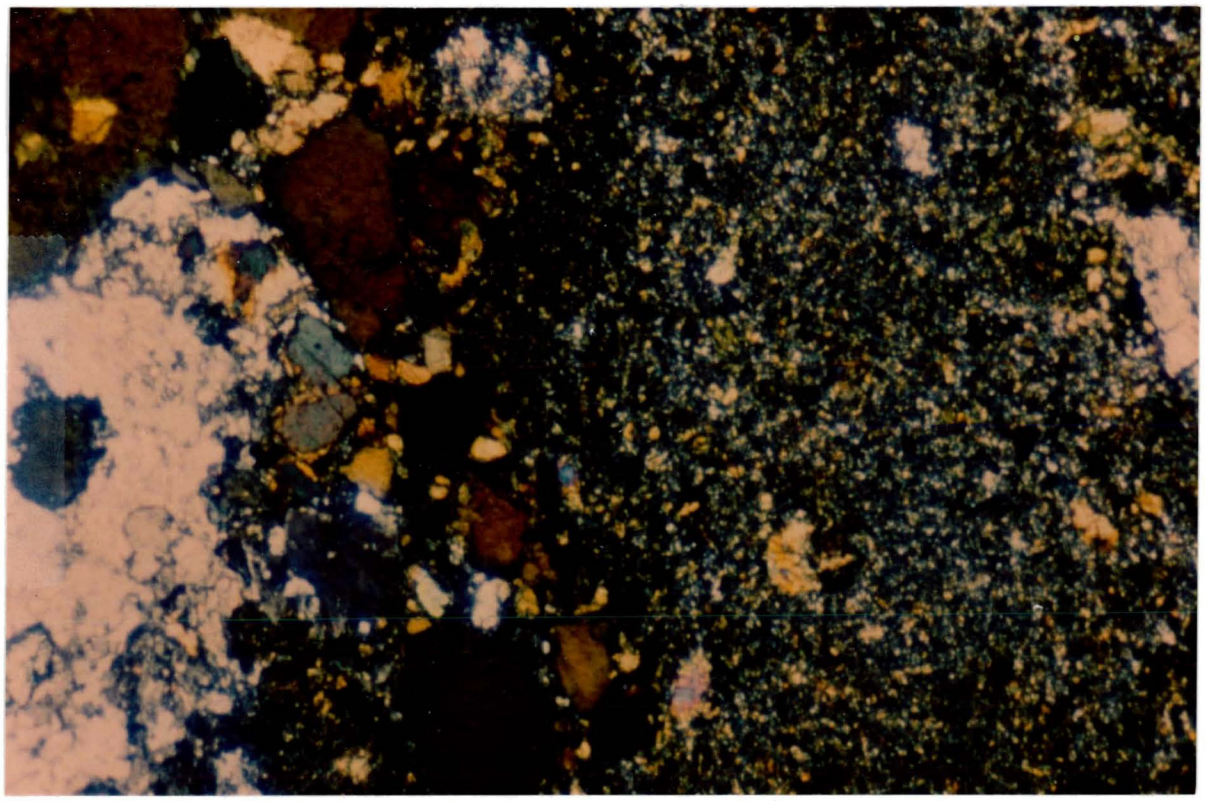

Plate 7.2 Sannaite dyke margin; note absence of phenocrysts in dyke as a result of flow differentiation (right side of photomicrograph) (fov 9.5mm; xpl).

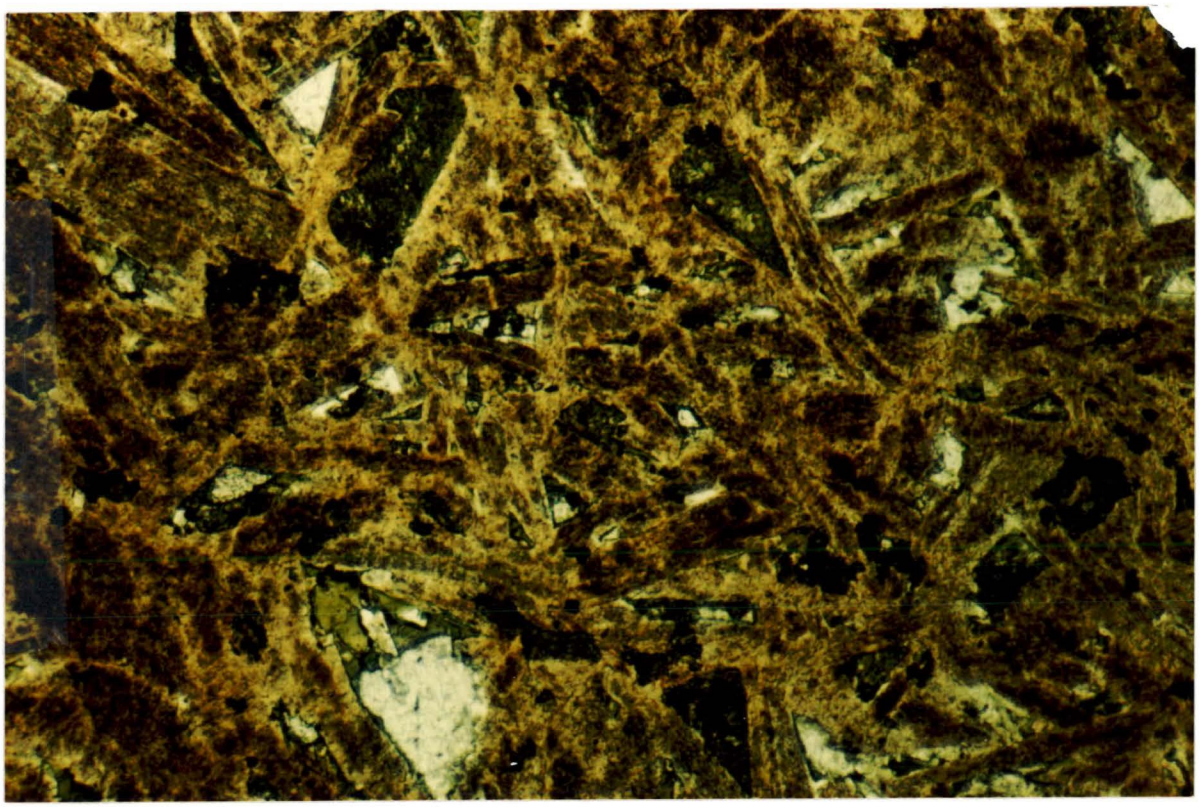

Plate 7.3 Tinguaite dyke centre; note the abundance of phenocrysts and the lack of alignment or preferred orientation suggestive of turbulent flow (fov 9.5mm; ppl).

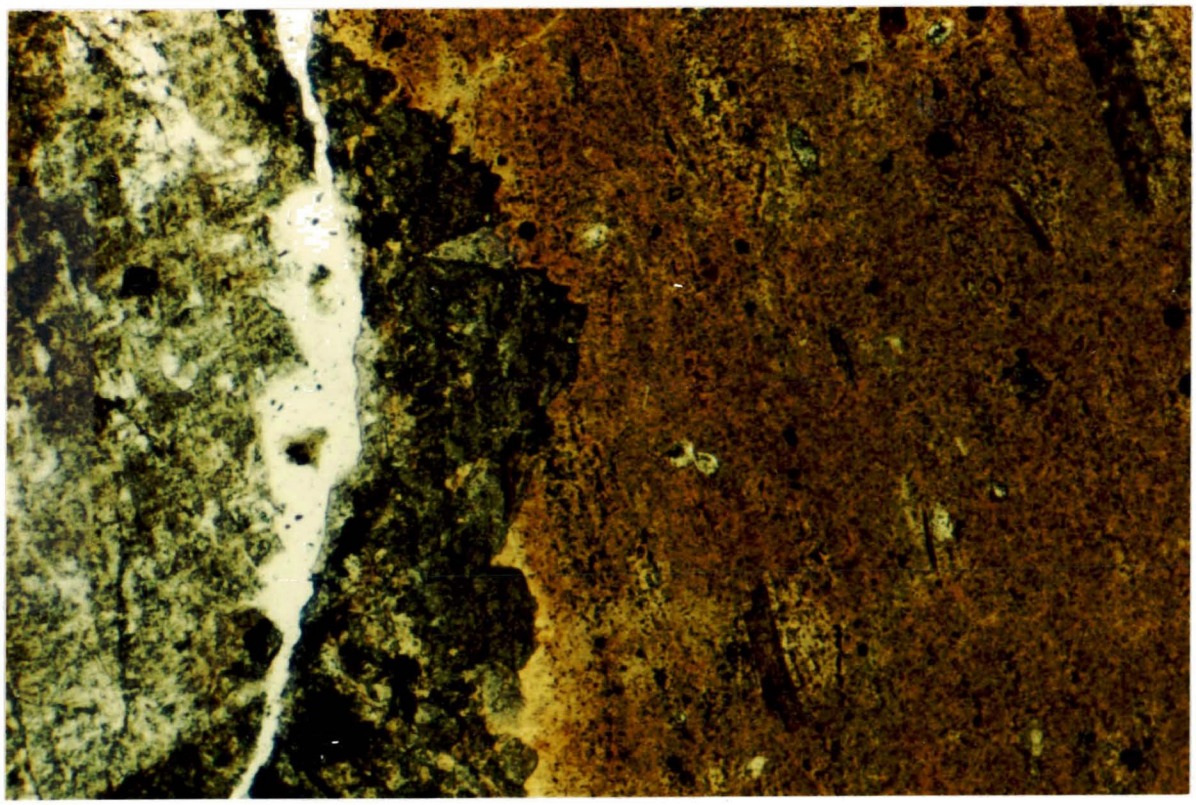

Plate 7.4 Tinguaite dyke margin; note lack of phenocrysts in dyke as a result of flow differentiation (right side of photomicrograph). Note also alignment of elongated crystals parallel to dyke margin, suggestive of laminar flow (fov 9.5mm; ppl).

is characterized by a very fine grained to glassy groundmass, and fewer smaller phenocrysts relative to the dyke centre. Most notably, in terms of its overall appearance, the aphanitic margin closely resembles a monchiquite (see Plate 2.6).

Plates 7.3 and 7.4 are photomicrographs of the centre and the margin, respectively, of a tinguaite. Although in hand specimen, this dyke does not clearly exhibit a chilled margin, these plates show that a considerable difference in grain size exists between the margin and the centre of the dyke, similar to the sannaite described above. In addition, inspection of Plates 7.3 and 7.4 gives some indication as to the mechanisms involved in dyke emplacement. In Plate 7.4, a definite alignment of elongate minerals parallel to the dyke/wall rock contact is observed, suggesting that fluid flow was laminar in this portion of the dyke. In Plate 7.3, no such alignment is observed, suggesting that flow was turbulent in the centre of the dyke.

COMPOSITIONAL OBSERVATIONS

The following observations may be made concerning the dyke margin/dyke centre compositional data:

a) In Table 7.1, the difference between the concentration of each major and minor element oxide in the margin and corresponding centre of each type of dyke rock is given. Generally, such differences are small (i.e. less than 1 weight%), however, a number of important differences are noted, as follows:

i) For the sannaite, the dyke margin is enriched in total Fe and depleted in MgO and SiO_2 relative to the dyke centre.

ii) For the quartz camptonite, the dyke margin is strongly depleted in SiO_2 and enriched in Fe_2O_3 relative to the dyke centre.

iii) For the amphibole camptonite, the dyke margin is enriched in SiO_2 and depleted in TiO_2 relative to the dyke centre.

iv) For the tinguaite, the dyke margin is enriched in K_2O relative to the dyke centre.

b) Figure 7.1 is an AFM diagram upon which the corresponding dyke margins and dyke centres are plotted. This diagram shows that in the case of the lamprophyres, dyke

Table 7.1 Major and Minor Element Chemistry of Coexisting Dyke Margins and Centres

Oxide	Sannaite Centre	Sannaite Margin	Diff	Quartz Camptonite Centre	Quartz Camptonite Margin	Diff	Ocellar Camptonite Centre	Ocellar Camptonite Margin	Diff	Monchiquite Centre	Monchiquite Margin	Diff
SiO2	47.71	44.56	3.15	55.81	47.32	8.49	46.75	47.73	-0.98	44.86	44.48	0.38
Al2O3	16.56	15.64	0.92	10.86	11.99	-1.13	12.84	13.08	-0.24	15.67	17.28	-1.61
Fe2O3	11.27	12.27	-1.00	5.45	11.54	-6.09	8.94	6.20	2.74	6.22	5.01	1.21
FeO	6.24	10.35	-4.11	6.85	6.67	0.18	7.29	6.02	1.27	4.50	7.15	-2.65
MgO	6.11	3.96	2.15	4.42	4.34	0.08	6.23	7.02	-0.79	8.75	6.65	2.10
CaO	7.20	6.22	0.98	9.64	10.32	-0.68	10.75	12.88	-2.13	10.33	10.48	-0.15
Na2O	1.12	1.02	0.10	3.21	3.54	-0.33	1.04	1.36	-0.32	2.35	1.12	1.23
K2O	2.01	2.59	-0.58	1.03	1.98	-0.95	1.53	1.44	0.09	2.44	2.56	-0.12
MnO	0.21	0.20	0.01	0.21	0.18	0.03	0.23	0.20	0.03	0.20	0.30	-0.10
TiO2	1.36	1.29	0.07	0.87	1.14	-0.27	0.92	1.01	-0.09	1.41	1.48	-0.07
P2O5	0.96	1.11	-0.15	1.06	1.43	-0.37	2.11	1.35	0.76	2.11	1.87	0.24
Total	100.75	99.21		99.41	100.45		98.63	98.29		98.84	98.38	

Table 7.1 (Cont.)

Amphibole Camptonite Centre	Amphibole Camptonite Margin	Diff	Tinguaite Centre	Tinguaite Margin	Diff
44.79	46.95	-2.16	63.20	62.77	0.43
15.73	16.45	-0.72	17.54	17.88	-0.34
6.20	7.01	-0.81	1.99	2.40	-0.41
4.87	4.15	0.72	0.44	0.37	0.07
6.65	6.04	0.61	0.32	0.11	0.21
10.33	9.48	0.85	2.84	2.44	0.40
2.05	1.12	0.93	6.09	6.52	-0.43
1.78	2.56	-0.78	4.50	6.03	-1.53
0.20	0.24	-0.04	0.17	0.10	0.07
2.75	0.80	1.95	0.36	0.38	-0.02
0.97	1.87	-0.90	0.76	0.34	0.42
96.32	96.67		98.21	99.34	

Figure 7.1 AFM diagram with data points for coexisting dyke margins and centres plotted

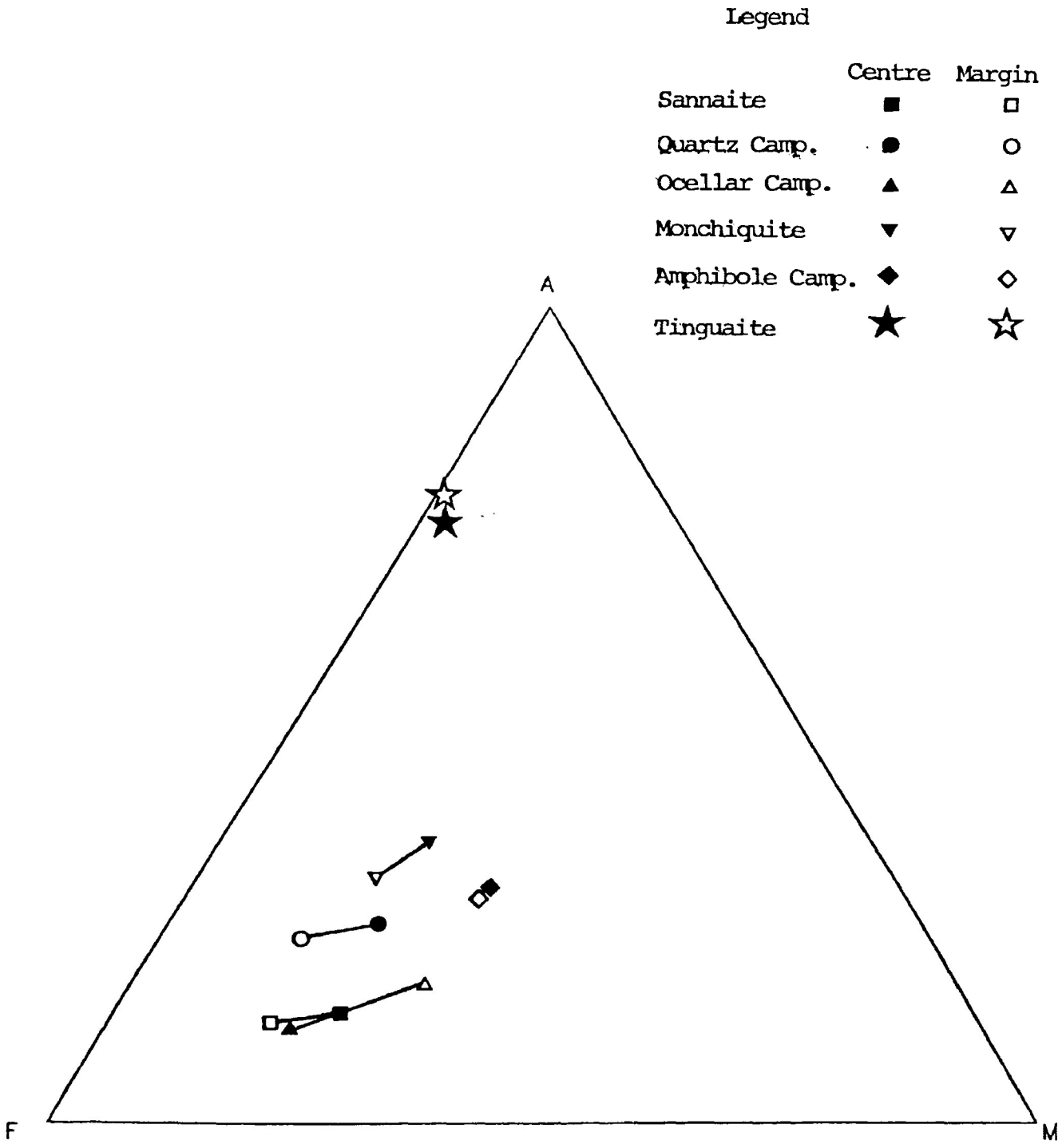

Table 7.2 Trace Element Chemistry of Coexisting Dyke Margins and Centres

Element	Sannaite Centre	Sannaite Margin	Diff	Quartz Camptonite Centre	Quartz Camptonite Margin	Diff	Ocellar Camptonite Centre	Ocellar Camptonite Margin	Diff	Monchiquite Centre	Monchiquite Margin	Diff
Rb	67	73	-6	89	84	5	76	145	-69	46	59	-13
Sr	622	717	-95	1434	1129	305	877	1120	-243	2361	2209	152
Ba	595	1325	-730	996	769	227	956	1120	-164	1168	1459	-291
Sc	41	29	12	20	17	3	15	16	-1	12	14	-2
Cr	658	325	333	68	111	-43	6	4	2	86	21	65
Co	125	136	-11	32	40	-8	71	91	-20	77	75	2
Y	33	35	-2	46	38	8	41	63	-22	26	25	1
Ta	5	8	-3	6	8	-2	4	5	-1	6	4	2
Nb	22	31	-9	33	25	8	25	26	-1	54	46	8
Hf	4	6	-2	4	6	-2	4	5	-1	5	5	0
Zr	243	319	-76	430	411	19	318	53	265	347	303	44
La	55.60	64.77	-9.17	43.88	42.02	1.86	83.55	93.85	-10.30	87.23	91.19	-3.96
Ce	128.22	94.12	34.10	90.06	88.25	1.81	163.12	174.44	-11.32	145.45	147.83	-2.38
Nd	54.21	41.03	13.18	36.74	31.33	5.41	64.59	69.06	-4.47	67.40	65.01	2.39
Sm	10.07	11.84	-1.77	10.59	10.48	0.11	11.36	13.17	-1.81	11.09	8.94	2.15
Eu	2.76	2.05	0.71	1.95	1.82	0.13	2.92	3.11	-0.19	2.75	2.82	-0.07
Tb	0.91	0.77	0.14	0.60	0.47	0.13	1.06	1.05	0.01	1.06	1.03	0.03
Yb	2.07	1.81	0.26	1.72	1.44	0.28	2.22	2.26	-0.04	2.07	2.24	-0.17
Lu	0.31	0.31	0.00	0.25	0.21	0.04	0.41	0.41	0.00	0.28	0.26	0.02
Th	6.14	13.88	-7.74	11.87	12.31	-0.44	8.00	7.27	0.73	9.45	5.32	4.13

Table 7.2 (Cont.)

Amphibole Camptonite Centre	Amphibole Camptonite Margin	Diff	Tinguaite Centre	Tinguaite Margin	Diff
284	275	9	253	388	-135
1081	968	113	116	111	5
2625	2090	535	367	388	-21
15	22	-7	0	0	0
181	335	-154	2	3	-1
150	100	50	56	67	-11
52	61	-9	64	138	-74
9	9	0	32	34	-2
108	88	20	124	116	8
5	5	0	34	29	5
371	403	-32	946	920	26
163.12	176.44	-13.32	479.69	484.80	-5.11
190.75	260.53	-69.78	686.27	648.08	38.19
71.19	94.53	-23.34	159.83	144.26	15.57
18.80	17.21	1.59	14.96	19.42	-4.46
3.07	3.81	-0.74	1.61	1.33	0.28
0.98	1.14	-0.16	1.81	1.83	-0.02
1.52	2.01	-0.49	5.29	6.96	-1.67
0.31	0.44	-0.13	0.67	1.19	-0.52
18.04	22.66	-4.62	35.95	33.23	2.72

Figure 7.2a

Chondrite Normalized REE Patterns of Dyke Margins vs Dyke Centres

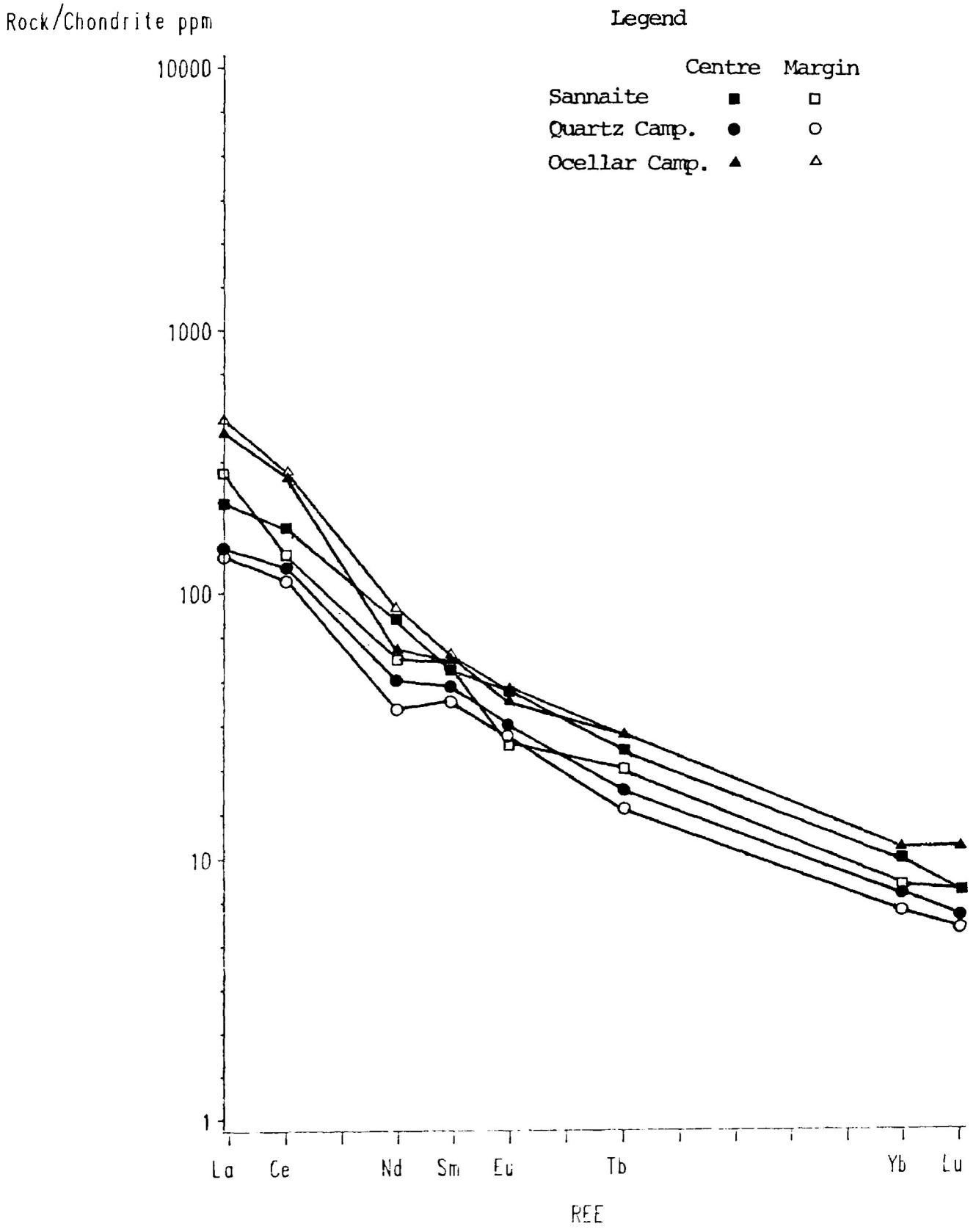

Figure 7.2b **Chondrite Normalized REE Patterns of Dyke Margins vs Dyke Centres**

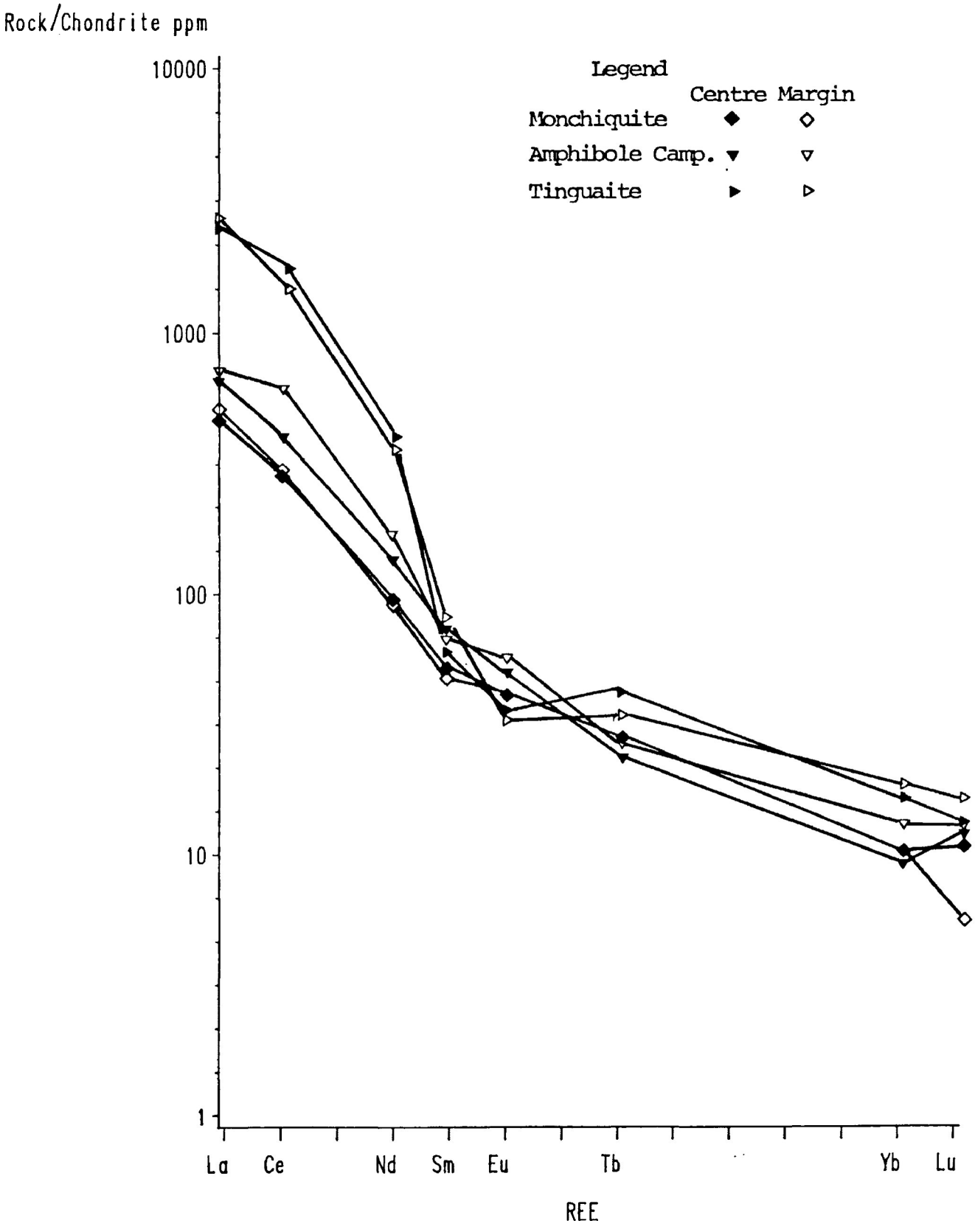

centres are apparently enriched in terms of MgO and total alkalis relative to dyke margins, although the opposite is true for the ocellar camptonite. Furthermore, in the case of the amphibole camptonite, the magnitude of this enrichment is small.

c) Table 7.2 shows that the distribution of trace elements between dyke margins and corresponding dyke centres exhibits no clear systematic pattern for any of the various types of dyke rocks.

d) Figures 7.2a and 7.2b are chondrite normalized REE plots of dyke margins and corresponding dyke centres. This diagram shows that in the case of the quartz camptonites there is a slight enrichment of all REE in dyke centres relative to dyke margins. Otherwise, there is no clear systematic difference between REE patterns for corresponding margins and centres.

CONCLUSIONS

The following conclusions may be drawn from the above observations:

a) Considerable textural differences exist between the margins and the centres of at least some of the Coldwell dyke

rocks, probably as a result of the type of flow regime operative in the dyke , and the temperature of the wall rock. According to Delaney and Pollard (1982), if a basic magma is flowing through a conduit in the host rock by laminar flow, then the contact temperature will be the median of the dyke magma temperature and the host rock temperature as a result of the reduced efficiency of heat transfer from the magma to the host rock. The tendency will be, therefore, for the dyke to develop a chilled margin, unless the host rock temperature is elevated. In the case of the Coldwell dyke rocks, there is, as noted previously, compelling evidence for the operation of laminar flow at the margins of the conduits of at least some of the dykes; these dykes also exhibit chilled margins. In the cases of dykes in which chilled margins are not well developed, then either laminar flow did not occur, probably as a result of a higher flow rate or lower viscosity, causing turbulent flow to dominate (Kille et al, 1986), or the host rock was at an elevated temperature, presumably as a result of its own recent intrusion (i.e. during the Centre 2 magmatic activity). The exact explantion is problematical, and will require further study.

b) The significant compositional differences observed can be explained by variations in phenocryst abundances across the various dykes, particularily in the case of the lamprophyres. Specifically:

i) The enrichment of the sannaite dyke centre in terms of SiO_2 and MgO is in good agreement with the observed concentration of clinopyroxene phenocrysts in the centre;

ii) The strong enrichment of the quartz camptonite dyke centre in terms of SiO_2 is in good agreement with the observed concentration of quartz phenocrysts in the centre; and

iii) The enrichment of the amphibole camptonite dyke centre in terms of TiO_2, and its depletion in terms of SiO_2, is in good agreement with the observed concentration of amphibole phenocrysts in the centre.

This form of flow differentiation is similar to that observed by Asquith (1973) in tertiary camptonite dykes in the Sacramento Mountains, New Mexico. In this case, however, the variable flow rates occur not within dykes but between dykes, resulting in a general enrichment of some dykes in terms of mafic phenocrysts; this enrichment is reflected in dyke compositions. Beyond this, however, flow effects apparently were not a significant mechanism for causing compositional differentiation in the various dyke rocks.

CHAPTER 8- PETROGENESIS

INTRODUCTION

The following sections describe the petrogenetic model developed for the Coldwell dyke rocks based on conclusions derived from mineralogical and petrographic observations together with the major, minor and trace element chemistry studies described in the preceding chapters.

FACTORS CONSTRAINING PETROGENETIC MODELS

The salient factors which will generally constrain the petrogenetic model developed to describe the evolution of the Coldwell dyke rocks are summarized below:

a) The various dyke rocks are volumetrically minor in terms of the Coldwell complex as a whole (see Chapter 1), so they, by themselves, are not likely to represent a large, distinct magmatic event, but are more likely an expression of a portion of such an event. This suggests an association with one of the magmatic centres i.e. Centres 1 or 2, since all of these dykes are cross-cut by Centre 3 material (see Chapter 1) (i.e. a derivation from the magmas which formed that centre).

b) With the exception of the quartz camptonites (see below), the dyke rocks represent a magmatic series, hereafter referred to as the Main Series, the most primitive of which are probably the sannaites, and the most evolved of which are the tinguaites (see Chapters 3 and 5). The dominant petrogenetic mechanism involved in the evolution of this series was fractional crystallization of olivine, small amounts of spinel (dominantly spinel ss and magnesiochromite), diopsidic to sahlitic (and acmitic) clinopyroxene in the case of the lamprophyres; pargasitic and hastingsitic, and, to a lesser extent kaersutitic hornblende in the case of all of the lamprophyres excepting the sannaites; and alkali feldspar in the case of the tinguaites (see Chapters 4 and 5). Note that the sannaites are not themselves primitive rocks, based on their Mg, Cr and Ni contents, and are therefore derived from some relatively less evolved source liquid (see Chapter 5).

c) Physico-chemical conditions in the magma varied during the evolution of the Main Series. Specifically:

i) A decrease in P_{total}, probably representative of an eruption from a deep-seated magma chamber to an intermediate-depth magma chamber, is recorded in the mineral

chemistry of the clinopyroxenes of the sannaites relative to those of the other Main Series lamprophyres.

ii) A subsequent decrease in $P_{tot_{s1}}$ is indicated by changes in the composition of zones in, and resorption of the higher-pressure cores of, the clinopyroxenes in the Main Series camptonites and monchiquites, suggesting a second eruption to a shallow magma chamber (see Chapter 3).

iii) An increase in P_{H_2O} following the crystallization of the sannaites is indicated by the abundance of primary hydrous mineralogy (i.e. amphibole, and to a lesser extent biotite) in the other Main Series lamprophyres as opposed to this rock type (see Chapter 2). Minor fluctuations in P_{H_2O} are reflected in minor zoning in the amphiboles (see Chapter 3).

iv) A continued increase in P_{H_2O}, or a subsequent increase following a decrease resulting from crystallization of the above hydrous phases, may be responsible for the de-polymerization of the melt and therefore in part responsible for the development of negative Eu anomalies in some of the tinguaites (see Chapter 5, and below).

v) P_{CO_2} was high throughout the evolution of the

Main Series (i.e. in the source region, and afterwards), as indicated by LREE enrichment in all of the dyke rocks (see Chapter 5), lack of HREE enrichment in the immiscible carbonate liquid represented by the carbonate-bearing ocelli (see Chapter 5), and possibly by the presence of the ocelli, and the compositional miscibility gap they represent (see Chapter 6).

vi) The Fe/Mg ratio of the magma increased during the evolution of the Main Series, as indicated by mineral zoning patterns, probably as a result of the ongoing crystallization of Mg-rich phases.

e) The magmas of the Main Series were periodically replenished by more primitive (i.e. more Mg-rich) magmas, presumably from greater depth, as evidenced by reversed zoning in clinopyroxene phenocrysts (see Chapter 4).

f) The ocellar and amphibole camptonites, and the monchiquites, are distinguished primarily on the basis of modal minerlogy and texture (see Chapter 2), and not chemistry (see Chapters 3 and 5), therefore, these types of dyke rocks may represent similar magmas which have been emplaced under different intrusive conditions.

g) The development of negative Eu anomalies in some of the tinguaites may be related to increased P_{H_2O} in those rocks; changes in the extent of alkali feldspar fractionation, temperature and f_{O_2} may be involved as well.

h) The quartz camptonites are distinguished from the lamprophyres of the Main Series, and therefore form a distinct series, hereafter referred to as the Quartz Series, on the basis of the following factors:

i) They apparently intrude only Centre 1 rocks, while the other types of dyke rocks are observed to intrude both Centre 1 and Centre 2 material (see Chapter 1);

ii) They are distinct from the other types of lamprophyres on the basis of all major and minor oxide contents (particularily SiO_2, but with the exception of MnO and P_2O_5) (see Chapter 3);

iii) They are distinct from the other lamprophyres on the basis of mineralogy, particularily in terms of the presence of primary quartz as a phenocryst phase, and in terms of clinopyroxene composition (i.e. uniformly augitic, as opposed to a range from diopsidic to sahlitic and acmitic

(in normally zoned crystals) as in the case of the other lamprophyres) (see Chapter 4); and

iv) They are distinct from the other lamprophyres on the basis of some trace element abundances, particularily the LREE, in which they are relatively depleted, and on the basis of the behaviour of some trace elements, such as Ce relative to La (see Chapter 5).

The above observations form the basis for the petrogenetic model described in the following section.

PROPOSED PETROGENETIC MODEL FOR THE COLDWELL DYKE ROCKS

Figures 8.1 and 8.2 are schematic diagrams depicting the sequence of events which define the evolution of the Main Series and the Quartz Series dyke rocks respectively. The following sections describe each petrogenetic series detail.

The Main Series

a) As noted in Figure 8.1, the proposed composition of the source liquid for the Main Series rocks is that of an alkali olivine basalt. This appears reasonable since:

Key to Figures 8.1 and 8.2

Abbreviations

Source Liquids

Alk Ol Basalt (C)- Silica-contaminated Alkali Olivine Basalt
Alk Ol Basalt- Alkaline Olivine Basalt
Thoeliite- Quartz Thoeliite

Minerals

Ol- Olivine
Sp- Spinel (Spinel ss-magnesiochromite)
HCpx- High P (Low Ti) Clinopyroxene
MCpx- Medium P (Medium Ti) Clinopyroxene
LCpx- Low P (High Ti) Clinopyroxene
Hble- Hastingsitic-Pargasitic-Kaersutitic Hornblende
Kspar- Alkali Feldspar
Amph- Amphibole
Qtz- Quartz
Aug- Augite

Others

Inc P_{H2O}- Increasing P_{H2O}
Dec P_{H2O}- Decreasing P_{H2O}
Var P_{H2O}·F_{O2}·Com- Poorly-understood Variation of P_{H2O}·F_{O2} and Liquid Composition and Structure

Symbols

Source Liquid

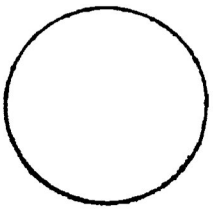

Crystallizing Phases

Resorbing Phases

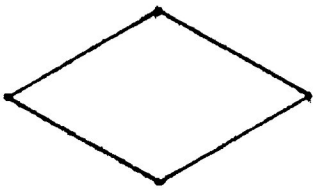

Physio-Chemical Change

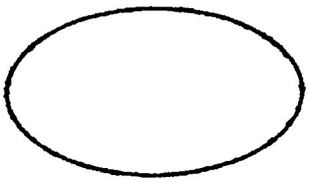

Final Assemblage

Next Event

Eruption

Figure 8.1 Schematic diagram depicting the evolution of the Main Series (see text)

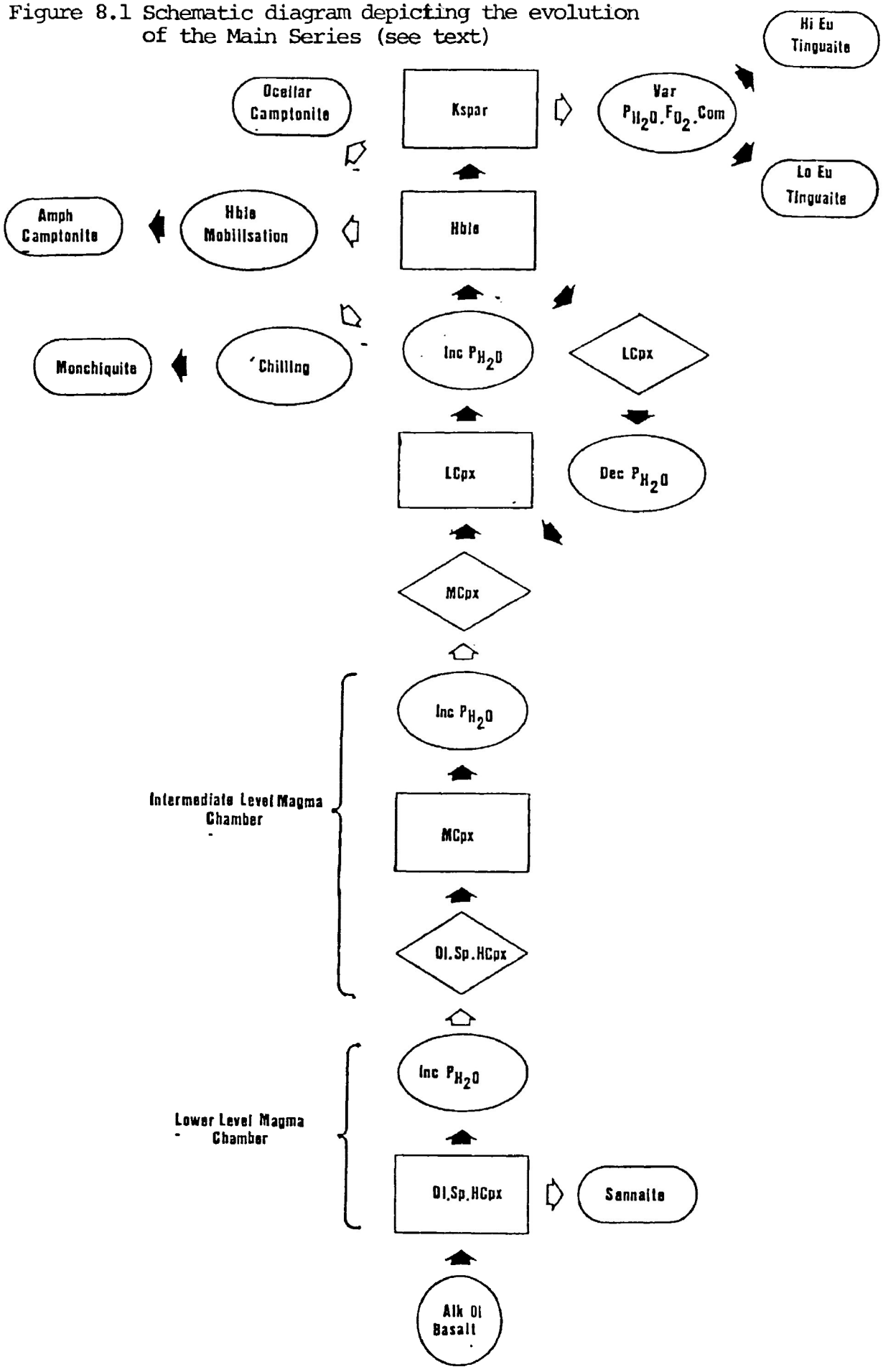

i) It is consistent with the observed compositions of the Main Series lamprophyres, since, as previously noted these themselves approximate alkali basaltic compositions (see Chapter 3), which have undergone some degree of evolution (see Chapter 5);

ii) It is consistent with the observed silica undersaturation observed throughout the Main Series rocks;

iii) The Main Series rocks are associated with the Centre 2 magmatic activity (see Chapter 1), this is also consistent with the observed silica undersaturation observed in the Centre 2 rocks; and

iv) The occurence of alkali olivine basalt at depth in the complex is reasonable considering the model of the general geology and structure of the complex developed by Mitchell et al (1983) (i.e. the occurrence of a large volume of ultramafic-mafic material underlying the complex; see Chapter 1).

The proposed alkali olivine basalt parent of the Main Series rocks probably represents a late-stage liquid associated with the terminal stages of the Centre 2 magmatic activity, and which has accumulated in the magmatic

"plumbing-system", since these dyke rocks commonly cross-cut the major intrusive units of that magmatic centre, but not those of Centre 3 (Chapter 1). This is a similar model to that suggested for the parental liquids of the lamprophyres of Ubekendt Ejland by Clarke et al (1983).

The source regions probably interacted with a CO_2 rich fluid, which caused LREE enrichment; this resulted in the generally LREE enriched REE distribution patterns observed throughout the Main Series rocks. This is consistent with the suggestion of Wendlandt and Harrison (1979) that metasomatism of a source region by a fluid carrying alkaline components, which is a precursor to alkaline magmatism such as that represented by the Coldwell complex, may also result in LREE enrichment if this fluid is rich in CO_2.

b) The alkali olivine basalt parental liquid underwent fractionation of high-Mg olivine, low-Ti diopside and a spinel phase (spinel ss-magnesiochromite); the relative abundance of these phases is unknown, although the spinel phase, which occurs only as small inclusions in olivine (see Chapters 2 and 3), probably did not crystallize in abundance. This fractionation occurred in a deep-seated magma chamber (i.e. high P environment, as indicated by the low Ti content of the clinopyroxene) which was probably part of the

"plumbing system" associated with the Centre 2 magmatism. Note that as these phases crystallized, the Fe/Mg ratio of the magma increased, as reflected by the increased Fe end-member contents in the outer zones of normally zoned olivine and clinopyroxene phenocrysts. Reversed zoning suggests that at least one episode of replenishment of the magma chamber by a more primitive (i.e. more Mg-rich) liquid (possibly more of the parental alkali olivine basalt), occurred. Crystallization of these anhydrous phases was probably accompanied by an increase in P_{H_2O}, however, either this increase was insufficient to promote, or physico-chemical conditions (e.g. P_{total}, T) were such that they prevented, the crystallization of significant volumes of hydrous phases (see below). The increase in P_{H_2O} may, however, have driven the eruption of quantities of the residual liquid plus cumulus phases from the magma chamber; this material was subsequently emplaced as sannaite dykes, the residual liquid crystallizing to a final assemblage in which alkali feldspar is the predominant feldspar phase. That this eruption was quite energetic is indicated by the abundance of large phenocrysts in these dykes (see Chapter 2 and Table 2.1); this suggests that the increase in P_{H_2O} was extensive, and that it was limitations imposed by the physio-chemical conditions in the magma that inhibited the crystallization of hydrous phases. Another portion of the

residual liquid plus cumulus crystals was passed on to a intermediate depth magma chamber.

c) That an intermediate-depth magma chamber was involved in the evolution of the Main Series magmas is suggested by the higher Ti contents in the cores of clinopyroxenes occurring in the camptonites and monchiquites than those of the sannaitic clinopyroxenes; the former clinopyroxenes thus crystallized at a lower P_{total} than the latter. Eruption of liquid from the lower-level chamber described in (b) above led to the resorption of the higher P cumulus phases, as indicated by the presence of resorbed olivine phenocrysts in the camptonites and monchiquites. Again, crystallization of the higher Ti (i.e. intermediate P) clinopyroxene was accompanied by an increase in P_{H_2O} which eventually resulted in the eruption of a quantity of the residual liquid plus phenocrysts from this chamber to shallow magma chamber.

As an alternative to the intermediate level chamber, as suggested by Scott (1980), if $P_{H_2O} > P_{load}$, such as prior to an eruption, then the latter clinopyroxenes may have crystallized under such high P_{total} conditions, which were not relieved by formation of hydrous phases due to unfavourable physio-chemical conditions. Following eruption, and consequent decrease in P_{H_2O} (and therefore P_{total}), the

former, higher Ti (i.e. intermediate P) clinopyroxenes crystallized, and the earlier formed phases underwent resorption. However, it is doubtful as to whether P_{H_2O} could remain high enough to promote such conditions for the sustained period of time represented by the large size of the sannaitic clinopyroxene phenocrysts, without being reduced by eruptions, unless new water were periodically added to the magma chamber. Residual liquid plus phenocrysts from the lower-level chamber were then erupted directly to the upper level chamber, so that no intermediate-level chamber is required.

d) After being passed on to the upper-level chamber, the intermediate P clinopyroxene underwent resorption, as evidenced by the rounded and embayed cores observed in clinopyroxenes in the camptonites and monchiquites. Crystallization of a low P (i.e. highest Ti content) clinopyroxene was promoted. Note that this low P clinopyroxene was also more Fe and Na rich than its higher P predecessors, as a result of changing magma composition. Crystallization of this low P clinopyroxene was again accompanied by an increase in P_{H_2O}. However, at this stage in the evolution of Main Series magma, physio-chemical conditions were such that the crystallization of hastingsitic to pargasitic, and, to a lesser extent, kaersutitic

hornblende was possible. Upon attaining a suitable P_{H2O}, as suggested by Scott (1980), such hornblende began to crystallize, possibly accompanied by resorption of the clinopyroxene. Hornblende crystallization continued until P_{H2O} was reduced below some critical value, at which point crystallization of low P clinopyroxene was re-initiated, and hornblende resorption may have ensued. As noted by Scott (1980), this cycle could repeat one or more times, however, there is little evidence to suggest that it was repeated more than once (see Chapter 3). Again, although the exact relative abundances of the two phases is unknown, there is evidence to suggest that greater quantities of hornblende crystallized:

i) The strong enrichment of the tinguaites in terms of silica relative to the lamprophyres (see below) suggests more extensive crystallization of relatively silica-deficient amphibole as opposed to more silica-rich clinopyroxene; and

ii) The presence of dykes rich in modal amphibole (i.e. amphibole camptonite), and the absence of dykes similarily rich in modal clinopyroxene, at this stage in the evolution of the Main Series, indicates the relative abundance of amphibole in the upper level magma chambber.

At some point, residual liquid plus cumulus phases were erupted from the chamber, under three distinct sets of conditions:

i) Eruption of approximately equal amounts of cumulus clinopyroxene and hornblende, (or some abundance of clinopyroxene relative to hornblende) plus residual liquid, accompanied by slow cooling during emplacement, resulted in the formation of the ocellar camptonites.

ii) Eruption of material as described in (i) above, accompanied by rapid cooling (i.e. chilling) during emplacement, resulted in the formation of the monchiquites. Such chilling will probably be the result of some combination of lower temperatures in the host rock, and the predominance of laminar flow over turbulent flow, as described in Chapter 7. Note that these conditions of formation for the monchiquites are in good agreement with those proposed by Rock (1977) i.e. abundant fractionation of amphibole followed by extensive chilling.

iii) Eruption of abundant cumulus hornblende relative to clinopyroxene (perhaps following accumulation of hornblende in the magma chamber resulting from an increase in P_{H_2O}; see Figure 8.1), accompanied by slow cooling during

emplacement, resulted in the formation of the amphibole camptonites.

Therefore, the above three types of lamprophyres are drawn from a common source, and are emplaced under different conditions. This is consistent with the observed compositional similarity between these rocks (see Chapter 3). At this point, carbonate ocelli, representing an immiscible carbonate liquid (see Chapter 6) were present in the erupted liquids as well, although the moment at which this immiscibility set in is not clear.

e) Continued fractionation of amphibole, and lesser amounts of clinopyroxene (see above), changes the composition of the residual liquid towards that of a tinguaite. As observed in Chapter 6, there is evidence to suggest that liquid approaching a tinguaite composition was present in the magma chamber, and was available to be mixed with the various camptonites and monchiquites which were being erupted and emplaced (i.e. as ocelli with compositions approaching those of the tinguaites occurring in some lamprophyres). Therefore, the magma chamber may, at this point, have been compositionally stratified, presumbably with the more felsic residual liquids concentrated towards the top of the chamber (Spera et al, 1986). When conditions became suitable, alkali

feldspar (i.e. anorthoclase) began to crystallize and fractionate from this residual liquid. Physico-chemical conditions (i.e. particularily P_{H_2O}, f_{O_2} and melt structure), varied at this time as well, albeit in some undetermined manner, and the result of this, in combination with variable degrees of anorthoclase fractionation, was the development of two distinct types of tinguaite magma i.e. those with negative Eu contents and low Sr contents, and those with no Eu anomalies and higher Sr contents.

The Quartz Series

a) Two possible compositions for the parental liquid of the Quartz Series are proposed. The first, that of a quartz thoeliite, is suggested by the following:

i) It is approximately consistent with the observed compositions of the quartz camptonites;

ii) It is consistent with the observed silica over-saturation observed throughout the Quartz Series; and

iii) Since the quartz camptonites are apparently associated with the Centre 1 magmatic activity (i.e. they are cross-cut by Centre 2 rocks; see Chapter 1), a quartz

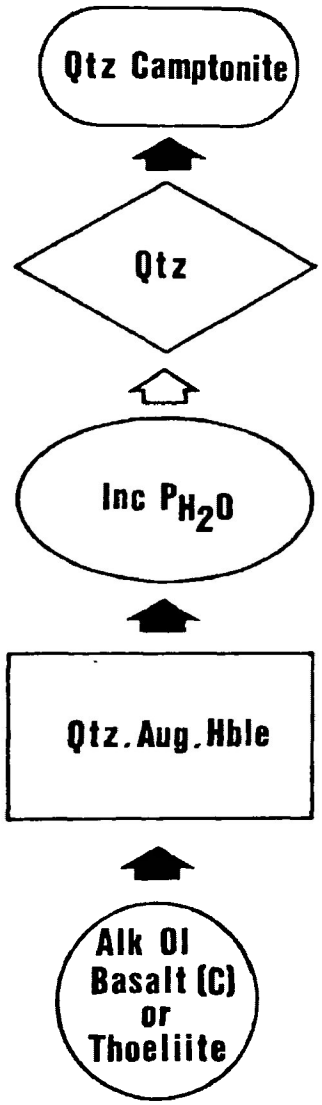

Figure 8.2 Schematic diagram depicting the evolution of the Quartz Series (see text)

thoeliite parent is consistent with the silica saturation / silica over-saturation observed in the Centre 1 gabbros and syenites.

The second possible source composition proposed is that of an alkali olivine basalt similar to that which is parental to the Main Series (see the preceding section dealing with those rocks), which has been contaminated with silica-rich material (note that this does not necessarily suggest inclusion of quartz grains, but rather incorporation of material which increases the silica content of the liquid). Although no direct evidence for such a contamination mechanism exists, it is possible that the Coldwell magmatism involved assimilation of lower crustal material which was relatively rich in terms of silica (Mitchell, pers. comm., 1987); isotopic studies of the rock involved may provide more insight into this. Note, however, that several points argue against such a common parental liquid for the Main Series and Quartz Series:

i) Point (iii) above;

ii) The different REE distribution pattern (i.e. MREE depleted) observed in the quartz camptonites as opposed to that observed throughout the Main Series rocks (see

Chapter 5), although this may only indicate a different evolutionary history; and

iii) The apparently lower Ca/Ca+Mg ratio of the Quartz Series magma, as reflected in the composition of clinopyroxenes in these rocks.

Either parental liquid (i.e. quartz thoeliite or alkali olivine basalt) is consistent with the structural/lithological model for the Coldwell complex proposed by Mitchell et al (1983), as described previously.

b) Quartz crystallized from the parental liquid, probably in a deep-seated magma chamber which was part of the Centre 1 "plumbing-system"; such a high pressure environment is necessary for the precipitation of primary quartz from a basic magma, as suggested by Nicholls et al (1973) (see Chapter 3), although a high degree of over-saturation of the magma with respect to silica (a function of the source composition or contamination; see (a) above) may relieve the pressure requirements to some degree. Augite, and small amounts of hornblende were also fractionated from the magma. Note that the paucity of amphibole in the quartz camptonites relative to the Main Series lamprophyres probably reflects a relatively low P_{H2O} in the former magma, which may be a

function of the composition of the parental magma, or may represent less extensive addition of water from external sources during the evolution of the magma.

c) A portion of the residual liquid plus cumulus crystals was erupted from the chamber. Following this eruption, physico-chemical conditions in the magma changed such that the quartz crystals were no longer in chemical equilibrium with the coexisting magma, resulting in resorption and formation of reaction rims around the quartz crystals as described in Chapter 3. The exact nature of these physico-chemical changes is problematical, but probably involves, at least in part, a decrease in P as the magma plus cumulus phases was emplaced at relatively shallow depths; geobarometric and geothermometric studies, which are beyond the scope of the present work, may more clearly define this. Another possibility (which may operate in conjunction with changes in P) is that the magma was contaminated with alkaline liquids which operated to reduce the silica activity in the magma to the point at which the quartz was no longer an equilibrium phase (Mitchell, personal communication). Such liquids are available in abundance during the emplacement of an alkaline intrusion (Rock, 1977). With quartz no longer being an equilibrium phase, the residual liquid crystallized upon emplacement to form a

silica-undersaturated assemblage (i.e. containing primary nepheline; see Chapters 2 and 3).

Late-Stage and Secondary Processes

Subsequent to emplacement, all dykes were subject to a variety of processes related to late-stage (i.e. deuteric) and secondary fluids, primarily involving replacement of primary phases (e.g. development of chlorite, uralite, serpentine, epidote, etc.) and deposition of secondary phases (e.g. haematite, calcite, zeolites, etc.), and to sub-solidus recrystallization (e.g. formation of scapolite from ocellar calcite). Details of the mineralogy of such phases are given in Chapter 3, and Chapter 6 in the case of ocellar minerals. Note that while the extent of such processes varies widely amongst the various dyke rocks, generally, alteration and physical decomposition are quite advanced.

The above model is a qualitative scheme to account for the observed features and chemistry of the various Coldwell dyke rocks. In terms of quantitative modelling, it may be possible to employ the method of O'Hara (1977), which describes in a quantitative sense the geochemical evolution of a basic magma during fractional crystallization of a periodically refilled magma chamber. Note that, in the case

of the Main Series, several such chambers would be modelled, taking into account the effects of changing P_{total} and P_{H_2O} on the model (note that O'Hara's (1977) method does not include specific terms for these parameters, however, it may be possible to incorporate such changes in the values of the distribution coefficients for the elements being modelled). While such modelling is beyond the scope of the present thesis, it may be a useful consideration for future work.

Significance of the Petrogenetic Model

Examination of literature dealing with the genesis of alkaline lamprophyres and related rocks shows that, depending upon specific petrological and geochemical characteristics of an occurrence, a variety of petrogenetic processes may be invoked to explain the origin of these rocks. For example:

a) Malpas et al (1986) propose that partial melting of a LREE-enriched upper mantle material gave rise to sannaite, aillikite and carbonatite dykes in the Aillik Bay dyke swarm. Eby (1985) suggests that partial melting of upper mantle garnet and spinel lherzolite produced the parental liquids of lamprophyres occurring in the Monteregian Hills and White Mountains igneous provinces, Quebec, although other genetic mechanisms were involved as well (see below);

b) Eby (1985) suggests that fractional crystallization of olivine, clinopyroxene and amphibole from the parental magma described above was involved in the formation of camptonites and monchiquites in the Monteregian Hills and White Mountains igneous provinces. Strong and Harris (1974), and Clarke et al (1983) postulate that fractional crystallization was the dominant genetic mechanism involved in the formation of lamprophyres in Central Newfoundland and Ubekendt Ejland, Greenland, respectively;

c) Rock (1979) proposes that mixing and hybridisation processes explain the genesis of the type monchiquites and associated lamprophyre dykes in the Serra de Monchique alkaline igneous province. Specifically, olivine-bearing monchiquites result from the incorporation of olivine into a foyaitic magma, while olivine-free monchiquites represent more complex mixing of nepheline syenite and theralite magmas; and

d) Maxey (1976) believes that liquid immiscibility between melteigite and carbonatite, and possibly syenite magmas are fundamental to the formation of all of the rocks of the Beemerville carbonatite-alkaline igneous complex, including the associated lamprophyres. In this case, several other processes, including fractional crystallization and

volatile enrichment, played subordinate roles as well. Similarily, Strong and Harris (1974) also suggest that liquid immiscibility played an important, albeit subordinate role in the origin of Central Newfoundland lamprophyres.

As described in the preceding sections, an origin by fractional crystallization best explains the observed characteristics of the Coldwell lamprophyres, although liquid immiscibility probably played a subordinate role, primarily being responsible for the development of ocelli. Note the models proposed by Eby (1985), Strong and Harris (1974) and Clarke et al (1983) are all quite similar to this model in a general sense (although details of the evolutionary schemes differ), in that abundant fractionation of mafic phases (e.g. clinopyroxene, olivine and amphibole) is an important or dominant genetic mechanism. Furthermore, in each of these occurrences, and in the Coldwell Complex, alkaline lamprophyre dykes also appear to post-date the main igneous activity in the region (determined from radiometric or structural evidence), which was itself apparently related to rifting of the continental lithosphere.

The above observation has significant implications in terms of understanding the nature and origin of alkaline lamprophyres and related rocks. Specifically, the Coldwell

occurrence offers further evidence that such rocks, at least in part, represent the emplacement of late-stage or residual magmas, following major rift-related alkaline igneous episodes, which have evolved by fractional crystallization of mafic phases under volatile-enriched conditions; this volatile-enrichment probably is a result of the accumulation of such components during the main igneous activity, and is responsible for the occurrence of abundant hydrous primary minerals, and the promotion of liquid immiscibility (i.e. ocelli), both of which features are characteristic of alkaline lamprophyres (Rock, 1977).

CHAPTER 9 CONCLUSIONS AND RECOMMENDATIONS FOR FURTHER WORK

The following sections, based on the information presented in this thesis, summarize the conclusions concerning the dyke rocks occurring the in Coldwell complex and present suggestions for further work involving these rocks.

Conclusions

a) Five types of mafic (i.e. lamprophyre) and one type of felsic (i.e. tinguaite) alkaline dyke rock are recognized as determined from field and petrographic observation. In approximate order of abundance these are:

i) ocellar camptonites
ii) analcite tinguaites
iii) sannaites
iv) quartz camptonites
v) amphibole camptonites
vi) monchiquites

Such a classification scheme is based primarily upon mineralogical and petrographic criteria (Rock, 1977) for the lamprophyres (i.e. camptonite, sannaite and monchiquite).

Note that classification based upon chemical criteria, using cluster analysis and multiple discriminant analysis of the whole rock major and minor element data, can effectively distinguish the quartz camptonites from the other types of lamprophyres, but is incapable of reliably separating the latter rock types.

b) Evidence from major and trace element data suggests that the ocellar and amphibole camptonites, the sannaites, the monchiquites and the analcite tinguaites form a magmatic series (the Main Series), with the tinguaites being the most evolved, and the sannaites possibly being the most primitive, members of that series. The quartz camptonites form a distinct group (the Quartz Series).

c) Consideration of trace element abundances (i.e. Ni and Cr) indicates that none of the Main Series lamprophyres represent primitive liquids. They have therefore undergone evolution from a volatile and LREE-enriched alkali olivine basalt parent probably related to the terminal stages of the Centre 2 magmatic activity according to the fractional crystallization model detailed in Chapter 8.

d) The quartz camptonites of the Quartz Series are similarily evolved rocks, being derived from a thoeliitic

parent related to the Centre 1 magmatic activity by the fractional crystallization model described in Chapter 8. Alternatively, a quartz-contaminated Centre 2 alkali olivine basalt parent may be involved in this model.

e) The above petrogenetic model is significant in that it implies that alkaline dyke rocks in similar occurrences (i.e. associated with alkaline intrusive complexes) may have similar origins (e.g. the lamprophyre dykes of Ubekendt Ejland; Clarke et al, 1983).

f) Carbonate ocelli occurring in all of the various lamprophyres are a result of immiscibility of a carbonate liquid in the silicate liquids from which these rocks crystallized. CO_2 vapour involved in this carbonate/silicate immiscibility may also be responsible for the LREE-enriched character of the dyke rocks.

Recommendations for Further Work

Additional work to characterize further the alkaline dyke rocks which are the subject of this thesis is suggested in the following sections.

a) Numeric modelling of the petrogenetic scheme

presented in Chapter 8 using various major, minor and trace element data would test the validity of the model and establish the possible extent of fractionation and abundance of various fractionating phases, as well as defining possible parental compositions.

b) Application of geothermometric and geobarometric methods to selected mineralogical data (e.g. clinopyroxene compositions) would to some extent define possible P-T conditions for the formation of the various rock types.

c) More detailed investigation of the structure and composition of the quartz phenocrysts and related phases occurring in the quartz camptonites may allow determination of the origin of this material. Isotopic studies of these rocks may assist in confirming or denying the inclusion of a crustal or country-rock component.

d) Detailed investigation of the mineralogy of each group of dyke rocks is desirable.

LIST OF REFERENCES

Ahrens L.H., 1953. A Fundamental law of geochemistry. Nature **172**, pg. 1148.

Ahrens L.H., 1954. The lognormal distribution of elements. Geochim. Cosmochim. Acta **5**, pp. 49-73.

Ahrens L.H., 1954. The lognormal distribution of elements (2). Geochim. Cosmochim. Acta **5**, pp. 121-131.

Allegre, C.J., Treuil, M., Minster, J.F., Minster, B. and Albarede, F., 1977. Systematic use of trace elements in igneous processes. Part I: Fractional crystallization processes in volcanic suites". Contrib. Mineral. Petrol. **64**, pp. 57-75.

Arth, J.G., 1976. Behaviour of trace elements during magmatic processes- A summary of theoretical models and their applications. J. Research U.S. Geological Survey **4**, pp41-41.

Asquith, G.B., 1973. Flow differentiation in Tertiary lamprophyres (camptonites), Sacramento Mountains, Otero County, New Mexico. Jour. Geology **81**, pp. 643-647.

Ayres, L.D., Lumbers, S.B., Milne, V.G. and Robeson, D.W., 1970. Ontario Geological Map, East Central Sheet, Ontario Department of Mines and Northern Affairs, Map 2198a.

Bacon, C.R. and Carmichael, I.S.E., 1973. Stages in the P-T path of ascending basalt magma: An example from San Quintin, Baja California. Contrib. Mineral. Petrol. **41**, pp. 1-22.

Bailey, D.K., 1964. Crustal upwarping- A possible tectonic control of alkaline magmatism. Jour. Geophysical Res. **69**, pp. 1103-1111.

Balint, F., 1977. The Neys diatreme, Coldwell alkaline complex, northwestern Ontario. Unpub. B.Sc. Thesis, Lakehead University, Thunder Bay, Ontario. 111 p.

Bogoch, R. and Margaritz, M., 1983. Immiscible silicate-carbonate liquids as evidenced from ocellar diabase dykes, S.E. Sinai. Contrib. Mineral. Petrol. 83, pp. 227-230.

Bergman, S.C., 1987. A review of the petrology of lamproites. Spec. Pub. Geo. Soc. London **30**, pp. 103-190.

Brooks, C.K., 1973. Rifting and doming in southern east Greenland, Nature Phys. Sci. **244**, pp. 23-25.

Brooks, C.K. and Platt, R.G., 1975. Min. Mag. London **40**, pp. 259-283.

Brooks, C.K. and Rucklidge, 1973. Contrib. Mineral. Petrol. **42**, pp. 197-212.

Brousse, R. and Rancon, J. Ph., 1984. Crystallization trends of pyroxenes from agpaitic phonolites (Cantal, France). Min. Mag. **48**, pp. 39-45.

Brownlow, A.H., 1979. "Geochemistry", Prentice-Hall, New Jersey, 498 p.

Carstens, H., 1982. Spherulitic crystallization in lamprophyric magmas and the origin of ocelli. Nature **297**, 493-494.

Chayes, F., 1956. "Petrographic Modal Analysis". J. Wiley & Sons, New York, 113 p.

Chayes, F., 1960. On correlation between variables of constant sum. Jour. Geophysical Research **65**. pp. 4185-4193.

Chayes, F., 1962. Numerical correlation and petrographic variation. Jour. Geology. **70**, pp. 440-452.

Chayes, F. and Kruskal, W., 1966. An approximate statistical test for correlations between proportions. Jour. Geology **74**, pp692-702.

Cheeney, R.F., 1983. Statistical Methods in Geology. G. Allen and Unwin, New York.

Clarke, D.B., Muecke, G.K. and Pe-Piper, G., 1983. The lamprophyres of Ubekendt Ejland, West Greenland: Products of renewed partial melting or extreme differentiation? Contrib. Mineral. Petrol. **83**, pp. 117-127.

Cocherie, A., 1986. Systematic use of trace element distribution patterns in log-log diagrams for plutonic suites. Geochim. Cosmochim. Acta 30, pp. 2517-2522.

Coleman, A.P., 1900. Heronite or analcite tinguaite. Ann. Rept. Bur. Mines of Ontario **9**, pp. 186-191.

Cooley, W.W. and Lohnes, P.R., 1962. "Multivariate Procedures for the Behavioural Sciences". J. Wiley & Sons, New York.

Cooper, A.F., 1978. Petrology of ocellar lamprophyres from W. Otago, New Zealand. Jour. Petrol. **20**, pp. 137-163.

Cox, K.G., Bell, J.D. and Pankhurst, R.J., 1979. "The Interpretation of the Igneous Rocks". George Allen and Unwin Ltd., London. 450 p.

Currie, K.L., 1980. A contribution to the petrology of the Coldwell alkaline complex, Northern Ontario. Geol. Surv. of Canada Bull. **287**

Davis, J.C., 1973. "Statistics and Data Analysis in Geolgy. J. Wiley & Sons, New York.

Deer, W.A., Howie, R.A. and Zussman, J., 1966. "An Introduction to the Rock Forming Minerals". Longman London.

Delaney, P.T. and Pollard, D.D., 1982. Solidification of basaltic magma during flow in a dyke. Amer. Jour. Sci. **282**, pp. 854-855.

Donaldson, C.H., 1985. The rates of dissolution of olivine, plagioclase and quartz in a basalt melt. Min. Mag. **49**, pp. 683-693.

Eby, G.N., 1980. Minor and trace element partioning between ocelli-matrix pairs from lamprophyre dykes and sills, Monteregian Hills petrographic province, Quebec. Contrib. Mineral. Petrol. **75**, pp. 269-278.

Edwards, A.C., 1976. A comparison of the methods for calculating Fe_{3+} contents of clinopyroxenes from microprobe analysis. N. Jb. Mineral. Mh. **11**, pp. 509-512.

Einarrson, S.A., 1972. Columbium (Niobium) deposits of Ontario. Ontario Dept. of Mines, Mineral Resources Circular **14**

Evans, J.W., 1901. A monchiquite from Girnar, Junagarth. Q. Jour. Geol. Soc. London **57**, pp38-52.

Ferguson, J. and Currie, K.L., 1971. Evidence of liquid immiscibility in alkaline ultrabasic dykes at Callander Bay, Ontario. Jour. Petrol. **12**, pp. 561-585.

Foley, S.F., 1984. Liquid immiscibility and melt segregation in alkaline lamprophyres from Labrador. Lithos **17**, pp. 127-137.

Gibb, F.G.F. and Henderson, C.M.B., 1977. Formation of analcime in the Dippin sill, Isle of Arran. Min. Mag. **41**, pp. 534-537.

Gibb, F.G.F. and Henderson, C.M.B., 1983. Felsic mineral crystallization trends in differentiating alkaline basic magmas. Contrib. Mineral. Petrol. **84**, pp. 355-364.

Gubac, J., 1986. On the character of distribution of chemical elements in nature. Math. Geo. **18**, pp. 429-432.

Hamm, H.M. anad Vieten, K., 1971. Zur berechnung der kristallchemischen Formel und des Fe^{3+}-Gehaltes von Klinopyroxen aus Elektronenstrahl-Mikroanalysen. N. Jb. Miner. Mh.,**1971**, pp 310-314.

Haskin, L.A. and Schmidt, R.A., 1971. "Rare earth distributions from researches in geochemistry; Vol. 2". John Wiley and Sons, 130p.

Hill, M.O., 1979. "TWINSPAN: A FORTRAN program for arranging multivariate data in an ordered two-way table by classification of individuals and attributes." Cornell University Press, Ithaca, N.Y.

Hinze, W.J. and Wold, R.J., 1982. Lake Superior geology and tectonics- overview and major unsolved problems. In "Geology and tectonics of the Lake Superior basin". R.J. Wold and W.J. Hinze Ed.GSA Memoir **156**, pp. 273-280.

Horne, R.R. and Thomson, M.R.A., 1967. Post-Aptian camptonite dykes in southeast Alexander Island. Bull. Brit. Antarctic Surv. **14**, pp. 15-24.

Hyndman, D.W., 1972. "Petrology of igneous and metamorphic rocks". McGraw-Hill Book Co., New York. 533p.

Joplin, G.A., 1966. On lamprophyres. J. Proc. R. Soc. N.S.W. **99**, pp37-44.

Kerr, P.F., 1977. "Optical mineralogy". McGraw-Hill Book Co., New York. 492p.

Kille, I.C., Thompson, R.N., Morrison, M.A., and Thompson, R.F., 1986. Field evidence for turbulence during flow of basalt magma through conduits from southwest Mull. Geol. Mag. **6** pp. 693-697.

Klasner, J.S., Cannon, W.F. and Van Schmus, W.R., 1982. The pre-Keewanawan tectonic history of the southern Canadian shield and its influence on the formation of the Midcontinent rift. In "Geology and tectonics of the Lake Superior basin". R.J. Wold and W.J. Hinze Ed. GSA Memoir **156**, pp 27-46.

Klecka, W.R., 1975. Discrimant analysis. In "Statistical Package for the Social Sciences, 2nd Ed." N.H. Nie, C.H. Hull, J.G. Jenkins, K. Steinbrenner and D.H. Bent, Ed. McGraw-Hill, New York. pp. 434-467.

Koch, G.S. and Link, R.F., 1971. "Statistical analysis of geological data". Dover Publications Ltd., New York.

Le Maitre, R.W., 1968. Chemical variation within and between volcanic series- a statistical approach. J. Petrol. **9**, pp. 220-252

Le Maitre, R.W., 1982. "Numerical petrology: Statistical interpretation of geochemical data". Elsevier Scientific Publishing Co., Amsterdam. 281p.

Leake, B.E., 1978. Nomenclature of Amphiboles. Am. Min. **63**, pp. 1023-1052.

Lilley, F.E.M., 1964. An analysis of the magnetic features of the Port Coldwell intrusive. Unpub. M.Sc. Thesis, Univ. of Western Ontario, London, Ontario.

Malpas, J., Foley, S.F. and King, A.F., 1986. Alkaline mafic and ultramafic lamprophyres from the Aillik Bay area, Labrador. Can. J. Earth Sci. 23, pp. 1902-1918.

Marriot, F.H.C., 1974. "The interpretation of multiple observations". Academic Press, London, 117p.

Mason, B., 1958. "Principles of Geochemistry". J. Wiley and Sons, Inc., New York.

Maxey, L.R., 1976. Petrology and geochemistry of the Beemerville carbonatite-alkalic rock complex, New Jersey. Geo. Soc. Amer. Bull. 87, pp. 1551-1559.

MacIntire, W.L., 1963. Trace element partition coefficients- A review of theory and applications to geology. Geochim. Cosmochim. Acta 27, pp. 1209-1261.

Metais, D. and Chayes, F., 1964a. Kersantites and Vogesites- a possible example of group heteromorphism. Yearb. Carn. Inst. Wash. 1963, pp. 196-199.

Metais, D. and Chayes, F., 1964b. Classifcation of lamprophyres; a possible petrographic application of multigroup discriminant function analysis. Yearb. Carn. Inst. Wash. 1963-4, pp. 182-185.

Michard, A. and Albarede, F., 1986. The REE content of some hydrothermal fluids. Chem. Geol. 55, pp. 51-60.

Miller, R.L. and Goldberg, E.D., 1955. The normal distribution in geochemistry. Geochim. Cosmochim. Acta 8, pp 53-62.

Milne, V.G., 1967. Geology of the Cirrus Lake-Bamoos Lake area, District of Thunder Bay. Ont. Dept. Mines Geol. Report No. 43.

Mitchell, R.H., 1985. A review of the mineralogy of lamproites. Trans. Geo. Soc. South Africa 88, pp. 411-437.

Mitchell, R.H. and Platt, R.G., 1977. Field guide to aspects of the geology of the Coldwell alkaline complex. Field guide of the 23rd annual meeting of the Institute on Lake Superior geology.

Mitchell, R.H. and Platt, R.G., 1978. Mafic mineralogy of ferroaugite syenite from the Coldwell alkaline complex, Ontario, Canada. Jour. Pet. **19**, pp. 627-651.

Mitchell, R.H. and Platt, R.G., 1982a. Mineralogy and petrology of nepheline syenite from the Coldwell alkaline complex, Ontario, Canada. Jour. Pet. 23, pp. 186-214.

Mitchell, R.H. and Platt, R.G., 1982b. Field Trip Guide Book; Proterozoic geology of the Northern Lake Superior area, GAC, pp. 42-61.

Mitchell, R.H., Platt, R.G. and Cheadle, S., 1983. A gravity study of the Coldwell complex, Northwestern Ontario, and its petrological significance. Can. Jour. Earth Sci. 20, pp. 1631-1637.

Moller, P. and Muecke, G.K., 1984. The significance of europium anomalies in silicate melts and crystal-melt equilibria: a re-evaluation. Contrib. Min. Petrol. **87**, pp242-250.

Nicholls, J., Carmichael, I.S.E. and Stormer, J.C. Jr., 1971. Silica activity and P_{total} in igneous rocks. Contrib. Min. Petrol. **33**, pp. 1-20.

O'hara, M.J., 1977. Geochemical evolution during fractional crystallization of a periodically refilled magma chamber. Nature **266**, pp. 503-507.

Pearce, J.A., 1976. Statistical analysis of major element patterns in basalts. Jour. Petrol. **17**, pp. 15-43

Philpotts, A.R., 1976. Liquid immiscibility: Its probable extent and petrogenetic sifnificance. Am. Jour. Sci. **276**, pp. 1147-1177.

Pirsson, L.V., 1900. On the monchiquites or analcite group of igneous rocks. Jour. Geol. **4**, pp. 680-683.

Poldervaart, A. and Hess, H.H., 1951. Pyroxenes in the crystallization of basaltic magma. Jour. Geol. 59, pp. 472-489.

Puskas, F.P., 1967. The geology of the Port Coldwell area. Ont. Dept. Mines Open File Rpt. No. 5014, Thunder Bay, Ont.

Rock, N.M.S., 1977. The nature and origin of lamprophyres: Some definition, distinctions and derivations. Earth Sci. Rev. 13, pp. 123-169.

Rock, N.M.S., 1978. Petrology and petrogenesis of the monchique alkaline complex, Southern Portugal. Jour. Petrol. 19, pp. 171-214.

Rock, N.M.S., 1979. Petrology and origin of the type monchiquites and associated lamprophyre dykes of Serra de Monchique, Portugal. Trans. Royal Soc. Edinburgh 70, pp. 149-170.

SAS Version 5, Statistics. 1985, SAS Institute, Cary, N.C. U.S.A.

Sahama, P., 1974. Potassium-rich alkaline rocks. In "The Alkaline Rocks", H. Sorensen, Ed. Wiley, New York, pp. 96-108.

Schnetzler, C.C. and Philpotts, J.A., 1970. Partition coefficients of rare-earth elements between igneous matrix material and rock-forming mineral phenocrysts- II. Geochim. Cosmochim. Acta 34, pp. 331-340.

Scott, P.W., 1976. Crystallization trends of pyroxenes from the alkaline volcanic rocks of Tenerife, Canary Islands. Min. Mag. 40, pp. 805-816.

Scott, P.W., 1980. Zoned pyroxenes and amphiboles from camptonites near Gran, Oslo region, Norway. Min. Mag. 43, pp. 913-917.

Skala, W., 1979. Some effects of the constant-sum problem in geochemistry. Chem. Geol. 27, pp. 1-9.

Smith, R.E., 1967. Segregation vesicles in basaltic lava. Am. Jour. Sci. 256, pp. 696-713.

Spera, F.J., Yuen, D.A., Greer, J.C. and Sewell, G., 1986. Dynamics of magma withdrawl from stratified magma chambers. Geology 14, pp. 723-726.

Streckeisen, A., 1978. Classification and nomenclature of volcanic rocks, lamprophyres, carbonatites and melitic rocks. N. Jb. Miner. Abh. 134, pp. 1-14.

Strong, D.F. and Harris, A., 1974. The petrology of Mesozoic alkaline intrusives of central Newfoundland. Can. Jour. Earth Sci. 11, pp, 1208-1219.

Sturchio, N., Muehlenbachs, K. and Seitz, M., 1986. Element redistribution during hydrothermal alteration of rhyolite in an active geothermal system: Yellowstone drill cores Y7 and Y8. Geochim. Cosmochim. Acta 50, pp. 1619-1631

Thompson, J.E., 1931. Geology of the Heron Bay area. Ann. Rept. Ont. Dept. Mines 40, pp. 21-39.

Treuil, M. and Varet, J., 1973. Criteres volcanologiques, petrologiques et geochimiques de la genese et de la differenciation des magmas basaltiques: exemple de l'Afar. Bull. Soc. Geol. Fr. 25, pp. 401-644.

Treuil, M., Joron, J.L., Jaffrezic, H., Villemant, B. and Calas, G., 1979. Geochimie des elements hygromagmaphiles, coeficients de partage mineraux/liquide et proprietes structurales de ces elements dans les liquides magmatiques. Bull. Mineral. 102, pp. 402-409.

Troger, W.E., 1939. Uber theralith und monchiquit. Zentralbl. Mineral., Abt. A., pp. 80-94.

Upton, B.G.J. and Wadsworth, W.J., 1971. Rhyodacite glass in Reunion basalt. Min. Mag. 38, pp. 152-159.

Villemant, B., Jaffrezic, H., Joron, J.L., and Treuil, M. Distribution coefficients of major and trace elements; fractional crystallization in the alkali basalt series of Chaine des Puys (Massif Central, France). Geochim. Cosmochim. Acta 45, pp. 1997-2016.

Walker, J.W.R., 1967. Geology of the Jackfish-Middleton area. Ont. Dept. Mines Geol. Rept. 50

Wendlandt, R.F. and Harrison, W.J., 1979. Rare earth partitioning between immiscible carbonatate and silicate liquids and CO_2 vapour: Results and implications of LREE enriched rocks. Con. Min. Petrol. **69**, pp. 409-419.

Williams, H., Turner, F.J. and Gilbert, C.M., 1955. "Petrography". Freeman, San Francisco.

Wimmenauer, W., 1973. Lamprophyre, semilamprophyre und anchibasaltique Gangesteine. Fortshcr. Mineral. **51**, pp. 3-67.

Wimmenauer, W., 1976. Remarks to the discussion on nomenclature of lamprophyres. Consultative Document, I.U.G.S. Subcommission (unpub.).

Appendix A

Analytical Methods

Appendix A- Analytical Methods

Whole Rock Major and Minor Element Data

The major and minor element data used in this work were collected by Dr. R. Mitchell and Dr. R.G. Platt using XRF and wet chemical methods.

Whole Rock Trace Element Data

Data for the following trace elements were provided by Dr. R. Mitchell and Dr. R.G. Platt: Ni, Cu, and Pb.

Data for the following trace elements were collected using pressed-powder pellet x-ray fluorescence spectrometry at Lakehead University: Rb, Sr, Y, Nb and Zr.

Data for the following trace elements were collected using instrumental and radiochemical neutron activation analysis at Lakehead University, using the research reactor at McMaster University, Hamilton, Ontario, for the activation process, according to methods described by Duffield and Gilmore (1979) and the MAC (1980): La, Ce, Nd, Sm, Eu, Tb, Yb, Lu, Co, Cr, Ba, Th, Ta, Sc, Cs and Hf.

Data for Li were collected using atomic absorption spectrophotometry at Lakehead University.

Mineral Analyses

Data for mineral analyses were collected by Dr. R. Mitchell and Dr. R.G. Platt using the EDS electron microprobe apparatus at Dalhousie University, Halifax, Nova Scotia, and Edinburgh, Scotland.

List of References

Duffield, J. and Gilmore, G.R., 1979. An optimum method for the determination of rare earth elements by neutron activation analysis. Jour. Radioanal. Chem. **48**, pp. 135-145.

Mineralogical Association of Canada, 1980. Short course in neutron activation analysis in the geosciences. Ed. G.K. Muecke. MAC Short Course Handbook **5**, 279p.

Appendix B

Data

Coldwell Dyke Rocks Whole Rock Major Element Data

Specimen No.	SiO2	Al2O3	Fe2O3	FeO	MgO	CaO	Na2O	K2O	MnO	TiO2	P2O5	H2O	CO2
Sannaites													
C1	44.60	11.63	3.01	7.18	8.65	15.63	1.17	1.82	0.21	0.98	0.79	3.45	0.51
C128	44.50	12.96	3.05	7.82	9.30	12.69	3.21	1.64	0.30	1.08	1.04	1.91	0.24
C454	45.81	10.73	4.48	4.64	10.30	15.10	2.05	0.16	0.23	0.95	0.73	2.34	1.80
C486	39.30	11.88	4.15	6.99	9.60	14.81	1.61	3.01	0.23	1.27	1.61	2.28	2.97
C458	43.64	16.29	5.61	8.68	6.08	8.32	4.11	0.57	0.30	2.08	0.92	3.55	0.00
C446	44.47	15.72	6.20	5.69	7.61	11.03	2.32	0.31	0.30	1.26	1.03	3.55	0.00
Quartz Camptonites													
C405	54.28	14.35	2.88	4.56	5.71	7.86	0.56	2.91	0.12	1.17	3.19	2.93	0.00
C453	56.05	13.79	0.00	7.22	5.67	3.87	3.63	3.63	0.12	1.00	0.52	0.00	0.00
C416	55.36	14.07	3.67	3.42	5.50	7.65	3.24	2.83	0.14	1.16	0.48	2.88	0.00
C430	52.20	14.86	4.05	4.08	5.66	8.45	2.86	2.04	0.14	1.24	0.65	2.61	0.77
C419	55.03	14.42	4.39	3.48	6.36	8.67	3.01	2.56	0.14	1.15	0.56	2.46	0.00
C461	56.05	13.62	2.59	4.35	6.25	4.95	3.76	2.46	0.18	1.01	0.62	3.27	0.96
Ocellar Camptonites													
C88	38.75	12.25	3.83	7.14	9.25	14.40	2.36	2.54	0.24	1.35	1.54	2.41	3.69
C74	45.60	14.82	4.41	5.26	6.35	8.15	4.81	3.36	0.35	1.06	0.65	2.68	2.34
C75	46.50	14.83	3.99	6.74	6.44	8.05	4.07	3.16	0.34	1.15	0.69	2.51	1.29
C81	44.80	15.22	3.07	8.66	6.65	10.41	3.73	1.95	0.25	1.14	0.89	2.15	0.80
C84	44.10	13.35	2.88	6.62	9.20	9.75	4.21	1.76	0.23	1.46	0.99	3.83	1.42
C85	46.40	14.27	2.78	8.31	7.15	10.77	3.86	1.89	0.22	1.12	0.88	1.73	0.41
C169	44.55	11.45	3.14	7.28	9.13	11.52	2.84	2.94	0.24	1.97	1.00	2.16	2.09
C97	46.26	14.37	3.09	7.28	6.58	8.87	2.66	2.20	0.44	0.98	0.67	4.32	2.16
C108	42.80	14.64	3.09	9.50	4.25	8.46	4.57	1.68	0.20	1.52	0.84	3.67	4.54
C113	44.65	14.52	4.39	8.74	4.80	7.85	4.78	0.51	0.23	2.68	1.71	3.43	1.54
C118	45.05	14.91	2.89	9.11	5.15	6.67	4.66	3.36	0.21	1.56	0.88	2.41	2.89
C92	45.30	14.71	2.92	11.58	3.50	6.75	4.90	1.39	0.33	1.21	0.95	3.58	2.71
C144	48.24	15.23	4.08	6.72	5.05	10.07	5.93	2.36	0.25	1.08	0.37	0.81	0.18
C135	41.05	13.86	3.06	8.57	6.40	13.85	2.77	2.68	0.27	1.13	1.82	2.01	2.25
C26b	44.90	14.63	3.76	6.74	6.45	9.23	3.77	1.92	0.23	1.51	1.60	3.08	2.34
C421	44.06	12.54	4.18	11.18	4.14	7.59	2.59	2.03	0.21	3.01	2.18	6.85	0.00
C576	44.60	13.88	3.37	6.75	7.95	9.82	3.61	2.54	0.21	1.41	1.03	2.80	1.94
C577	46.70	14.43	2.77	8.15	6.93	11.02	3.67	1.96	0.20	0.96	0.85	1.84	0.35
C583	45.80	15.19	3.59	8.03	6.10	9.98	3.62	2.44	0.20	1.01	0.92	2.52	0.42
C678	nd	nd	nd	nd	nd	nd	nd	nd	nd	nd	nd	nd	nd
Monchiquites													
C560	44.80	14.22	3.68	6.59	7.25	10.98	3.72	2.41	0.20	1.42	1.18	2.78	0.62
C581	42.78	17.26	4.24	6.80	6.04	6.88	4.36	3.02	0.21	1.02	0.67	4.59	1.28
C569	44.44	13.73	4.26	6.36	7.58	13.20	3.20	2.25	0.19	1.02	0.86	1.80	0.92
C586	41.60	12.84	4.62	4.56	6.34	13.93	3.28	2.73	0.18	1.31	0.89	3.69	2.90
Amphibole Camptonites													
C553	44.48	14.50	3.43	6.72	6.48	11.25	3.77	2.34	0.22	1.59	1.03	2.43	0.99
C240	35.95	12.32	5.28	8.36	5.63	12.37	3.90	1.96	0.32	2.32	2.39	3.10	5.72
C295	45.90	17.29	3.49	6.94	3.74	6.68	4.81	4.09	0.19	2.16	0.51	3.10	0.78
C296	nd	nd	nd	nd	nd	nd	nd	nd	nd	nd	nd	nd	nd
C555	46.90	15.12	4.59	4.83	4.98	8.86	5.30	2.20	0.21	1.13	0.93	3.09	1.54
Tinguaites													
C161	61.28	16.76	2.14	0.52	0.14	4.15	6.17	6.27	0.06	0.37	0.10	0.54	1.76
C166	59.88	15.96	0.82	3.48	0.10	3.39	6.92	4.76	0.15	0.31	0.07	0.54	3.63
C507	61.54	20.81	0.73	1.22	0.66	1.85	5.88	6.86	0.11	0.29	0.05	0.00	0.00
C79	58.77	16.95	3.45	3.28	1.29	1.74	7.10	5.66	0.19	0.54	0.09	1.08	0.18
C168	58.52	17.29	2.95	4.00	0.48	1.71	6.16	5.70	0.18	0.62	0.30	1.53	0.73
C76	59.21	20.39	1.49	0.76	0.42	3.95	8.00	2.09	0.09	0.24	0.15	0.09	2.97
C667	60.30	17.52	4.33	1.12	0.59	1.54	6.96	4.40	0.27	0.59	0.12	1.26	0.29

Coldwell Dyke Rocks Whole Rock Major Element Data

Specimen No.	SiO2	Al2O3	Fe2O3	FeO	MgO	CaO	Na2O	K2O	MnO	TiO2	P2O5	H2O	CO2
C478	60.83	18.05	4.99	0.96	0.17	2.00	5.16	5.45	0.12	0.05	0.07	0.99	1.03
C618	64.46	15.46	2.64	2.36	0.21	1.54	5.66	5.05	0.16	0.49	0.10	1.17	0.70
C202	nd	nd	nd	nd	nd	nd	nd	nd	nd	nd	nd	nd	nd
C210	nd	nd	nd	nd	nd	nd	nd	nd	nd	nd	nd	nd	nd
C209	nd	nd	nd	nd	nd	nd	nd	nd	nd	nd	nd	nd	nd
C633	68.90	17.98	2.47	0.40	0.16	0.03	9.05	0.01	0.01	0.21	0.17	0.11	0.36

Table A.3 Trace Element Abundances of a Representative Suite of Coldwell Centre 2 Dyke Rocks
(All values in ppm)

Rock Type	Sample	Ba	Rb	Sr	Hf	Zr	Ta	Nb	Sc	Co	Cr	Ni	Cu	Pb	Li	Cs	
Sannaite	C1	199	42	293	3.93	206	3.79		26	56					24	0	
	C128	1291	68	901	5.40	244	5.46	95	29	51		129	31	19			
	C454	335	9	670	4.45	182	3.92	56	44	54	93	210	55	0			
	C486	1011	99	1293	4.96	270	9.48	176	23	53	620	250	71	9			
	C458	801	29	1090	1.85	253	4.67	89	18	50		42	65	49			
	C446	350	12	2040	5.43	245	6.02	95	23	61		128	62	0.30	24	0	
	Mean	665	43	1048	4	233	6	102	27	54	357	152	57	15	24	0	
	Std Dev	437	35	597	1	33	2	44	9	4	373	81	16	20	0	0	
Quartz Camptonite	C405	848	97	645	6.29	221	9.31	89	16	35		105	65	13			
	C453	1102	123	336	6.16	222	8.85	98	14	34		105	48	15			
	C416	786	96	653	6.19	222	8.96	94	16	39		142	71	14			
	C430	930	46	723	7.18	236	5.02	72	20	44	5	111	77	7	8	1	
	C419	819	74	645	3.81	206	7.43	85	18	37	16	155	63	13	12	4	
	C461	948	69	413	6.02	224	9.49	95	15	34	336	111	50	6			
	Mean	906	84	569	6	222	8	89	17	37	119	122	62	12	10	3	
	Std Dev	115	27	156	1	10	2	9	2	4	188	21	11	3	3	2	
Ocellar Camptonite	C88	1056	68	1679	5.36	274	9.97	189	22	50		211	79	6	0	1	
	C74	790	188	639		131		44				159	34	6			
	C75	623	143	826		144		47				148	70	2			
	C81	1271	67	881		196		69				101	109	32			
	C84	969	60	692		227		95				170	126	21			
	C85	1232	64	952		189		67				95	93	11			
	C169	1239	160	892	5.62	241	4.76	84	29	65		268	133	13			
	C97	1352	116	755		226		86				106	52	4			
	C106	461	65	744		193		58				57	43	2			
	C113	833	28	687		309		91				23	25	5			
	C118	942	134	871		192		60				65	56	0.40			
	C92	795	55	777	4.85	211	3.79	65	13	39		17	16	71			
	C144	637	156	575	6.35	318	5.68	101	25	37		82	55	27			
	C135	1422	94	1752	5.65	275	7.68	118	14	52		76	86	21	90	0	
	C26b	2403	63	1854	4.93	226	7.49	123	19	69		106	100	5			
	C421		40	470		451						21	56	3			
	C576	1575	80	1130	7.25	264	5.46	106	24	42	41	147	117	9			
	C577	1180	64	1000	3.98	213	4.42	72	27	62	28	98	97	4			
	C583	1299	108	108	4.53	217	4.40	77	23	62	22	83	93	25			
	C678	1224	60	547	7.64	348	5.68		14	66	1						

	Mean	1121	91	892	6	242	6	86	21	54	23	107	76	14	45	1
	Std Dev	432	45	434	1	74	2	34	6	12	17	65	34	17	64	1
Monchiquite	C560	2894	74	2352	5.08	232	10.27	126				130	101	5		
	C581	929	168	670		167		54	19	51	20	64	49	0		
	C569	1081	77	665		229		91				143	104	5		
	C586	1611	77	1210		203		183				169	120	15		
	Mean	1629	99	1224	5	208	10	114	19	51	20	127	94	6		
	Std Dev	893	46	794		30		55				45	31	6		
Amphibole	C553	2812	174	1649	5.40	403	7.88		19	46	519					
Camptonite	C240															
	C295	1671	170	1098		224		122				28	90	1		
	C296	1301	109	1008	8.05	272	9.77		6	58	0.10				82	1
	C555	2538	227	1806	5.22	557	8.52		13	35	17				52	5
	Mean	2081	170	1390	6	364	9	122	13	46	179	28	90		67	3
	Std Dev	712	48	396	2	149	1		7	12	295				21	3
Tinguaite	C161	94	214	34	17.20	879	12.70	217	3	45		5	6	2		
	C166	124	163	70		823		206				9	6	50		
	C507															
	C79	26	163	26		1107		326				11	2	30		
	C168	1347	128	99		551		168				5	21	5		
	C76	346	140	140		1132		206				1	7	96		
	C667	44										2	2	29		
	C478	132	453	27	31.70	1732	32.10	487	0.13	9		6	18	22		
	C618	50	202	19	14.88	725	14.45	211	10	18	2	5	11	4		
	C202	2662	381	749	13.55	718	19.70	94	1	11	1				38	11
	C209	484	176	289	24.50	891	30.50		0.11	10						
	C210	655	140	265	22.55	1196	33.32	143	0.12	19	3				12	56
	C633	317	212	114	11.20	293	32.30	465	0.35	32		1	4	51		
	Mean	523	216	167	19	913	25	252	2	21	2	5	9	32	25	34
	Std Dev	771	105	214	7	379	9	132	4	13	1	3	7	30	18	32

Rock Type	Sample	Th	Y	La	Ce	Nd	Sm	Eu	Tb	Yb	Lu
Sannaite	C1	7.22	38	83.76	147.45	66.58	11.42	2.84	1.08	1.80	0.26
	C128	10.99	34	117.84	204.92	90.29	16.78	4.70	1.32	2.62	0.38
	C454	5.75	28	75.80	122.98	86.82	11.69	3.38	1.17	1.65	0.28
	C486	16.80	39	128.33	228.42	167.98	21.13	5.86	1.92	2.98	0.39
	C458		33	89.57	178.79	72.32	12.05	3.73	1.24	2.20	0.03
	C446	10.42	32	125.38	217.62	87.98	15.23	4.21	1.37	2.20	0.30
Quartz Camptonite	C405		27								
	C453		28								
	C416		27								
	C430	12.45	26	72.18	112.32	46.11	7.99	1.74	0.49	1.71	0.03
	C419	9.89	26	64.05	158.51	48.88	7.45	2.41	0.95	2.89	0.04
	C461	19.44	26	68.26	132.66	77.14	9.71	2.41	0.92	2.74	0.37
Ocellar Camptonite	C88		39								
	C74		24								
	C75		25								
	C81		29								
	C84		32								
	C85		28								
	C169		31								
	C97		29								
	C108		25								
	C113		39								
	C118		26								
	C92	8.62	34	83.64	158.35	71.89	13.88	3.82	1.28	2.19	0.31
	C144	19.75	47	132.26	200.99	69.14	12.33	2.84	0.98	3.24	0.48
	C135	10.40	43	154.07	277.04	121.46	22.59	6.30	1.82	2.80	0.39
	C26b	15.54	35	154.96	291.41	100.21	16.78	5.35	1.03	2.45	0.31
	C421		68								
	C576	11.21	32	139.73	264.89	89.58	13.68	4.30	1.34	2.22	0.26
	C577	9.89	28	88.44	172.41	105.00	13.60	3.61	1.32	2.81	0.39
	C583	10.61	30	95.45	142.51	93.49	12.77	3.31	1.55	2.24	0.33
	C678	12.54	66	111.34	219.45	83.63	14.65	3.59	0.87	2.53	0.04
Monchi-quite	C560	12.30	34	163.43	328.61	94.63	16.22	4.56	1.76	2.37	0.03
	C581	9.67	24	76.08	139.95	45.85	9.14	2.60	0.85	1.93	0.03
	C569		27								
	C586		22								
Amphibole Camptonite	C553	15.77	50	159.75	255.60	139.34	17.15	5.32	1.60	2.51	0.36
	C240										
	C295		17								
	C296	6.21	16	46.36	101.00	36.66	5.08	2.28	0.64	1.00	0.02
	C555	11.33	59	185.49	236.53	82.40	13.76	3.36	0.73	1.82	0.03
Tinguaite	C161		51								
	C166	45.78	42	295.15	415.64	119.05	17.89	1.73	1.14	3.73	0.01
	C507										
	C79		80								
	C168		34								
	C76		54								
	C667										
	C478	133.00	95	484.80	648.08	144.26	19.31	1.33	1.83	6.96	0.01
	C618	28.12	47	164.12	252.71	123.12	16.59	0.89	1.62	4.47	0.61
	C202	28.29	72	177.73	286.86	135.06	16.58	4.94	1.87	4.57	0.58
	C210	54.77	52	202.83	341.40	156.44	20.87	5.93	2.59	7.51	0.96
	C209	48.50	54								
	C633	74.30	74								

Clinopyroxene Analyses

	SiO2	Al2O3	TiO2	Fe2O3	FeO	MgO	CaO	Na2O	K2O	MnO	Cr2O3
Sannaite											
core	53.39	2.39	0.11	1.94	0.83	17.99	22.13	0.32	0.02	0.05	1.03
rim	49.34	4.80	1.11	7.98	3.44	12.42	17.49	2.44	0.21	0.28	0.01
grdmss	49.80	4.81	0.97	3.28	4.96	13.22	22.10	0.60	0.03	0.17	0.12
core	52.87	2.86	0.29	1.47	2.15	16.60	23.44	0.31	0.01	0.07	0.23
rim	53.24	0.97	0.01	3.07	7.63	11.67	22.68	1.27	0.03	0.57	0.06
core	53.53	2.35	0.17	1.61	1.28	17.58	22.19	0.26	0.01	0.04	0.73
	53.48	2.49	0.17	1.81	1.04	17.44	22.37	0.28	0.02	0.06	0.88
rim	51.85	2.80	0.66	3.36	3.64	14.62	21.81	0.80	0.02	0.17	0.30
grdmss	51.42	3.38	0.78	4.40	3.81	12.89	21.93	1.25	0.04	0.23	0.04
core	51.41	4.13	0.39	1.88	3.22	15.82	22.61	0.45	0.02	0.08	0.11
	52.07	3.93	0.51	3.49	3.49	15.25	21.52	1.06	0.03	0.19	0.06
	50.92	3.43	0.93	3.78	5.20	13.47	21.97	0.84	0.02	0.40	0.14
	50.56	3.49	1.07	3.32	6.08	13.10	22.07	0.57	0.03	0.23	0.04
rim	48.81	3.89	0.79	7.00	2.85	13.70	22.11	2.12	0.44	0.26	0.00
core	53.51	2.18	0.14	1.72	1.08	17.98	22.60	0.28	0.02	0.05	0.84
	52.82	2.66	0.17	2.50	0.22	17.57	22.38	0.38	0.02	0.07	1.36
	52.91	2.62	0.15	2.59	0.14	17.59	22.09	0.34	0.02	0.07	1.59
rim	51.68	4.21	0.39	5.17	2.17	12.94	21.76	1.54	0.05	0.22	0.87
Quartz Camptonite											
grdmss	49.28	5.31	0.81	2.33	5.33	16.33	18.50	0.15	0.00	0.07	0.55
core	51.11	1.20	0.21			11.67	18.61	0.44	0.00	0.58	0.00
rim	48.12	6.19	1.47	3.83	4.38	14.74	19.93	0.42	0.00	0.10	0.22
core	49.10	4.70	1.08	4.10	8.18	13.57	18.20	0.93	0.00	0.22	0.00
	49.23	4.60	0.89	3.13	9.23	13.48	18.40	0.66	0.00	0.18	0.00
	48.97	4.58	0.91	2.93	9.48	13.39	18.26	0.56	0.00	0.13	0.00
rim	50.47	4.12	0.65	2.15	4.68	16.14	20.53	0.19	0.00	0.15	0.57
grdmss	49.11	4.81	1.26	2.79	7.07	15.33	18.93	0.17	0.00	0.24	0.14
grdmss	48.91	4.33	1.34	3.30	7.21	13.35	20.62	0.37	0.07	0.00	0.00
grdmss	49.43	4.04	1.26	3.03	6.27	14.20	21.19	0.28	0.00	0.21	0.12
core	50.15	5.21	0.87	2.12	6.09	15.98	19.00	0.19	0.00	0.06	0.12
rim	48.36	5.94	1.49	3.47	5.81	15.12	18.97	0.28	0.00	0.00	0.15
core	49.31	6.99	0.90	3.08	4.18	15.96	18.85	0.34	0.00	0.00	0.71
rim	49.24	6.45	1.04	3.05	6.99	15.42	17.64	0.51	0.00	0.14	0.00
Ocellar Camptonite											
core	51.29	3.94	0.75	3.18	4.64	14.54	20.81	0.79	0.00	0.24	0.00
core	48.25	6.45	1.40	4.49	3.03	13.01	21.70	0.85	0.00	0.16	0.04
core	49.14	5.87	0.92	3.38	2.17	14.44	22.02	0.60	0.00	0.09	0.35
rim	45.13	8.72	2.67	6.17	2.59	11.44	22.10	0.58	0.00	0.12	0.03
core	49.73	4.28	0.46	4.18	8.99	9.46	20.75	1.43	0.00	0.43	0.04
	50.79	3.89	0.34	3.70	7.64	10.97	20.76	1.32	0.00	0.38	0.03
	47.59	6.19	1.13	3.77	3.26	13.49	21.99	0.72	0.00	0.28	0.07
rim	48.08	6.46	1.23	3.92	3.05	13.40	21.90	0.69	0.00	0.13	0.11
core	49.67	5.20	0.92	3.24	2.33	14.52	22.65	0.58	0.00	0.09	0.26
core	49.10	5.91	1.31	4.03	3.86	13.04	21.23	0.64	0.00	0.12	0.20

	52.02	3.83	0.78	1.57	3.91	15.59	21.78	0.00	0.00	0.00	0.18
rim	51.48	4.00	0.81	1.75	4.45	15.12	21.53	0.00	0.00	0.00	0.31
core	51.92	4.00	0.57	1.46	3.68	16.69	21.14	0.00	0.00	0.14	0.46
rim	47.74	5.90	1.86	3.35	5.21	12.64	21.99	0.00	0.00	0.13	0.00
grdmss	50.90	5.20	0.71	2.47	2.11	15.69	21.17	0.00	0.00	0.15	1.26
grdmss	51.88	4.26	0.52	1.90	2.58	16.52	21.25	0.00	0.00	0.16	1.02
grdmss	50.65	5.30	0.82	2.28	2.40	15.58	21.07	0.00	0.00	0.13	0.85
core	47.51	5.41	1.02	4.71	5.83	9.71	20.57	1.21	0.00	0.43	0.07
rim	49.25	6.08	1.03	3.57	2.40	14.11	22.10	0.60	0.00	0.11	0.34

Monchiquite

grdmss	48.93	5.61	1.31		8.46	13.77	21.42	0.24	0.00	0.12	0.00
grdmss	49.44	5.82	1.18	3.05	3.92	13.98	22.34	0.32	0.00	0.00	0.20
core	50.49	4.06	0.46	3.01	8.62	11.04	21.09	0.94	0.00	0.38	0.00
	48.71	6.08	1.06	3.72	6.94	11.01	21.33	0.74	0.00	0.18	0.10
	49.15	6.02	1.26	3.04	3.41	14.05	22.36	0.22	0.00	0.07	0.28
rim	46.25	8.25	2.16	4.67	5.21	10.72	22.38	0.34	0.00	0.08	0.00
core	50.41	3.13	0.18	2.39	12.10	9.94	20.79	0.89	0.00	0.55	0.00
	50.22	4.62	0.81	2.00	4.15	14.44	22.47	0.14	0.00	0.00	0.23
rim	46.05	7.29	2.50	5.38	4.08	11.05	22.63	0.38	0.00	0.20	0.00
grdmss	50.40	3.80	0.35	3.17	9.73	10.68	21.15	1.06	0.00	0.41	0.08
core	48.33	6.57	1.53	3.22	4.92	12.58	21.85	0.20	0.00	0.14	0.00

Amphibole Camptonite

core	48.62	6.38	1.03	4.03	4.46	12.30	21.25	0.94	0.00	0.00	0.00
	48.23	6.86	1.07	4.52	4.39	11.52	21.36	1.12	0.00	0.13	0.00
	48.86	6.33	1.10	3.65	1.59	14.03	22.51	0.31	0.00	0.07	1.01
rim	48.28	5.88	1.22	3.64	4.71	12.69	21.91	0.59	0.05	0.00	0.00
core	48.18	6.69	1.37	3.76	4.88	12.41	21.70	0.56	0.00	0.00	0.00
	48.53	6.09	1.53	3.52	2.83	14.05	22.59	0.28	0.00	0.00	0.05
	49.78	5.10	1.00	2.67	4.73	14.11	21.92	0.35	0.04	0.05	0.00
rim	49.12	5.86	1.18	3.58	4.51	12.75	22.05	0.63	0.00	0.00	0.00
grdmss	50.11	5.72	0.88	2.65	3.07	14.39	22.91	0.23	0.04	0.06	0.50
grdmss	51.24	3.75	0.72	2.48	4.99	13.99	22.33	0.51	0.00	0.00	0.00
grdmss	48.67	6.68	1.41	3.77	3.67	13.00	22.09	0.51	0.00	0.00	0.05

Tinguaite

core	52.52	1.87	3.84		22.21	0.22	3.70	14.26	0.00	0.63	0.00
rim	51.38	1.24	3.89		23.38	0.30	2.18	14.32	0.00	0.56	0.00
core	47.32	4.13	1.53		16.87	6.12	20.90	1.69	0.00	0.61	0.00
rim	47.39	3.00	1.14		16.98	6.16	21.33	1.25	0.00	0.74	0.00
core	48.02	4.14	1.27		14.30	7.88	21.35	1.27	0.00	0.38	0.00

Amphibole Analyses

	SiO2	Al2O3	TiO2	Fe2O3	FeO	MgO	CaO	Na2O	K2O	MnO	Cr2O3
Sannaite											
grdmss	37.65	15.71	1.84		17.64	7.93	11.77	2.38	1.79	0.32	0.02
grdmss	38.42	15.02	2.12		16.36	9.04	11.49	2.13	1.52	0.29	0.01
grdmss	37.74	16.17	2.17		15.95	8.93	11.76	2.12	1.63	0.28	0.02
core	38.74	15.04	2.13		16.57	8.74	11.80	2.03	1.52	0.30	0.02
rim	38.83	13.55	2.08		18.60	7.92	11.49	2.08	1.83	0.34	0.04
core	39.15	14.86	1.84		15.26	9.84	11.79	2.23	1.56	0.26	0.01
rim	39.41	13.21	1.88		18.14	8.47	11.54	2.24	1.74	0.30	0.03
grdmss	39.14	13.80	2.27		16.32	10.26	11.93	2.47	1.44	0.11	0.00
grdmss	38.85	14.03	2.53		15.16	10.98	11.82	2.58	1.39	0.11	0.00
grdmss	40.13	12.86	2.10		18.05	9.72	11.77	2.59	1.42	0.30	0.00
Quartz Camptonite											
core	40.47	12.54	0.94		17.61	9.66	11.55	2.99	1.43	0.34	
rim	40.43	9.80	1.80		23.05	6.82	10.50	2.89	1.44	0.66	
grdmss	41.17	9.52	2.35		22.85	6.61	10.57	2.85	1.41	0.53	
grdmss	40.19	10.09	1.87		23.09	6.46	10.60	3.58	1.53	0.52	
core	43.61	12.00	0.70		12.17	13.12	12.26	2.92	0.14	0.22	
core	44.01	11.39	0.46		12.03	13.60	12.50	2.42	0.28	0.20	
grdmss	38.68	12.19	6.73		13.85	11.50	11.08	2.45	1.17	0.00	0.00
core	39.08	11.87	6.67		14.32	11.06	11.32	2.75	1.14	0.17	0.00
rim	37.80	12.28	7.67		13.20	11.27	11.34	2.35	1.13	0.04	0.00
Monchiquite and Ocellar Camptonite											
grdmss	38.33	12.05	7.09		13.40	11.38	11.24	2.47	1.18	0.07	0.00
grdmss	37.80	11.23	0.20		28.11	4.01	11.31	2.24	2.25	0.54	0.00
grdmss	37.44	11.67	0.17		27.92	4.04	10.81	2.56	2.09	0.54	0.01
core	38.76	14.01	3.04		13.57	10.88	11.68	2.02	1.77	0.37	
rim	39.67	11.69	2.12		19.92	7.78	11.35	1.99	1.89	0.47	0.11
core	38.67	12.76	2.56		19.43	7.91	11.47	1.66	1.90	0.18	
grdmss	39.36	12.22	1.97		20.21	7.65	11.39	2.10	2.00	0.54	
grdmss	39.64	12.48	2.60		17.70	8.92	11.44	2.45	1.47	0.26	
grdmss	38.88	12.50	2.82		17.71	9.19	11.49	1.91	1.62	0.39	
core	37.68	14.67	2.86		19.68	7.51	11.45	1.93	1.81	0.31	
rim	40.04	11.77	3.08		20.43	8.14	11.45	2.69	1.05	0.10	
core	40.23	11.62	2.60		19.91	8.42	11.47	2.93	1.13	0.15	
rim	39.76	10.59	1.10		23.62	7.30	11.30	2.60	1.14	0.38	
grdmss	39.75	11.62	1.34		23.53	7.18	11.59	3.07	0.91	0.45	
grdmss	38.94	11.38	1.21		24.42	6.67	11.48	2.89	1.11	0.33	
grdmss	35.46	15.41	2.05		20.06	6.42	11.70	1.71	2.36	0.49	0.00
grdmss	55.39	1.09	0.00		6.55	20.05	12.36	1.17	0.01	0.21	0.12
grdmss	35.36	16.37	1.95		17.32	8.08	11.65	1.64	2.36	0.37	0.00
Amphibole Camptonite											
core	39.86	13.08	4.25		11.70	12.95	11.78	2.45	1.87	0.00	

rim	40.23	12.77	3.53	14.96	11.22	11.48	2.37	1.67	0.17
core	39.98	13.00	3.75	14.80	11.06	11.25	2.77	1.62	0.11
rim	39.12	12.31	3.48	18.99	8.54	11.21	2.65	1.59	0.43
grdmss	39.32	12.54	3.52	18.40	9.02	11.28	2.68	1.63	0.17

Tinguaite

pheno	49.09	0.58	0.07	37.31	0.00	4.88	4.69	0.68	1.51
pheno	50.26	0.39	0.00	33.89	2.41	5.16	4.28	0.51	1.47
pheno	48.98	0.74	1.07	34.03	0.68	1.31	6.65	0.99	1.34
pheno	49.36	1.19	0.81	32.62	3.09	5.56	4.22	0.75	1.30
pheno	50.02	0.46	0.74	31.71	2.46	2.14	7.57	0.81	1.84
pheno	49.07	0.67	1.49	34.20	0.85	1.47	6.30	0.97	0.99

Feldspar Analyses

	SiO2	Al2O3	TiO2	FeO	MgO	CaO	Na2O	K2O	MnO	BaO
Sannaite										
grdmss	54.51	27.76	0.09	0.05	0.05	0.14	5.61	9.51		
grdmss	55.88	27.06	0.09	0.83	0.46	0.64	6.06	7.70	0.30	
grdmss	54.89	28.00	0.06	0.09	0.03	0.11	5.56	9.90	0.00	
grdmss	54.44	27.98	0.06	0.07	0.04	0.09	5.44	9.90	0.30	
grdmss	68.94	19.55	0.00	0.00	0.05	0.00	11.38	0.00	0.00	
grdmss	68.35	19.82	0.00	0.00	0.00	0.24	11.52	0.00	0.00	
grdmss	69.01	19.64	0.00	0.00	0.00	0.05	11.42	0.00	0.00	
grdmss	68.29	19.23	0.00	0.80	0.50	0.47	10.78	0.00	0.00	
Quartz Camptonite										
grdmss	54.39	28.50	0.00	0.68	0.12	11.30	5.07	0.52		
grdmss	55.19	27.61	0.00	0.56	0.07	10.17	5.70	0.51		
grdmss	56.89	26.09	0.00	0.89	0.31	8.61	6.51	0.72		
grdmss	55.84	27.34	0.00	0.52	0.00	10.10	5.92	0.01		
grdmss	55.27	27.58	0.00	0.25	0.00	9.88	5.58	0.93		
grdmss	55.34	28.03	0.00	0.28	0.00	10.05	5.58	0.93		
grmdss	66.48	21.96	0.00	0.15	0.00	2.60	9.13	0.96		
grdmss	65.97	22.13	0.00	0.19	0.00	2.88	9.88	0.88		
grdmss	66.96	21.79	0.00	0.22	0.28	2.17	10.11	0.87		
grdmss	65.20	22.44	0.06	0.15	0.00	3.20	9.48	0.78		
grdmss	65.42	22.12	0.00	0.17	0.00	2.88	9.93	0.90		
grdmss	62.95	23.92	0.00	0.23	0.00	4.96	9.02	0.68		
grdmss	62.41	24.65	0.00	0.19	0.00	5.72	8.47	0.62		
Ocellar Camptonite										
grdmss	50.65	31.19	0.00	0.33	0.00	13.62	3.75	0.12	0.00	
grdmss	51.63	30.69	0.00	0.26	0.00	12.96	4.18	0.11	0.00	
grdmss	52.39	30.06	0.00	0.35	0.00	12.06	4.67	0.13	0.00	
grdmss	50.87	30.64	0.00	0.38	0.00	13.06	3.87	0.16	0.00	
grdmss	52.52	30.02	0.00	0.19	0.00	12.11	4.66	0.04	0.00	
grdmss	50.92	30.64	0.00	0.09	0.00	13.06	4.04	0.05	0.00	
grdmss	56.72	27.09	0.00	0.15	0.00	8.85	7.23	0.00	0.00	
grdmss	51.79	30.67	0.00	0.48	0.21	12.59	4.19	0.21	0.00	
core	52.05	30.14		0.27	0.00	12.13	4.80	0.06	0.00	
rim	65.47	21.14	0.07	0.17	0.00	1.96	10.09	0.00	0.00	
grdmss	51.96	30.08	0.00	0.55	0.16	12.03	4.63	0.27	0.00	
core	54.53	28.86	0.00	0.00	0.00	10.60	5.68	0.08	0.00	
rim	59.07	25.88	0.06	0.20	0.00	7.47	8.22	0.00	0.00	
grdmss	57.40	26.74	0.00	0.15	0.00	8.29	7.35	0.00	0.00	
grdmss	53.00	29.78	0.00	0.63	0.23	11.45	4.91	0.32	0.00	
grdmss	53.62	29.60	0.15	0.17	0.00	11.52	5.53	0.13	0.00	

grdmss	53.60	29.29	0.00	0.07	0.00	11.37	5.41	0.05	0.00	
grdmss	53.05	29.86		0.18	0.00	11.80	4.97	0.11	0.00	
grdmss	66.75	20.34	0.00	0.23		0.96	10.45	0.15		0.27
grdmss	67.10	20.12	0.00	0.00	0.00	1.12	10.47	0.11		0.21
grdmss	66.68	20.45	0.00	0.00	0.20	1.05	10.55	0.16		
grdmss	52.80	28.87	0.00	0.50	0.00	11.91	4.21	0.51		0.24
core	54.97	27.93	0.00	0.38	0.00	10.81	4.75	0.41		
rim	59.85	24.61	0.00	0.29	0.00	6.64	6.50	1.10		0.54
grdmss	60.65	23.87	0.00	0.27	0.00	5.98	7.02	1.34		0.47
grdmss	59.27	24.49	0.00	0.34	0.00	6.69	6.52	1.18		0.41
grdmss	52.22	29.54	0.00	0.79	0.00	12.80	4.24	0.28		
megacryst	62.95	23.92	0.00	0.23	0.00	4.96	9.02	0.68		
grdmss	69.04	20.11	0.07	0.39	0.06	0.35	11.61			
grdmss	69.98	20.47	0.00	0.20	0.00	0.60	11.51	0.06		
grdmss	52.08	30.04	0.00	0.36	0.00	9.96	4.73	0.86		
grdmss	53.86	29.30	0.07	0.15	0.00	11.19	5.44	0.10		

Amphibole Camptonite

grdmss	53.36	29.21	0.00	0.25	0.00	11.44	5.39	0.16		
grdmss	53.38	29.43	0.09	0.30	0.00	11.53	5.34	0.13		
grdmss	52.02	29.77	0.00	0.24	0.00	8.47	4.58	2.39		
grdmss	52.26	29.85	0.00	0.40	0.00	11.19	5.58	0.38		
grdmss	52.18	30.03	0.00	0.10	0.00	12.34	4.89	0.09		
grdmss	64.73	21.04	0.00	0.20	0.01	2.29	8.12	0.20		
grdmss	63.39	19.14	0.06	0.76	0.50	1.83	8.28	0.22		
grdmss	66.24	19.66	0.00	0.28	0.00	2.61	10.99	0.00		
grdmss	67.99	19.77	0.00	0.01	0.04	0.39	9.81	0.00		
core	54.43	28.53	0.00	0.32	0.00	9.98	5.87	0.46		
rim	68.36	19.32	0.00	0.01	0.03	0.12	11.49	0.01		

Tinguaite

phen	66.66	19.02	0.00	0.15	0.00	0.22	6.63	8.21		
phen	67.20	19.23	0.00	0.31	0.00	0.08	7.15	7.72		
phen	64.56	18.44	0.00	0.63	0.00	0.00	5.14	9.75		
phen	66.65	18.41	0.00	1.21	0.24	0.00	7.83	6.66		
phen	66.65	19.25	0.00	0.31	0.00	0.27	6.35	8.54		
phen	66.28	21.09	0.00	0.25	0.00	0.55	10.02	0.97		
phen	65.75	21.16	0.00	1.49	0.13	0.55	9.54	0.77		
phen	66.64	21.19	0.00	0.21	0.00	0.37	10.04	0.91		
phen	67.68	19.83	0.00	0.23	0.00	0.53	10.88			
phen	68.49	20.26	0.00	0.00	0.00	0.51	11.67			

Olivine Analyses

	SiO2	Al2O3	TiO2	FeO	MgO	CaO	Na2O	K2O	MnO
Ocellar Camptonite									
core	39.74	0.10	0.00	10.74	48.26	0.33	0.04	0.00	0.18
rim	39.12	0.10	0.02	16.61	43.46	0.61	0.04	0.00	0.39
core	39.39	0.09	0.00	12.39	46.96	0.38	0.04	0.00	0.21
core	39.09	0.08	0.00	13.58	45.93	0.43	0.04	0.00	0.27
core	38.73	0.12	0.01	17.47	42.91	0.45	0.04	0.00	0.29
core	38.97	0.08	0.00	14.16	45.50	0.45	0.05	0.00	0.27
Monchiquite									
core	39.81	0.00	0.00	11.07	47.47	0.27	0.00	0.00	0.06
	38.64	0.00	0.00	17.30	42.50	0.21	0.00	0.00	0.27
rim	38.63	0.00	0.00	18.71	41.20	0.19	0.00	0.00	0.21
core	39.76	0.00	0.00	12.79	46.99	0.23	0.00	0.00	0.11
core	39.12	0.00	0.00	12.76	45.91	0.35	0.00	0.00	0.24

Biotite Analysees

	SiO2	Al2O3	TiO2	FeO	MgO	CaO	Na2O	K2O	MnO	Cr2O3
Sannaite										
grdmss	35.86	15.41	2.42	19.04	12.57	0.02	0.08	9.24	0.27	
grdmss	35.19	16.39	2.41	19.40	12.05	0.42	0.00	6.78	0.28	
grdmss	35.46	15.36	3.31	18.41	12.57	0.01	0.07	8.81	0.24	0.04
grdmss	39.72	10.10	0.48	8.80	22.42	0.18	0.35	8.26	0.18	0.02
Quartz Camptonite										
grdmss	32.52	15.25	3.36	22.58	8.57	0.39	0.16	7.20	0.33	0.00
grdmss	32.92	15.77	7.00	15.88	12.72	0.00	0.56	7.33	0.17	
Ocellar Camptonite										
grdmss	31.08	17.28	2.72	19.82	10.81	0.07	0.48	7.12	0.29	
grdmss	37.03	14.22	0.72	18.25	14.04	0.00	0.00	9.65	0.24	
grdmss	37.78	14.78	0.85	16.30	14.50	2.33	0.62	7.36	0.24	0.13
grdmss	32.35	15.23	7.19	20.77	9.44	0.00	0.51	6.99	0.29	
Monchiquite										
grdmss	31.51	15.71	0.99	23.74	11.64	0.31	0.13	5.45	0.37	0.00

Amphibole Camptonite

grdmss	31.27	17.43	2.82	19.02	11.08	0.10	0.50	7.34	0.28

Spinel Analyses

	SiO2	Al2O3	TiO2	FeO	MgO	CaO	Na2O	K2O	MnO	Cr2O3
in olivine		15.56	1.38	26.91	11.15				0.22	44.98
in olivine		12.18	1.14	28.49	10.38				0.00	48.86
in olivine		15.75	1.30	27.25	11.35				0.22	45.30
in olivine		12.58	1.34	25.58	10.40				0.05	47.69

Other Analyses

	SiO2	Al2O3	TiO2	FeO	MgO	CaO	Na2O	K2O	MnO	Cr2O3
Nepheline Analyses										
lamp	41.88	32.99	0.03	0.74	0.00	0.78	16.11	6.82		
tinguaite	44.65	32.03	0.00	0.59	0.00	0.79	17.25	3.66		
Analcite Analyses										
tinguaite	54.73	23.65		0.09			11.15	0.09		
Sphene Analyses										
	30.23	1.97	34.63	1.67		27.55				
	30.27	1.87	36.29	1.43		28.09				
	30.32	0.27	38.49	1.14		28.32				
Magnetite Analyses										
	0.31	4.23	0.05	95.60	0.06	0.02				
Carbonate Analyses										
grdmss	0.01	0.03	0.00	0.05	0.06	54.14	0.01	0.00	0.15	
ocellus	0.00	0.00	0.00	2.67	1.26	54.82	0.00	0.00	1.47	
veinlet	0.01	0.00	0.00	0.03	0.05	54.23	0.00	0.00	0.25	
Scapolite Analyses										
rep f'spar	55.01	22.89	0.00	0.18	0.00	7.38	8.06	0.90		

ocellar	53.92	24.30	0.00	0.15	0.00	8.30	8.38	0.65	
ocellar	50.17	25.56	0.00	0.13	0.00	12.03	6.57	0.55	

Epidote Analyses

ocellar	37.59	23.22	0.02	10.64	0.11	20.78	3.10	0.00	0.05
grdmss	37.56	24.33	0.03	10.51	0.62	21.36	0.00	0.00	0.17
grdmss	38.37	26.37	0.47	7.39		23.59			0.21

Chlorite Analyses

grdmss	28.99	15.77		25.98	15.20	0.48			0.33
ocellar	29.60	15.98		25.21	16.20	0.43			0.40
ocellar	29.35	15.36		25.57	15.64	0.48			0.33
grdmss	28.43	15.21		24.67	15.01	0.21			0.45

Zeolite Analyses

grdmss	46.68	32.41		0.79		1.04	3.66	5.99	0.66
ocellar	63.79	18.35	0.11	0.05	0.03	0.07	0.08	15.98	
ocellar	51.95	24.35	0.00	0.00	0.00	0.88	12.59	0.13	0.11
ocellar	36.32	30.45	0.00	0.00	0.01	13.00	3.25	0.01	0.00
veinlet	43.49	23.85				27.07			